SYNTHESIS AND CHARACTERIZATION OF MULTIWALL CARBON NANOTUBES USING MICROWAVE HEATING FOR REMOVAL OF HEAVY METALS

MUBARAK MUJAWAR

A THESIS SUBMITTED IN FULFILMENT OF THE REQUIREMENTS FOR THE DEGREE OF DOCTOR OF PHILOSOPHY

FACULTY OF ENGINEERING
UNIVERSITY OF MALAYA
KUALA LUMPUR

2015

ORIGINAL LITERARY WORK DECLARATION

Name of Candidate: MUBARAK MUJAWAR (I.C/Passport No.: F7864962)

Registration/Matric No.: KHA110085

Name of Degree: Doctor of Philosophy (Ph.D.)

Title of Project Paper/Research Report/Dissertation/Thesis ("this Work"):

SYNTHESIS AND CHARACTERIZATION OF MULTIWALL CARBON NANOTUBES USING MICROWAVE HEATING FOR REMOVAL OF HEAVY METALS

Field of Study: Chemical Engineering

I do solemnly and sincerely declare that:

(1) I am the sole author/writer of this Work;
(2) This Work is original;
(3) Any use of any work in which copyright exists was done by way of fair dealing and for permitted purposes and any excerpt or extract from, or reference to or reproduction of any copyright work has been disclosed expressly and sufficiently and the title of the Work and its authorship have been acknowledged in this Work;
(4) I do not have any actual knowledge nor ought I reasonably to know that the making of this work constitutes an infringement of any copyright work;
(5) I hereby assign all and every rights in the copyright to this Work to the University of Malaya ("UM"), who henceforth shall be owner of the copyright in this Work and that any reproduction or use in any form or by any means whatsoever is prohibited without the written consent of UM having been first had and obtained;
(6) I am fully aware that if in the course of making this Work I have infringed any copyright whether intentionally or otherwise, I may be subject to legal action or any other action as may be determined by UM.

Candidate's Signature **Date:**

Subscribed and solemnly declared before,

Witness's Signature **Date:**

Name:

Designation: Department of Chemical Engineering,

Faculty of Engineering, University of Malaya, Kuala Lumpur, 50603, Malaysia

Tel. /Fax: +60105491759/03- 79675319

ABSTRACT

Carbon nanotubes (CNTs) are among the most eminent materials in the first rank of the nanotechnology revolution. The most eye-catching features of these structures are their electronic, mechanical, optical and chemical characteristics, which open a way for future applications. A new method is introduced for synthesis of CNTs by gas phase, single stage microwave assisted chemical vapor deposition (MA-CVD) using ferrocene as a catalyst and acetylene (C_2H_2) and hydrogen (H_2) as precursor gases. A fast CNTs growth and ambient reaction condition, lowers the cost, and simplifies the procedure leading to a high yield synthesis of high-quality CNTs with minimal impurity are among the characteristics of the MA-CVD. Production of CNTs depends on various process parameters such as microwave power, radiation time, and gas ratio of C_2H_2/H_2 and further investigation was based on the central composite design (CCD) for optimization. The morphology and structures of multiwall carbon nanotubes (MWCNTs) produced were characterized using Field Emission Scanning Electron Microscope (FESEM), Transmission Electron Microscope (TEM) and Thermo Gravimetric Analysis (TGA). FESEM and TEM analyses revealed that the uniformly dispersed vertical alignment of MWCNTs have diameters ranging from 16 to 23 nm and 30 micron long and high BET surface area of 206 m^2/g. The TGA analysis showed that the purity of MWCNTs produced is around 98% purity. Results reveal that the optimized conditions for MWCNTs production were 900 W microwave power, 35 min radiation time, and 0.6 gas ratio of C_2H_2/H_2. Removal of heavy metal from industrial waste water leads to the biggest challenge nowadays due to it the novel MWCNTs samples are tested for performances in the removal of heavy metals. The effect of process parameters such as pH, MWCNTs dosage, agitation speed and adsorption time were investigated using a CCD. The optimization and kinetic study on the removal of

Pb (II), Cd (II), Cu (II) and Zn (II) using novel MWCNTs was conducted. Maximum adsorption capacities (qm) for Pb (II), Cd (II), Cu (II) and Zn (II) ions were obtained as 104.2, 88.62, 99 and 90.9 mg/g, respectively. Analysis of results revealed that the optimum conditions for the highest removal (99.9%) of Pb (II) and (98.8%) Cd (II) were recorded to have pH 5, MWCNTs dosage 0.1 g, contact time 22.5 min for Pb (II) and 50 min for Cd (II) and agitation speed of 160 rpm, respectively, with the initial concentration of 10 mg/l. In addition, statistical analysis revealed that the optimum conditions for the highest removal (99%) of Cu (II) and (99.9%) Zn (II) were recorded to have pH 5.5, and pH10 MWCNTs dosage 0.1 and 0.05 g, contact time 35 min for Cu (II) and 60 min for Zn (II) and agitation speed of 160 rpm for Cu (II) and 120 rpm for Zn (II) respectively. The Langmuir and Freundlich isotherm models matched the experimental data very well and adsorption kinetic obeyed pseudo-second for Pb (II), Cd (II), Cu (II) and Zn (II). The results proved that MWCNTs can be used as an effective adsorbent due to the high adsorption capacity as well as the short adsorption time needed to achieve equilibrium.

.

ABSTRAK

Karbon nano-tiub (CNTs) adalah salah satu penemuan yang paling menarik dalam revolusi sains nano. Kepentingan dalam CNTs semakin meningkat kerana sifatnya yang unik dari segi elektronik, mekanikal, optik dan ciri kimianya yang menjanjikan pelbagai kegunaan pada masa akan datang. Satu cara baru telah diperkenalkan untuk menghasilkan CNTs dengan fasa gas, di mana pengeluaran CNTs dioptimumkan menggunakan Microwave seperingkat Pemendapan Wap Kimia Terbantu(MA-CVD) menggunakan ferrocene sebagai pemangkin dan acetylene (C_2H_2) dan hidrogen (H_2) sebagai gas pelopor. Pertumbuhan CNTs yang cepat dan keadaan reaksi ambien, dapat mengurangkan kos, dan memudahkan prosedur akan membawa kepada hasil sintesis yang tinggi, menghasilkan CNTs yang berkualiti tinggi dengan kadar ketidakaslian yang minimum adalah antara ciri-ciri MA-CVD. Pengeluaran CNTs bergantung kepada pelbagai parameter proses seperti kuasa gelombang mikro, masa radiasi, dan nisbah gas C_2H_2/H_2. Kesan parameter ini telah disiasat berdasarkan konsep pusat reka bentuk komposit (CCD) untuk pengoptimuman. Morfologi dan struktur multi- inding CNT (MWCNT) dihasilkan telah dicirikan menggunakan beberapa peralatan seperti Field Emission Scanning Electron Microscope (FESEM), Transmisi Mikroskop Elektron (TEM) dan Thermo Gravimetrik Analisis (TGA). Analisis FESEM dan TEM mendedahkan bahawa MWCNT bertaburan seragam dengan penjajaran menegak s mempunyai diameter antara 16 ke 23 nm seta panjang 30 mikron. MWCNTs yang dihasilkan mempunyai luas permukaan BET yang tinggi iaiyu 206 m^2/g. Analisis TGA menunjukkan keaslian MWCNTs dihasilkan adalah sekitar98% keaslian. Dengan menggunakan kaedah CCD, hasil kajian menunjukkan bahawa analisis statistik mendedahkan keadaan optimum untuk penghasilan MWCNTs adalah 900 W kuasa gelombang mikro, 35 minit masa radiasi dan nisbah gas 0.6 bagi C_2H_2/H_2.

Penyingkiran logam berat dari air sisa industri merupakan cabaran terbesar masa kini, dengan ini sampel MWCNT yang baru ini diaplikasikan bagi menentukan prestasi penyingkiran logam beratnya. Pengoptimuman dan kajian kinetik bagi penyingkiran Pb (II), Cd (II), Cu (II) dan Zn (II) menggunakan MWCNTs yang baru ini juga dijalankan. Kapasiti penjerapan maksimum (qm) untuk Pb (II), Cd (II), Cu (II) dan Zn (II) ion yang diperoleh masing-masing pada 104.2, 88.62, 99 dan 90.9 mg/g. Keputusan analisis menunjukkan bahawa keadaan optimum untuk penyingkiran tertinggi Pb (II) iaitu 99.9% & Cd (II) iaitu 98.8% telah direkodkan mempunyai pH 5, MWCNTs dos 0.1 g, masa sentuhan 22.5 untuk Pb (II) dan 50 minit untuk Cd (II) dengan masing-masing mempunyai kelajuan pengadukan 160 rpm, yang mana kepekatan awalnya adalah 10 mg/l. Tambahan itu, analisis statistik pula mendedahkan bahawa keadaan optimum untuk penyingkiran tertinggi Cu (II) & Zn (II) telah direkodkan mempunyai pH 5.5, dan pH10 MWCNTs dos 0.1 dan 0.05 gram, masa sentuhan 35 untuk Cu (II) dan 60 minit untuk Zn (II) dengan kelajuan pengadukan 160 untuk Cu (II) dan 120 rpm untuk Zn (II). Kedua-dua model isotermal Langmuir dan Freundlich berpadanan dengan data uji kaji dengan baik dan penjerapan kinetik mematuhi pseudo-kedua untuk Pb (II), Cd (II), Cu (II), & Zn (II). Oleh itu, kesemua ujian telah membuktikan bahawa MWCNTs merupakan penjerap yang efektif untuk penyingkiran logam berat dari rawatan air sisa dan proses pemisahan kerana kapasiti penjerapan yang tinggi serta masa penjerapan yang pendek diperlukan bagi mencapai keseimbangan.

ACKNOWLEGMENTS

In the name of Allah, the Most Gracious and the Most Merciful.

First of all, the author would like to raise his hand of syukur (appreciation) to Allah (S.W.T) for the guidance, wisdom and barakah for all these years till now, where he has reached to this important destination of his journey in life to accomplish his goal.

Every success is paid through the continuous and diligent effort. As for the author, it is a success to finish the project as well as the report within the time. This success was not meant for only the author, but the rest of people who have contributed to the completion of this work and the author would like to extend a word of thanks and express his gratitude and appreciation to all of them.

Author wish to express his sincere gratitude to the chairman of the supervisory committee, Prof. Dr. Jayakumar Natesan Subramanian Nayagar, and members of the supervisory committee, Assoc. Prof. Dr. Jaya Narayan Sahu and Prof. Dr. Ezzat Chan Abdullah for their valuable guidance, thoughtful ideas, keen interest, encouragement and support at all stages of this work. The author is proud and honored to work with them and it was a delightful and enriching experience.

Finally, the author presents his most heartfelt and warmest appreciation to the great parents and parents in law (may ALLAH SWT bless and reward them), brothers and sisters who always encouraged and supported him during the study period. Special and heartiest gratitude to the author's dearest wife, Muna Tasnim and son, Muhammad Fayyad, for their invariable encouragement, endless sacrifices, patience, understanding, ideas and inspirations from time to time in finishing the Doctorate of Philosophy in Chemical Engineering smoothly and timely.

TABLE OF CONTENTS

LIST OF FIGURES

LIST OF TABLES

LIST OF ABBREVIATIONS

List of abbreviations

CNTs	Carbon Nanotubes
SWCNTs	Single walled Carbon nanotubes
MWCNTs	Multiwalled Carbon Nanotubes
FESEM	Field Emission Scanning Electron Microscope
TEM	Transmission Electron Microscope
HRTEM	High Resolution Transmission Electron Microscope
XRD	X-ray Diffraction
TGA	Thermogravemetric analysis
MW	Microwave
ANOVA	Analysis of variance
DOE	Design of Experiment
PLV	Pulsed laser vaporization
CCD	Central composite design
CNTs	Carbon Nanotubes
DWCNTs	Double walled Carbon nanotubes
MPECVD	Microwave plasma enhanced chemical vapor deposition
MA-CVD	Microwave Assisted-Chemical Vapour Deposition
FESEM	Field Emission Scanning Electron Microscope
TEM	Transmission Electron Microscope
HRTEM	High Resolution Transmission Electron Microscope
XRD	X-ray Diffraction
TGA	Thermogravemetric analysis

MFCNTs	Metal- Filled Carbon nanotubes
FTIR	Fourier Transform Infrared

LIST OF APPENDICES

CHAPTER I

INTRODUCTION

1.1 Overview

Research on new materials technology is attracting the attention of researchers all over the world. Developments are being made to improve the properties of the materials and to find alternative precursors that can give desirable properties of the materials. Nanotechnology, which is one of the new technologies, refers to the development of devices, structures, and systems whose size varies from 1 to 100 nanometers (nm). The last decade has seen the advancement in every side of nanotechnology, such as: nanoparticles and powders, nanolayers and coats, electrical optic and mechanical nanodevices, and nanostructured biological materials. Nanotechnology is estimated to be influential in the next 20-30 years, in all fields of science and technology (Harris and Harris, 2001). Great interest has recently been developed in the area of nanostructures carbon materials. Carbon nanostructure materials are becoming of considerable commercial importance with interest growing rapidly over the decade or so since the discovery of buckminsterfullerene, carbon nanotubes (CNTs), and carbon nanofibers (CNFs) (Dresselhaus and Avouris, 2001). CNTs and CNFs are among the most eminent materials in the first rank of revolution nanotechnology. The most eye-catching features of these structures are their electronic, mechanical, optical and chemical characteristics, which open a way for future applications. These properties can even be measured on single nanotube and nanofiber. For commercial application, large quantities of purified CNTs are needed (Dresselhaus et al., 1996; Ebbesen, 1997b).

Fundamental and practical CNTs researches have shown possible applications to almost all the scientific areas, such as aerospace science, bioengineering, environmental, energy,

materials, industry, medical and medicine, science, electronic computer, security and safety, waste water treatment, bioscience and science education. They are known to be superior to any other existing material in mechanical, electrical, and hydrogen storage characteristics. Various synthesis methods have been developed aiming at bulk production of CNT by mainly looking into ways at controlling their characteristics and morphologies. Conventional methods of synthesizing CNT are Laser Ablation (Journet and Bernier, 1998), Electric Arc Discharge (Thess et al., 1996), and Chemical Vapor Deposition (Bethune et al., 1993; Cassell et al., 1999; Liu et al., 2004).

In recent years, microwave irradiation has attracted the attention of chemists and engineers due to its capability of molecular level heating, which leads to homogeneous and quick thermal reaction (Brunetti et al., 2007; Dallinger and Kappe, 2007). It is of current development of new techniques for the efficient and the selective synthesis of CNTs and CNFs, and other carbon nanostructures at the cheapest possible cost. One such possibility is the use of microwave radiation, which over the past few years has played an important role as a thermal tool in organic synthesis due to considerable advantages over conventional methods (Lidström et al., 2001). The use of microwave radiation in the synthesis and functionalization of CNTs or other nanostructures is advantageous because it provides a fast and uniform heating rate that can be selectively directed towards a targeted area. The first report of the production of carbon nanostructures with microwaves was made by (Ikeda et al., 1995) who synthesized fullerenes from microwave-induced naphthalene-nitrogen plasma at atmospheric pressure inside a cylindrical coaxial cavity. Kharissova, (2004) has reported the synthesis of vertically aligned CNTs using a domestic microwave oven. Unlike conventional heating, microwave heating has a higher heating rate, which results from the intrinsic transition of electromagnetic energy to thermal energy by a

molecular interaction with the electromagnetic field, rather than heat transfer by conduction or convection (Vázquez and Prato, 2009).

Water resources are being polluted from various sources such as metallurgy, mining, tannery, chemical manufacturing, fossil fuel, battery manufacturing industries and the production of plastics, involving the use of metal compounds, particularly as heat stabilizers etc (Bansal, 2005; Muyibi et al., 2008). The types of emerging pollutant are also increasing while the traditional pollutants are not efficiently solved yet. Removal of toxic metals is one of the biggest challenges in ensuring safe water for all as well as protecting the environment (Bansal, 2005; Muyibi et al., 2008). It might cause several health problem to human such as nervous system damages, renal kidney disease, mental retardation, cancer and anemia (Calderón et al., 2001; Friberg, 1979; Li, Wang, et al., 2002). There are many conventional methods that are being used to remove the metal ions that include oxidation and reduction (Ling, 2010), precipitation (Wirojanagud et al., 2004), membrane filtration (Kim and Anderson, 1994), ion exchange (Wójtowicz and Stoklosa, 2002) and adsorption (Choi et al., 2006; Rao et al., 2007; Ye and Yu, 2010). Among the above methods, the promising process for the removal of metal ions from water and wastewater is adsorption, because some of the used adsorbent can be regenerated by suitable desorption process and it is highly effective and economical (Choi et al., 2006; Rao et al., 2007; Ye and Yu, 2010). Several adsorbents have been studied for adsorption of metal ions such as activated carbon (AC) (Kim and Anderson, 1994), fly ash (Weng and Huang, 2004), peat (Ho and McKay, 1999a) sewage sludge ash (Pan et al., 2003), zeolite (Biškup and Subotić, 2005), and biomaterials (Li et al., 2004). However, these adsorbents suffer from low adsorption capacities or removal efficiencies of metal ions. Until now, the process of removing these metal ions has not reached the optimum condition which is still in lower efficiency of

removal. The high performance of CNTs in separation process technology is becoming a major concern of development. In the treatment process of adsorption, CNTs is used as a new absorbents to replace AC. In order to optimize the efficiency of the removal, the study of CNTs as new absorbent is being developed. It is a member of carbon family that has novel properties with the special characteristic of the shape and properties of CNT is used to optimize the process of absorption in the removal of heavy metal ions in wastewater treatment. Many researchers have studied the removal of heavy metals using CNTs for water treatment, which are still in experimental stages only, but it may consider them to be very much promising at least at the pilot plant level. It is convinced that waste water treatment in large scale to remove heavy metals and separation in conjunction with CNTs is expected to create a major breakthrough in the coming future.

1.2 Problem Statement and Significance of Study

Generally, there are few techniques employed to produce CNTs such as electric- arc discharge, laser ablation and Chemical Vapor Deposition (CVD). Among these, technique, CVD is very different from the other two common methods used for CNTs production, namely; arc discharge and laser ablation (Ebbesen and Ajayan, 1992; Journet et al., 1997; Thess, et al., 1996). At the moment, arc discharge methods generally produce larger quantities of impure material and produces a small amount of CNTs yield (Journet and Bernier, 1998). Whereas for laser ablation, the method was said to be uneconomical feasible due to high laser power required and involves high-purity graphite rods, as well as it produces small amounts of nanotubes (Guo et al., 1995). The material prepared by these techniques has to be purified using chemical and separation methods (Kokai et al., 2002). None of these techniques are scalable (Guo, 1995) to make the industrial quantities needed

for many applications (e.g., In composites), and this has been a bottleneck in nanotube research and development (R&D).

In recent years, work has focused on developing microwave assisted chemical vapor deposition (MA- CVD) (Bower, Zhou, et al., 2000; Dallinger and Kappe, 2007; Hong et al., 2003) which is one of the most popular method to produce CNTs using C_2H_2 and H_2 as precursors, while Argon (Ar) acts as parching gas. MA - CVD seems to be the most promising method for possible industrial scale-up due to the relatively low growth temperature, high yields and high purities that can be achieved (Fu et al., 2013; Liu and Ting, 2003; Méndez et al., 2003). It is of current general interest that the development of new techniques for the efficient and the selective synthesis of CNTs at the cheapest possible cost. One such possibility is the use of microwave radiation, which over the past few years has played an important role as a thermal tool in organic synthesis due to considerable advantages over conventional methods. MA- CVD is a very promising process with respect to large-scale production of different kinds of carbon nanostructures materials as for example for multi, and single-walled carbon nanotubes. The economic, social, environmental and public health implications of decreasing water quality are a worldwide threat. Water resources are being polluted from various sources. Different types of emerging pollutants have been increasing while the removal of traditional pollutants is not solved efficiently. Environmental issues and its consequences effect towards the living creatures and fauna on earth has been a serious problem for the past few decades. In regards to this issue, water pollution has been highlighted as one of the most crucial issues which needs an abrupt solution to avoid further impact on the environment. One of the main contributions to water pollution issue would be the emission of heavy metal ions from extensive industries. Many methods have already been discovered and established to adsorb

these heavy metals from the contaminated waste water streams. Adsorption is enclosed to be one of the highest efficient methods due to its simplicity and flexibility. However, due to the lack of significant adsorbent, this method is still unable to reach its peak demand and meets the environmental regulations regarding the emission heavy metal into the surround environment. Therefore, overcome this problem, to optimize the efficiency of the removal, the study of novel multiwall carbon nanotube (MWCNTs) as new absorbent is being developed. With the special characteristic of shape and properties, a MWCNTs is used to optimize the process of absorption in the removal of heavy metal ions. Hence, MWCNTs are the most promising candidate for removal of heavy metal from wastewater treatment and separation process.

1.3 Research Philosophy

In this research, single stage mass production of CNTs using microwave technology for various industrial applications. In our innovation microwave-assisted synthesis, including fast CNTs growth and ambient reaction condition, low growth temperature, high surface area, high adsorption capacity, less pollution and energy saving, and simplifies the procedure leading to a high yield synthesis of high-quality CNTs with minimal impurity. It is of current general interest the development of new techniques for the efficient and the selective synthesis of CNTs at the cheapest possible cost. CNTs are in the limelight globally as a new dream material in the 21st century and are broadening their niche applications to almost all the scientific areas, such as waste water treatment, materials industry. However, synthesis conditions have major influences on the nature of the CNTs product formed. Reaction conditions, including microwave power, gas ratio, and radiation time. The nature and composition of metallic catalysts leading to the CNTs formation

which in turn affects the properties of the final product have to be still explored to understand these influences. In addition, CNTs have great attention as a novel type of adsorbent due to their extraordinary properties such as chemical stability, mechanical and thermal stability, and the high surface area which leads to various applications including waste water treatment, hydrogen storage, and protein purification. Removal of heavy metal from industrial waste water leads to the biggest challenge nowadays. In order to reduce environmental problems, the CNTs are promising candidates for the adsorption of heavy metals

1.4 Research Objectives

This study embarks on the following objectives:

i. To produce high purity and high yield CNTs using microwave assisted chemical vapor deposition (MA-CVD).

ii. To investigate the effect of process parameters on CNTs such as microwave power, radiation time and gas ratio of C_2H_2/H_2.

iii. To optimize the process parameters on CNTs production by varying microwave power, radiation time and gas ratio C_2H_2/H_2 using central composite design (CCD) to produce high quality and high yield of CNTs.

iv. To optimize the process parameters such as agitation speed, pH, CNTs dosage and contact time by using CCD for the removal of heavy metals Pb (II), Cd (II), Cu (II) and Zn (II) from aqueous solution.

v. To study the adsorption isotherm and adsorption kinetics on the removal of heavy metals from aqueous solution.

1.5 Research Methodology

In this research, CNTs is produced using microwave assisted chemical vapor deposition (MA-CVD). In order to achieve high purity of CNTs, the process parameters were optimized, such as gas ratio (C_2H_2/H_2), radiation time, microwave power, using Design Expert® version 6.0.8. The characterization of produced CNTs in order to achieve high yield and high purity of CNTs were used for the removal of heavy metals. Application of CNTs on synthetic water polluted with toxic metals (Pb (II), Cd (II), Cu (II) and Zn (II)) to study the adsorption behavior. In addition, optimization of the adsorption conditions such as pH, CNTs dosage, contact time, and agitation speed using CCD Futhermore, thermodynamics and kinetic study of each heavy metal adsorption were conducted.

1.6 Outline of the Thesis

This thesis comprised of five chapters, as follows:

Chapter I include a brief background overview of CNTs synthesis using microwave assisted CNTs and application of CNTs in heavy metal removal. The problem statement and philosophy of the research work are mentioned, followed by the objectives of the research, and finally the research methodology.

Chapter II discusses the background of CNT structure and properties, a summary of production of CNTs using CVD and microwave assisted synthesis of CNTs. It also explains various parameters influences the production of CNTs and comparison between the technique was made. In addition, the nature of different heavy metal removal issuing modified and non modified CNTs for removal of heavy metals were explained in detail. Furthermore, previous removal studies on heavy metals using CNTs were discussed.

Finally the theoretical background of adsorption isotherm and kinetic models were elaborated.

Chapters III discusses the detailed research methodology of optimization of CNTs production using microwave heating, as well as the method of detail experimental procedure for production CNTs and follow up the characterization of CNTs analysis. Detail deigns experiment for production of CNTs as well as optimization of heavy metals removal are described in this chapter.

Chapter IV The results are mainly focused on the optimization of process parameters on CNTs synthesis and detail characterization of CNTs. The preparation conditions were statistically optimized using central composite design (CCD) to produce the high quality and high weight of CNTs. The optimized condition of MWCNTs sample has proven to be an outstanding adsorbent for the removal of heavy metals such as, Pb (II), Cd (II), Cu (II) and Zn (II) from aqueous solution. The studies on the isotherm kinetic and isotherm model were developed and investigated as well. In addition, the thermodynamic parameters were also investigated.

Chapter V The optimization the process parameters for CNTs synthesis using the single stage MA-CVD is investigated in this chapter. In order to produce high purity and high yield of CNTs microwave power and catalyst play a vital role in the synthesis and controlling diamter of CNTs. The optimized CNTs was tested for efficiency of removal of heavy metals such as Pb (II), Cd (II), Cu (II) and Zn (II) from aqueous solution. Our results proved novel CNTs is the best adsorbent for removal of heavy metals with high adsorption capacity compared to existing literature review. Furthermore, for future work different catalyst may be used for synthesis of CNTs via microwave heating and tested for other heavy metals such as As^{+6}, Ni, Hg etc.

CHAPTER II

LITERATURE REVIEW

2.1 History of carbon nanotube (CNTs)

The most popular is the identification of the structure of the fullerenes in 1985 by (Kroto et al., 1985). A further study in 1991 by (Iijima, 1991) discovered the multi-walled carbon nanotubes (MWCNTs) and single-walled carbon nanotubes (SWCNTs), whereas the SWCNTs were independently discovered by (Iijima and Ichihashi, 1993) and (Bethune, et al., 1993). Earlier to the discovery of nanotubes, the significance of the investigations made on carbon fibers with diameters bigger than 7 nm was not clear until the connection between fullerenes and nanotubes was revealed. One of the articles (Ball, 2001) reported a decade before the discovery of nanotubes, stated that nanotubes were unintentionally produced by chemists experimenting on methane in the late nineteenth century (Hughes and Chambers,1989). In 1960, nanoscale scrolls of graphite were produced by (Bacon, 1960). The truth is that Iijima, who has generated a mixture of scrolls and tubes by using his own procedure (Amelinckx et al., 1995; Mordkovich et al., 1998; Y. Maniwa, 2001), suggests that Bacon may have also done this. In the previous study, showed a hollow carbon fibre with nanometer-scale diameters using a vapor-growth technique (Oberlin et al., 1976). Wiles and Abrahamson also, found “mats of small fibres” in on one electrode when sparks were passed between two graphite electrodes. (Gibson, 1992) reported that, (Davis et al., 1953) were the first to see a nanotube, but some researchers like (Monthioux and Kuznetsov, 2006), agreed that the credit should be given to (Radushkevich and Lukyanovich, 1952) in 1952 for producing first nanometric-sized carbon filaments. The researchers (Baker et al., 1972) who investigated on the growth of vapor grown carbon

fibres may have also yieldedvaporubes because tfibershnique used nowadays to produce nanotube is similar. Recently, (José-Yacamán et al., 1993) using chemical vapor deposition (CVD) have made a large achievement in synthesis and the application of CNTa large achievement investigations in the synthesis and application of CNTs has been studied wisely (José-Yacamán, et al., 1993).

2.2 Structure of carbon nanotubes

With the revolutionary discovery of fullerenes and CNTs, different research fields in the domain of carbon experienced an enormous boom. Fullerenes are spherical molecules, the smallest of which composed of 60 carbon atoms that are arranged like the edges of the hexagons and pentagons on a football. Nanotubes can be described as a rolled-up tubular shell of graphene sheet see Fig. 2.1, which is made of benzene-type hexagonal rings of carbon atoms. The body of the tubular shell is thus mainly made of hexagonal rings (in a sheet) of carbon atoms, whereas the ends are capped by half-dome shaped half-fullerene molecules (Gogotsi, 2006). Due to their special one-dimensional form, they have interesting physical properties like they have metallic or semiconducting electrical conductivity depending on the chirality's of the carbon atoms in the tube. Nanotubes have a large geometric aspect ratio which promoted them to be use in different applications such as electrode material in super capacitors and hydrogen storage material for the fuel storage or as field emitters in flat panel displays (Srivastava et al., 2003).

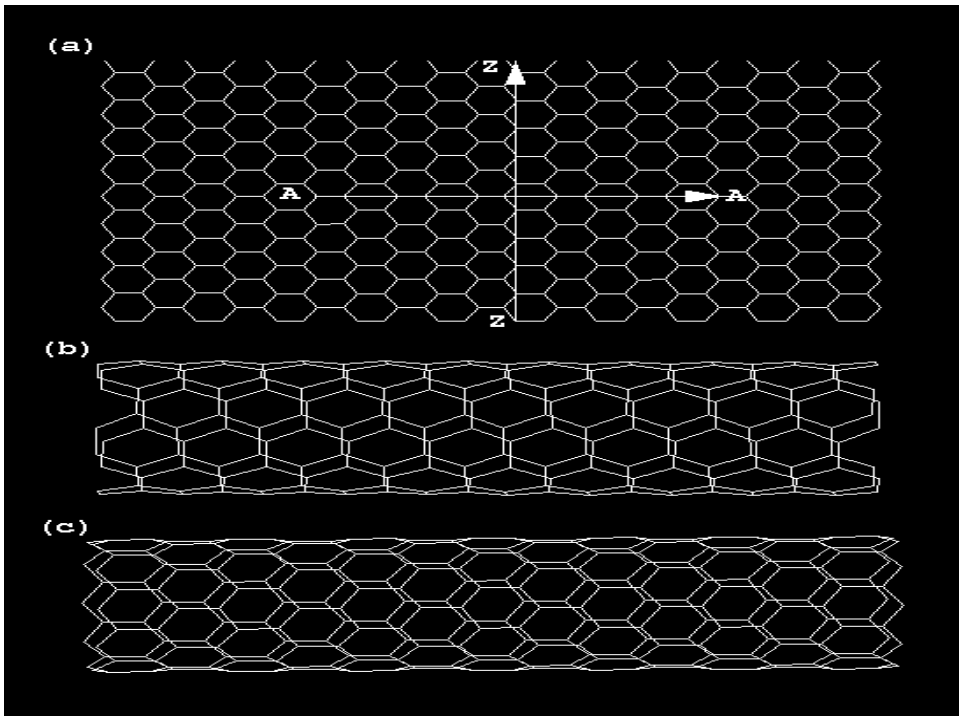

Figure 2.1: (a) A graphene sheet made of C atoms placed at the corners of hexagons forming the lattice with arrows AA and ZZ denoting the rolling direction of the sheet to make (b) a (5,5) armchair nanotube and (c) a (10,0) zigzag nanotube (Srivastava, et al., 2003).

CNTs may be classified into three different types: armchair, zigzag, and chiral nanotubes, depending on how the two-dimensional graphene sheet is "rolled up". Fig. 2.2 shows the three structural categories of SWCNTs. Fig. 2.2 (a) shows the zig-zag SWCNT which is named for the pattern of hexagons as one move circumferentially around the body of the tubule. Fig. 2.2 (b) shows the second form known as chiral SWCNT and is believed to be the most commonly occurring SWCNT. The name chiral means handedness and indicates that the tubes may twist in either direction. While, Fig. 2.2 (c) shows the third structures named armchair SWCNT, which describes one of the two conformers of cyclohexane, a

hexagon of carbon atoms, and describes the shape of the hexagons as one move around the body of the tubule (Baughman et al., 2002)

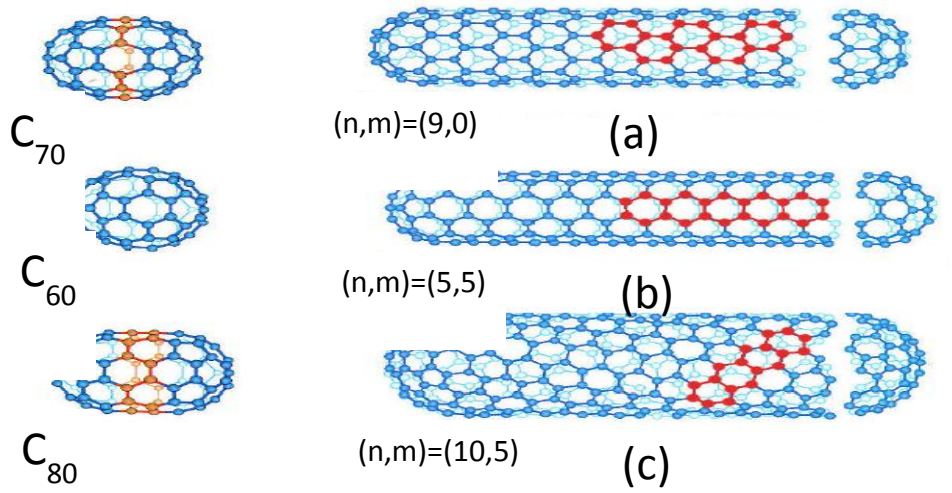

Figure 2.2: (a) Zig-Zag Single-Walled Nanotube. (zig-zag pattern around circumference and m = 0), (b) Chiral Single-Walled Nanotube (twisting of hexagons around tubule body. (c) Armchair Single-Walled Nanotube. Note the chair-like pattern around circumference and n = m (Gogotsi, 2006; Harris and Harris, 2001).

The geometry of the chiral SWCNT lies between that of the armchair and zigzag SWCNTs as shown in Fig. 2.3 (A-G) (Baughman, et al., 2002). A SWCNT can be described as a rolled up graphene sheet that is closed at each end with half of a fullerene. Fig. 2.3 (A) armchair, (B) zigzag, and (C) chiral SWCNTs. Projections normal to the tube axis and perspective views along the tube axis are on the top and bottom, respectively. (D) Tunneling electron microscope image showing the helical structure of a 1.3-nm-diameter chiral SWCNT for projection normal to the tube axis. (E) Transmission electron microscope (TEM) image of a MWCNT containing a concentrically nested array of nine

SWCNTs. (F) TEM micrograph showing the lateral packing of 1.4-nm-diameter SWCNTs in a bundle. (G) Scanning electron microscope (SEM) image of an array of MWCNTs grown as a nanotube forest. Fig. 2.4 shows the nanotube is usually characterized by its diameter d_t and the chiral angle θ ($0 \leq |\theta| \leq 30°$). The chiral vector C_h is defined with the two integers (n, m) and the basis vectors of the graphene sheet (Dresselhaus and Avouris, 2001; Harris and Harris, 2001; Saito et al., 1993) .

$$C_h = n*a_1 + m*a_2 \qquad (2.1)$$

The so-called chiral vector of the nanotube, C_h, where a_1 and a_2 are unit vectors in the two-dimensional hexagonal lattice, and n and m are integers. Another important parameter is the chiral angle, which is the angle between C_h and a (Kiang et al., 1998).

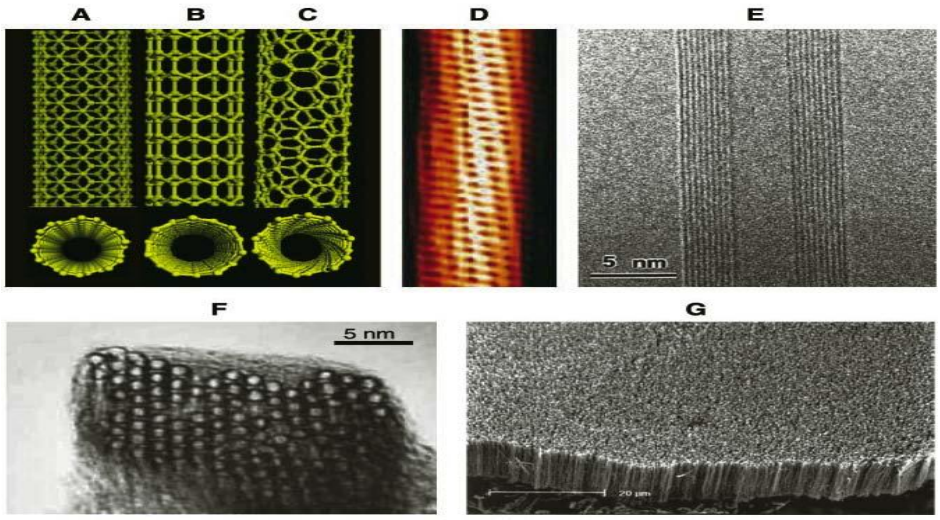

Figure 2.3: Schematic illustrations of the structures of CNTs (Baughman, et al., 2002).

In order to discriminate between different types of CNTs, the chiral angle and vector play an important role in determining the important properties of nanotubes. Armchair nanotubes are formed when n = m and the chiral angle is 30°. Zigzag nanotubes are formed when either n or m is zero and the chiral angle is 0°. All other nanotubes, with chiral angles intermediate between 0° and 30°, are known as chiral nanotubes. The properties of

nanotubes are also determined by their diameter, which depends on n and m. A nanotube is usually characterized by its diameter d_t and the chiral angle θ ($0 \leq |\theta| \leq 30°$). The integers (n, m) determine d_t and θ (Baughman, et al., 2002; Dresselhaus et al., 1995).

$$d_t = \frac{1}{\pi}\sqrt{n^2 + m^2 + nm}, \quad \sin\theta = \frac{\sqrt{3}m}{2\sqrt{n^2 + m^2 + nm}} \tag{2.2}$$

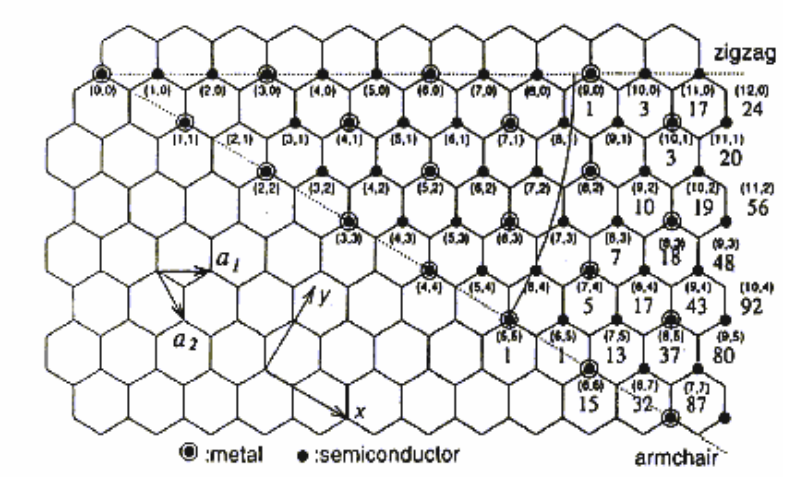

Figure 2.4:Diagram showing rolling direction of nanotube (Dresselhaus, et al., 1996).

Fig. 2.5 shows, there are two main types of CNTs with high structural perfection; they are SWCNTs, which consist of a single graphite sheet seamlessly wrapped into a cylindrical tube and MWCNTs, which comprise an array of concentric cylinders (Odom et al., 1998). The image of TEM with high resolution shows the spacing between of inter shell found to vary from 0.34, augmenting with the diameter of tube diminishing. The biggest spacing for the smallest diameter is allocated in the high curve, following in a distasteful force augmented, linked to the diameter diminished by the shells of CNTs (Gogotsi, 2006; Saito, et al., 1993). The value of 0.34 nm spacing in the bulk graphite crystal is approximately that of the CNTs. However, a closer study revealed that the mean value of the interlayer spacing

is 0.3444 ± 0.001 nm; the values in CNTs are larger, by a few percent, than those in the bulk graphite crystal (Ru, 2000). According to theoretical calculations the distance between two layers is d = 3.39 Å, slightly bigger than in graphite. Based on TEM images, the interlayer separation of d = 3.4 Å is commonly reported for MWCNT (Ebbesen, 1997a).

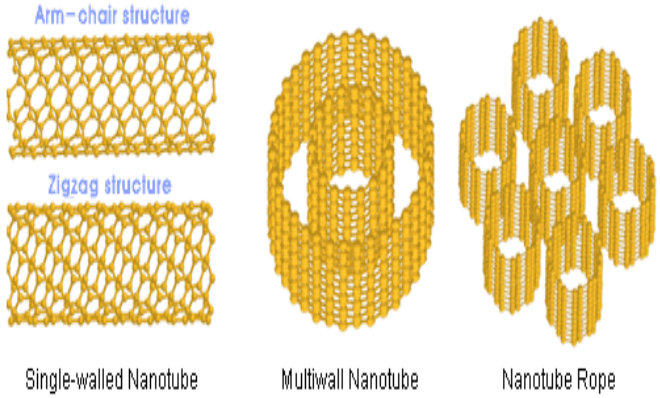

Figure 2.5: Different types of CNTs (Ebbesen et al., 1993; Saito, et al., 1993).

2.3 Properties of carbon nanotubes

A SWCNT has three different structures as described before, SWCNT can be either metallic or semiconducting, according to their chirality's vector (n, m). A metallic nanotube is found when the difference n-m is a multiple of three. If the difference is not a multiple of three, a semiconducting nanotube will be formed. Besides, it is also possible to connect nanotubes with different chiralities creating nanotube heterojunctions, which can shape a variety of nanoscale molecular electronic device components (Saito, 1998) single and multi-wall nanotubes have very good elasto-mechanical properties. These structural and material characteristics of nanotubes point towards their possible use in making the next generation of extremely lightweight with highly elastic and very strong composite

materials. CNTs have high aspect-ratio structures with good electrical and mechanical properties. Consequently, the applications of nanotubes in field-emission displays, and scanning probe microscope tips for metrology have started to materialize in the commercial sector.

2.3.1 Electronic Properties

Carbon nanotubes have some different electrical properties. One of the important properties of CNT is that it can exhibit the characteristics of a metal or a semiconductor depending on their chiral vector. Electronic structure, usually characterized using electron scanning microscopy (Satishkumar et al., 2000). One possible use of the CNTs is as a diode. One can view CNTs as giant conjugated molecular wires with a conjugation length corresponding to the whole length of the tube. Carbon has four valence electrons of which three are strongly bound to neighboring atoms, giving graphene its very high in-plane rigidity (Andriotis et al., 2000; Collins and Avouris, 2000; Schujman et al., 2002) considered CNTs with junctions to be of potential value in nanoelectronics; for such applications, it is important to be able to connect the CNTs of different chirality and diameters. Nanotube fabrication was via a pyrolysis method. The fourth electron is delocalized and shared by all the atoms, thus allowing for electronic current transport. However, because of its particular structure graphene is electronically between a semiconductor and a metal.

Depending on their chiral vector, CNTs with a small diameter are either semi-conducting or metallic. The differences in conducting properties are caused by the molecular structure that results in a different band structure and thus a different band gap. The differences in conductivity can easily be derived from the graphene sheet properties (Collins and Avouris,

2000). It was shown that a (n,m) nanotube is metallic as accounts that: n=m or (n-m) = 3i, where i is an integer and n and m are defining the nanotube. The resistance to conduction is determined by quantum mechanical aspects and was proved to be independent of the nanotube length by (Tans et al., 1997). The small size (diameter) of nanotubes in combination with their transport properties is vercombinationve in this context. CNT technology offers a new approach that may turn out to be more suitable for devices with nanometer-scale dimensions.

2.3.2 Mechanical Properties

The basal-plane elastic modulus of graphite is one of the largest of any known material. CNTs are the strongest fibers that are currently known. The reason for that, the carbon atoms form a planar honeycomb lattice in which each atom is connected via a strong chemical bond to three neighbor atoms. Therefore, these compounds are potentially suitable for applications in composite materials that need anisotropic properties. CNTs have a very large Young Modulus in their axial direction. The Young Modulus of SWCNT is up to 1TPa, which is more than 4 times greater than steel (230 GPa) while the density is only 1.3 g/cm^3 (Qian et al., 2002). From this study, estimated that the tensile stress at fracture in the CNT was ~ 55 GPa, based on polymer-NT specimens and if the stress is transferred to the CNTs via the interface shear mechanism (Schadler et al., 1998; Wagner et al., 1998) directly measured the tensile strength of MWCNTs made by CVD by pulling on very long (~2 mm) ropes with a tensile strength of 1.72 ± 0.64 GPa. The tubes had an inner diameter and outer diameter of 12 and 30 nm, respectively, and spacing of about 100 nm between the tubes. Account for this spacing, they use the effective cross sectional area. They treat the CNTs was parallel resistors of conductance 1/R by measuring this value; they estimate the

rate at which the tubes break. They measured the tensile strength of the ropes to be an order of magnitude lower than that of graphite whiskers.

Pan et al. (1999) were employed tensile strength of 20 mm long ropes consisting of soundly aligned SWCNT ropes, made by catalytic decomposition of hydrocarbons, in direct tensile strength measurements. The average tensile strength of SWCNT rope composites was high as 3.6 ± 0.4 GPa, that of carbon fibers. The tensile strength of SWCNT bundles was extrapolated to be 2.3±0.2 to 14.2±1.4 GPa by taking into account the volume fraction of SWCNT bundles in the mini-composite. Tensile strengths of single SWCNT estimated to be as high as 22.2±2.2 GPa. The ropes consist of roughly aligned bundles, which consist of well-aligned SWCNTs. Li et al (2005) was prepared bulk CNTs samples by spark plasma sintering. The prepared bulk CNTs material exhibited brittle fracture similar to that of common ceramics. Its fracture toughness was around 4.2 MPa $m^{1/2}$ while flexural strength was 50 MPa due to the weak bonding between CNTs. CNTs bridging was found during the development of the crack induced, which provides a possibility of CNTs tough material.

2.3.3 Thermal Conductivity Properties

Despite the significant amount of research on carbon nanotubes, the thermal conductivity of individual single-wall carbon nanotubes has not been well established. The thermal conductivity of carbon nanotubes is higher than most known material ranges (Hone, 2001). Thermal conductivity values of aligned ropes of SWNTs at room temperature have been measured to be greater than 200w/m.k, while mats of nanotubes possess a thermal conductivity of 35w/mK (Hone, 2001). This property of carbon nanotubes can be exploited for the development of thermal interface material. Molecular dynamics simulation results range from several hundred to 6600 W/m K and existing theoretical predictions range from

several dozens to 9500 W/m.k To clarify the several-order-of-magnitude discrepancy in the molecular dynamics simulation to systematically examine the thermal conductivity of several individuals (10, 10) single-wall carbon nanotubes as a function of length, temperature, boundary conditions and molecular dynamics simulation methodology by (Jennifer, 2007).

2.3.4 Field Emission

Carbon nanotube films are excellent field emitters, producing large emission currents at relatively low applied electric fields which were best known as field emitters of any material (Bonard et al., 1998). Recently, studies have shown that carbon nanotubes have promising electron field emission properties compared to the conventional field emitters, with low emission threshold fields (Saito et al., 1997). The smaller the tips radius of curvature, the more concentrated the electric field were leading to increased field emission. Besides that, CNTs also was utilized as a source for field emission due to its astonishing characteristics such as small diameter, high surface area and high aspect ratio. In this case, high aspect ratio means that only a little amount of CNTs will be needed to provide the same electrical conductivity as high dosage of other substances. Field emission or also known as field electron emission is a process which results from tunnelling electrons from the tip of a metal into a vacuum field, usually under the utilization of a strong electric field (Che et al., 1998). It was also discovered that the light is emitted in the visible part of the spectrum, which is lured by the electron field emission.

2.4 Production of carbon nanotubes

Generally, there are few techniques employed to produce CNTs such as electric- arc discharge, laser ablation and CVD. By using any of these techniques, different type of CNTs, can be produced such as vapor grown, carbon fiber and types of carbon nanostructure materials.

In the arc discharge, a vapor is created by an arc discharge between two carbon electrodes with or without catalyst. In the laser ablation technology, a high achievement laser beam, impose to a volume of the carbon, containing feedstock gas (methane or carbon monoxide). Laser ablation produces a very small amount of pure nanotubes, while an arc-discharge method produces in general large amounts of the impure material. Production of CNTs using CVD is the most promising method for possible industrial scale-up due to the relatively low growth temperature. In this process any hydrocarbon in the presence of a catalyst (Fe/Co/Ni) at high temperature (600 to 1000^{o}C) produce large amount and high purities of CNTs.

2.4.1 Electric - arc discharge

Electric - arc discharge is known to be the most common technique and also one of the oldest ways in the CNTs production. This method is known to be a traditional and simple device to produce high temperature needed to evaporate carbon atoms in plasma. (Iijima, 1991) was the one who first observed the CNTs structure using this method. Electric arc vaporizes a hollow graphite anode packed with a mixture of transition metals (such as Fe, Co or Ni) and graphite powder. The inert gas flow is maintained at 50-600 Torr. Nominal conditions involve 2,000 to 3,000 ^{o}C, 100 amps and 20 V (Ebbesen and Ajayan, 1992; Iijima, 1991; Journet and Bernier, 1998; Jung et al., 2003; Kiang et al., 1995). The variation

of process parameters such as flow rate, gas pressure, and metal concentration is needed to obtain the highest yield of CNTs which occurred in 'pillar-like tubes' either in single-walled tubes or multi- walled tubes. The structures of the nanotubes produced are usually short tubes. SWCNTs with diameters ranging from 0.6 to 1.4 nm and 10 nm diameter MWCNTs, this method is relatively easy to be implemented and 30% yield will be obtained. The content of impurities in CNTs produced is higher compared to other methods, and the consistency of the shape, wall, and lengths of the tubes are somewhat random (Journet and Bernier, 1998).

Two carbon electrodes are used in the carbon arc discharge technique to produce an arc by digital current (DC). Fig. 2.6 shows schematic of arc-discharge to produce CNTs. Initially, the two electrodes are kept independent. The electrodes are kept in a vacuum chamber and an inert gas is supplied to the chamber. The inert gas increases the speed of carbon deposition. Once the pressure is stabilized, the power supply is turned on (about 20 V). The positive electrode is then gradually brought closer to the negative one to strike the electric arc. The electrodes become red hot and a plasma form. Once the arc stabilizes, the rods are kept about a millimeter apart while the CNT deposits on the negative electrode. Once the specific length is reached, the power supply is cut off and the machine is left for cooling. Precaution needed for the important parameters are; 1) the control of arcing current and 2) the optimal selection of inert gas pressure in the chamber (Ebbesen, 1997a; Sinha and Yeow, 2005).

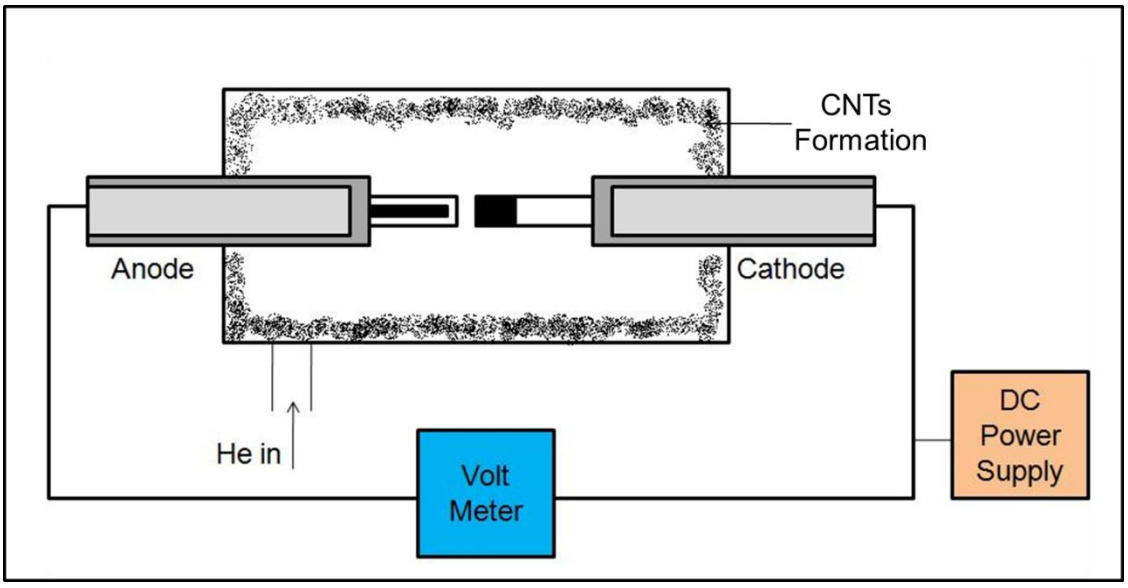

Figure 2.6: Schematic of arc-discharge to produce CNTs adopted from (Ebbesen, 1997a).

The CNTs are usually produced by striking an arc between graphite electrodes a atmosphere (He or Ar), this method also produces carbon soot materials which contain fullerence molecules (Iijima, 1991). The carbon arc provides a suitable instrument to create high temperatures required to vaporize carbon atoms into a plasma (>3,000 ^{o}C) (Ebbesen, et al., 1993; Seraphin et al., 1993). Normally the yield and purity of CNTs are based on the sensitivity of gas pressure vessel occurred between the electrodes, current density, inert gas pressure and stability. A very high ionization potential (Ebbesen, 1997a) makes gasses such as He atmosphere gives good results, perhaps due to its very high ionization potential (Ebbesen, 1997a) However, some works (Gamaly and Ebbesen, 1995) also reported the use of methane or hydrogen atmosphere. The well-cooled electrodes and arc chamber will be useful in maximizing the yield of CNTs.

For the MWCNT production, the conditions are optimized during arc discharge utilizing the DC current between two graphite; usually for water-cooled electrodes with diameters between 6 and 12 mm in a chamber filled with He sub atmospheric pressure, the soot

produced is minimized and 75% of evaporated carbon is made to deposit onto the opposite graphite cathode surface from graphite anode. The deposited pyrolytic was removed from the cathode that consists of 3 to 4 layers having 0.3 to 0.4 cm thickness that needs to be grind for the carbon deposit on morphology and yield of product. The grinding of the sample was carried out in three ways, the mortar and pestle, ball milling with alumina balls and tungsten carbide grid. Depending upon the nature of grinding the sample, the morphology of the sample is quite different from each. The optimal conditions were at 20 to 25 V, 50 to 100 amps. The DC, current density 90 A/Cm^2 and the He pressure maintained at 500 Torr. This method is a variant and easy process to produce high quality of CNTs having 15 to 60 nm in diameter. However, this technique is not a regular and unstable method and the yield of CNTs is very less. From these methods, the amount of CNT on the cathode surface and electrode gap is not constant, as the results, the current flow is not uniform throughout and electric field is non-homogenous. The temperature distribution and density of carbon vapor is not uniform and the impurities present on the surface of CNT collected are not constant, the consequent current flow is not uniform throughout and electric field is non-homogenous. Hence, the temperature distribution and density of carbon vapor are not uniform and impurities were present on the surface of CNTs. To solve these problems that occur during the synthesis of CNTs, many researchers (Byszewski et al., 1997; Gamaly and Ebbesen, 1995) have conducted the studies to understand the mechanism of nanotube to produce a large scale synthesis of MWCNTs using these techniques (Ebbesen and Ajayan, 1992).

Lee and Kim et al., (2002) used the plasma rotating arc discharge to produce large amount of CNTs where high velocity has been adopted to rotate the graphite anode for the synthesis of CNTs. The stable plasma was generated by the rotation of the anode with the distribution

of the microdischarges homogeneously. The acceleration of the carbon vapor perpendicular to the anode is generated by the rotation of the centrifugal force. It does not condense on the cathode surface, but collected on the graphite collector that was placed at the periphery of the plasma. The nanotube yield increases as the rotation speed of the anode increases and the collector becomes closer to the plasma. The optimal condition includes the high density of carbon vapor created by the uniform and high temperature plasma for nucleation and sufficient temperature of collectors for the nanotube growth. The plasma rotating electrode process is a continuous process of the stable discharge and it is expected to perform the mass production of high quality nanotubes.

The CNTs have been produced by using plasma arc jets in large quantities by optimizing the quenching process in an arc between the graphite anode and cooled copper electrode (Colbert et al., 1994; Hatta and Murata, 1994; Ishigami et al., 2000) reported for the continuous synthesis of CNTs using a simplified arc discharge. This method requires only a DC power supply, graphite electrodes and a container of liquid nitrogen continuous synthesis need for pumps, seals, water-cooled vacuum chambers, etc. The advantage of these techniques is simplified as no purging is required and the liquid nitrogen provides a protective oxygen-free environment as well as being the source of buffer gas during the arcing process, which are necessary for the production of CNTs by the conventional arc discharge. They reported that the reaction can run in a continuous fashion and can be scaled for industrial applications with a CNT yield comparable to that of an optimized conventional arc reaction. In general, high quality of MWCNT is produced at a high production rate as these nanotubes have four to eight layers and have long and straight parallel walls with only occasional surface contamination. In fact, the tubes grown using the liquid-nitrogen method appear to have consistently cleaner surfaces than tubes grown

using other methods. The tubes are composed only of carbon and show no evidence of nitrogen incorporation. This carbon arc nanotube synthesis method eliminates nearly all the complex and expensive equipments associated with conventional nanotube growth techniques. The most important feature of this new synthesis method is that there appear no obvious cost or technology obstacles to scale the method for high-quantity production.

Shi et al., (1996) produce a high yield synthesis and growth mechanism of carbon nanotube using arc discharge. The optimal condition of nanotube growth; 100 A DC, and 500 Torr He, the deposit with high yield nanotube bundles is synthesized. From the appearance of the deposit and the directions of nanotube bundles and nanotubes, it is proven that they are not parallel to the hat of electric field so that it can be further justified that the growth of nanotubes does not mainly depend on the electric field but the temperature gradient. It is also proven that the existence of nanosize particles in the carbon vapor is a necessity of the nucleation of the nanotubes. The intense heat of the plasma, the arc, the yttrium carbide or other clusters reach the cathode together with carbon vapor and condense on the cathode to form nuclei the diameters of the nanotubes depend on that of nuclei. The high yield is due to the large amount of nuclei which spurt from the anode together with carbon vapor for nanotubes to grow. The formation of single-layered (SL) CNTs has been studied using different elements and compounds. (Ata et al., 1994; Kiang, Goddard Iii, et al., 1996; Kiang et al., 1994; Kiang, Dresselhaus, et al., 1996; Lambert et al., 1995; Lin et al., 1994; Saito, Kawabata, et al., 1995; Saito et al., 1996; Saito, Okuda, et al., 1995; Seraphin et al., 1994; Zhou et al., 1994) reported that to produce SL, the CNTs are synthesized by catalytic assistance of rare-earths in a carbon arc. The tube length ranged from 10 to 100 nm depending on the catalytic activity of the elements, while diameters were 1.8-2.1 nm

regardless of the elements. The Y, La, and Ce, which are the three rare-earth elements with the lowest vapor pressures, denoted the highest activity among the elements investigated. The vapor pressure is a crucial factor for the formation of SL tubes by using arc-evaporation of carbon and metal catalysts.

Seraphin and Zhou, (1994) reported that SWCNTs are produced in high yield by mixed catalysts. The high-density preparation of single-wall tubes in the presence of mixed catalysts of the types Fe/Ni and Co/Ni, in the soot as well as in the weblike deposits forming in the chamber (Satio, 1994). Diameters cover the range from 0.9 to 3.1 nm. Park et al (2002) reported that High yield of SWCNT has been synthesized by DC arc discharge under low pressure of He gas with a small amount of a mixture of nickel and iron powders. The highest yield of CNTs was obtained at a low pressure of 100 Torr with 5 wt % of metal mixture. In addition, to produce high yield with low gas pressure they used sulphur as a promoter to improve the yield and quality of SWCNTs. The SWCNTs were also prepared by using various oxides (Y_2O_3, La_2O_3, CeO_2) as catalysts (Saito, et al., 1995). For the Ni-Y-graphite mixtures, (Journet, et al., 1997) studied the Large-scale production of SWCNTs by the electric-arc technique and found that high yields (70-90%) of SWCNTs having diameter range 1.4 nm can be produced. This Ni-Y mixture is now used worldwide for production of SWCNTs in high yield. Shi et al., (2000) reported large-scale production of SWCNTs under the arc conditions of 40~50 A DC and He pressure of 500 or 700 Torr by using a graphite rod with a hole filled with the powder of a mixture of Y-Ni alloy and graphite or CaC_2-Ni and Ni as anode.

Liu et al., (2000) studied the synthesis of macroscopically long ropes of well-aligned SWCNTs by hydrogen and Ar. The electric arc was operated at 150 A DC under an atmosphere of 150 Torr H_2 and 50 Torr Ar. They obtained ~2g/h SWCNT bundles, the

production of SWCNTs in the ropes about 30%, and the diameter of SWCNTs is about 1.72 nm. Ando et al., (2000) a reported mass production of SWCNTs by the arc plasma jet method. The production rate of the cotton like soot was significantly higher than that by conventional DC are discharged evaporation, and the highest yield was 1.24 g/min and with purity 50%. The diameter of each SWCNT was determined to range from 1.28 to 1.52 nm. Takizawa et al., (1999) reported on the effects of environmental temperature for synthesizing SWCNTs by arc vaporization. The production rate of SWCNTs by burning of a Ni-Y catalyzed carbon pellet is investigated by varying the environment temperature (Tenv). The yield of SWCNTs indicates a maximum in the Tenv range between 400 and 600 ^{o}C. At 600 ^{o}C, the yield reaches > 70 wt%, while the yield is similar to 30 to 40 wt% for the sample prepared at room temperature. It was also reported that the Tenv plays an important role in the high yield synthesis of SWCNTs as well as to select the metal catalysts.

Recently, (Ando and Zhao, 2006) reported about the synthesis of MWCNT and SWCNT using DC arc discharge. Ambient gas played an important role, and pure hydrogen gas was the best gas for obtaining high crystallinity of MWCNTs which obtained less than 0.4 nm diameters. SWCNT synthesis by an arc discharge, the incorporation of catalytic metal particles in a graphite anode is necessary, and SWCNTs are obtained as soot in an evaporation chamber. By an arc-plasma-jet method wherein two electrodes are placed at a sharp angle, the yield of soot, including SWCNTs is increased by decreasing the amount of cathode deposit.

2.4.2 Laser ablation

The pulsed laser vaporization (PLV), or laser ablation, is a newer method currently being developed to create nanotubes. Similar to the arc-discharge, this method vaporizes the carbon and later deposits it onto a substrate. In 1995, the Smalley's group at Rice University reported that the synthesis of CNTs by laser vaporization becomes an efficient route for the synthesis of bundles of SWCNTs with a narrow distribution. In this method, a piece of graphite target is vaporized by laser irradiation under high temperature in an inert atmosphere. The MWCNTs were found when a pure graphite target was used (Guo, et al., 1995). The quality and yield of these products have been found to depend on the reaction temperature. The best quality is obtained at 1200 ^{o}C reaction temperature. At lower temperatures, the structure quality decreases and the CNTs start presenting many defects. As soon as small quantities (few percents or less) of transition metals (Ni, Co) playing the role of catalysts are incorporated into the graphite pellet, products yielded undergo significant modifications and SWCNTs are formed instead of MWCNTs. The yield of SWCNTs strongly depends on the type of metal catalyst used and it is seen to increase with furnace temperature, among other factors. A high yield with about 50% conversions of transition-metal/graphite composite rods to SWCNTs was reported in the condensing vapor in a heated flow tube (operating at 1200 ^{o}C) (Guo, et al., 1995).

Fig. 2.7 shows the setup of the laser furnace, which consists of a furnace, a quartz tube with a window, a target carbon composite doped with catalytic metals, a water-cooled trap, and flow systems for the buffer gas to maintain constant pressures and flow rates (Ando et al., 2004; Guo, et al., 1995) . A laser beam (typically a YAG or CO_2 laser) is introduced through the window and focused onto the target located in the center of the furnace. The target is vaporized in high-temperature Ar buffer gas and forms SWCNTs. The Ar flow rate

and pressure are typically 1 cm.s^{-1} and 500 Torr, respectively. The SWCNTs produced are conveyed by the buffer gas to the trap, where they are collected. The vaporization surface is kept as fresh as possible by changing the focus point or moving the target (Thess, et al., 1996).

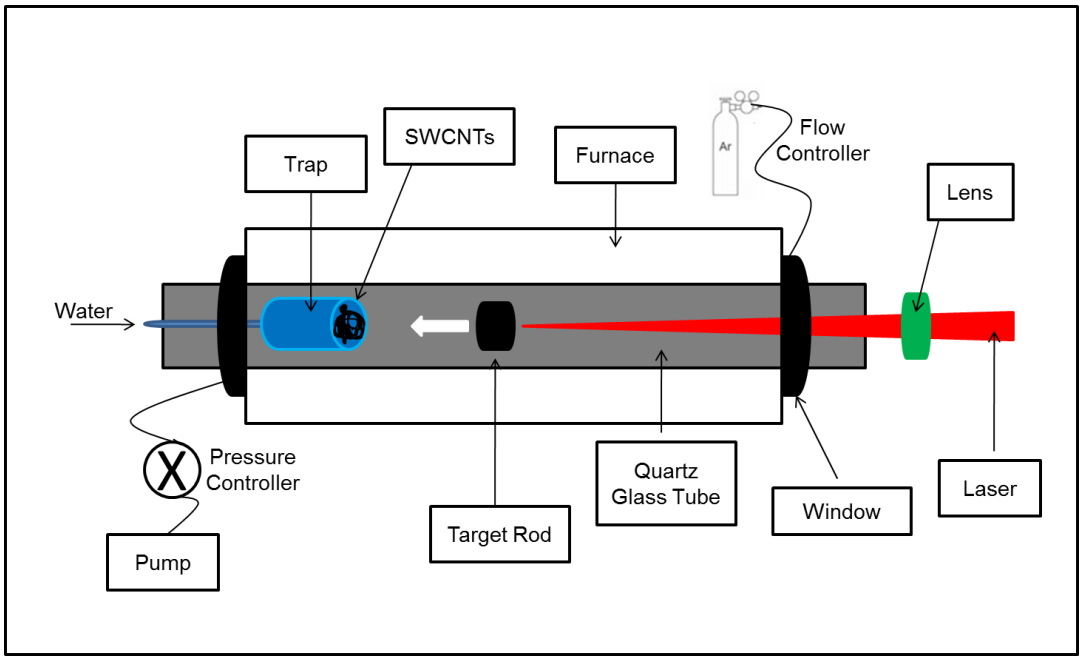

Figure 2.7: Diagram of laser furnace apparatus to produce CNTs adopted from Ando et al. [82].

Thess et al., (1996) reported crystalline ropes of metallic CNTs using the laser ablation. In this method, by producing CNTs, intense laser pulses were utilized to ablate the carbon target. The pulsed laser-ablation of graphite in the presence of an inert gas and catalyst formed SWCNTs at 1200 ^{o}C and yield of SWCNT of more than 70% with a mixture of carbon – nickel -cobalt mixture. Maser et al., (1998) studied the Production of high-density SWCNT material by a simple laser-ablation. This method, continuous-operating CO-laser in combination with a vertical evaporation chamber has been successfully employed to

produce high-quality SWCNT material. This system allows effective laser-target–gas-plasma interactions, and therefore shows that the local condition near the evaporation zone plays an important role in the formation of SWCNTs (the diameter of SWCNT is 1.1 to 1.6 nm). Similarly, (Muñoz et al., 2000), reported that the production of SWCNTs under Ar, nitrogen and He atmospheres in the pressure range of 50 to 500 Torr uses a continuous wave 10.6-mm CO_2 laser. Both Ar and nitrogen can be equally used as a buffer gas to synthesize SWCNTs in high yield between 200 and 400 Torr. Below 200 Torr, the amount of SWCNTs in the soot is drastically decreased and the materials are dominated by amorphous carbon. Negligible amounts of SWCNTs were formed using He as ambient gas.

Dillon et al., (2001) denoted that the synthesis of SWCNTs was investigated at room temperature with a porous target, and at the 1200 ^{o}C with a dense target. The tube diameters were shifted to smaller sizes with increasing pulse power in both cases. Kokai et l., (2002) noticed that the synthesized SWCNT are 1.2–1.4nm in diameter, and aggregates of single-wall carbon nanohorns (SWCNHs) by CO_2 laser vaporization in Ar gas under pressures of 150 to 60 Torr. At 150 Torr, SWCNTs with smaller diameters were synthesized together with amorphous carbon. With an increase in the gas pressure, the yield of SWCNTs decreased, the tube diameters increased, and SWCNH aggregates were synthesized. At 60 Torr, most of the products were SWCNH aggregates. Similarly, (Yudasaka, Kokai, et al., 1999) mentioned that the formation of SWCNTs from a target is composed of graphite, Ni, and Co, compared the use of a pulsed CO_2 laser with the use of a pulsed Nd: YAG laser. They noticed that the laser experiments revealed the porous targets of graphite-Co-Ni (nitrate) yielded twice as much SWCNT material from the standard metal carbon target. Eklund et al., (2002) reported that the first use of ultrafast laser pulses for large-scale production of SWCNTs is by the PLV technique. Very high production rates were achieved

using only 20% of the nominal average power of the 1KW where carbons soots rich in high quality bundles of SWCNTs were produced at ≈1. 5 g/h. Similarly, (Jiang et al., 2004) CNTs were synthesized in an atmospheric chamber by irradiating a metal-catalyst containing graphite target with a 2 KW continuous wave CO_2 laser and capturing the soot in flowing distilled water to facilitate continuous, rapid production. The ablation products, swept away by an Ar flow and collected in the distilled water, were further purified to result in a yield of 50%. The growth rate of purified aggregate ranged from 0.5 to 2 g/h depending on the laser power. The average diameter and length of nanotubes were 1.3 nm and 1.5 μm, respectively. The major benefits of this technique are the absence of vacuum and high-temperature furnace associated with the traditional pulsed laser, and scalability to meet the industrial production levels. Many researchers have been synthesizing SWCNT with high yield at the 1200 ^{o}C in the presence of CO/Ni, graphite/bi- metal targets (Bandow et al., 1998; Bower et al., 1998; Rinzler et al., 1998; Yudasaka, Ichihashi, et al., 1999; Yudasaka et al., 1997; Yudasaka, Sensui, et al., 1999)] or Rh/Pd (Kataura et al., 1998). In the early stages of MWCNT with pure graphite target (Guo, 1995; Journet and Bernier, 1998).

Both arc discharge and laser ablation produce some of the most high quality nanotubes, but suffer from the following disadvantages which limit their use as large scale industrial processes:

(1) They are both energy extensive methods where a large amount of energy is required to produce an arc or laser used for the ablation processes. Such a huge amount of energy is not only impossible but also uneconomical for large scale production.

(2) Both methods require solid carbon/graphite as target which has to be evaporated to produce nanotubes. It is difficult to get such large graphite to be used as target in industrial process which limits its exploitation as large scale process.

(3) Both processes grow nanotubes in highly tangled form, mixed with unwanted forms of carbon or catalysts. Thus, the CNTs produced by these processes require purification to obtain purified and assembled forms. The designing of such refining processes is difficult and expensive.

(4) The growth temperature of both methods is higher than other CNT production. As a result, the crystalline and perfection of arc-produced CNTs are generally high, and the yield per unit time is also higher than other methods.

(5) The by-products in the case of the arc-discharge and laser-ablation techniques are fullerenes, graphitic polyhedrons with enclosed metal particles, and amorphous carbon.

2.4.3 Chemical vapor deposition (CVD)

The CVD is essentially a thermal dehydrogenation reaction whereby a transition metal catalyst e.g, iron, nickel, or cobalt is used to lower the temperature required in order to 'crack' a gaseous hydrocarbon feed into carbon and hydrogen. The CVD is a versatile process suitable for the manufacturing of coatings, powders, fibers, and monolithic components. With the CVD, it is possible to produce most metals, many nonmetallic elements such as carbon and silicon as well as a large number of compounds, including carbides, nitrides, oxides, intermetallics, and many others. This technology is now an essential factor in the manufacturing of semiconductors and other electronic components in

the coating of tools, bearings, and other wear-resistant parts and in many optical, optoelectronic and corrosion applications.

The CVD may be defined as the deposition of a solid on a heated surface from a chemical reaction in the vapor phase. Hugh et al., (1999) reported that it is a class of vapor-transfer process, which is atomistic in nature that is the deposition species are atoms or molecules or a combination of these.

The CNTs samples were produced in the reactor as shown in Fig. 2.8; it comprises a quartz tube of 50 mm OD, 40 mm ID and 1500 mm length extended through two furnaces. The catalyst ferrocene was placed in a ceramic boat located inside the ceramic tube at the centre of the first furnace. The growth of CNTs took place at the second furnace and collected in ceramic boats which were placed at the center of the second furnace. The system was initially flushed with Ar in order to ensure an oxygen free environment. In the meantime, the second furnace was heated to the desired reaction temperature. Heating was continued until a steady state condition is achieved. The flow of Ar was then stopped and the first furnace was switched on till the temperature reached 150 ^{o}C. The gas flow for C_2H_2 along with H_2 was immediately released. The reaction was carried out for the desired reaction time when the reaction is completed. The CNT produced in the ceramic boats as well as on the inner walls of the second furnace was collected and weighed separately (Mubarak et al., 2011).

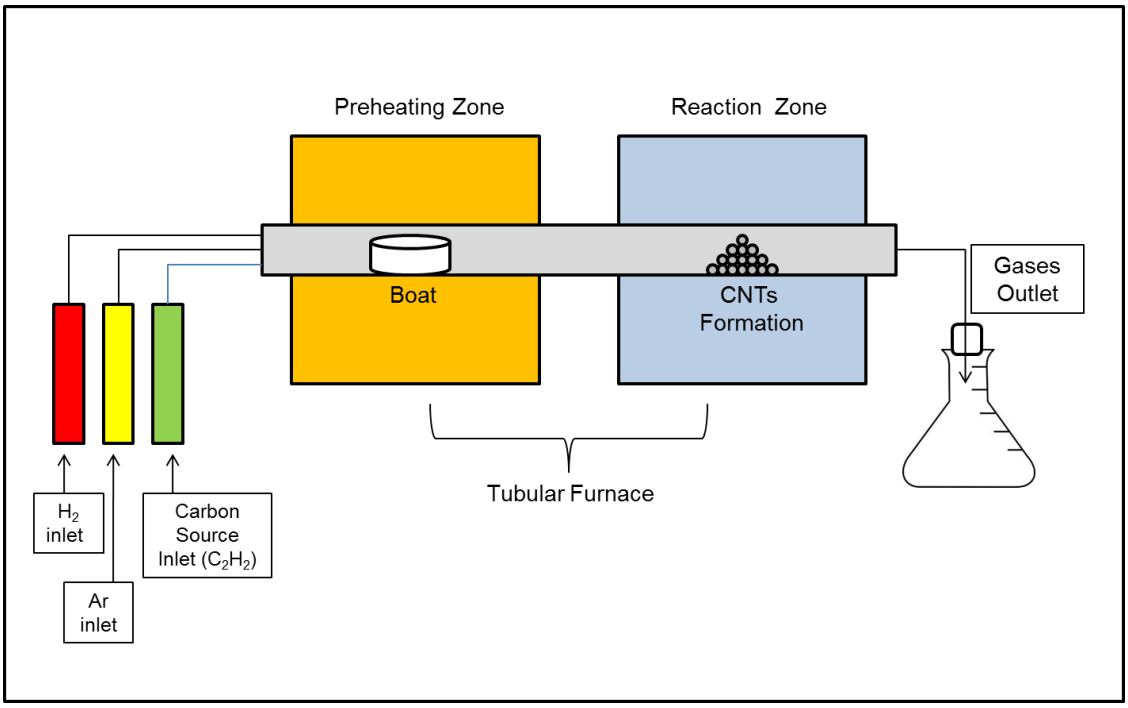

Figure 2.8: Diagram of CVD to produce CNTs adopted from (Mubarak, et al., 2011).

2.4.3.1 Advantages of CVD

Recently, the CVD used in the synthesis of CNTs has attracted much attention because it has many advantages compared to arc discharge and laser ablation. The CVD has several important advantages, which make it the preferred process in many cases. These can be summarized as follows (Hugh, 1999). The CVD is a relatively uncomplicated and flexible technology, which can accommodate many variations, and the reaction process and reactor design is simple as the reaction is easy to control and manipulate. Easily available raw material abundance in the form of gases. With the CVD, it is possible to coat almost any shape of almost any size. Unlike other thin film, techniques such as sputtering CVD can also be used to produce, vertically aligned nanotubes, fibers, monoliths, foams and powders.

The CVD is economically competitive.

The CVD of CNT involves flowing carbon precursor gases such as benzene, methane, acetylene, carbon monoxide or ethanol into a chamber containing one or more heated objects to be coated. The chemical reactions occur on or near the hot surfaces resulting in the deposition of thin film on the surface. The CVD synthesis is achieved by taking carbon species in the gas phase and using an energy source, such as the resistively heated furnace, in this case, to impart energy to gaseous carbon molecules. The process usually involves high temperature decomposition of hydrocarbons in hydrogen over the catalyst, which is pre-deposited on the solid substrate. A typical reactor and thermal decomposition of acetylene precursor in a hydrogen atmosphere are employed in the CVD process. The decomposition reaction generates carbon atoms, which reach the surface of the substrate and diffuse into tiny islands of melted catalyst which dissolve the carbon atoms forming a metal-carbon solution. When this high temperature solution becomes supersaturated, carbon precipitates, thus providing the "building bricks" for growth of the CNT structures. Transition metals such as Fe, Co, and Ni are frequently used as catalysts. The metal catalyst can stay on top of the CNT forming a cap encapsulating the CNTs (Kuang et al., 2000). In some cases, it remains at the bottom of the CNT, which promotes a bamboo-shaped morphology Lee and Park et al., (2000) reported that the described growth mechanism is very simplistic, and it postulates that carbon atoms from the gas phase are transported through the melted carbon-catalyst solution to the growth surface of the CNT. This process is based on the vapor liquid solid (VLS) mechanism. The different process variables playing key roles in the yield and quality of the synthesized nanotubes include the reaction temperature, reaction time, gas flow rates, kind of process steps performed during the run, quality and quantity of the Substrate/Catalyst particle and techniques employed to bond the

catalyst particle on the substrate sample. Manipulating any one of them can lead to a totally different breed of nanotubes, and may also affect the nanotube yield and the ability to purify the product of the synthesis. Table 1 illustrates the review of synthesis of CNTs using CVD.

The CVD deposits hydrocarbon molecules on top of the heated catalyst material. Metal catalysts dissociate with the hydrocarbon molecules. The CVD produces both SWCNTs and MWCNTs. The CVD process uses hydrocarbons as the carbon source. Hydrocarbons flow through the quartz tube or ceramic according to (Muataz, 2003), where it is heated at a high temperature (Sinnott et al., 1999). The energy source is used to "crack" the molecule into reactive atomic carbon. Then, the carbon diffuses towards the substrate, which is heated and coated with a catalyst (usually a first row transition metal such as Ni, Fe or Co) where it will bind. CNTs will be formed if the proper parameters are maintained. Excellent alignment, as well as the positional control on the nanometer scale, can be achieved by using the CVD (Muataz, 2003). Control over the diameter, as well as the growth rate of the nanotubes can also be maintained (Cao et al., 2007; Gulino et al., 2005; Kuo et al., 2006; Lee, Lyu, et al., 2002; Liu et al., 2003; Masao Yamaguchi, 2008; Nikolaev, 2004; Ren et al., 1999; Tatsuki et al., 2003; Yudasaka et al., 1995). Recently, the study shows the synthesis of CNTs using CVD with different hydrocarbon, carbon source, such as ethane (Tomie et al., 2010), ethylene (Narkiewicz et al., 2010), acetylene (He et al., 2011), methane (Palizdar et al., 2011), xylene (Atthipalli et al., 2011; Shirazi et al., 2011), eventually their mixture (Li, He, et al., 2010), ethanol (Hou, 2011; Santangelo et al., 2010) or isobutene (Yong et al., 2011). In the case of gaseous carbon source (Shukla et al., 2010), the CNTs was efficiently grown relying on the reactivity and concentration of gas phase intermediates produced together with reactive species and free radicals as a result of

hydrocarbon decomposition. Thus, to obtain the most efficient intermediates, which have the potential of chemisorption or physisorption on the catalyst surface to initiate CNT growth, the expectation has been made that production should be done in the gas phase.

2.4.3.2 Vapor Phase Growth

Vapor phase growth is one of the synthesis methods which have been used to produce carbon nanotubes (José-Yacamán, et al., 1993). The production of carbon nanotubes can be obtained directly by supplying reaction gas and catalytic metal in the chamber without a substrate, this method also called floating catalyst chemical vapor deposition (Muataz, 2003). The catalyst is introduced in the flowing gas stream, e.g. in form of volatile organometallic molecules like ferrocene and nickel. This method has been suggested as a good method for mass production of carbon nanostructure materials and fiber (Cheng et al., 2004; Muataz, 2003).

Fig. 2.9 shows a schematic diagram of a vapor phase growth apparatus. The flow controller for the gas flow rate is placed in one corner and a ceramic boat for catalytic metal powder in the chamber. Two furnaces are placed in the reaction chamber. In the first furnace, vaporization of catalytic carbon is maintained at a relatively low temperature while higher temperature is maintained in the second furnace where the synthesis occurs. The hydrocarbon gas in the first furnace will not decompose, while the low temperature in this furnace will be supplied to vaporize the catalysis. During the vaporization of the catalyst fine catalytic particles will form. When this particle reaches the second furnace, the decomposed carbons are absorbed and diffused on the surface of the catalytic metal particles (Lee, et al., 2002; Nikolaev et al., 1999; Ren, et al., 1999).

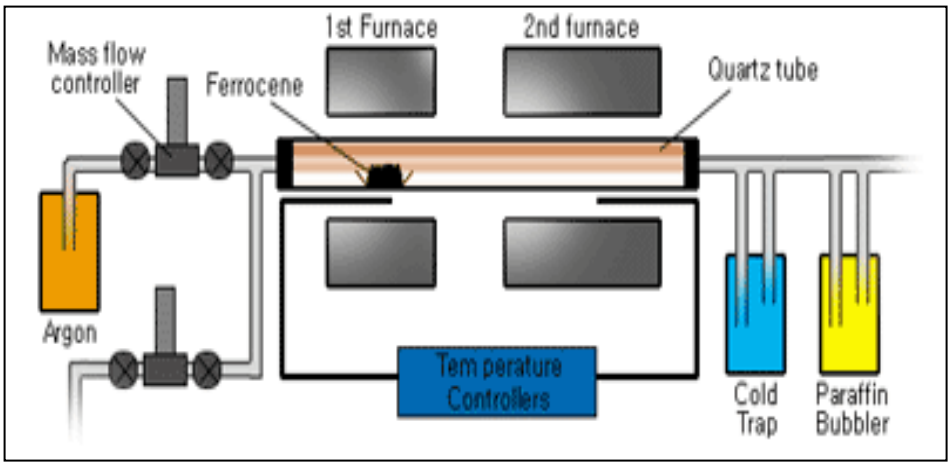

Figure 2.9: Schematic diagram of a vapor phase growth apparatus (Nikolaev, et al., 1999)

Liu et al., (2003) simultaneously has synthesized single-walled carbon nanotubes (SWCNTs) and double-walled carbon nanotubes (DWCNTs) by catalytic decomposition of CH_4 over Fe–Mo/Al_2O_3 catalyst. High-resolution transmission electron microscopy observation showed that carbon materials produced consist of about 70% SWCNTs and about 30% DWCNTs. The diameters of SWCNTs are in the range of 0.8–1.5 nm while the outer and inner diameters of DWCNTs are in the range of 1.75–3.1 and 0.95–2.3 nm, respectively. Raman analysis indicates that the synthesized SWNTs and DWCNTs have high-quality graphite structure. Tatsuki et al., (2003) were synthesized DWCNTs in high-yield (>80%) by catalytic chemical vapor deposition (CCVD) of acetylene over well dispersed metal particles (typically Co/Fe binary system) embedded in heat resistant zeolites at temperatures above 900 °C. The synthetic yield of DWCNTs has been sensitively affected by the reaction conditions of the CCVD such as zeolite support materials, the sintering of the metal particles, hydrocarbon sources and reaction temperatures. High-resolution transmission electron microscopy together with Raman spectroscopy shows that the outer tube diameter varies from 3 to 6 nm with inner–outer

tube separations of 0.36–0.37 nm, which is much larger than the interlayer distance of graphite (0.335 nm).

Teo et al., (2003), has been studied the formation mechanisms involved in the growth of carbon nanotubes by spray pyrolysis. Both iron and nickel were used as catalysts for growth, and nanotubes were produced using thermal chemical vapor deposition for comparison. Transmission electron microscopy was used to analyze the encapsulated metal catalyst particles found within the tubes, and the dimensions and location of these particles were recorded. CNTs grown by spray pyrolysis were found to have encapsulated particles in both the middle and end of the tubes, with large length to diameter ratios. As a result of these observations, it is concluded that nanotubes grown using spray pyrolysis are formed via an open-ended, root growth mechanism. Additionally, the presence of multiple, high aspect ratio particles within single tubes is explained by an additional growth theory. During the continued growth of these CNTs, metal atoms or nanoscale metal catalyst particles deposit in the open ends of growing tubes, forming new particles and helping to prevent tube closure. CNTs grown with thermal CVD did not contain similar elongated particles or particles along the middle of the tubes, indicating that this new growth mechanism is only applicable in the case of tubes grown via spray pyrolysis or other vapor phase CVD growth methods.

Qui et al., (2004a) have been successfully synthesized SWCNTs from coal gas with ferrocene as catalyst by catalytic chemical vapor deposition. The results lead to believe that coal gas is an ideal carbon-containing precursor for preparing SWCNTs. This new approach to SWCNTs should be of potential in the production of carbon nanotubes in large scale. Many works are needed to further establish the influence of process parameters on the formation, yield and quality of the SWCNTs, and to clarify the possible synergic effects

of gaseous species in the coal gas. Murakami et al., (2003) were synthesized high purity SWCNTs from ethanol by the catalytic CVD method. The yield of SWCNTs was characterized based on TGA complemented by Raman and TEM analyses. The effects of CVD reaction time and pre-reduction of catalytic metal in the yield and quality of synthesized SWNTs were investigated. The SWCNT yield of more than 40% was achieved over the weight of zeolite support powder with Fe/Co catalyst, which corresponded to more than 800% yield over the weight of the catalytic metal, within the CVD reaction time of 120 min assuring as-grown high quality.

Kobayashi et al., (2004) has been investigated SWCNT growth using a novel Fe_3O_4 nanoparticle catalyst synthesized with a simple organic chemistry process. They characterized the structure of the grown SWCNTs through scanning electron microscopy (SEM), atomic force microscopy (AFM) and microscopic Raman spectroscopy. Discrete nanoparticles with a uniform diameter of ~4 nm could be deposited on Si substrates with a thermal oxide layer by spin coating with a nanoparticle solution. Nanoparticles prepared under optimum conditions remained discrete and uniform without aggregation even after CVD process and their diameters were reduced to ~1.7 nm due to decomposition reactions during CVD. These nanoparticles were found to have remarkable catalytic activity in the CVD growth of the SWCNTs. SWCNTs with diameters of around 1 nm were produced from the reduced nanoparticle catalyst. The diameters of the grown SWCNTs were closely correlated with those of the catalytic nanoparticles and tended to be slightly smaller than the particle size.

Kuo et al., (2005) have been synthesized MWCNTs using a chemical vapor deposition floating feeding method in a vertical reactor. They were systematically examined Effects of the preparation variables on the average diameter of carbon nanotubes using the fractional

factorial design (FFD), the path of the steepest ascent, and central composite design (CCD) coupled with the response surface methodology. Factorial design study, the main and interactive effects of reaction temperature, methane flow rate, and chamber pressure were concluded to be the key factors influencing the diameter of MWCNTs. Two empirical models, representing the dependence of the diameter of carbon nanotubes at the vicinities around maximum (420 nm) and minimum (15 nm) on the reaction temperature and methane flow rate, were constructed in two independent CCD studies. These models, shown as contour diagrams, indicated that the diameter of carbon nanotubes generally increased with increasing reaction temperature and methane flow rate. Based on both models, the diameter of MWCNTs from 15 to 420 nm can be controlled precisely by using a continuous CVD fabrication method.

Flahaut et al., (2005) has been reported the influence of catalyst preparation conditions for the synthesis of carbon nanotubes by CCVD. Catalysts were prepared by the combustion route using either urea or citric acid as the fuel. They found that the milder combustion conditions obtained in the case of citric acid can either limit the formation of carbon nanofibers (defined as carbon structures not composed of perfectly co-axial walls or only partially tubular) or increase the selectivity of the CCVD synthesis towards CNTs with fewer walls, depending on the catalyst composition. It is thus for example possible in the same CCVD conditions to prepare (with a catalyst of identical chemical composition) either a sample containing more than 90% double- and triple-walled CNTs, or a sample containing almost 80% double-walled CNTs.

Gulino et al., (2005) has been successfully used ethane as an active and efficient carbon source in a large-scale synthesis of high quality carbon nanotubes by CVD over Fe/Al_2O_3 catalyst with an iron loading of 20 wt.% . The carbon nanotube yield of 20 g per gram of

catalyst per hour was obtained at a synthesis temperature of 660 °C. The active phase for growing carbon nanotubes is a mixture of metastable iron carbide (Fe_3C) and α-Fe, which were formed in situ by the ethane dissociation followed by carbon diffusion through the starting a-Fe phase similar to that reported in the literature. The reaction products only contained multi-walled carbon nanotubes with very homogeneous diameters between 20 and 40 nm and lengths up to several hundred nanometers without any trace of other impurities such as nanoparticles or amorphous soot. The high yield of the MWCNT significantly decreases the amount of the catalyst in the final product and the product can be used directly without the need for post-synthesis treatment in order to remove the catalyst. Ethane is an active carbon source for growing MWCNTs with high yield and selectivity. The CNTs formation at the reaction temperature 750 °C contains amorphous soot and carbon nanoparticles mixed with nanotubes.

Synthesis of MWCNTs through a catalytic chemical vapor deposition method using a floating reactant method and subsequent thermal treatment up to 2600 °C in a large quantity (Kim, Hayashi, et al., 2005b). Main characteristics of these nanotubes are (1) relatively wide distribution of diameters ranging from 20 to 70 nm and linear, long macro-morphology (aspect ratio >100), (2) highly straight and crystalline layers, (3) high purity through removal of metallic impurity, (4) very low interlayer spacing (0.3385 nm) and low R value (I_D/I_G = 0.0717), (5) high G' intensity over intensity of G band (G'/G = 0.85). The unusual microstructure of thin multi-walled carbon nanotubes with a partially facetted cross-sectional shape caused by thermal treatment is mainly ascribed to abrupt density changes (from 1.89 to 2.1 g/cm^3) within a confined nanosized space, accompanying with the phase separation.

Harris et al., (2005) has been synthesized preferential oriented multi-walled carbon nanotubes by injection CVD using either cyclopentadienyliron dicarbonyl dimer or cyclooctatetraene iron tricarbonyl as the iron catalyst source. The catalyst precursors were dissolved in toluene as the carrier solvent for the injections. The concentration of the catalyst was found to influence both the growth (i.e., MWCNT orientation) of the nanotubes, as well as the amount of iron in the deposited material. The multi-walled carbon nanotubes contained as little as 2.8 (wt %) of iron. The material was deposited onto tantalum foil and fused silica substrates. The CNTs were characterized by scanning electron microscopy, transmission electron microscopy, and Raman spectroscopy and thermogravimetric analysis. This synthetic route provides a simple and scalable method to deposit MWCNTs with a low defect density, low metal content and a preferred orientation.

Pinault et al., (2005) has been reported a study of the initial stages of growth of aligned MWCNT synthesized by CCVD of liquid aerosol obtained from toluene/ferrocene solution A special experimental procedure has been developed to stop the process after short durations (30 s to 2 min). Two different pyrolysis temperatures are considered: 800 and 850 ^{o}C. Both scanning and transmission electron microscopy (SEM, TEM) coupled with energy-dispersive X-ray (EDX) analyses are used in order to determine the location of catalyst particles and to examine their chemical nature, morphology and size distribution when nanotubes start to grow. During the early stages (30s), they observe the formation of a layer of catalyst particles on silicon substrates before the growth of nanotubes. X-ray diffraction (XRD) and X-ray photoelectron spectroscopy (XPS) measurements indicate the occurrence of iron oxide (C-Fe_2O_3 or Fe_3O_4). In addition, XPS analysis reveals the formation of graphite-like carbon, demonstrating that iron oxide particle catalyst the decomposition of toluene vapor. SEM and TEM observations show that these particles are

most often located at the nanotube root, suggesting a base growth mechanism responsible for the formation of aligned nanotube when prolonging growth time (2 min).

Reported a systematic study on the controlled growth of large areas of aligned multi-wall carbon nanotube arrays, from ferrocene–benzene precursor, and of nanotube junctions from ferrocene–thiophene precursor, without hydrogen addition, using an injection CVD method easy to scale up for industrial production (Tapasztó et al., 2005). A detailed study is presented of how the synthesis parameters such as growth temperature, active solution flow rate; catalyst concentration or sulfur addition can control the properties and morphology of the grown nanotube mat. Nanotube junctions with a considerable yield can be grown by adding sulfur to the synthesis process. The sulfur addition also results in growth of carbon nanocones (CNC) in the lower temperature regime of the furnace. Observation of single-wall carbon nanotubes using Scanning tuning microscopy (STM) investigations provides further indication that under properly chosen conditions SWCNTs can be grown with similar continuous processes.

2.4.3.3 CVD Method using Substrate Catalyst

In this method substrates like silicon (Si), Silicon dioxide (SiO_2), and aluminium are used to deposit different types of catalysts such as Fe, Ni, Co on the substrate. After the substrate was washed with distilled water and diluted HF solution, the substrate was placed in a ceramic boat. The ceramic boat is positioned in the center of the CVD furnace as shown in Fig. 2.10. Very thin film of catalyst will be deposited over the substrate catalyst when the catalyst is injected with hydrocarbon source into the chamber of the furnace tube. During the injection of the hydrocarbon with catalyst precursor, the organic catalyst will decompose into fine cluster catalysts and will deposit over the substrate.

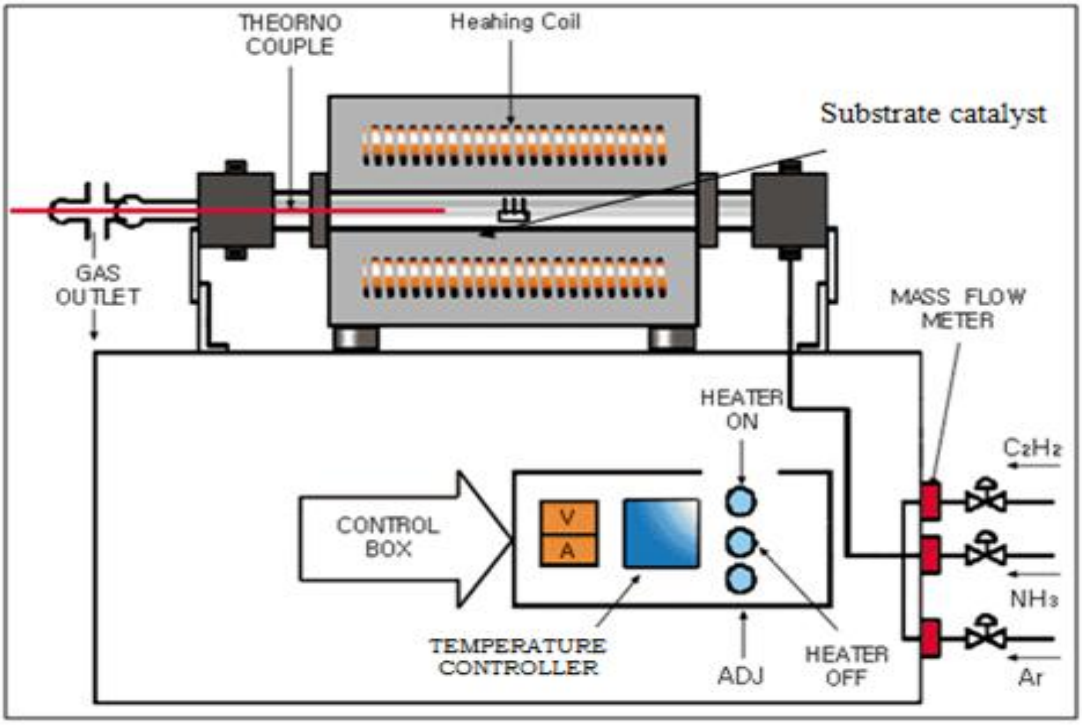

Figure 2.10: Schematic diagram of thermal CVD apparatus (Zheng et al., 2002).

Chen and Wu (2005) have been study the effect of thickness ratio of Ni:Cr on the density and alignment of CNTs synthesized by CVD (Changing the layer thickness ratio of Ni:Cr can change the density and alignment of CNTs dramatically. It is found the density and alignment can be controlled by adjusting the thickness ratio of Ni: Cr. Meanwhile, the catalyst encapsulated in the CNT was confirmed to be a Ni by EDX and HRTEM measurement. They conclude that only Ni has catalysis and Cr acts as dispersant in these experiments. Thus, their investigations are significant in providing a better understanding of the acting of catalyst and the controlling of the desirable density and alignment of CNTs for various applications. Xu et al., (2005) have been explained the importance of substrates in chemical vapor deposition by using two different substrates such as Kaolin plate and ceramic plate. Kaolin supported cobalt catalyst was used on these substrates, also without

substrate and the catalytic decomposition of C_2H_2 was carried out at the optimal temperature (750 °C) in nitrogen atmosphere. They produced two kinds of carbon nanostructures, carbon nanotubes and carbon spheres.

The peculiar ability of transition metals such as iron, cobalt and nickel to catalyze CNT formation is mostly linked to their catalytic activity for the decomposition of carbon compounds, their ability to form carbides and the possibility for carbon to diffuse through and over the metals extremely rapidly (Sinnott, et al., 1999). The metals used to catalyze CNT formation are most often transition metals, in particular iron, cobalt and nickel. Many of the papers available in the literature about the growth of CNTs on iron based catalysts report growth of MWCNTs (Fan, Wan, et al., 1999; Lee, et al., 2002) for production of CNTs Many groups also obtained SWNTs (Kim, Hayashi, et al., 2005a; Nikolaev, et al., 1999). Most of the reported results obtained with cobalt-based catalysts concern formation of MWCNTs (Ago et al., 2000; Pinheiro et al., 2003), a few others SWNTs (Colomer et al., 2000; Geng et al., 2002). Mixtures of transition metals are often observed to be more efficient for CNT production than one metal alone. Iron-nickel alloys are found to produce MWCNTs (Maroto Valiente et al., 2000), iron– cobalt alloys seem to produce rather SWNTs (Willems, Konya, et al., 2000) obtained SWNTs with a nickel–cobalt alloy (Dai et al., 1996). The catalyst nanoparticle would therefore not disturb the electronic transport properties of the nanotube by forming a Schottky barrier. Nevertheless, palladium has been used a little as a catalyst for CNT formation, as described in (Vajtai et al., 2002). These three papers report growth of MWNTs. Other metals than iron, cobalt, nickel or palladium have been used as a catalyst. These metals are generally, but not necessarily non-active catalysts alone, but at any rate are used to improve the performance of the ‘‘classical’’ catalysts when added to them in different quantities. Molybdenum is the most important,

added to iron (Cassell, et al., 1999; Harutyunyan et al., 2002) or to cobalt (Huh et al., 2003). Table 2.1 illustrates the review of synthesis of CNTs using CVD.

Table 2.1: Summary of CVD process

Reaction Condition						
Catalyst and substrate	**Carbon source**	**Temp. (^oC)**	**Time**	**Flow rate of gases (ml/min)**	**Product Quality**	**Ref.**
Co, Fe, Cu/SiO_2, Zeolite, clay	C_2H_2	700	30 min	C_2H_2 ~8 N_2 ~75	MWCNTs (71-76%) and SWCNTs (low yield)	(Fonseca et al., 1996)
Co-Mo, Co-V, $Co-Fe/SiO_2$, Zeolite	C_2H_2	700	60 min	C_2H_2 ~30 N_2 ~300 NAY/CA (5%wt by CO-V,Co-Fe and CO-MO)	MWCNTs	(Willems, Kónya, et al., 2000)
Co-Mo ,Co-Ni	CO	1200	60 min	CO ~1200 (flow in chamber) The CO pressure was held at ~100 Torr	SWCNTs (1-5 nm in diameter)	(Dai, et al., 1996)
Co-Mo (1:2)/SiO_2	CO	700	60 min	CO ~100	MWCNTs (4%) & SWCNTs (88%)	(Kitiyanan et al., 2000)
Co, Ni, Fe/MgO	H_2/CH_4 (4:1)	1000	10 min	H_2 ~300 CH_4 ~75	SWCNTs (1-5 nm in diameter (70-80%)	(Colomer, et al., 2000)
Fe-Mo, Fe-Ru/Al_2O_3-SiO_2	CH_4	900	30 min	CH4 ~6000	SWCNTs (~42 wt%)	(Cassell, et al., 1999)
Mg0.9Co0.1Mo0 .025 O	H_2/CH_4	1000	30 min	18 mol% CH_4 CH_4 ~250	SWCNTs /DWCNTs ~ 64wt%	(Flahaut et al., 2003)

					(>80% 0.5 –5 nm diameter)	
Fe/Al_2O_3	CH_4	900	10 min	-	DWCNTs (1-6 nm diameter)	(Cumings et al., 2003)
Fe-Mo,	CH_4	875	30 min	CH_4 : Ar (1:1 ratio)	DWCNTs (in high yields)	(Endo et al., 2005)
Fe, Co, Ni/Al_2O_3 SiO_2 $Fe(CO)_5$	C_2H_4	800-1000	10 min	C_2H_4 ~30 N2 ~80	SWCNTs or thin MWCNT (3-12 nm diameter)	(Cheung et al., 2002)
Fe, Si-substrate	C_2H_5OH	900	30 min	Ar + H2 (6%) ~20	SWCNTs (4 cm length)	(Zheng et al., 2004)
Fe/Mo, SiO2/Si	CH_4	900	7 min	CH_4 (~1500) H_2(~125)	SWCNTs	(Franklin et al., 2001)
Al/Fe/Mo, Si-substrate	C_2H_2	1000	5 s	C_2H_2 ~50-250	SWCNTs (~1.3nm diameter)	(Lacerda, Teh, et al., 2004)
Fe,Co, Zeolite powder Mo,Co	C_2H_5OH C_2H_5OH	700-800 800	30 min	C_2H_5OH vapour (5 Torr),Ar C_2H_5OH vapour (10 Torr), Ar-H2(3%)	SWCNTs (>40 wt%) Mat of SWCNTs	(Maruyama et al., 2002)
Metallocene $M(C_5H_5)_2$ (M=Fe, Co, Ni)	C_6H_6	900	120 min	Ar (75%) H_2 (25%) $Ar+H_2$ ~50 & 1000	MWCNTs	(Sen et al., 1997)
$M(C_5H_5)_2$ (M=Fe,Co,Ni), Fe(CO)5	C_2H_2 CH_4	1100 1373	60 min 60 min	Ar ~975 H_2 ~25 C_2H_2 ~50 Ar ~950, H_2 ~50,CH4-50	SWCNTs (diameter 1-2 nm)	(Satishkumar et al., 1999; Satishkumar et al., 1998)
Fe $(C_5H_5)_2$,	Coal gas	850-950	30 min	Coal ~50-200	SWCNTs (1-2nm diameter)	(Qiu et al., 2004b)
Fe $(CO)_5$	CO	800-1200	60 min	CO (<10 atm)	SWCNTs (0.7-1.4 nm)	(Nikolaev, 2004; Nikolaev, et al., 1999)
Fe $(CO)_5$	CO	1050	60 min	CO (30 atm)	SWCNTs (450 mg/h)	(Kim et al., 2003)
Ba/Ca	C_2H_2	700	30 min	C_2H_2 ~ 60ml/min	MWCNT (100-300nm)	(Eftekhari et al., 2006)

				H_2/Ar ~10:1		
Si3N4	C_2H_2	800-1000	5 to 30 min	C_2H_2 ~(0.5-100m bar)	SWCNT (1-5nm	(Kasumov et al., 2007)
Si	C_2H_2	600-750	15 min	H_2 ~(0-400 cm^3/min) C_2H_2 ~ 50 cm^3/min Ar $(Fe(CO)_5$ ~(100-300 cm^3/min)	MWCNT	(Kuo, et al., 2006)
Ni/SiO_2-Al_2O_3	CH_4	850-1000	10 min	H_2/CH_4	MWCNT (16-100 nm)	(Bustero et al., 2006)
Ni	C_2H_2	550	60 min	C_2H_2 ~10-90 sccm	MWCNT (40-80 nm)	(Cao, et al., 2007)
$Si/SiO_2/Al_2O_3$	C_6H_{12}	750	5 min	C_6H_{12} (50 mbar) H_2~400	MWCNT (10 nm)	[153]
$Fe_2CO/Al2O3$	C_2H_4	750	10 min	C_2H_4~(50-200), Ar~80,H_2~80	MWCNT (50 nm)	(Magrez et al., 2011)
Si/SiO_2	CH_4	900	20 Min	CH_4~500 sccm, H_2~500	SWCNT (5 nm)	(Liu et al., 2009)
Fe	PP,PE, PVC	800	30 Min	Ar~ 500, H_2 ~30sccm	MWCNT (29-34 nm)	(Yang et al., 2010)
NiO/HZSM-5 zeolite	PP	500-800	35 Min	Plastic feed rate 80 g/h, Hydrogen gas concentration 72.21 vol.%	MWCNTs (15-25 nm)	(Liu et al., 2011)
Ni/Fe/CO/ HZSM-5 Zeaolite	PP,PE PVC, PET	400-900	1-60 min	Ar to H_2 (50:3 vol %)	MWCNTs 10-50 nm	(Bazargan and McKay, 2012)
Fe	C6H6	750	5-240 min	Ar~100 sccm	MWCNT (2nm).	(McKee et al., 2009)

2.4.3.4 Microwave assisted Chemical Vapor Deposition (MA-CVD)

Recently, a microwave-assisted synthesis is enabling technology that has been extensively used in organic synthesis (Brunetti, et al., 2007; Dallinger and Kappe, 2007; Nuchter et al., 2004). Microwave-assisted modification of CNTs is non-invasive, simple, fast,

environmentally friendly, and clean method as compared to traditional methods. Usually, the use of the microwave facilitates and accelerates reactions, often improving relative yields. In case of microwave-assisted functionalization of CNTs, microwave irradiation of CNTs and CNFs reduces the reaction time and gives rise to products with higher degrees of functionalization than those obtained by the conventional thermal methods (Vázquez and Prato, 2009). Interestingly, suggest a competitive effect of microwave irradiation that both promotes functionalization and removes some functional groups that are initially present (Liu et al., 2007). On the other hand, Vazquez and co-workers, 2009 show that a solvent-free technique combined with microwave irradiation produces functionalized nanotubes in just 1 h of reaction, paving the way to large scale production of functionalization (Nuchter, et al., 2004). Although materials are heated differently by microwaves, the maximum temperature is determined primarily by the dielectric properties of the receptor. The microwave heating of carbon-based materials gives rise to hot spots that appear as small sparks or electric arcs, with local temperature higher than 1100 °C. These hot spots have been well established as the thermal sensitizer upon microwave irradiation in the fields of organic synthesis, environmental remediation, preparation of catalysts, and carbon nanostructures (Kharissova, 2004). According to the previous study reported by Mendez et al., (2003), microwave heating was used to produce carbon nanotubes from graphite by applying microwave power of 800 W, oven temperature approximately at 1200 ^{o}C for 60 min. This study also shows that no catalyst was employed and graphite was directly targeted for microwave heating as graphite does not require a preliminary heating. Along with graphite, few other samples such as sucrose-graphite, boric acid with graphite were also tested with this microwave heating method. By doing this, the formation of nanotubes and nanofibers for sucrose-graphite sample was observed (Méndez, et al., 2003). The same

yield for boric acid and graphite with an additional yield of micro particles was also observed. Hong et al., (2003) report a method for the synthesis of CNTs by microwave irradiation. CNTs were successfully synthesized by microwave heating of the catalyst loaded on various supports such as carbon black, silica powder, or organic polymer substrates (Teflon and polycarbonate). Microwave (2.45 GHz, 800 W) irradiation used acetylene as a hydrocarbon source, and 3D transition metals and metal sulfides were used as the catalysts. Kharissova et al., (2004) developed a study for obtaining long and aligned carbon nanotubes with or without Fe filling by a highly efficient one step technique**.** Ferrocene was utilized as a catalyst to synthesise the aligned carbon nanotubes (CNTs) by heating it through microwave irradiation. However, in this study, used a catalyst (Fe) and a silica fused target. Microwave heating allows the growth of vertically aligned.

Lee, (2007) reported that, synthesis of CNTs on various supports, even on organic polymer substrates, by microwave heating of the catalysts under atmospheric pressure was conducted in order to establish a better understanding of the influence of chemical structures and processing conditions on the properties of CNTs which are directly synthesized on polymeric and organic materials through microwave irradiation. Benito et al., (2009b) reported that, the microwave-hydrothermal treatment determines the chemico-physical properties of Co-Zn-Al catalysts obtained by calcination of layered double hydroxide at 500 °C. The treatment affects to the distribution of the cations within the layers of the precursors because of an improved order. This effect is also observed in the catalysts. The kinetic study of carbon growth from the catalytic decomposition of methane indicates that the treatment improves the activity and the stability of the Co-Zn-Al catalyst. However, remarkable differences between the different aged catalysts are not found. This observation is in agreement with the results obtained by characterization, the greatest

changes in the properties are observed in the sample aged for the shortest period of time. On the other hand, the transmission electron microscopy results show that the carbon products obtained also depend on the duration of microwave-hydrothermal treatment, producing a change of the type of the nanofilaments formed (herringbone carbon nanofibers or multi-walled carbon nanotubes) and of the quantity of amorphous carbon produced. In addition, Zajickova et al., (2009) reported that, the microwave operating in the atmospheric pressure was successfully applied to the fast deposition of MWNTs on the substrate without necessity of any vacuum or heating equipment. Different ways to generate in situ and ex-situ catalytic nanoparticles for the carbon nanotube growth were tested. Dense straight standing nanotubes were successfully prepared on silicon substrates with or even without barrier SiO_x layer and oxidized Al layer. Therefore, it was possible to produce CNTs directly on conductive Si and used them as electron-emitting electrode of the gas pressure sensor. The CNTs grown in microwave torch were also intended to create a gas sensor based on the changes of electrical resistance measured between two planar electrodes connected by CNTs.

Zeng et al., (2010) reported that microwave-assisted pyrolysis of methane on the growth and morphology of carbon nanostructures (carbon nanospheres and CNTs) in the absence of a catalyst was studied. A vertical quartz tube was placed in a 2.45 GHz domestic microwave oven to carry out the experiment. A microwave absorber material carbon/carbon composite without mineral content was placed in the tube, which acted like a catalyst for nanostructure growth. Flushing the nitrogen before performing the experiments eliminated the oxygen from the cavity. The reaction was performed in a mixed gas flow CH_4/N_2 (ratio of 1:4) for 60 min and then the substance deposited on the quartz wall was used for further analysis. The results demonstrated that microwave-assisted pyrolysis is a novel and

promising approach for synthesizing carbon nanostructures. Besides, the experimental conditions, such as methane to nitrogen ratio, reaction temperature, and total gas flow rate, affected the nature of the produced nanostructures.

Vivas-Castro et al., (2011) reported that, synthesis of carbon nanotubes and other carbon nanostructures by microwave irradiation is simple and low-cost. With this technique and under various preparation conditions obtained nanostructured material from a graphite/iron acetate powder mixture using a commercial microwave oven as an energy source. Microwave absorption by the powder mixture results in pyrolysis of iron acetate. Decomposition of the acetate provides metallic iron nanoparticles that act as catalysts in the synthesis of nanotubes and other carbon nanostructures. Different type of nanostructured carbon can be obtained by variation of preparation conditions. Direct irradiation of (vacuum sealed) quartz ampoules, and attenuated irradiation by partial submerging the ampoules in water provide examples of the variety of nanostructures that can be obtained at different stages of microwave exposure. Reactions are very fast and may become so violent that can cause explosions of the ampoules. To avoid any accidents, the sites inside the microwave oven with maximum radiation intensity should be determined before. Exposure to microwaves and temperature gradients are static, resulting in the growth of well oriented and aligned MWCNTs arrays. Bekarevich et al., (Bekarevich et al., 2012) MWCNTs and few-layer graphene sheets have successfully grown on Si and polyimide substrates at relatively low temperature of 230 to 260°C by the microwave-excited surface wave plasma technique. Graphite-encapsulated Ni nanoparticles have been used as the catalyst for growing CNMs in NH_3/CH_4 plasma. It has been found that bias voltage and the nature of the substrate can greatly influence the CNMs structure.

Recently, Konno et al., (2013) reported that CNTs can be directly prepared by microwave plasma decomposition of Methane over Fe/Si activated by biased hydrogen plasma. In this research, using Fe/Si catalyst, methane was decomposed to H_2 and CNTs by microwave. After the hydrogen plasma treatment, both methane and hydrogen gas mixtures (ration 1:4) were flowing into the reactor, exposed to power of 500W for 30 min reaction time at temperature of 600^{o}C. Resulting CNTs' diameter reaches a maximum value of 22.5 nm at treatment time of 20 min and a minimum value of 9.8 nm at treatment time of 30 min. The maximum height of the MWCNTs increases with increasing plasma treatment time, and reaches 30.7 nm at 10 min.

2.4.3.5 Microwave Plasma Chemical Vapor Deposition (MP-CVD*)*

In Plasma enhanced-CVD method, carbon nanotube was growth over the substrate catalyst, which is coated with a catalyst, but the substrate, is located inside the plasma. In this method, usually the source of the plasma is RF- (radio frequency), MW- (microwave) or a DC-plasma (direct current). The plasma enhanced CVD method generates a glow discharge in a chamber or a reaction furnace by a high frequency voltage applied to both electrodes. Fig. 2.15 shows a schematic diagram of typical plasma CVD apparatus with a parallel plate electrode structure and a substrate is placed on the grounded electrode. Hydrocarbon such as methane (CH_4) and hydrogen (H_2) gas mixture with a ratio of 1% CH_4 to 99% H_2 is used at a total pressure between 1 to 40 mbar and a temperature of 900 °C to produce CNTs (Bower, Zhu, et al., 2000; Küttel et al., 1998; Ren, et al., 1999).

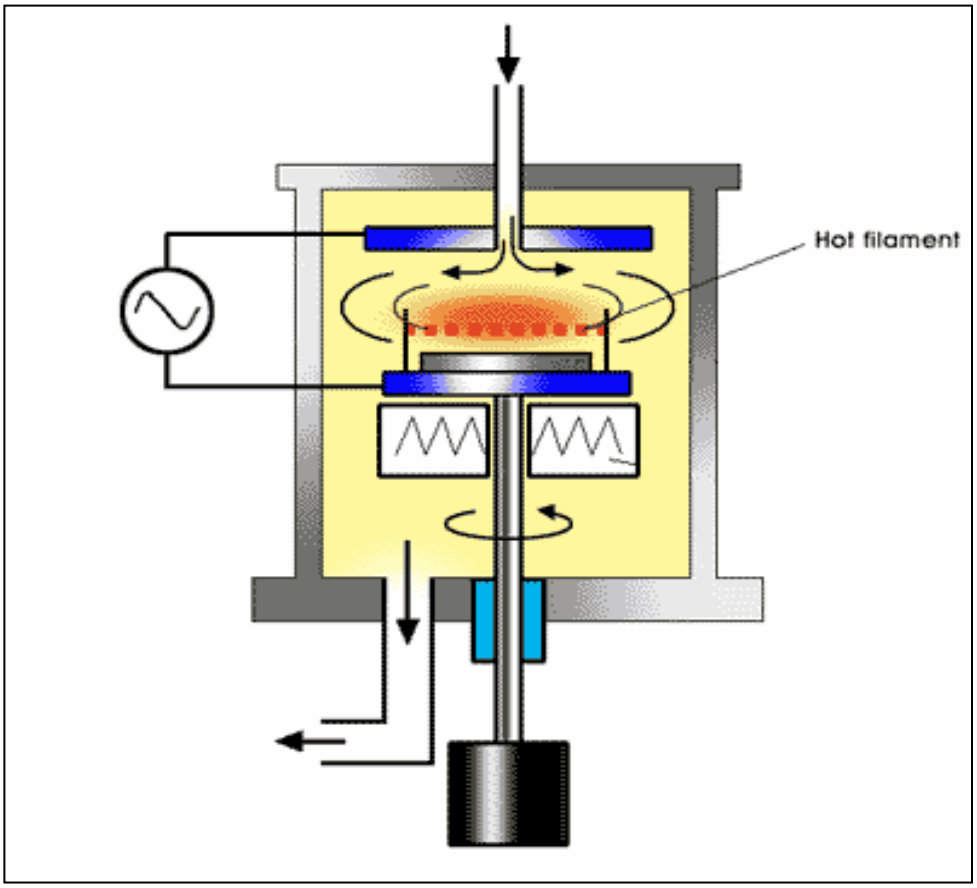

Figure 2.11: Schematic diagram of Plasma Enhanced CVD apparatus (Bower, Zhou, et al., 2000)

Huang et al., (1998) reported that synthesizing CNTs on low temperatures, by using microwave plasma enhanced chemical vapor deposition (MPE- CVD). The lowest reported growth temperature when that research was being conducted was 666 ^{o}C (Huang et al., 1998). Choi et al., (2000) carried out an investigation on producing CNTs a lower temperature (520 ^{o}C) by MPE -CVD using Ni as the growth catalyst and Si as the substrate. For the carbon source, CH_4 and H_2 was used. The plasma power was set to 400 W and the reaction time for CNT growth varied from 50 to 100 min. Characterization of the grown CNTs shows uniformly graphitized CNTs were synthesized with a high density, which proves that pure carbon nanotubes were grown at a very low temperature on Si substrates

coated with Ni catalyst using MPE-CVD with CH_4/H_2 gas mixtures. Chhowalla et al., (2001) reported, the growth of vertically aligned CNTs using a direct current plasma enhanced chemical vapor deposition system is reported. The growth, properties is studied as a function of the Ni catalyst layer thickness, bias voltage, deposition temperature, C_2H_2:NH_3 ratio, and pressure. It was found that the diameter, growth rate, and areal density of the CNTs are controlled by the initial thickness of the catalyst layer. The alignment of the CNTs depends on the electric field the growth occurs by diffusion of carbon through the Ni catalyst particle, which rides on the top of the growing tube.

Chen et al., (2002) reported that high yield multi walled carbon nanotubes can be obtained by MP-CVD maintained at a low temperature. In their study, shows that usage of carbon dioxide as a substitute of hydrogen gas, mixed with methane gas for the carbon source gas system provides a high yield and good alignment of CNTs that is obtainable by maintaining a lower temperature of the gas system. Microwave heating of Fe-deposited-Si substrate was done for 20 min at temperatures lower than 330 ^oC with microwave power of 300 W. Rather than using the conventional reaction gas mixtures such as hydrogen-methane, hydrogen-acetylene and hydrogen-benzene, a different approach by using methane with carbon dioxide is considered as a successful method in producing high quality CNTs (Chen, et al., 2002).

Liu and Ting (2003) investigated on the growth of CNTs using microwave plasma enhanced chemical vapor deposition. In their study, synthesized CNT uses a microwave with 1500 W and an iron containing liquid compound, Ferrofluid as the catalyst for CNT growth. Ferrofluid was sprayed onto Si which was used a substrate prior to the heating process. Gas mixtures of CH_4 and H_2 were utilized as the carbon source. The reaction time and the temperature allowed in the plasma were 5 min and 1100 ^oC respectively. Grown

CNTs were studied for characterization and it can be concluded that Liu obtained uniform and oriented CNTs with an average length of 12 micrometer and methane concentration and plasma power affects the diameter of CNTs being grown (Liu and Ting, 2003). Taniguchi et al., (2005) reported that, a study in preparation of dense CNTs film using microwave plasma-enhanced chemical vapor deposition where dense, vertically aligned CNT . As in for this study, a carbon source gas where a mixture of acetylene and hydrogen was used. Microwave power of heating was kept at 900W and 800 ^{o}C respectively, and growth experiment was done for about 10 min. Besides that, heat pre-treatment for the catalyst was not required for this study. The growth of the carbon nanotubes was evident on the Co-catalyzed substrate which was buffered with a TiN layer. Observation on the growth rate behavior was recognized and reported earlier (Bower, Zhou, et al., 2000; Bower, Zhu, et al., 2000). The CNTs were characterized by a relatively large inner diameter 4 nm and thinner wall thickness 2–5 concentric layers. Dense, aligned CNTs grown from the laser-ablated catalytic nanoparticles would be applicable for the vertical wiring of an ultra-large scale next generation integrated circuit (Taniguchi, et al., 2005).

Quinton et al., (2013) reported that, thermal (T-CVD), MPE-CVD, and floating catalyst thermal CVD (FCT-CVD). Methane gas was introduced into the microwave as a source of carbon and Fe use as a catalyst. T-CVD provided the largest diameter tubes, with catalysts residing mainly at the CNT/diamond interface. The MPE-CVD process yielded a non uniform defective CNTs, and FCT-CVD resulted in the smallest diameter CNTs with catalyst particles imbedded throughout the length of the nanotubes. The Raman spectroscopic analysis suggested that T-CVD had the lowest disordered carbon to graphite intensity ratio of 0.3 followed by FCT-CVD of 0.83 and the highest by MPE -CVD of 1.94. T-CVD also produces large diameter CNTs that are otherwise clean, with minimal tubular

defects or additional catalytic contaminants. MPE-CVD is sometimes the preferred method for larger scaled applications.

Nie et al., (2013) prepared CNTs by placing a conductive polymer and ferrocene under the microwave, where the polymer was the microwave acceptor and the simple microwave oven in air at room temperature, without the need of an inert gas atmosphere or other gas feeds. Although this convenient and ultrafast method did not require any complex apparatus, high temperature or inert atmosphere, the need to synthesize the conductive polymer layer increased the complexity and cost substantially. In their study reported that, a one-step and low-cost CNTs fabrication method by a single carbon fiber triggering the pyrolysis of ferrocene under microwave field. CNTs were synthesized in 15 to 20 S by a single carbon fiber initiating the pyrolysis of ferrocene under microwave field without any other chemicals. The growth of CNTs can also be triggered by other carbonaceous materials and influenced by their configurations. The CNTs prepared by the method described here have a graphitic structure that is better than the commercial MWCNTs of the same diameter. The precise mechanism of CNTs growth is still under investigation.

2.5 Comparison of nanotube synthesis methods

Although many methods have been developed for synthesis the MWCNTs and SWCNTs, only the first three methods which are the electric arc-discharge, laser ablation and CVD are widely adopted. In the arc discharge, a vapor is created by an arc discharge between two carbon electrodes with or without catalyst. In the laser ablation technology, a high achievement laser beam imposes to the volume of the carbon, containing feedstock gas (methane or carbon monoxide). Laser ablation produces a very small amount of pure nanotubes, while an arc-discharge produces in general large amounts of the impure

material. The production of CNTs using CVD is the most promising method for possible industrial scale-up due to the its relative simplicity of operation, process control, energy efficiency, the raw material used, capability to scale up as large unit operation, high yield and purity. In this process, any hydrocarbons in the presence of a catalyst (Fe/Co/Ni) at high temperature (600-1000 ^{o}C) can produce large amount of high purities of CNTs. Compared with conventional heating technques, microwave heating has additional advantages as follows: higher heating rates selective heating, greater control of heating process, no direct contact between the heating source and heated materials, and reduced equipment size. In addition, So, to overcome this shortcomings, MA-CVD seems to be the most promising method for possible industrial scale-up due to the relatively low growth temperature, high surface area, high adsorption capacity, less pollution and energy saving. Low cost and high yield of CNTs for industrial application Single stage production of carbon nanotubes using microwave heating compared to the conventional method which requires multiple stage. A comparison of these techniques according to the synthesis temperature, nanotube graphitization, yield and relative CNTs quantity is shown in Table 2. The CVD process is very simple, easily reproducible, highly selective (SWCNTs or MWCNTs alignment, diameter, length) and can be scaled to produce by the kilogram. Based on these attributes the CVD is the most promising synthesis method for producing large qualities of CNTs at a low cost.

Table 2.2: Comparison of Arc-discharge, Laser ablation and CVD

Process	**Arc-Discharge**	**Laser ablation**	**CVD**	**Ref**
Reaction temperature	3000 to 4000 ^{o}C	3000 ^{o}C	500 to1100 ^{o}C	(Ebbesen, et al., 1993; Journet and Bernier, 1998)
Per unit design cost	High	High	Low	(Ando, et al., 2004; Thess, et al., 1996)
Nanotube selectivity	Low	Low	High	(Muataz, 2003)
Source of carbon	Difficult	Difficult	Easy available	(Cao, et al., 2007)
Purification of CNT (high impurities)	High	High	Low	(Fonseca, et al., 1996)
CNTs yield	<30%	≈70%	95-99%	(Colomer, et al., 2000; Fonseca, et al., 1996)
Process nature	Batch	Batch	Continuous	(Cassell, et al., 1999; Zheng, et al., 2004)
Process parameter control	Difficult	Difficult	Easy to control	(Bustero, et al., 2006; Kim, et al., 2003)
Energy requirement	High	High	Low	(Nagaraju et al., 2002)
Reactor design	Difficult	Difficult	Easy to design reactor	(Kong et al., 1998)
Nanotube graphitization	High	High	Middle	(Pérez-Cabero et al., 2004; Zhu et al., 2003)

2.6 Factors influencing the growth mechanism of carbon nanotubes

Among the parameters that influence the growth mechanism of CNTs are the catalyst, carrier gas, substrate, and temperature of synthesis, reaction time and the flow rate of carrier gas. Most effective and widely used catalysts are Fe/Co/Ni. The rationale for using these metals lies in the phase diagrams for these metals and carbons. At a high temperature, carbon has a finite solubility in these metals, which leads to the formation of metal-carbon solutions and therefore the aforementioned growth mechanism. Li et al., (2010) reported that the growth process, catalysts plays an important role in controlling the structure of

SWCNTs. Also observed systematically studied the size-controlled synthesis of Fe-based nanoparticles and the CVD growth of SWCNTs, especially the horizontally aligned SWCNTs, catalyzed by these produced nanoparticles. Some new catalysts were also developed. Among them, Cu is shown to be a superior catalyst for growing SWCNT arrays on both silicon and quartz substrates and Pb was a unique catalyst from which one can obtain SWCNTs without any metallic contaminant. SWCNTs prepared with both Cu and Pb was very suitable for building high-performance nano-devices. These studies were also very helpful in further understanding the growth mechanism of SWCNTs. The growth rate of CNT is a function of catalyst particle size and the diffusion rate of carbon through the catalyst. As the catalyst particle size increases, the growth rate will decrease. Meanwhile, the growth rate of CNTs is directly proportional to the diffusion rate of carbon through the catalyst (Kim, et al., 2003). Widely used catalyst materials in CNT synthesis is cobalt (Couteau et al., 2003; Nagaraju, et al., 2002; Sinha et al., 2000), iron (Chen et al., 2003; Rohmund et al., 2000), titanium (Chen, et al., 2003), nickel (Klinke et al., 2001; Zeng et al., 2002) a couple of zeolites and combinations of these metals and/oxides (Mukhopadhyay et al., 1999; Ning et al., 2002; Su et al., 2000; Wang et al., 2001). Another factor that may influence the productivity of the catalyst material is the dispersion level of the catalyst material. Large particles and aggregates instead of fine and well dispersed particles may be inactive for nanotube growth (Kong, et al., 1998) and well-dispersed catalyst systems may result to a narrower size distribution of the synthesized nanotubes (Hernadi et al., 1996). Most commonly used, CNT precursors are methane, (Douven et al., 2012; Fan, Chapline, et al., 1999; Kong, et al., 1998; Li et al., 1996) ethylene, (Satishkumar, et al., 1998), acetylene, (Sen, et al., 1997) benzene, (Wei et al., 2002) xylene, (Endo, 1991) and carbon monoxide, (Nikolaev, et al., 1999). (Endo et al., 1993; Endo, 1992) reported the CNT

growth from pyrolysis of benzene at 1100 ^{o}C, whereas (José-Yacamán, et al., 1993) got clear helical MWCNTs at the 700 ^{o}C from acetylene. The carrier gas also affects the growth of CNTs. Carrier gas such as H_2 and Ar effects the growth of CNTs. Hydrogen is the most effective carrier gas as it provides a reducing atmosphere and scavenges oxygen. However, excess hydrogen will push the reaction in the opposite direction which is not desirable. Nitrogen has been found to be effective for the growth of bamboo type CNTs by delaying the surface of passivation of the catalyst particle and enhance carbon diffusion through the catalyst. Ammonia has been thought to provide large amounts of hydrogen that suppresses the carbon supply and enhances the tube formation. The growth of CNTs is observed to be strongly substrate dependent. The high surface roughness pores and defects of substrate will promote the growth of nanotubes that have surface defects. The amount of substrate crystallinity also affects the ability for CNTs growth and nucleation.

On the crystalline surface of substrate, the growth of SWCNTs seems to be favored, while on amorphous and polycrystalline surface, the MWCNTs growth is preferred. The growth mechanism of CNTs can be categorized into two modes that are the base growth mode and the tip growth mode depending on the interaction of the catalyst particle with the substrate. The rate of reactions is a strong function of temperature, thus it is expected that the concentration of each species will vary with temperature. At a low temperature, a decrease in the formation of CNTs formation has been observed, possibly due to the partial deactivation of catalyst (Pérez-Cabero, et al., 2004). It is reported that lower synthesis temperatures than optimum synthesis temperature result in lower CNTs yield in the product (Sinha, et al., 2000). It is also reported that the reaction temperature plays an important role in the alignment properties and diameter of the synthesized nanotubes (Singh et al., 2003). Generally, the CNT growth temperature (or reaction temperature) used is between 550 ^{o}C

and 1000 ^{o}C, and reaction temperature may vary according to the catalyst support material pair. Zhu et al., (2003) synthesized the CNT on graphite fibers by the thermal CVD. They showed that the CNTs can only be grown in a limited temperature range. At low growth temperatures, only a carbon layer is formed on the fiber surface. However, at high temperatures, the diffusion rate of iron particles into carbon fibers was enhanced and the nanotube growth possibility is reduced. Li et al., (2002) synthesized the CNTs with nanocrystalline Ni/metallic oxide catalyst from decomposition of methane. When the reaction temperature is higher than 1000 K, the CNTs can be obtained. At lower temperatures, the formation of carbon fibers is observed. (Chiang and Sankaran, 2008) reported that production of CNTs at below 400 ^{o}C, no appreciable change was observed in the particle size distribution for Ni particles, indicating that the temperature is too low for nucleation and growth and also enhanced growth rates and lowering of activation energy and growth temperature. The typical reaction time is approximately 60 minutes, but the reaction time also depends on the desired CNTs amount. Furthermore, deviations of the optimum reaction time for the specific synthesis suffer from the quality of the final product (Nagaraju, et al., 2002). It is also noted that the yield is proportional to the time of reaction. Han et al., (2002) studied the influence of flow rate of precursor and carrier gas, and it is found that if the flow rate of carrier gas is increased, with the precursor flow rate remain constant, the mean diameter of CNTs will decrease. If the flow rates of both carrier and precursor gas are increased, the diameter essentially remains constant, but the growth rate will increase. Abdullahi et al., (2012) reported that the decomposition of methane for MWCNTs growth among other factors such as operating conditions is dependent on the catalyst and the loading of the active specie for methane decomposition, catalyst preparation and pre-treatment such as the calcination and reduction in hydrogen. A kinetic

model is developed for the decomposition of methane during growth of MWCNTs over 20 wt % nickel–alumina catalyst by CVD. The activation energy for methane decomposition on Ni–Al_2O_3 catalyst was 37.1±3.5 kJ/mol was also observed.

In addition, (Kumar and Ando, 2010) reported that growth mechanism and mass production of CNTs by CVD with the effect of material aspect such as roles of hydrocarbon, catalyst and catalyst support. Besides, discussion has been made on the growth-control aspects such as the effects of temperature vapor pressure and catalyst concentration in the CNT diameter distribution and single- or multi-wall carbon nanotube. Recently, Danafar et al., (2009) reported out of different techniques, catalytic CVD in a fluidized bed is the most promising technique for large scale production of CNTs. Bulk production of CNTs depends on the gas flow rate, hydrocarbon concentration, temperature, size and shape of the initial agglomerate and catalyst loading and size. The gas flow rate affects the mass transfer coefficient, the size and shape of the agglomerate influences the internal diffusion of gas within the pore, the temperature, hydrocarbon concentration and catalyst loading determines the reaction rate. The morphology of CNTs depends on the type and size of catalyst and the carbon supply rate.

2.7 Heavy Metals

New era industries have immensely improved the living standard of human being. But however, these modern industries also pose serious adverse impacts on our living surrounding. One of the major environmental concerns is the water pollution by the heavy metals. Heavy metals in water are the main preoccupation for many years because of the toxicity towards aquatic-life, human beings and also the environment (Stafiej and Pyrzynska, 2007). Even though trace amounts of heavy metals are vital for the human

body, they are considered as harmful when they become excessive. Contrasting with organic pollutants, most of which are susceptible to biological degradation, heavy metal ions do not end product that is harmless to the environment. The contamination of crucial concern includes lead, cadmium, mercury, zinc, copper, chromium, silver, Stannum, and other mutagenic nature which also makes up the earth's surface (Cho et al., 2009; Hyung and Kim, 2008; Mubarak et al., 2013; Mubarak et al., 2014; Xu et al., 2008). Contamination of heavy metals exists in aqueous wastes of various industries, such as mining operations, tanneries, metal plating, alloy industries and smelting (Masciangioli and Zhang, 2003). The process involves industries such as metal plating and battery manufacturing can be counted as the primary source for cadmium pollution in water (Wang, Gong, et al., 2007). The types of emerging pollutant are also increasing while the traditional pollutants are not efficiently solved yet. Removal of toxic metals is one of the biggest challenges in ensuring safe water for all as well as protecting the environment (Bansal, 2005). It might cause several health problems such as nervous system damages, renal kidney disease, mental retardation, cancer and anemia (Calderón, et al., 2001; Friberg, 1979; Li, Wang, et al., 2003; Li, Wang, et al., 2002; Vuković et al., 2010). As a result, the standard B discharge limit of these metals under the Malaysian-Enrironmental Quality Act 1914 (Sewage and Industrial Effluents) 1979 are kept below 1.0 mg/L (MDC, 1997)' The maximum limit under the standard is 0.02 mg/L for Cd- 0.50 mg/L for Pb (II) and 1"0 mgLeach for Zn, Ni, Cu and Cr (III). Despite their potential toxicity (Aziz et al., 2008) various types of metal compounds end up in the rivers. Carbon nanotubes (CNTs) as a new member in the adsorbent family, which was first reported in 1991 (Iijima, 1991), have been proven for its high efficiency in the removal of heavy metal ions from aqueous solutions due to its remarkable mechanical (Dai and Mau, 2001; Terrones, 2003), chemical properties

(Javey et al., 2003) and electrical (Collins et al., 1997); on the same note, CNTs have large specific surface area, high thermal and chemical stabilities and provision for large scale synthesis making a good candidate for adsorption kinetics (Li, Ding, et al., 2003; Li, 2004; Mubarak, et al., 2013); besides, its light mass density (Chen et al., 2008) have made them one of the successful adsorbents to be integrated with the removal of heavy metal ions from aqueous solutions (Kabbashi, 2011; Li, Liu, et al., 2010; Mubarak, et al., 2013). Therefore, CNTs are the most promising candidate for removal of heavy metal from waste, particularly in water treatment and separation processes. Due to high surface area, it could be potential to remove toxic metals for the production of high purity water (Colt, 2006).

2.7.1 Carbon nanotubes Adsorption

There are two main types of CNTs with high structural perfection; they are SWCNTs, which consist of a single graphite sheet seamlessly wrapped into a cylindrical tube and MWCNTs, which comprise an array of concentric cylinders (Odom, et al., 1998). They have been treated as the most promising nanostructured materials and the prospect of developing novel carbon-based nonmaterial has excited worldwide interest among researchers (Luo et al., 2000). The CNTs have the large adsorption capacity, which is mainly attributable to their pore structure, surface area and the existence of a wide spectrum of surface functional groups. The mechanisms by which the metal ions are sorbed onto CNTs are very complicated and appear attributable to electrostatic attraction, sorption-precipitation and chemical interaction between the metal ions and the surface functional groups of CNTs (Rao, et al., 2007). Consequently, CNTs serve an important role in the removal of some organic salts, toxic dyes and heavy metals from water.

Human activities affect the natural geological and biological redistribution of heavy metals through pollution of the air, water and soil. The primary anthropogenic sources of heavy metals are point sources such as mines, foundries, smelters and coal-burning power plants, as well as diffuse sources such as combustion by-products and vehicle emissions. Heavy metal removal is one of the most essential processes in wastewater treatment. The CNTs adsorption is one of the well known methods in removing heavy metals or other traces in waste water. The adsorption capacity is an aspect to be highlighted where the successfulness of heavy metal removal is based on the maximum amount of the traces that can be attracted to and held on to the surface of the CNTs. Many researchers have studied and explained about the adsorption capacity of the CNTs in their studies which will be discussed further.

2.7.2 Heavy metals removal using CNTs

Zinc is one of the famous heavy metals occurring in waste water. In water, Zn ion may associate or react with neutral or ionic compounds to form inorganic salts, stable organic complexes or inorganic or organic colloids. The quantity of Zn ion available in water from each of these forms is dependent upon the solubility of these forms, the pH and temperature, the total amount of the Zn form present in water and the presence of other metal ions, organic compounds and inorganic compounds. Zn ion exhibits high toxicity to aquatic organisms and it may cause high chronic toxicity in some cases. For example, the aquatic toxicity is evidence indicating that the Zn ion is highly toxic to aquatic organisms and has a high potential to bioaccumulate. Therefore, it is important to remove Zn from waste water during the treatment. Lu and Chiu, (2006b) in their study explained on the trend of the graph obtained from the adsorption capacity of Zn^{2+} onto the CNTs, where

adsorption increases when the pH is adjusted from 1-8, achieving maximum between pH 8-11 and decreased at pH 12. The time taken for the adsorption to reach the equilibrium for the SWCNTs and MWCNTs are 60 min while for the powdered activated carbon (PAC) it took 120 min. A comparison on the adsorption of Zn^{2+} between the CNTs and commercial PAC was also carried out. With the initial Zn^{2+} concentration range of 10 to 80 mg l^{-1}, the maximum adsorption capacities of Zn^{2+} calculated by the Langmuir model for the SWCNTs, MWCNTs and PAC were 43.66, 32.68 and 13.04 mg g^{-1} respectively. The time taken to reach equilibrium was short and they suggested that in order to obtain high adsorption capacity, the SWCNTs and MWCNTs are used in the applications for the Zn^{2+} removal from water. In another case study, Lu et al., (2006b) reported that the amount of Zn^{2+} sorbed onto the CNTs increased with a rise in temperature. Using the same conditions, the Zn^{2+} sorption capacity of the CNTs was much greater than that of the commercially available PAC, reflecting that the SWCNTs and MWCNTs are effective sorbents. The thermodynamic analysis revealed that the sorption of Zn^{2+} onto the CNTs is endothermic and spontaneous. The Zn^{2+} ions could be easily removed from the surface site of the SWCNTs and MWCNTs by a 0.1 mol/L nitric acid solution and the sorption capacity was maintained after 10 cycles of the sorption/desorption process. This suggests that both the CNTs can be reused through many cycles of water treatment and regeneration. Recently, Mubarak et al., (2013) reported that the removal of Zn^{2+} using functionalized CNTs and magnetic biohcar. Statistical analysis revealed that the optimum conditions for the highest removal of Zn^{2+} are at pH 10, dosage 0.09 g, agitation speed and time of 120 rpm and 120 min respectively. The removal efficiency of Zn^{2+} for an initial concentration of 1.1 mg/L using functionalized CNT was 99% and using magnetic biochar was 75%.

Not only the Zn ion could be removed by the CNTS adsorption, other studies show that some other trace elements such as Ni, Pb, Cd, chromium (Cr) and Cu can also be absorbed by this powerful agent, the CNTs. Yang et al., (2009) in their study of adsorption of Ni^{2+} on oxidized MWCNTs found that adsorption capacity increases with the increase of pH in the pH range of 2 to 9 from zero to ~99%. They found that oxidized MWCNTs were the most suitable material for the solidification and pre-concentration of Ni^{2+} from aqueous solutions. In another article, Kandah and Meunier, (2007) reported on their achievement in adsorption of some heavy metals using functionalized CNTs. With a large adsorption capacity, they also reported on the ability of the CNTs to remove some organic dyes from water. In their study, for both produced and oxidized CNTs, the Langmuir model determined 18.083 and 49.261 mg/g, respectively, as the maximum Ni^{2+} adsorption uptake. These two sets of isotherm models suit well with the experimental data. Therefore, it concluded that the experiment was successful where the CNTs were found to be the most effective nickel ion absorbent based on higher adsorption capacity as well as the adsorption time taken which was set to be at an equilibrium state (Kandah and Meunier, 2007).

Chromium at low-level exposure can irritate the skin and cause ulceration. Long-term exposure can cause kidney and liver damages as well as damaging the circulatory and nerve tissues. Once again, it is important to eliminate such traces in our waste water by the aid of the CNTs. Atieh, (2011a) has reported using carbon nanotubes supported by AC to remove Cr^{6+} ions from polluted water. The highest adsorption capacity by using an AC coated with carbon nanotubes adsorbent obtained from the batch adsorption experiment was 9.0 mg/g. Therefore, it can be concluded that the AC coated with carbon nanotubes is most effective for the removal of chromium ions. Di et al., (2006) reported that removal of Cr^{6+} from drinking water using ceria nanoparticles supported on aligned carbon nanotubes

(CeO_2/ACNTs). The largest adsorption capacity of CeO_2/ACNTs reaches 30.2 mg g^{-1} at an equilibrium Cr^{6+} concentration of 35.3 mg l^{-1} at pH 7. They also concluded that the adsorption capacity of the CeO_2/ACNTs is 1.5 times higher than that of the AC, 2 times higher than that of Al_2O_3 and 1.8 times higher than that of ball-milled ACNTs. The high adsorption capacity, wider range of pH values makes CeO_2/ACNTs a good candidate material for removal of Cr^{6+} from drinking water. Hu et al., (2009) reported that the removal of Cr^{6+} from aqueous solution using oxidized MWCNTs. The maximum removal of Cr^{6+} was found at low pH, and the adsorption kinetics of Cr^{6+} were suitable for pseudo-second order models. The removal of chromium mainly depends on the occurrence of redox reaction of adsorbed Cr^{6+} on the surface of oxidized MWCNTs to the formation of Cr^{3+} and subsequent the sorption of Cr^{3+} on MWCNTs appears as the leading mechanism for chromium uptake to MWCNTs. To remove the anionic chromate ($CrO4^{2-}$) from waste water, functionalized CNTs were found to be the most suitable compared to unmodified CNTs in terms of the adsorption capacity, Xu et al., (2011). The authors explained on the reason of the CNTs showing an excellent adsorption capability of anionic chromate, which was because of the interaction of $CrO4^{2-}$ with the surface oxygen-containing functional groups on the modified CNTs. Hence, functionalized CNTs once again can be potentially employed in adsorbing heavy metal from waste water.

Lu and Su, (2007) reported that MWCNTs were thermally treated to remove natural organic matter (NOM) in aqueous solution. The amount of adsorbed NOM onto CNTs increased with a rise in initial NOM concentration and solution ionic strength, but decreased with a rise in solution pH. Also concluded that the performance of adsorption using raw CNTs and Treated CNTs and granular activated carbon (GAC). The result proved that treated CNTs have best NOM adsorption performance compared to others.

Besides Zn and Cr, Pb is also one of the famous heavy metals occurring in waste water. Pb compounds are generally soluble in soft and slightly acidic water. Pb waterworks were often applied in past days and these may still be present in old buildings. The Pb from pipes may partially dissolve in the water flowing through. It occurs in almost all water resources as well as waste water. Despite its toxicity, the presence of lead in the water may affect the human and marine lives' health. Therefore, again, the discussion on the CNTs to absorb the lead from waste water is still going on. Wang et al., (2007) reported that, the role of functional groups in the adsorption of Pb^{2+} to create a chemical complex adsorption. It is reported that 75.3% of Pb^{2+} adsorption capacity was achieved. The Pb^{2+} is in the form of PbO, $Pb(OH)_2$, and the $PbCO_3$ is adsorbed on the surface of the acidified MWCNTs which is only 3.4% of the total Pb^{2+} adsorption capacity. They concluded that the Pb^{2+} species adsorbed acidified MWCNTs on the ends and at the defect sites. Wang et al., (2007) reported that men oxide-coated carbon nanotubes (MnO_2/CNTs) was used to remove Pb^{2+} from aqueous solution. The Pb^{2+} removal capacity of MnO_2/CNTs decreased with the decrease of pH. From the Langmuir isotherms, maximum adsorption capacity was 78.74 mg/g, comparing with CNTs, significant improvement of Pb^{2+} adsorption shows MnO_2/CNTs can be good Pb^{2+} absorbers. The adsorption of Pb^{2+} by MnO_2/CNTs occurred first 15 min of contact time, and equilibrium reach at 2hr, also kinetics adsorption described was pseudo-second-order rate equation. Wang et al., (2007) in the study on the adsorption of acidified MWCNTs to Pb^{2+} found that the experiment met the Langmuir model. The results demonstrate a high adsorption capacity of acidified MWCNTs for Pb^{2+}. The reason stated was due to the formation of oxygenous functional groups on the surface of the CNTs. Salt formation or complex deposited occurred on the surface of CNTs when acidified MWCNTs react with Pb^{2+}. The adsorption contact time to reach equilibrium is about 20

minutes, which proven be shorter than AC (reported to be 120 minutes). Besides the discussion at an adsorption contact time, the authors also stated that Pb^{2+} can be easily regenerated from the acidified MWCNTs by adjusting the solution to pH 2. In another study, Kabbashi et al., (2009) discussed on the removal of Pb^{2+} which has reached the maximum value 85% or 83% at pH 5 or 40 mg/L of the CNTs, respectively. Higher correlation coefficients from the Langmuir isotherm model indicates the strong adsorptions of Pb^{2+} on the surface of CNTs (adsorption capacity Xm = 102.04 mg/g). The results indicate that the highest percentage removal of Pb^{2+} (96.03%) can be achieved at pH 5, 40 mg/L of CNTs, contact time 80 minutes and agitation speed 50 r/min.

The effectiveness of an adsorbent depends on the adsorptive properties of their surface. Adsorption takes place when a solid surface is in contact with a solution and tends to accumulate a surface layer of solute molecules created by the imbalanced surface forces. Moradi et al., (2011) explained on the interaction between some heavy metal ions such as Pb^{2+}, Cd^{2+} and Cu^{2+} ions from aqueous solution adsorbed by single walled carbon nanotube (SWCNTs) and the carboxylate group functionalized single walled carbon nanotube (SWCNT-COOH) surfaces. The maximum adsorption capacities (qm) for Pb^{2+}, Cu^{2+} and Cd^{2+} ions onto the SWCNT-COOH obtained are 96.02, 77.00 and 55.89 mg/g, respectively, and by the SWCNTs are 33.55, 24.29 and 24.07 mg/g, respectively. The thermodynamic parameter values showed that the adsorption of ions on the SWCNT-COOH and SWCNTs at 283 to 313 K is spontaneous and endothermic

One of the most hazardous heavy metals is cadmium (Cd). Cd, when in humans, long-term exposure to it is associated with renal dysfunction. Therefore, it is essential to remove Cd during the wastewater treatment in order to save our lives and the nature. Li et al., (2003) in their article discussed on the adsorption of Cd^{2+} by the CNTs. The adsorption capacity is

highly dependent on the pH where H_2O_2 oxidizes the CNTs to reach an equilibrium state with a high adsorption capacity at lower pH and it is more obvious compared to the HNO_3 and $KMnO_4$ oxidized CNTs. The experiments of the CNT dosage effect on the Cd^{2+} adsorption reflect that the adsorption capacity for $KMnO_4$ oxidized CNTs has a sharper increase in the CNT dosage from 0.03 to 0.08 g per 100 ml than the as-grown, H_2O_2 and HNO_3 oxidized CNTs and its removal efficiency almost reaches 100% at the CNT dosage of 0.08 g per 100 ml. This shows that the CNTs again managed to adsorb Cd^{2+} with high adsorption capacity.

In order to prove the efficiency of CNTs in adsorbing heavy metals Gao et al., (2009) studied on the adsorption of Ni, Cu, Zn and Cd from aqueous solutions on CNTs oxidized with concentrated nitric acid, which was carried out in single, binary, ternary and quaternary systems of the complexity of adsorption of metal from multi-component solution on the CNTs oxidized. They studied with the effect of process parameters such as the pH value, initial concentration of ions, the surface chemistry of the adsorbent, the kind and number of components in the adsorption system and the ratio of the metal ion species in solution. For the single and binary systems, it was revealed that the amount adsorbed on the CNTs oxidized followed the order of Cu^{2+} (aq) >Ni^{2+} (aq) > Cd^{2+} (aq) > Zn^{2+} (aq). A good correlation between the amount adsorbed and standard electrode potential was discovered indicating that the redox process may serve a role in the mechanism of adsorption. Meanwhile, for the ternary and quaternary systems, the adsorption was more complex. The order of amount adsorbed at the same concentration was Cu^{2+} (aq) > Cd^{2+} (aq) > Zn^{2+} (aq) >Ni^{2+} (aq). Stafiej and pyrzynska (2007) reported that adsorption characteristics of some divalent metal ions (Cu, Co, Cd, Zn, Mn, Pb). The effect of metal ions removal at pH9 was Cu^{2+} > Pb^{2+} > Co^{2+} > Zn^{2+} > Mn^{2+}. Li et al., (2004) reported that

different heavy metals (Pb^{2+}, Cu^{2+} and Cd^{2+}) adsorption using oxidized CNTs. The maximum adsorption capacities of Pb^{2+}, Cu^{2+}, and Cd^{2+} ions by oxidized CNTs calculated from Langmuir isotherm were 63.29, 23.89 and11.01 mg/g respectively in the following order Pb^{2+}>Cu^{2+}>Cd^{2+}. Their kinetic models of first, pseudo second and second order rate model fit the experimental data better than the two others. For initial metal concentration 30 mg/l the adsorption rate of Pb^{2+},Cu^{2+} and Cd^{2+} are 0.033,0.049 and 0.096 mg/g.min respectivey, in the order of Cd^{2+}>Cu^{2+}>Pb^{2+}. Rao et al., (2007) reported that, the sorption capacities of metal ions to different CNTs follow roughly the order: Pb^{2+} >Ni^{2+} >Zn^{2+} >Cu^{2+} >Cd^{2+}. The sorption capacities of metal ions by raw CNTs are very low, but significant, increase after oxidizing by HNO_3, NaOCl, and $KMnO_4$ solutions such surface oxidized CNTs show great potential as superior sorbents for environmental protection applications. The sorption mechanism appears mainly attributable to chemical interaction between the metal ions and the surface functional groups. The order of heavy metal ions removed from aqueous solutions by CNTs mentioned above shows that their adsorption does not depend clearly on the ionic radius of metal ions, but depend on properties of CNTs such as ionic strength, pH, foreign ions, CNT mass, contact time, initial metal ion concentration, and temperature. However, synthesis conditions have major influences on the nature of the CNTs product formed. Reaction conditions, including temperature, gas composition, and the nature and composition of metallic catalysts leading to the CNTs formation which in turn affects the properties of the final product still need to be explored in order to understand these influences.

Copper is an essential substance to human life, but in high doses, it can cause anemia, liver and kidney damages as well as stomach and intestinal irritation. This is the reason why copper becomes an unwanted material in wastewater. Li et al., (2010) reported that the

environmentally friendly adsorbent, the CNTs immobilized by calcium alginate (CNTs/CA) was prepared to adsorb copper. Its copper adsorption properties were investigated via equilibrium studies. Experimental results showed that copper removal efficiency of the CNTs/CA is high and reaches 69.9%, even at a lower pH of 2.1. The copper adsorption capacity of the CNTs/CA can attain 67.9 mg/g at the copper equilibrium concentration of 5 mg/L. In other cases, Li et al., (2001) reported that the adsorption isotherms were the best fluoride adsorption of Al_2O_3/CNTs. It occurs at a pH range of 5 to 9 with the adsorption capacity for Al_2O_3/CNTs of about 13.5 times higher than that of the AC-300 carbon and 4 times higher than that of the c-Al_2O_3 at an equilibrium fluoride concentration of 12 mg/l. The broad range of the pH values and high adsorption capacity of the Al_2O_3/CNTs indicates its suitability to be applied in fluoride removal from water.

Similar work has been reported by Ruparelia et al. (2008) to remove heavy metals such as the cadmium, lead, nickel and zinc studied on carbon nanomaterials (CNMs), the adsorption capacity of nanocarbon (NC), nanoporous carbon (NPC) and activation were tested. Nanoporous carbon was the best among other adsorbents due to its ion exchange with acidic, oxygen containing functional groups introduced by activation during the post treatment process as well as due to its unique nanoporous structure. They concluded that nanoporous carbon has a good potential in water treatment applications.

Many CNT applications require handling in solution-phase; however, CNTs have proven difficult to disperse in solvents (Ausman et al., 2000). Chemical modification of SWCNTs is often required for more versatile suspension capabilities and enablement of certain applications. This has encouraged greater exploitation of their intrinsic properties, as well as the capability to modify these properties. In particular, the functionalization of CNTs is required for their aqueous suspension and to allow for molecular interactions with

biological systems. Non-modified CNTs was surfactants that have been found to associate with CNTs via van der Waals interactions through their hydrophobic chains, rendering CNTs hydrophilic and able to disperse in aqueous environments. SWCNTs can be isolated from aggregated bundles (Strano et al., 2003), allowing for spectroscopic probing of individual SWCNTs. Surfactants have been used to prevent nonspecific interactions between SWCNTs and protein surfactants with modified head groups have also been used to link SWCNTs to specific molecules (Chen et al., 2001). Kim et al., (2005b) reported that lipids comprise a class of molecules that interact with CNTs similarly to surfactants. This class of molecule offers control of its interactions with CNTs through modification of their hydrophobic chains, while also providing versatility of the functionality that they impart through the modification of their head groups. Among these, chemical interaction between the heavy metal ions and the surface functional groups of CNTs is the major adsorption mechanism. Table 2.3 and 2.4 illustrates the brief summary of the removal of heavy metals using non-modified and functionalized CNTs.

Table 2.3: Brief summary of removal of heavy metal using non-modified CNTs.

Adsorbate & Adsorbent CNTs	**Initial Concentration (mg/L)**	**Optimised condition**	**Adsorption Capacity (mg/g)**	**Surface Area (m^2/g)**	**Reference**
Pb^{2+} MWCNTs	10-80	pH5, CNTs dosage 0.05 g, Temperature 280-321k	1	134	Li et al., (2002)
Pb^{2+} MWCNTs AC	10-60	pH5, Temperature 298 to 323K CNTs dosage1g, Equilibrium time 20 to120	4 18	162.16 1124.58	(Wang, Zhou, Peng, Yu, & Chen, 2007)
Zn^{2+} SWCNTs MWCNTs PAC	10-80	pH (8-11) Contact time 60 min	43.66 32.68 13.04	423 297 852	(Long and Yang, 2001)
Ni^{2+} As-produced CNTs	10-200	pH(2-8) Adsorption time,20-50 min CNTs dosage 20 mg	18.083	134	(Kandah and Meunier, 2007)
Ni^{2+} Sr^{2+} MWCNTs /iron oxides	6	pH6.5, CNTs dosage 2g, Temperature 298K	9.18 NA	88.53 NA	(Chen et al., 2009)
Pb^{2+},Cu^{2+} Cd^{2+} CNTs	5-60	pH5, CNTs dosage 0.05g, Temperature 298K	62.50 27.03 9.30	98.69	(Hsieh et al., 2006)

Cd^{2+} As grown CNTs	1.1-9.50	pH (2-12), CNTs (0.05-0.20 g), Contact time 4 hour	1.1 to 3.5	122	(Li, Wang, et al., 2003)
Cr^{6+} Normal AC AC coated with CNTs	0.5	pH(2-4), Contact time 60 min, Agitation speed 100-200 rpm	8.25 9.0	123 755.8	(Di, et al., 2006)
Cu^{2+} As-produced CNTs	43.1	pH (2-9), Ionic strength-0.01M, Temperature 280-320K, CNT dosage 0.5g/l.	8.25	82.2	(Wu, 2007)

Table 2.4: Brief summary of removal of heavy metals using functionalized CNTs.

Adsorbate &Adsorbent CNTs	**Initial Concentration (mg/L)**	**Optimised condition**	**Adsorption Capacity (mg/g)**	**Surface Area (m^2/g)**	**Reference**
Pb^{2+} Oxidized MWCNTs	10-60	pH5, Temperature 298 -323K, CNTs dosage 1g	59	237.33	(Wang, Zhou, Peng, Yu, & Chen, 2007)
Pb^{2+} Oxidized MWCNTs Pristine Annealed	10-100	Temperature 298K Oxidation 1 to 6 hr CNTs dosage 0.025	91 7.2 21	195.49 162.1 253.8	Wang et al., (2007)

Pb^{2+} Oxidized MWCNTs	1.0	pH7, Temperature 298K, Contact time 36 hours, CNTs dosage 3g	2.06–11.70	197	(Xu, et al., 2008)
Pb^{2+} Oxidized CNTs	10-80	pH5, Contact time 10 min, Temperature 298K CNTs dosage 0.05g	28	153	(Li, Di, et al., 2005)
Pb^{2+} Cu^{2+} Cd^{2+} Oxidized MWCNTs	10-60 5-30 2-15	pH(6-11), CNT dosage 0.05-0.3g	97.08 28.49 10.86	NA	Li et al., (2003)
Cu^{2+} Zn^{2+} Pb^{2+} Cd^{2+} Co^{2+} Oxidized CNTs	100-1200	pH7, Temperature-298K	50.37 58.00 101.05 75.84 69.63	NA	(Tofighy and Mohammadi, 2011)
Pb^{2+} MWCNTs	10-80	pH5, CNTs dosage 0.05g, Temperature 280-321K	15.6	145	Li et al., (2002)
Cd^{2+} Oxidized CNTs	1	pH7, CNTs dosage 10 mg, Contact time 120 min, Agitation speed 150 rpm Temperature 298K	34.36	NA	Kabashi et al., (2011)
Cd^{2+} Oxidized MWCNTs and ethylenediamine-functionalized MWCNTs (e-MWCNT)	0.1-5	pH(5.5-6.5), Temperature 318K, CNTs dosage 1mg Contact time 5-120 min	23.32 25.7	78.49 101.24	(Vuković, et al., 2010)

Cd^{2+} Oxidized CNTs HNO_3 $KMnO_4$ H_2O_2	1.1-9.50	pH (2-12) CNTs dosage (0.05-0.20 g) Contact time 4 hrs	5.1-11.8 11-19 2.6 -8.4	154 128 130	(Li, Wang, et al., 2003)
Cu^{2+} HNO_3-modified NaOCl-modified	43.1	pH (2-9), Ionic strength 0.01M, Temperature 280-320K, CNTs dosage 0.5g/l	13.87 47.39	64.3 94.5	(Wu, 2007)
Ni^{2+} MWCNTs (oxidized)	2-24	pH (2-9), Contact time 2 hours	NA	197	(Yang, et al., 2009)
Ni^{2+} (aq) Cu^{2+} (aq) Zn^{2+} (aq Cd^{2+} (aq) Oxidized CNTs	1–5	pH (2-12), Reaction time 4hr, CNTs dosage 0.15g	NA	77	(Gao, et al., 2009)
Ni^{2+} (aq) Oxidized CNTs	10-200	pH(2-8) Adsorption time 20-50 min, CNTs dosage 1g	49.261	145	(Kandah and Meunier, 2007)
Ni^{2+} Oxidized SWCNTs MWCNTs	10-80	pH(1-8), CNTs dosage 0.05 g, Agitation speed 180 rpm	47.85 38.46	397 307	(Lu and Liu, 2006)
Ni^{2+} Oxidized SWCNTs MWCNTs	10-80	pH7, CNTs dosage 1g, Contact time 12hour	47.86 38.46	380 323	(Lu et al., 2008)(84)

Ni^{2+} Oxidized CNTs	10-200	pH(2-8) Adsorption time 20-50 min CNTs dosage 20 mg	49.261	145	(Kandah and Meunier, 2007)

.

CHAPTER III

Experimental Methodology

3.1 Intoduction

This chapter is divided into two parts: experimental materials and experimental methods for production of CNTs and characterization of the produced CNTs. Details of materials, equipments and experimental procedures used are further discussed in this section.

3.2 Materials

There are three types of gases used in the production of CNTs namely, H_2 (99.99% purity), C_2H_2 (99.9%) and Ar (99%). All are analytical grade supplied by MOX Sdn. Bhd.

3.3 Catalyst

Ferrocene catalyst for analytical grade was purchased from Merck and used as received

3.4 Methods

Fig. 3.1 shows the flow chart of the overall experiment conducted throughout the research.

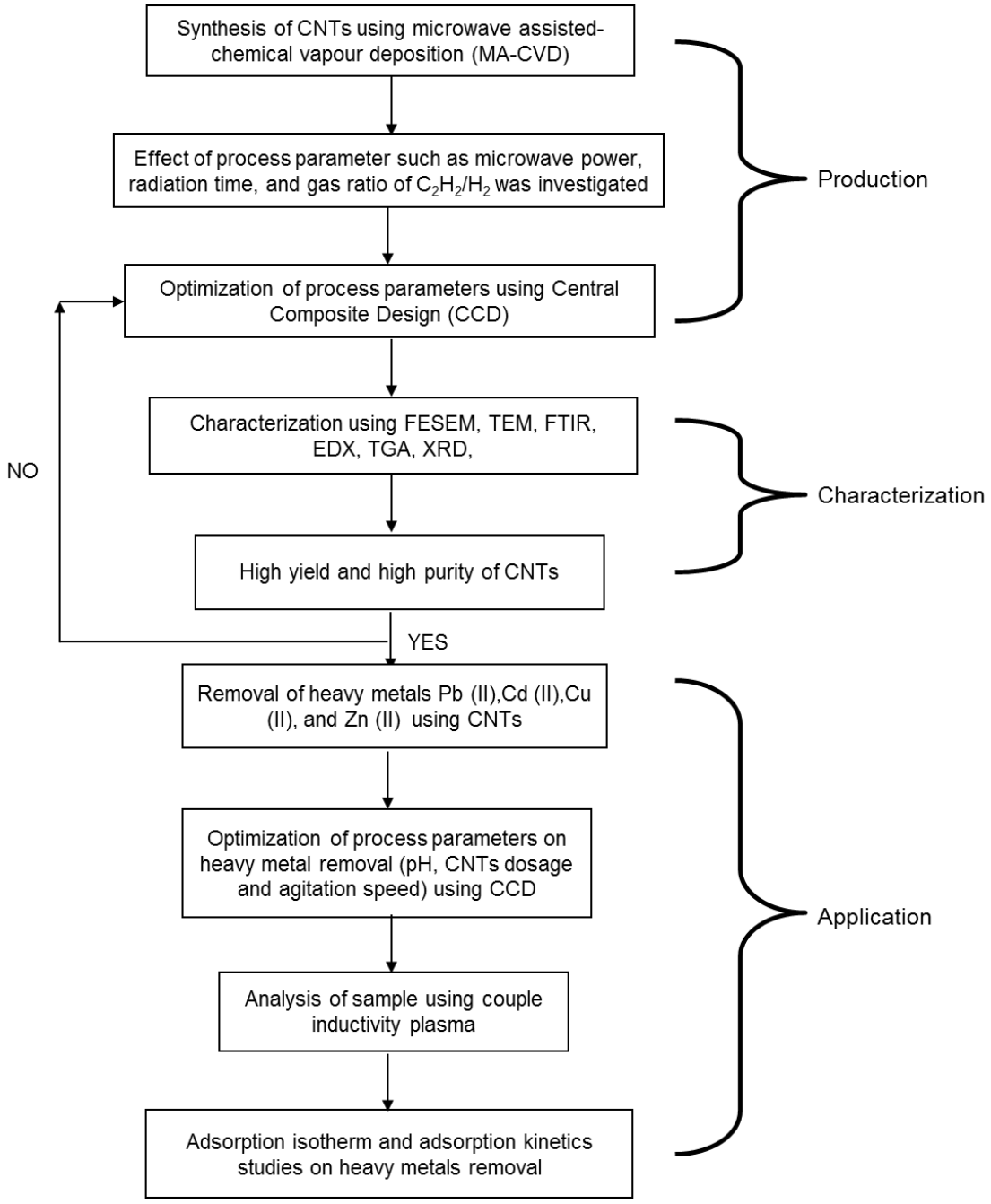

Figure 3.1: Flow chart of the overall experiment.

3.5 Production of CNTs using MA-CVD

Fig. 3.2 shows schematic of horizontal tubular microwave model Synotherm-T1500, (China) reactor for the production of CNTs. It comprised a quartz tube of 55 mm OD, 50 mm ID and 615 mm length. Ferrocene catalyst was placed at the entrance of the chamber

and quartz boat size was placed at the middle of the reaction chamber. The system was initially flushed with Ar in order to ensure an oxygen free environment. The gas flow rate of C_2H_2 and H_2 was free mixed before entering into the tubular microwave chamber using gas mixer Model KM-20-2, (Germany). The reaction was carried on for the desired time period and on completion, the total amount of CNTs produced in the quartz boats was collected and weighed.

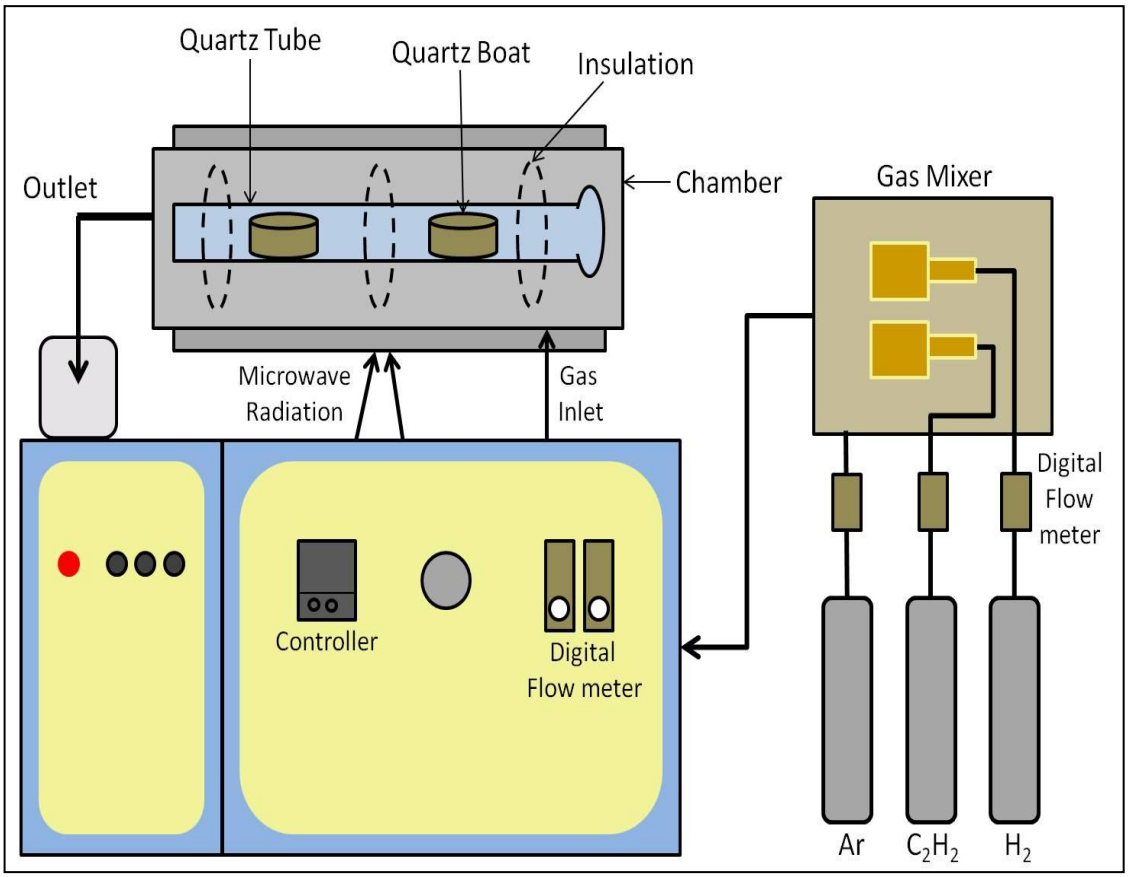

Figure 3.2: Schematic of MA-CVD for CNT production.

3.6 Design of experiment for CNTs production

Response surface methodology is a well know approach to optimizing the effects of multiple variables on the properties of prepared products using a combination of mathematical and statistical techniques (Amirhasan et al., 2007; Veziri et al., 2008). The

CNTs production parameters were studied using the standard response surface methodology with a central composite design (CCD). This method was chosen for fitting a quadratic surface with a minimum number of experiments. It also helps analyze the interaction between the effective process parameters and identify the factor settings that optimize response (Amirhasan, et al., 2007). Table 3.1 shows the ranges and levels of the dependent variables in this study, microwave power (A), radiation time (B) and gas ratio of C_2H_2/H_2 (C). The lower and upper values of each parameter (microwave power, radiation time and gas flow rates of C_2H_2/ H_2) were chosen based on previous study on the production of CNTs (Fonseca et al., 1998; Lacerda, Teo, et al., 2004; Mubarak, et al., 2011; Satishkumar, et al., 1998; Willems, et al., 2000). Acetylene flow rate was fixed at 40 ml/min and H_2 flow rate was being varied and catalyst was fixed to 0.2 g (Couteau, et al., 2003; Delzeit et al., 2002; Pérez-Cabero, et al., 2004). The CCD for three factors, two replicate, and two center points per block were selected for CNTs production because there were three parameters to be optimized. The total number of experimental runs for the production of CNT samples determined by the statistical software through the design of the experiment (DOE) were 24. The responses for each run based on the weight of CNTs (grams) were further statistically analyzed by the software for the determination of the optimum preparation conditions. Hence, this design was selected to reduce the number of experiments.

Table 3.1: A lower and upper limits for CCD experiments design for CNTs production

Factor	Name	Units	Low	High
A	Microwave Power	W	600	1200
B	Radiation time	min	10	60
C	Gas Ratio (C_2H_2/H_2)	-	0.2	1

3.7 Preparation of stock solution

Analytical grade Pb (II), Cd (II), Cu (II) and Zn (II) standard solution which was obtained from Merck was used to prepare stock solutions containing 1000 mg/L of Pb (II), Cd (II), Cu (II) and Zn (II) metal ions which were further diluted with distilled water to obtain the required concentrations. As for this research, the initial concentration of Pb (II), Cd (II), Cu (II) and Zn (II) metal ions was set to 10 mg/L and the prepared solution were used for batch adsorption experiments.

3.7.1 Optimization of removal of heavy metals

A batch adsorption experiment was performed by using conical flask of 250 ml of 10.0 mg/L of Pb (II) Cd (II) Cu (II) and Zn (II) agitated with varying dosages of CNTs and other variable parameters according to the design obtained from the Design of Expert (DOE). The lower and upper values of each parameter (pH, CNTs dosage, agitation speed and time) were chosen based on previous study on the removal of Pb (II), Cd (II), Cu (II) and Zn (II) (Azouaou, et al., 2010; Biškup and Subotić, 2005; Li, Luan, et al., 2003a, 2003b; Li, Wang, et al., 2002; Li, et al., 2010; Li, 2004; Lu, et al., 2006b; Machida et al., 2004; Meena et al., 2008; Mubarak, et al., 2013; Tofighy and Mohammadi, 2011; Ye and Yu, 2010). The parameters used for this research is as shown in Table 3.2, 3.3. 3.4 and 3.5 for Pb (II), Cd (II), Cu (II) and Zn (II) respectively. Statistical optimization of process parameters, pH,

CNTs dosage, agitation speed and time using CCD with two centre points and one replicate was selected for the optimization process for removal of Pb (II), Cd (II), Cu (II) and Zn (II) from aqueous solution. The total number of experimental runs for the each heavy metal removal samples determined by the statistical software through the design of the experiment was 26 runs. The initial pH of the stock solution was adjusted by using 1 M of NaOH by adding in a few drops of the alkaline solution in the 250 ml of 10 mg/L of Pb (II), Cd (II), Cu (II) and Zn (II) until the desired pH was obtained. The CNTs were then added into the 250 ml of 10 mg/L of Pb (II), Cd (II), Cu (II) and Zn (II) solutions and it was agitated according to the parameters displayed in Table 3.2, 3.3, 3.4 and 3.5. At the end of each interval of the time, the suspensions were shaken and centrifuged at 4000 rpm for 10 min and the supernatant was withdrawn and filtered by using the ADVANTEC qualitative filter paper no. 161 having a pore size of 3 µm. The filtrates were analyzed for contaminants by inductively coupled plasma optical emission spectrometry (ICP-OES) (Perkin Elmer 7000 DV) using a Perkin-Elmer multimetal standard solutions. The experimental errors of ICP-OES were within the range of ±2.461% to ±2.983%. The Zn (II) residual concentrations were measured from the standard calibration curve. All the data presented are the average of three replicates. Differences between the initial and the equilibrium metal ion concentrations determine the amount of metal ions being absorbed. The adsorption capacity of CNTs at a specific time, t as for the adsorption kinetic study were calculated by using equation (3.1) while the adsorption equilibrium for Pb (II), Cd (II), Cu (II) and Zn (II) was determined by equation (3.2).

$$q_t \text{ (mg/g)} = [(C_o - C_t)V] / m \quad (3.1)$$

$$q_e \text{ (mg/g)} = [(C_o - C_e)V] / m \quad (3.2)$$

where Co represent the initial concentration of Pb (II), Cd (II), Cu (II) and Zn (II) solution (mg/L), q_t represents the concentration of Pb (II), Cd (II) , Cu (II) and Zn (II) at time t (mg/g), C_e represents the equilibrium concentration of Pb (II),Cd (II), Cu (II) and Zn (II) (mg/L) respectively, V represents the volume of Pb (II) Cd (II) , Cu (II) and Zn (II) stock solution (L) and m indicates the weight of the adsorbent used (g).

Table 3.2: Experimental design for batch adsorption of Pb (II) removal using CCD.

Factor	**Name**	**Units**	**Low**	**high**	**Low coded**	**High coded**
A	pH		4	6	-1	1
B	Agitation Speed	rpm	120	200	-1	1
C	MWCNTs dosage	g	0.05	0.15	-1	1
D	Contact Time	min	5	40	-1	1

Table 3.3: Experimental design for batch adsorption of Cd (II) removal using CCD

Factor	**Name**	**Units**	**Low**	**high**	**Low coded**	**High coded**
A	pH		4	6	-1	1
B	Agitation Speed	rpm	120	200	-1	1
C	MWCNTs dosage	g	0.05	0.15	-1	1
D	Contact Time	min	20	80	-1	1

Table 3.4: Experimental design for batch adsorption of Cu (II) removal using CCD.

Factor	Name	Units	Low	high	Low coded	High coded
A	pH		2	8	-1	1
B	Agitation Speed	rpm	120	200	-1	1
C	MWCNTs dosage	g	0.05	0.15	-1	1
D	Contact Time	min	10	60	-1	1

Table 3-5: Experimental design for batch adsorption of Zn (II) removal using CCD.

Factor	Name	Units	Low	high	Low coded	High coded
A	pH		8	12	-1	1
B	Agitation Speed	rpm	120	200	-1	1
C	MWCNTs dosage	g	0.05	0.15	-1	1
D	Contact Time	min	10	110	-1	1

3.7.2 Adsorption iostherms study

Adsorption equilibrium capacities of heavy metals on CNTs at various equilibrium heavy metals concentrations were studied in the best fit adsorption isotherm model. To understand the interaction between the metal ion and the adsorbent, a number of models such as Langmuir, Freundlich, Temkin and Dubinin –Radushevich isotherm models were applied to analyze the experimental data. In order to study the adsorption process shake flask experiments were carried out for 2 h at room temperature, as obtained in the optimization process. The adsorption study was performed using various Pb (II), Cd (II), Cu (II) and Zn

(II) concentrations from 10 to 80 mg/L were employed to perform adsorption equilibrium isotherm experiments. The adsorption runs were conducted at conditions of pH 5, pH5, pH 5.5 and pH 10 and CNTs dosage of 0.1, 0.1, 0.1 and 0.05g for Pb (II) Cd (II), Cu (II) and Zn (II) respectively. On the other hand, agitation speed of 160 rpm for Pb (II), Cd (II) and Cu (II), while, 120 rpm for Zn (II). The sample was collected at various time intervals (5 to 120 min) the equilibrium concentration was achieved before 1 hour and conformed after 2 h. At the end of each interval of the time, the solution was filtered by using filter paper. The final Pb (II), Cd (II), Cu (II) and Zn (II) concentration was determined by inductively coupled plasma optical emission spectrometry (ICP-OES) (Perkin Elmer). Differences between the initial and the equilibrium metal ion concentrations determine the amount of metal ions being adsorbed. The adsorption capacity of CNTs at a specific time, t as for the adsorption kinetic study was calculated by using Equation (3.1 and 3.2)

The Langmuir isotherm for the adsorption of heavy metals on CNTs was determined from plotting the relation between equilibrium concentrations Ce of heavy metals adsorption in the X-axis versus Ce/qe in the Y-axis. The linearized Langmuir equation is represented as follows:

$$\frac{C_e}{q_e} = \frac{1}{K_L \cdot q_m} + \left(\frac{1}{q_m}\right) C_e \qquad (3.3)$$

Where q_e (mg/g) and C_e (g/L) are the amount of adsorbed heavy mteals per unit weight of adsorbent and the unadsorbed heavy metals concentration in solution at equilibrium, K_L is the equilibrium constant or Langmuir constant related to the ffinity of binding sites (L/g) and q_m represents a particle limiting adsorption capacity when the surface is fully covered with heavy metals (maximum adsorption capacity) and assists in the comparison of

adsorption performance. q_m and K_L were calculated from the slope and intercept of the straight line C_e/q_e versus Ce graph.

Freundlich isotherm for the adsorption of heavy metals on CNTs was also studied by plotting the relation between ln Ce in the X-axis versus ln qe in the Y-axis.The linearised Freundlich equation was expressed by logarithmic as follows:

$$\ln\ q_e = \ln K_F + 1/n \ln\ C_e \qquad (3.4)$$

Where q_e (mg/g) is the amount of adsorbed heavy metals per unit weight of the adsorbent at equilibrium, K_F is a Freundlich constant that shows the adsorption capacity of adsorbent, and n is a constant which shows the greatness of the relationship between adsorbate and adsorbent. n and K_F were determined from the slope and intercept of the linear plot of ln qe versus ln Ce.

The Temkin isotherm contains a factor that explicitly taking into the account of adsorbent–adsorbate interactions. By ignoring the extremely low and large value of concentrations, the model assumes that the heat of adsorption (function of temperature) of all molecules in the layer would decrease linearly rather than logarithmic with coverage. The isotherm can be represented by the following equation:

$$q_e = \frac{RT}{b} \ln(AC_e) \qquad (3.6)$$

$$q_e = \text{B ln A} + \text{B ln } C_e \qquad (3.7)$$

where B=RT/b, R is universal gas constant (8.314 J mol^{-1} K^{-1}), T defined as absolute temperature (K), b is the Temkin constant related to heat of adsorption (J mol^{-1}) and A the

Temkin isotherm constant (L g^{-1}). The constants A and B are calculated from the slope and intercept of qe versus ln Ce plot.

Dubinin–Radushkevich isotherm is generally applied to express the adsorption mechanism with a Gaussian energy distribution onto a heterogeneous surface. The model has often successfully fitted high solute activities and the intermediate range of concentration data. The isotherm can be expressed by the following equation.

$$ln\ q_e = ln\ q_m - K\varepsilon^2 \quad (3.8)$$

Where K and ε^2 are Dubinin –Radushkevich isotherm constant. The saturation adsorption capacity q_m and K were calculated from the intercept and slope of ln qe versus ε^2.

3.7.3 Adsorption kinetics

Adsorption kinetics have been proposed to elucidate the adsorption mechanism. The mechanism of adsorption depends on the physical and chemical characteristics of the adsorbent as well as on the mass transport process. In order to investigate the mechanism of adsorption of magnesium on magnetic biochar derived from rice husk and examine the potential rate, the capability of pseudo-first order (Langergren, 1898) and pseudo-second order (Ho and McKay, 1999b) kinetic model were examined in this study.

The differential equation of a pseudo first order kinetic is as follows:

$$\frac{dq_t}{dt} = K_1\ (\ q_e - \ q_t) \quad (3.9)$$

Integrating Equation (3.9) for the boundary conditions t=0 to t = t and q_t = 0 and $q_t = \ q_t$ gives:

$$Log(q_e - \ q_t) = logq_e - \left(\frac{K_1}{2.303}\right)t \quad (3.10)$$

Where q_e and q_t refers to the amount of adsorbed (mg/g) at equilibrium and at any time t respectively while K_1 is the equilibrium rate constant h^{-1}. The rate constant was calculated from the slope of the straight line of plot $Log(q_e - q_t)$ versus t.

On the other hand, a pseudo second order equation based on the adsorption capacity is expressed in the form:

$$\frac{dq_t}{dt} = K(q_e - q_t)^2 \quad (3.11)$$

Integrating the equation above for the boundary conditions, t=0 to t = t and q_t = 0 and $q_t = q_t$ rearranging the final equation as:

$$\frac{t}{q_t} = \frac{1}{K_2 . q_e{}^2} + \frac{1}{q_e} \quad (3.12)$$

Where K_2 is the equilibrium rate constant (g /(mg.h)). K_2, q_e were calculated from the intercept and slope of the straight line plot of t/q_t versus t.

3.8 Characterization of CNTs

The scanning electron microscopy (Brand: Zeiss Model: Auriga) was used to characterize the morphology (diameter and the length) of the deposited powder, while the structure was characterized using the transmission electron microscopy (TEM) for the selected sample. The SEM gives good results in characterizing the length and the diameter of the CNT and because it is used to scan only the surface of the sample, but it cannot be used to distinguish between the structure of the CNT, while the TEM is the best way to distinguish between them.

3.8.1 Field Emission Scanning Electron Microscopy

Field Emission Scanning electron microscopy (FESEM) model Zeiss Auriga, Japan, has an ultimate lateral resolution of a nanometer (depending on the type of the electron gun employed), making it a useful alternative to light microscopy for detailed examination of material having micro and nano structures. FESEM makes use of a tightly focused, energetic electron beam, which is swept across the surface of the sample in a raster-scan pattern (this is similar to how the cathode ray tube in your TV works). Secondary electrons are emitted from the sample and detected, which forms the image observed.

3.8.2 Transmission Electron Microscopy

Transmission electron microscopy (TEM) provides the visualization of the internal structure of specimens by the use of transmitting electrons. Because electrons have a much smaller wavelength than that of visible light, microscopy-using electrons offers a much greater (50,000x) resolving power than light microscopy. Because electrons have a very limited range transiting matter, TEM samples must be very thin and they must be placed in a vacuum inside the instrument. The structure of the CNT was characterized using TEM model Hitachi H-7100, Japan and high-resolution TEM (HRTEM) model JEOL JEM 2100F, Japan.

3.8.3 Thermogravimetric Analysis

TGA measures changes in weight of a sample with increasing temperature. Moisture content and presence of volatile species can be determined by this technique. Computer controlled graphics can calculate weight percent losses. The dynamic thermogravimetric were carried out on small samples (about 10 mg) with an airflow rate of 300 cm^3/min. The

maximum temperature was 1100 ℃ and the typical heating rate was 10° per minute. The purity measurements of CNTs were carried out by using TEM images and TGA. The TEM images were taken from various locations of the sample. After finishing the scanning of the sample, serial analysis was carried out in order to measure the purity. The purity of the CNT was determined by Thermogravimetric Analysis (TGA) model Pyris diamond TG/DTA, USA. The TGA was used to study the thermal stability of the products in order to distinguish the deposited carbons according to their different thermal stability level.

3.8.4 BET surface area

Physical characterization of CNTs produced at the optimum condition was analyzed with Autosorb 1 surface area analyzer by nitrogen adsorption at -77 K. Prior to analysis, the samples were degassed at 200 ^{o}C for 3 hrs. Surface area was calculated by the BET (Brand: Quanta Chrome Model: Autosorb 6B) equation using the nitrogen adsorption data. The adsorbed nitrogen volumes and various equilibrium pressures, and BET surface area of the sample were reported using the computer - monitoring system.

3.8.5 Raman spectra Analysis

The graphitization of the CNT samples was determined by using Raman spectroscopy model Renishaw inVia, USA at a wavelength of 532 nm with green laser excitation.

3.8.6 XRD analysis

The crystalline information of CNTs was observed using XRD patterns by using model Siemens D-500 X-ray, diffractemeter, USA.

3.8.7 Inductively Couple Plasma

The heavy metal ion concentrations were measured by Inductively Couple Plasma (ICP) at 283.307 nm, 228.802 nm, 327.393 nm and 206.2 nm Zn (II) for Pb (II) Cd (II), Cu (II) and Zn (II) respectively.

3.8.8 FTIR analysis

Fourier Transform Infrared (FTIR) spectroscope (Brand: Bruker, Model: IFS66v/S) was used to analyze the CNTs for determination of the surface functional groups.When light travels across the boundary between two materials causes reflection of some of the light. The proportion of reflected light is a function of the angle of incidence, θi, at which the light encounters the boundary. By measuring the attenuated total reflection as a function of wavelength, an adsorption spectrum of absorbing medium is obtained.

CHAPTER IV

RESULTS AND DISCUSSION

4.1 Introduction

In this research, microwave induced MWCNTs synthesized using the single stage MA-CVD, using acetylene and hydrogen as the precursor gases, and ferrocene as catalyst. The effect of process parameters such as microwave power, radiation time and gas ratio of C_2H_2/H_2 was investigated. The preparation conditions were statistically optimized using central composite design (CCD) to produce the high quality and high weight of MWCNTs and detailed characterization of MWCNTs was investigated. The optimized condition of MWCNTs has high BET 206 m^2/g surface area and proved to be an outstanding adsorbent for the removal of Pb (II), Cd (II), Cu (II) and Zn (II) from aqueous solution. The statistical optimization of process parameters such pH, MWCNTs dosage and agitation speed and time of removal of Pb (II), Cd (II), Cu (II) and Zn (II) were investigated using novel MWCNTs. The studies on the isotherm kinetic (Langmuir, Freundlich, Temkin and Dubinin isotherm) and isotherm model (pseudo-first order and pseudo-second order) were developed and furthermore thermodynamic parameters were investigated on Pb (II), Cd (II), Cu (II) and Zn (II) adsorption are also reported in this chapter.

4.2 Effect of process parameters on synthesis of CNT

CNTs production requires the knowledge of optimum microwave power, radiation time and gas ratio of C_2H_2/H_2 ratio. The effects of process parameters on the synthesis of the CNT were studied to enhance higher yield with high purity. The effects of each process parameter were further discussed in the following section.

4.2.1 Effect of microwave power

The effect of microwave power on the weight of CNTs and purity is illustrated in Fig. 4.1 The microwave power influence on the structure of the carbon nanomaterials has been emphasized. It is generally accepted that carbon materials are formed by the carbon atom dissolving, diffusing, and precipitating through the catalyst droplets in a CVD process (Ishioka et al., 1993; Ishioka et al., 1992; Kato et al., 1993; Muataz, 2003; Mubarak, et al., 2011). The dissolving, diffusing and precipitating rates of the carbon atoms are affected by both the carbon atom concentration and the microwave power. It was found that increase in microwave power from 600 to 900 W (the temperature inside microwave for 250 to 520 ^{o}C) increase weights and purity of CNTs was observed. Therefore, a maximal CNTs growth rate and high purity (98%) occurs at 900W (temperature of 520 ^{o}C where both of the carbon diffusion and catalyst activity are optimized (Hayashi et al., 2006; Huang, Chuang, et al., 2003). The carbon solubility and diffusion in catalyst metals have been recognized as important factors for CNT growth, but are difficult to quantify. When the microwave power was less than 900 W, the size of the catalyst was very small and the diffusion rate of C atoms onto Fe particle was also low, for this reason small amount of carbon nanostructure materials were formed. By increasing the microwave power, the size of the Fe catalyst increased, and this leads to the gradual growth of the C atoms on the catalyst. At a low microwave power, a decrease in the formation of CNTs has been observed, possibly due to the partial deactivation of catalyst and the carbon concentration from the decomposition of C_2H_2 over an iron catalyst is certainly low (Pérez-Cabero, et al., 2004; Taniguchi, et al., 2005). Furthermore, increase microwave power to 1000 W (the temperature inside microwave of 540 ^{o}C and above), and above decreased the weight of

CNTs and purity due to weight loss of carbon (Chhowalla, et al., 2001; Huang, Wang, et al., 2003). This is due to the diffusion rate of iron particles into carbon fibers was enhanced and the CNT growth possibility is reduced (Brunetti, et al., 2007; Kim, Kim, et al., 2005; Li, Chen, et al., 2002). Another possible reason is related to the catalyst distribution on the substrate, the available carbon flux arriving on the catalysts, and the carbon solubility and diffusion in catalysts, which are controlled by process parameters including the inputs of a gas ratio and microwave power. Microwave power a vital role in the formation of high weight of CNTs and high purity of CNTs.

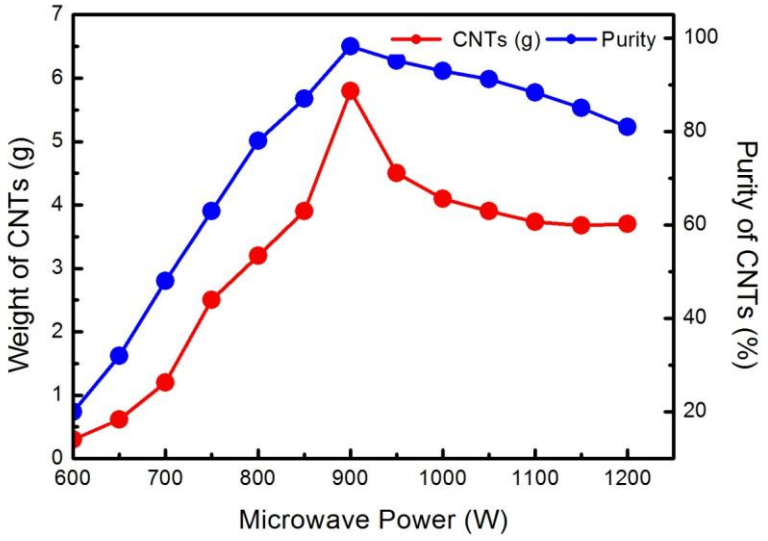

Figure 4.1: Effect of microwave power on weight of CNTs and purity.

4.2.2 Effect of radiation time

Fig. 4.2 shows the effect of microwave radiation time on the weight of CNTs. Besides microwave power, radiation time is an important process variable for synthesis of high weight of CNTs. It was clearly observed that as radiation time increases from 10 to 35 min increased in the amount of CNTs formation was also observed. The maximum amount of

CNTs (5.8 g) was produced at the radiation time of 35 min. It is also observed that when the radiation time was 10 min, only a small amount of CNTs (0.3 g) formed due to the diffusion rate of Fe particles and C atoms which were very low. When the reaction time was increased, the growth time needed to grow the CNTs increased, reaching a maximum at 35 min. Further increase in radiation time decreases in the amount of CNTs deposited. The typical reaction time is approximately 60 min, but the reaction time also depends on the desired CNTs amount. Furthermore, deviations of the optimum reaction time for the specific synthesis suffer from the quality of the final product. It is also noted that the yield is proportional to the time of reaction (Nagaraju, et al., 2002; Nuchter, et al., 2004). In other word, the radiation time in MA-CVD did not appear to be a major factor in controlling the formation of the CNTs. However, it has a pronounced effect on the purity and the weight of CNTs.

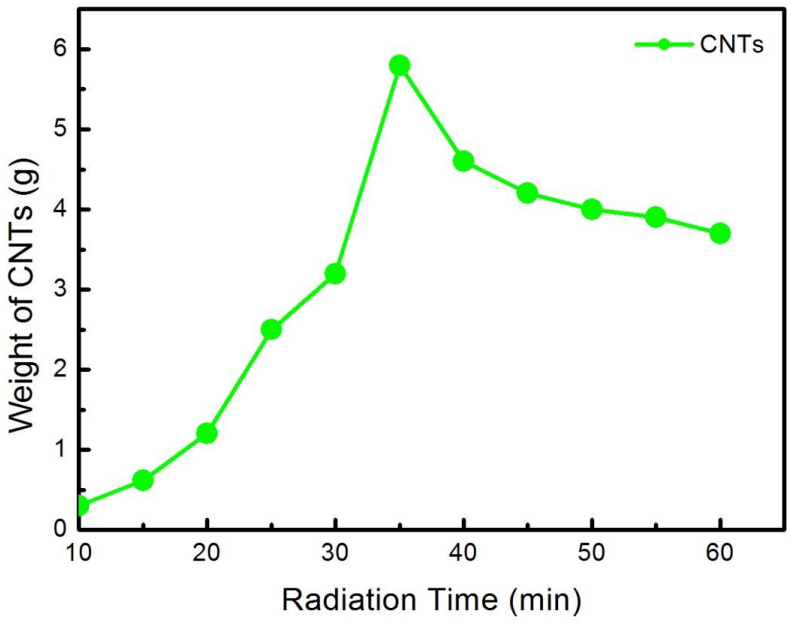

Figure 4.2: Effect of radiation time on weight of CNTs.

4.2.3 Effect of Gas ratio

Gas ratio (C_2H_2/H_2) plays a significant role in the formation of CNTs as being the carrier and reactant gas in the floating catalyst method. Fig. 4.3 shows the effect of gas ratio of weight of CNTs produced. It was clearly observed that as the gas ratio (0.2 to 0.6) increase, the amount of CNTs also increased drastically. The C_2H_2/H_2 input had a slight effect on decreasing the weight of CNTs after 0.6 gas ratio. For most of the situations, CNT growth rates increased with increasing gas ratio, the maximal amount of CNTs enhanced at microwave power 900 w with a gas ratio of 0.6 (Kuo, et al., 2006; Quinton, et al., 2013). A further increase in the gas ratio decreased the amount of the CNT was observed. Synthesis of CNTs depends on the gas flow rate, hydrocarbon concentration, microwave power, size and shape of the initial agglomerate and catalyst loading and size. The gas flow rate affects the mass transfer coefficient, the size and shape of the agglomerate influences the internal diffusion of gas within the pore, the microwave power, hydrocarbon concentration and catalyst loading determine the reaction rate. The morphology of CNTs depends on the type and size of catalyst and the carbon supply rate (Danafar, et al., 2009; Vázquez and Prato, 2009). Hence, the effect of gas ratio and microwave power is very important parameter for synthesis of high quality and high amount of CNTs.

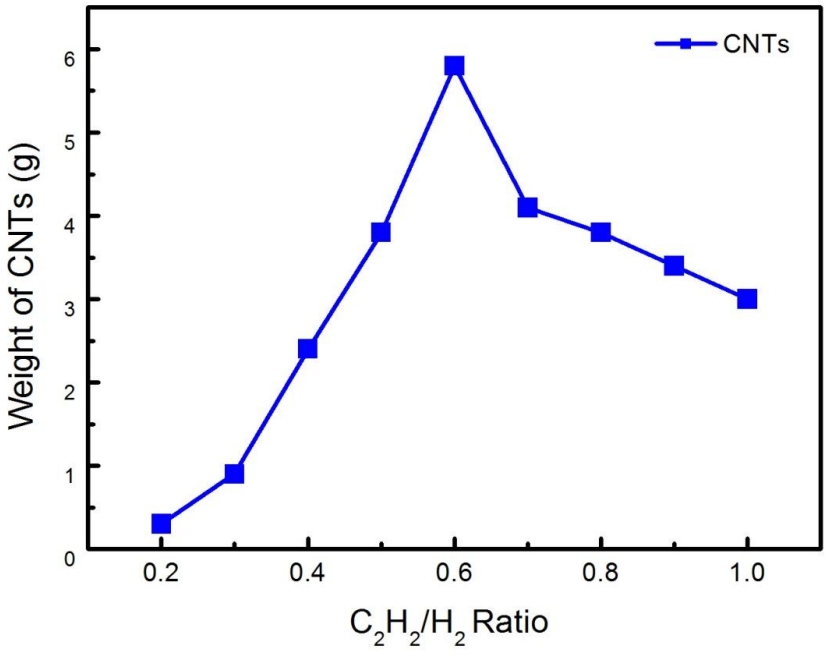

Figure 4.3: Effect of gas ratio on weight of CNTs at optimal CNTs.

4.3 Statistical optimization of CNTs production

CCD was employed to attain all possible combinations of all the input factors with minimum number of experimental runs that could possibly optimize the response within the region of three dimensional observation spaces. The results from the experiments were analyzed using analysis of variance (ANOVA) in the design of experiment (DOE). The variables such as microwave power, radiation time, and gas ratio of C_2H_2/H_2 were employed for the analysis in the design to obtain the weight of CNTs.

Detailed overview of design expert software as shown in appendix E. In addition, a detailed experimental array of CNTs production using microwave heating as shown in appendix A. The results from the analysis are shown in Table 4.1 the regression equation that models the relationship between the variables was presented. In equation (4.1) the significance of the

model parameters was assessed by the values of probability>F-values, lack of fit, and also the curvature of F. The pattern of interactions between the variables is indicated by these coefficients. The variables with low probability levels contribute to the model, whereas the others can be neglected and eliminated from the model. The larger the magnitude of F-value and smaller the probability>F-values indicate the higher significance of the corresponding coefficient. The probability value is the probability of obtaining a value at least as extreme as the one actually obtained. For a significant and convincing coefficient, the probability values must be smaller than 0.05. The ANOVA of the quadratic regression model demonstrates the significances of the model. For this optimization study, the ANOVA of quadratic regression model demonstrated that the model was highly significant, as evident from the Fisher's F-test with a very low probability value [(Prob > F) = 0.0001]. The fisher F-test value signifies how the mean square of the regressed model compared to the mean square of the residuals (errors). Note that the greater the F value, the more efficient the model. Meanwhile, lower probability (P value) demonstrates the higher significance of the regression model. The F-test which is 26.01 implies that the model is significant. ANOVA shows an F test value of less than 0.05 implies that the model is also significant. Furthermore, the value of the correlation coefficient (R^2 = 0.99) and the adjusted determination coefficient (R^2Adj=0.98) are both very close to one, indicating a high significance of the model. The developed model Equation (4.1) is as follows.

Weight of CNT = 5.28 +0.44 * A +0.14 * B -0.11 * C -2.55* A^2 -0.74 * B^2 -1.44 *C^2

+0.088* A * B -0.069 * A * C +0.088 * B * C (4.1)

Consequently, variables A, B, C, AB, AC and BC were significant model terms. This indicates that the microwave power (A), radiation time (B) and gas ratio (C) were highly significant as the values of Probe >F was 0.002. The ANOVA of the quadratic regression

model demonstrates the significances of the model. In the analysis of CNTs yield through the coefficient values from the equation of regression model, it is shown that the microwave power gives higher positive effect as compared to the radiation time. On the other hand, gas ratio of C_2H_2/H_2 is giving negative effects. Thus, in short, the coefficient values obtained show that all the process parameter chosen to be investigated in the optimization experiments influenced the weight of CNTs in the production process. The effect of each interaction process parameter was further analyzed by statistical software and the discussion regarding the matter are noted in the following section. Fig. 4.4 shows theoretical values versus the experimental values for CNTs yield. It was clearly shown that the theoretical values obtained were quite close to experimental values, indicating that the model developed was successful in bridging the correlation between process parameters to the yield of CNTs.

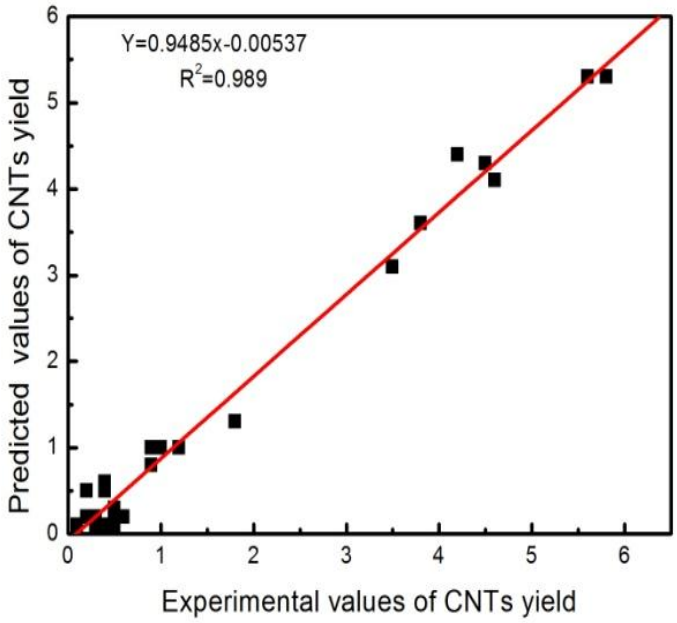

Figure 4.4: Relationship between Predicted and Experimental values of yield of CNTs

Table 4.1: ANOVA for the selected factorial Model for CNTs production.

Source	Sum of squares	DF	Mean square	F Value	Prob > F	Status
Model	78.33	9	8.7	26.01	0.0001	Significant
A	3.36	1	3.56	6.54	0.002	
B	0.34	1	0.34	0.63	0.004	
C	0.22	1	0.22	0.4	0.053	
A^2	17.61	1	17.61	32.39	0.0001	
B^2	1.47	1	2.71	2.71	0.012	
C^2	5.60	1	10.31	10.31	0.006	
AB	0.12	1	0.12	0.23	0.063	
AC	0.076	1	0.076	0.14	0.071	
BC	0.12	1	0.12	0.23	0.064	
Residual	7.61	14	0.54		0.0234	
Lack of fit	6.48	5	1.3	10.36	0.65	Insignificant
Pure Error	1.13	9	0.13			
Cor Total	85.96	23				

4.3.1 Effect of process parameters on CNTs production

The 3D response surface and the contour plots are the graphical representation of the regression equation in order to determine the optimum values of the variables (Ishioka, et al., 1992). The main target of response surface is to obtain the optimum values of the variables efficiently in such a way that the response is maximized (Veziri, et al., 2008). The maximum predicted value is referred by the surface confined in the smallest ellipse in the contour diagram. The perfect interaction between the independent variables can be shown when elliptical contours are obtained (Mubarak, et al., 2011; Veziri, et al., 2008). Each contour curve represents an infinitive number of combinations of two test variables. The graphical representations of the model equation facilitate an examination of the effect of process parameters on CNTs production, 3D surface and contour plots between

production factors were obtained using the DOE. The effect of each interaction process parameter was further analyzed by statistical software and the discussion regarding the matter are noted in the following section.

4.3.2 Effect of radiation time and microwave power on weight of CNTs

Fig. 4.5 (a-b) represents the contour and 3-dimensional plot of the production of CNTs affect by variables are radiation time and microwave power to weight of CNTs. All the 3-dimensional surface and contour plot is almost perfectly elliptical indicated that a good interaction between radiation time and microwave power. It was observed that the weight of CNT reached to the maximum when the radiation time and microwave power is at its center point. Further increase in radiation time and microwave power resulted in weight of CNT decreased. Due to deviations of the optimum radiation time for the specific synthesis suffer from the quality of the final product. On the other hand, when the microwave power was less than 900 W, the size of the catalyst was very small and the diffusion rate of C atoms onto Fe particle were also low, for this reason small amount of carbon nanostructure materials were formed. From the observed increase in microwave power from 600 to 900 W increase the in weight of CNT linearly increased (Benito et al., 2009a; Choi, et al., 2000; Ikuno et al., 2002; Lacerda, et al., 2004). At 900 W microwave power, the size of the Fe catalyst increased, and this leads to the gradual growth of the C atoms on the catalyst (Huang, Chuang, et al., 2003). Further increase in microwave power from 900 to 1200 W decrease in weight of CNT (Clauss et al., 2010; Hong, et al., 2003; Muataz et al., 2003; Vivas-Castro, et al., 2011) . This is due to the diffusion rate of iron particles into carbon fibers was enhanced and possibly lead to the decrease of the CNT growth (Li, Chen, et al., 2002; Zeng, et al., 2010). It is also noted that the weight of CNTs is proportional to the

radiation time (Nagaraju, et al., 2002). In other word, the radiation time in MA-CVD did not appear to be a major factor in controlling the formation of the CNTs. However, it has a significant effect on the purity and the weight of CNTs. Hence, microwave power plays a vital role in the formation of high yield and high quality of CNTs (Huang, Wang, et al., 2003; Lee et al., 2013).

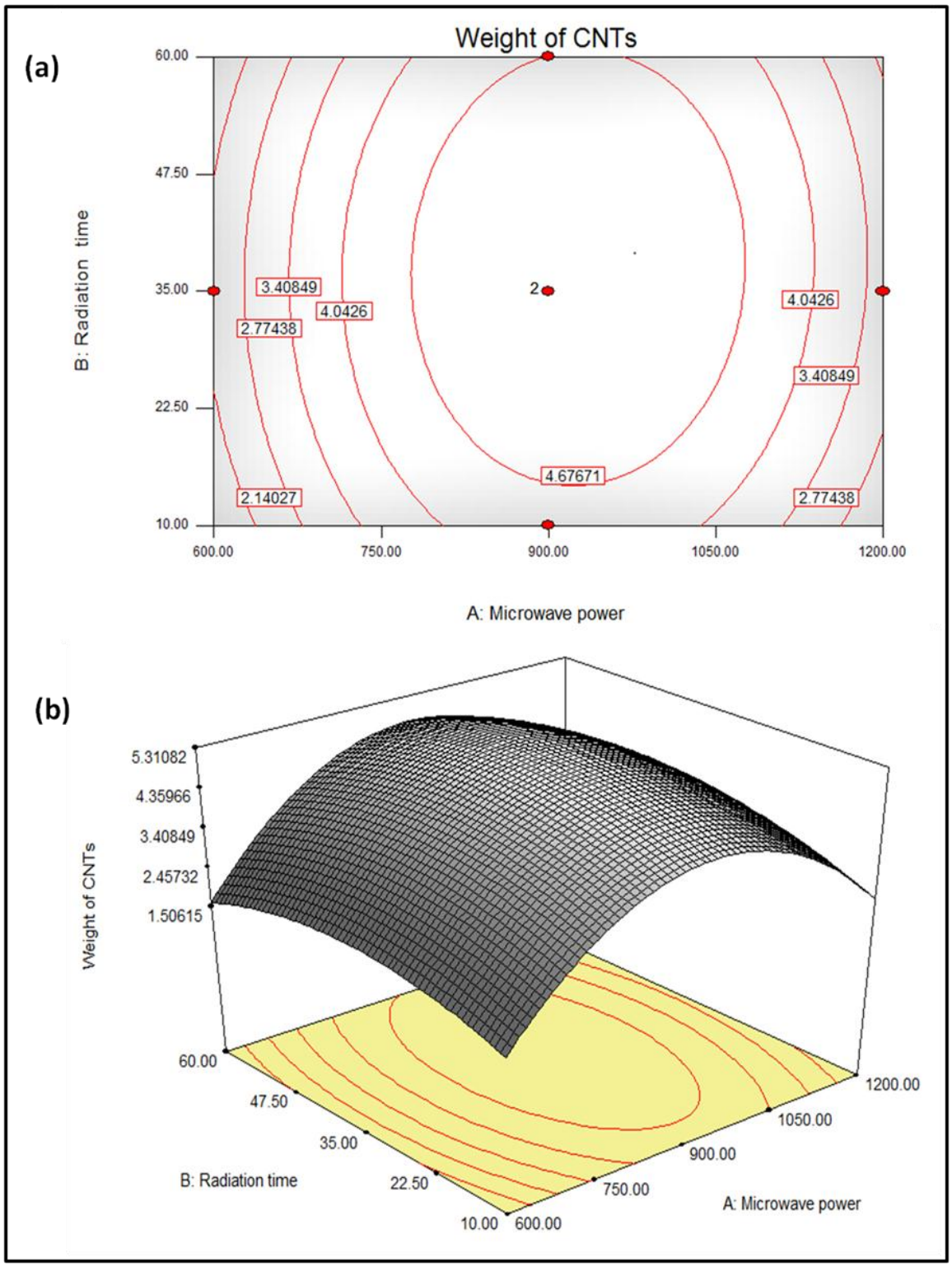

Figure 4.5: (a-b): Effect of radiation time and microwave power on CNT production.

.

4.3.3 Effect of gas ratio and microwave power on weight of CNT

Fig. 4.6 (a-b) shows the interaction between gas ratio and microwave power. It was observed that 3-dimensional surface and contour plot is perfectly elliptical indicated that all interaction was perfectly optimized to obtain the high weight of CNTs (Ishioka, et al., 1993; Ishioka, et al., 1992; Kato, et al., 1993). The weight of CNT reached to the maximum when the gas ratio and microwave power are at 0.6 and 900 W respectively (Hayashi, et al., 2006; Kuo, et al., 2005; Kuo, et al., 2006). By increasing and decreasing both parameters from its center point will result in decreasing the weight of CNTs. A further increase in the gas ratio of 0.6 to 1 and microwave from 900 to 1200 W decreased the amount of the CNT was observed. Production of CNTs depends on the hydrocarbon concentration, gas flow rate, microwave power, size and shape of the initial agglomerate and catalyst loading and size. The gas flow rate affects the mass transfer coefficient, the size and shape of the agglomerate influences the internal diffusion of gas within the pore, the microwave power, hydrocarbon concentration and catalyst loading determine the reaction rate. The growth rate of CNTs is a function of catalyst particle size and the diffusion rate of carbon through the catalyst (Kim, et al., 2003). The morphology of CNTs depends on the type and size of catalyst and the carbon supply rate (Danafar, et al., 2009). Therefore, the effect of gas ratio and microwave power is very important parameter for synthesis of high quality and high amount of CNTs (Kuo, et al., 2005; Lee, et al., 2002; Teng et al., 2013).

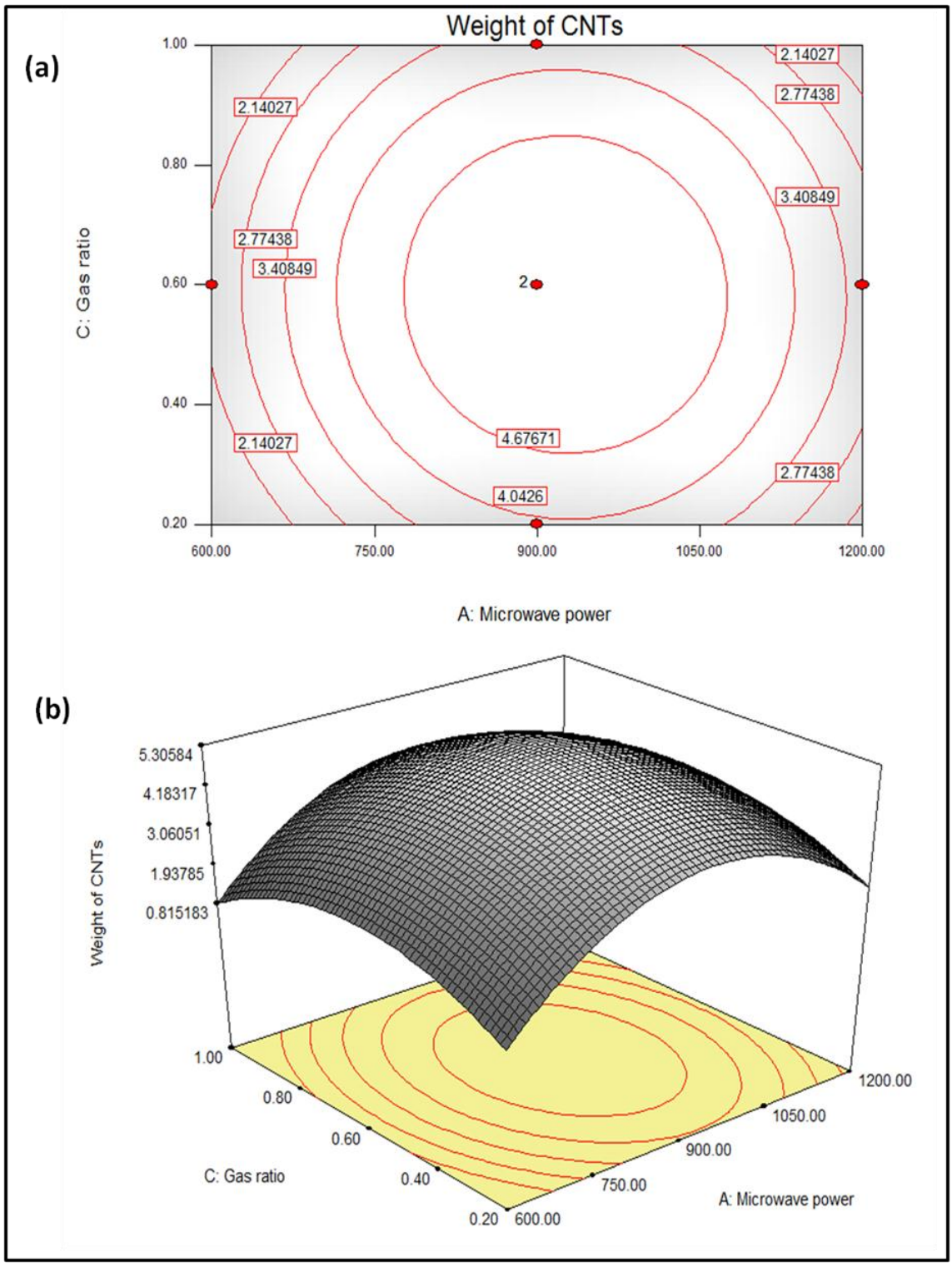

Figure 4.6: (a-b): Effect of gas ratio and microwave power on CNT production.

4.3.4 Effect of gas ratio and radiation time on weight of CNT

Fig. 4.7 (a-b) shows the interaction between gas ratio and radiation time. 3-dimensional and contour plot indicated that almost elliptical indicated that there is good interaction between gas ratio and radiation time. The mid- point interaction for gas ratio and radiation time shows the highest weight of CNTs obtained. Further increase in radiation time from 35 to 60 min and gas ratio of 0.6 to 1.0 resulted in weight of CNTs decreased (Han, et al., 2002; Vázquez and Prato, 2009). The typical radiation time is approximately 60 min, but the radiation time also depends on the desired CNTs amount. Furthermore, deviations of the optimum radiation time for the specific synthesis suffer from the quality of the final product (Liu, et al., 2007; Nagaraju, et al., 2002; Nuchter, et al., 2004; Willems, et al., 2000). It is also noted that the yield is proportional to the time of reaction. Hana et al. (2002) studied the influence of flow rate of precursor and carrier gas, and it is found that if the flow rate of carrier gas is increased, with the precursor flow rate remain constant, the mean diameter of CNTs will decrease. If the flow rates of both carrier and precursor gas are increased, the diameter essentially remains constant, but the growth rate will increase. On the other hand increase in gas ratio after 0.6 resulted in decreasing the weight of CNTs. Hence the gas ratio is a vital factor that can influence the formation of the growth mechanism of CNTs.

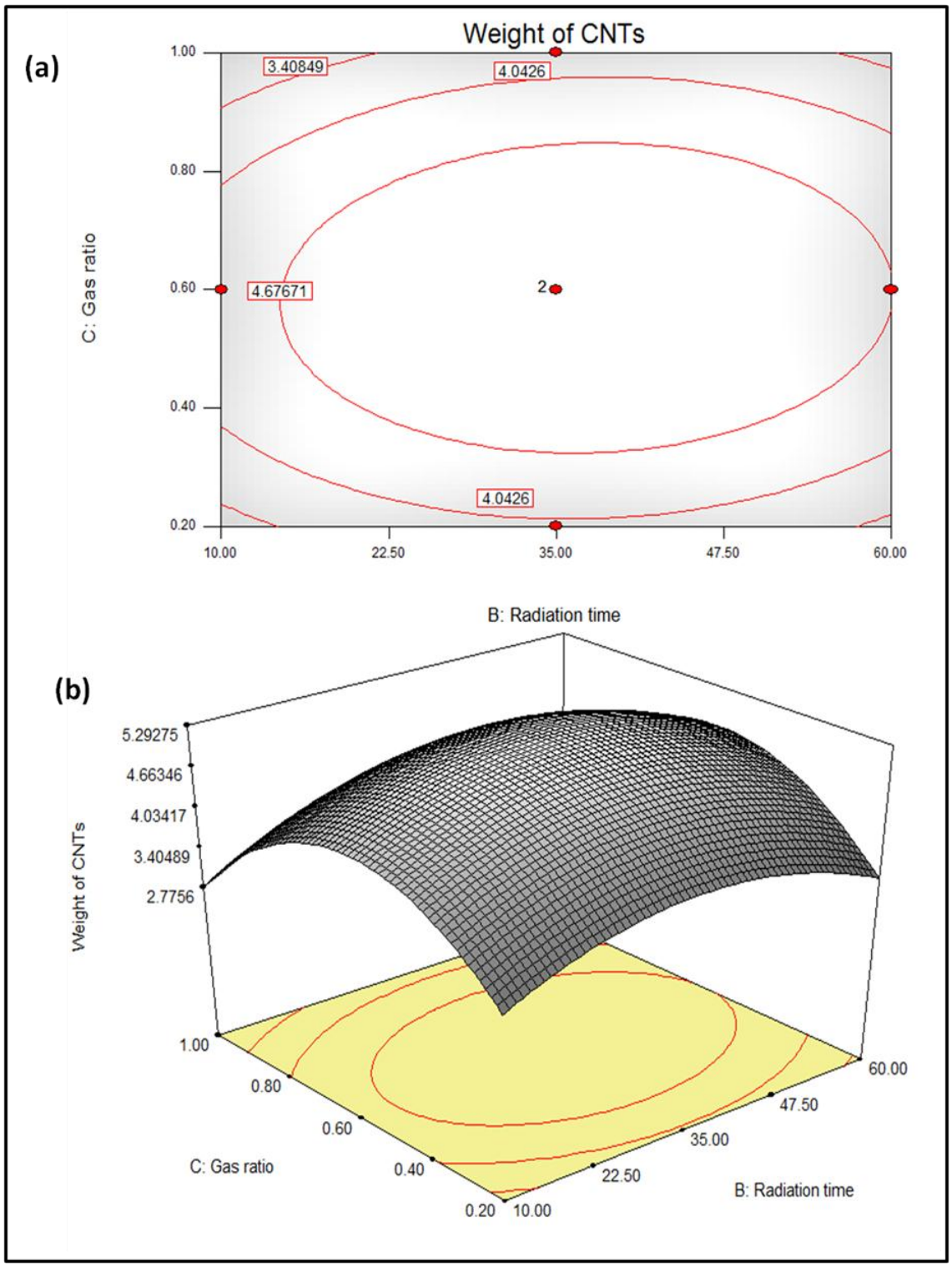

Figure 4.7: (a-b): Effect of gas ratio and microwave power on CNT production.

For the best fit regression of the model, the regression equation and the coefficient of determination R^2 was evaluated. The determination coefficient, R^2 and adjusted R^2 values represented the proportion of variation in the response data explained by the predictors. The model gave a $R^2 = 0.996$, which means 97 % of the variance; microwave power, radiation time, and gas ratio (C_2H_2/H_2) were best fitted to the model selected. The statistical analysis gave four comparative solutions for the production of CNTs based on the weight of CNTs as shown in Table 4.2. If the desirability value is less than one, it means optimization was achieved. From the solution obtained from the design it showed the desirability of getting a value of 0.97, which mean that 97 % of optimization was achieved.

Table 4.2: Validation study for selection of best yield, high quality and high purity of CNTs

Number	**Microwave Power (W)**	**Radiation time (min)**	**Gas ratio C_2H_2/H_2**	**Weight of CNTs (g)**	**Desirability**
1	900	35	0.6	5.8	0.97
2	900	33	0.58	5.4	0.91
3	900	32	0.57	5.34	0.89

Based on the statistical result the optimum production conditions for the selected CNT were; microwave power 900 W, radiation time 35 min, and gas ratio of C_2H_2/H_2 0.6. The optimization process parameter was related to similar work done by (Amirhasan, et al., 2007; Das et al., 2006; Kuo, et al., 2005; Otsuka et al., 2004; Veziri, et al., 2008) to produce high yields and high purity of the CNT. From their observation microwave power, and gas flow rate played a tremendous role in the formation of the CNT. Table 4.3 Shows a review on the microwave assisted synthesis of CNTs.

Table 4.3: Review on microwave assisted synthesized CNTs

Catalyst	Time (min)	Carbon Source	Temp (^oC)	Microwave Power (W)	CNT Type	Diameter (nm)	Reference
Fe	35	C_2H_2/H_2	520°C	900	MWCNTs	10-23	This Study
Si	30-90	graphite	1200	800	MWCNTs	50-400	(Méndez, et al., 2003)
Catalytic Cobalt (Co)	0.5-10	C_2H_2	800	900	CNTs	4	(Taniguchi , et al., 2005)
Pd-CO	10	CH4	750	600	MFCNTs	50	(Hayashi, et al., 2006)
Co-Zn-Al mixed oxides	300	CH_4	125	800	MWCNTs	20-30	(Benito, et al., 2009a)
Fe	5 S	Iron melonate+ Prussin blue	1000	800	MWCNT	30-60	(Clauss, et al., 2010)
Fe	120	graphite	>1000	1000	MWCNT	10-30	(Vivas-Castro, et al., 2011)
Fe	6	CH_4	594-597	750	SWCNTs	45-100	(Teng, et al., 2013)
Ferrocene	30	C_2H_2	600	6000	MWCNTs	50-80	(Fu, et al., 2013)
Ni	3	CH_4	600	800	MWCNTs	60	(Lee, et al., 2013)

4.3.5 Effect of perturbation plot on weight of CNTs

Among the parameters that influence the growth mechanism of CNTs is the catalyst, gas flow rate and microwave power. Most effective and widely used catalysts are Fe/Co/Ni. The rationale for using these metals lies in the phase diagrams for these metals and carbons. At a high temperature, carbon has a finite solubility in these metals, which leads to the

formation of metal-carbon solutions and therefore the aforementioned growth mechanism. Using the selected quadratic model, the optimization goal was set to a targeted response prediction and statistically validated the observed experimental data, the numerical optimization tool in CCD was used to generate contour maps from which optimum experimental conditions (design points) were identified. The three experimental factors could be used as axes for the contour maps, it was necessary to choose the factors that were most sensitive to the response by using perturbation plots. In generating the perturbation plots, all the factors were plotted on the same response graph. These plots show how the response changes as each factor moves from a chosen reference point (in this case the middle of the design space or the midpoint of each factor range). The response (weight of CNTs) was therefore plotted against the deviation from the reference point of the interaction of all factors over its entire range as shown in Fig. 4.8. From the observation of the perturbation plots exhibit good interaction with all the process parameter such as microwave power (A), radiation time (B) and gas ratio (C). This indicates that the response (weight of CNTs) is more sensitive to changes in factors A and C than to changes in factor B. The range of process parameters such as microwave power (600 to 1200 W), radiation time (10 to 60 min) and gas ratio of C_2H_2 (0.1 to 1). The range of process parameters was selected based on the previous study (Cao, et al., 2007; Cheung, et al., 2002; Douven, et al., 2012; McKee, et al., 2009) .

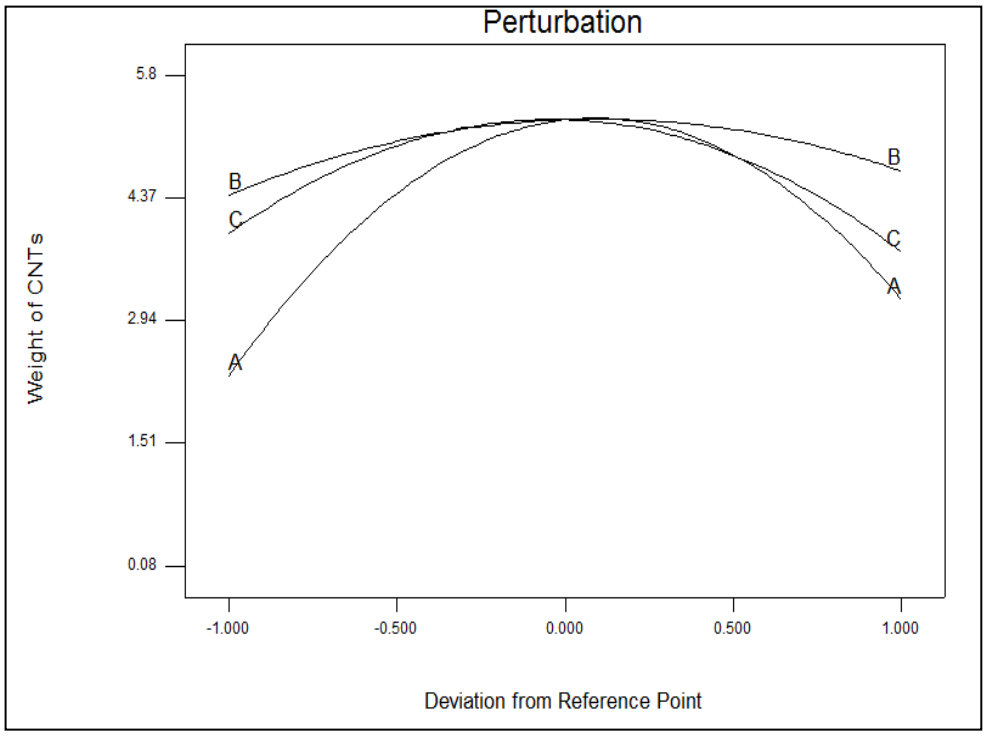

Figure 4.8: Effect of perturbation plot of CNTs production.

4.4 Characterization of selected CNT samples produced

4.4.1 Field Emission Scanning Electron Microscope

The CNT produced at optimal production conditions was examined by FESEM as shown in Fig. 4.9 (a-c). The quality of CNTs, in terms of crystallinity and impurity content is dependent on the conditions of synthesis, the use of hydrocarbon gas and metal nanoparticle catalysts. High purity and high of CNTs array were observed in Fig. 4.9 (a-c). FESEM images at different magnifications, i.e. 1000, 1000,000 and 2000,000 nm scales. These produced CNT is free from impurity was observed from the all the images and clear CNTs was observed. It also shows that these CNT are tens of microns long with uniform diameters. The bulk morphology of long CNT is filmed like and oriented. The produced CNTs have the vertical alignment of CNT could be observed with the diameter of CNTs

ranging from 15 to 23 nm. These images indicate that despite the long growth time and centimeter length, the tubes grew vertically without any interruption until the catalyst activity was terminated. The uniform diameter of CNTs shows that CNTs produced were in homogenized form. These results are in good agreement with previous researchers (Kuo, et al., 2006; Masao Yamaguchi, 2008; Mubarak, et al., 2011).

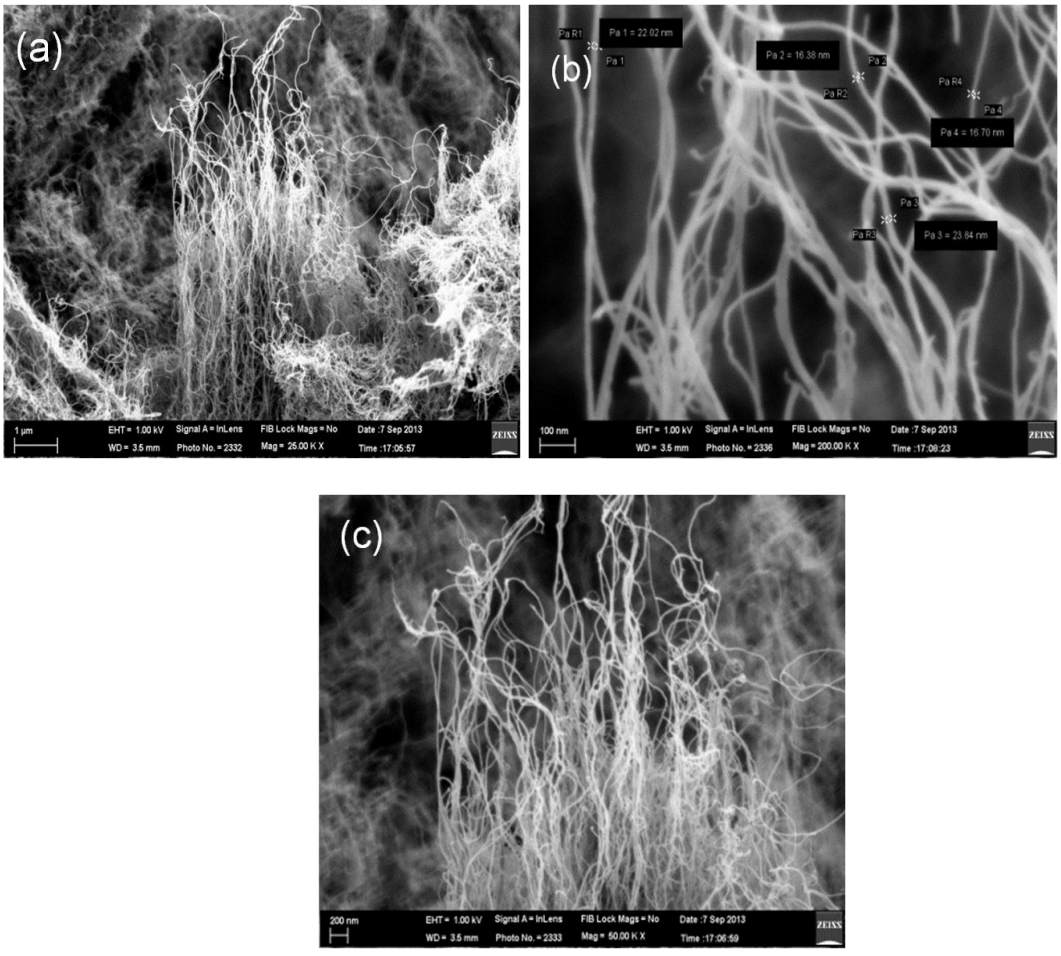

Figure 4.9: (a-c): FESEM image of CNTs produced at optimal conditions.

4.4.2 Transmission Electron Microscope

TEM images reveal the internal structure of CNTs produced at optimal production conditions with different magnification scale as shown in Fig. 4.10 (a-c). It was clearly observed that produced CNTs were hollow and tubular in shape. The dark spots represent

the Fe catalyst nanocrystals encapsulated in carbon graphic layers give evidence of tip growth mechanism (Kumar and Ando, 2010). It was also observed that the shape of the catalyst, which served as a seed during the production process, is important because the produced CNTs are assumed to follow the shape of the catalyst. This fact is obvious in the TEM images and we see some CNTs follow the shape of the catalyst. Therefore, produced CNTs were high purity, uniform diameter distribution with no deformity in the structure was observed in TEM images.

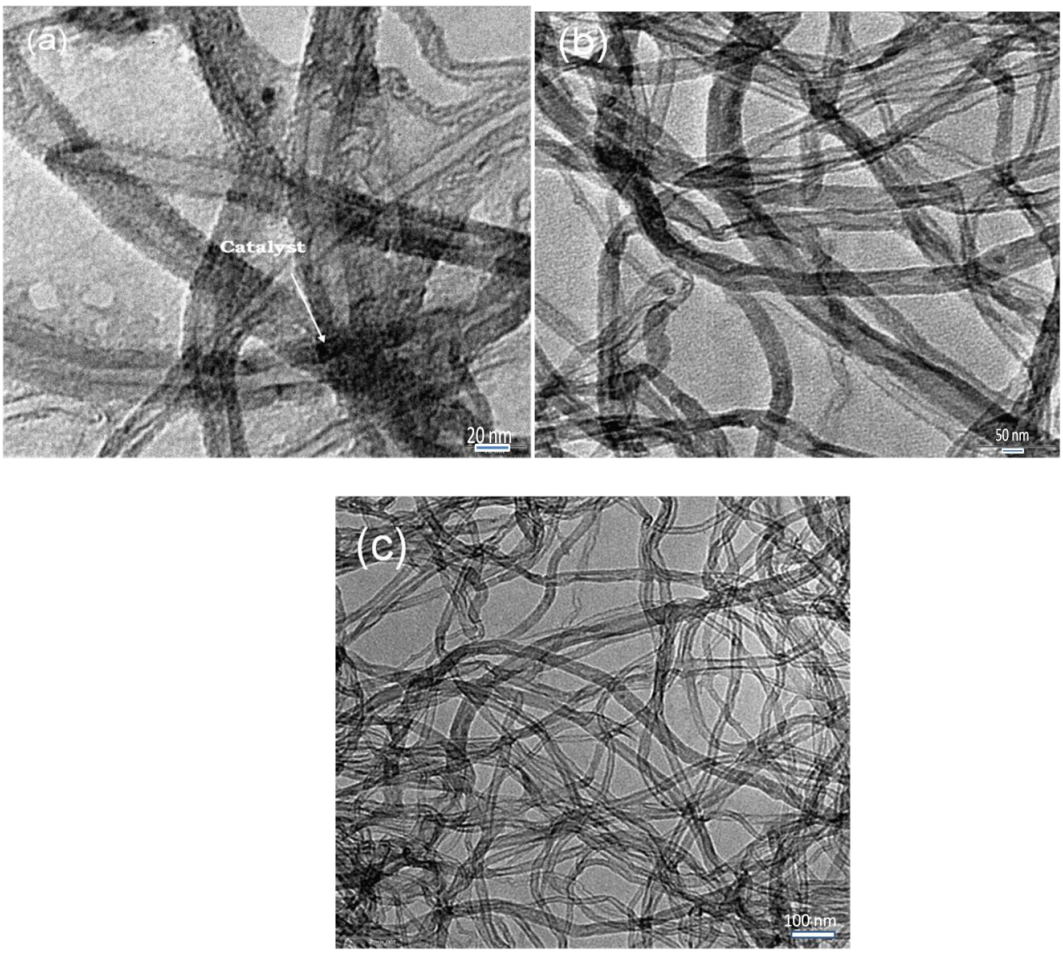

Figure 4.10: (a-c): TEM images of the selected CNT prepared at optimal condition.

4.4.3 High Resolution Transmission Electron Microscope

Fig. 4.11 (a-d) shows the HRTEM images of CNTs at different magnification scale. Fig. 4.11 (a-b), a highly ordered crystalline structure of CNTs, revealing that the structure of this multiwall carbon nanotube (MWCNTs) is a waving structure of graphite sheets at a short range. Most inner graphite sheets have straight fringes, but the outer graphite sheets were waving fringes, indicating a defective crystalline structure. The clear fringes of graphitic sheets are well separated by 5 nm and aligned with a tilted angle of about 2° toward the tube axis.The space of graphite layers in the MWCNT is 0.34 nm meanwhile the outer and inner diameters of MWCNT are 5 and 10 nm, respectively. Fig. 4.11 (c-d) provides evidence that the twisting and winding CNTs are MWCNTs. The length of product CNTs is estimated at more than several tens of micrometers. Some dark spot was observed on the surface of MWCNTs, these sports may be a catalyst particle on top. HRTEM image shows at high resolution indicates that there were about multi layers graphitic walls of the of CNTs grown at 900 W were observed. The TEM image shows that there were about 17 graphitic walls of the multi layers CNTs grown at optimal production conditions. Hence, HRTEM result proved that produced CNTs were appeared in tubular and hollow shape (Chen, et al., 2002; Mubarak, et al., 2011; N. Grobert and Zhu, 1999).

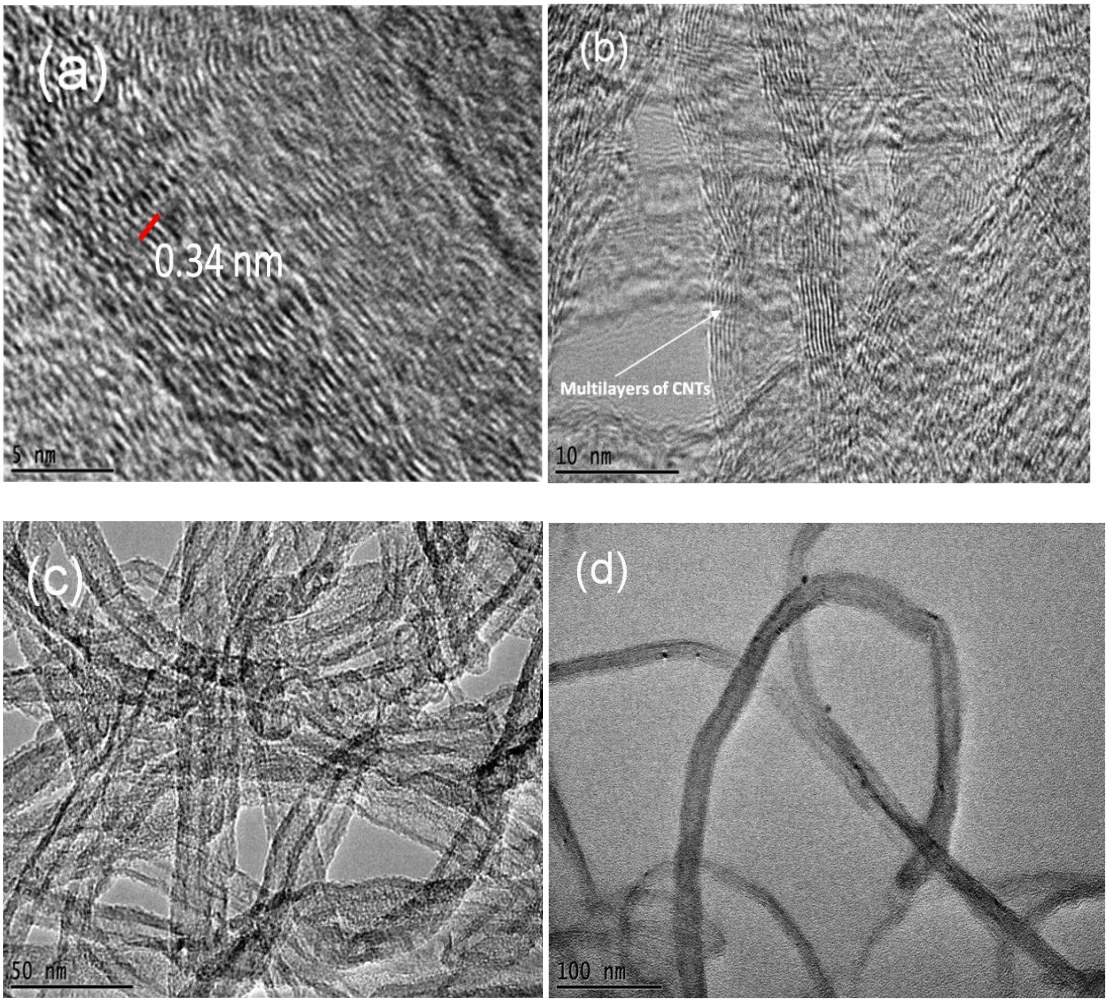

Figure 4.11: (a-d): HRTEM image of CNT prepared at optimal conditions.

4.4.4 Thermogravimetric Analysis

TGA of the CNT was used to examine the purity of the selected CNT. The variations of the CNT mass with respect to temperatures at specific time are shown in Fig. 4.12 TGA analysis shows a single peak at one distinct zone, implying high purity of the CNTs. Moreover, the peak corresponds to the decomposition of one element only, since no other peaks are observed. There is a very slight loss of weight between 50 to 100^{o}C, which correspond to the loss of water from the catalyst support. The weight loss in the range of

335 to 350 ^{o}C is a result of oxidation of amorphous carbon (Chen, Chen, Chen, et al., 2002; Kim, Kim, et al., 2005; Moon et al., 2001) and the weight loss in the range of 480 to 620 ^{o}C is due to oxidation of CNTs (Kim, Kim, et al., 2005). The observed flat profiles between 620 and 850 °C showed that the metal catalyst and support are not volatile below 800 °C and thus remain as residue of TGA. The weight loss indicates the purity and yield of CNTs and the higher the weight loss, the higher is the purity of CNTs. From the TGA analysis, we concluded that the produced CNTs have almost 98% purity. The above finding proved by previous research (Das, et al., 2006; Huang, Wang, et al., 2003).

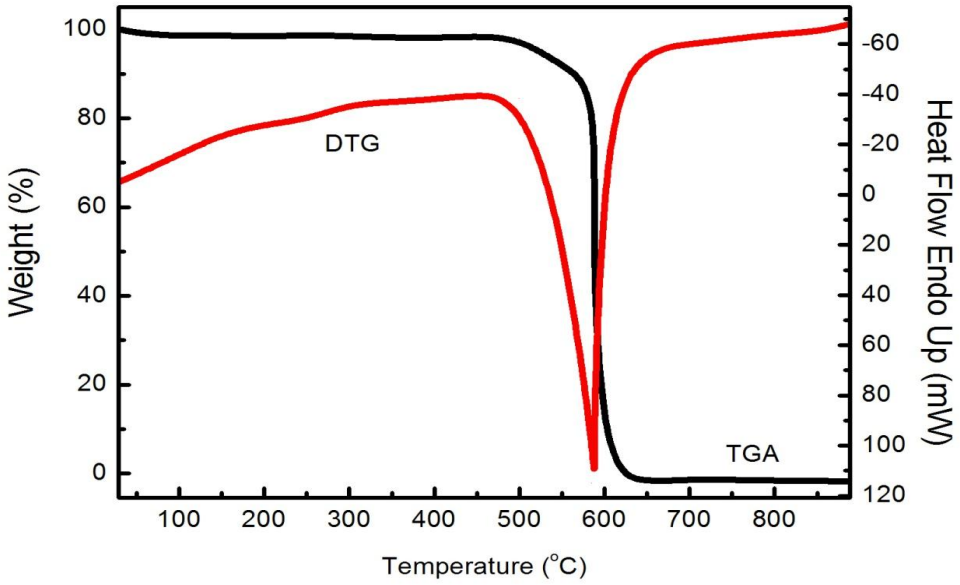

Figure 4.12: TGA analysis of the CNT produced at optimal conditions

4.4.5 X-ray Diffraction

The crystalline information of MWCNTs with average diameters of 15-23 nm is shown in Fig. 4.12, where these x-ray diffraction (XRD) patterns was measured at a scan rate 1^{0}/min from 20^{0} to 80^{0}. Two main crystalline peaks C (101) and C (002), are clearly centered at 45^{o} and 26^{o} on these XRD patterns, indicating the presence of a graphite crystalline

structure on these MWCNTs. This phenomenon suggested that the crystalline quality of the graphite structure on the MWCNTs becomes poor with an increase in the average diameter. In addition, the broad diffraction peak (centered at 45^{o}) between 43^{o} and 46^{o} may be attributed to the contribution of Fe (110) (centered at 44.7^{o}). This result suggests the presence of Fe particles, possibly due to the aggregation of Fe atoms from the catalyst precursor. The diffraction peaks associated with Fe_3C and Fe phases are in agreement with other reports (Das, et al., 2006; Gulino, et al., 2005; Kuo, et al., 2005).

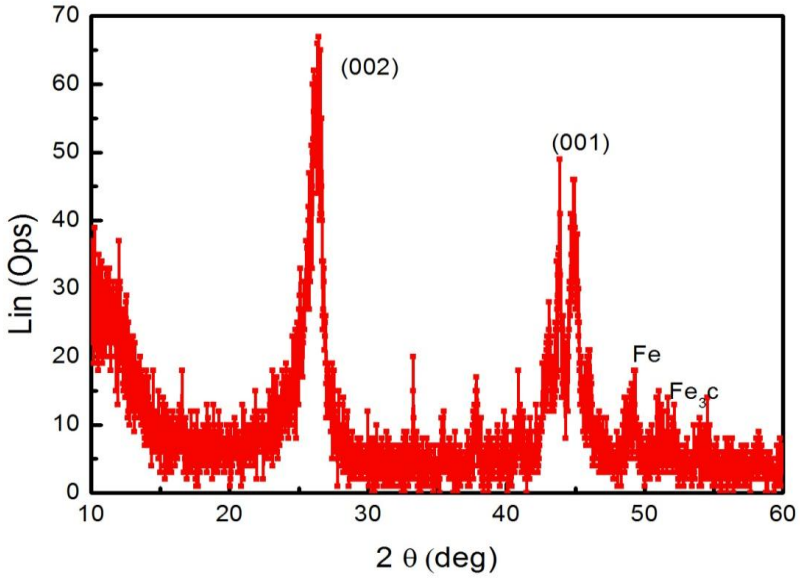

Figure 4.13: XRD patterns of CNT prepared at optimal conditions.

4.4.6 Raman spectroscopy

The quality of the CNTs was assessed Raman spectroscopy as shown in Fig. 4.13. Two prominent Raman features are observed with the CNTs with D (disordered)-band and G (graphite)-band. The D-band (1330 cm^{-1}) is representative of the defects and disorder associated with the CNTs, such as open caps, wall defects and amorphous carbon deposits

(Eklund et al., 1995). The D-band arises from shifts in the phonon modes of the CNTs that are caused by perturbations in the symmetry of the tubes (Pimenta et al., 2001; Qian et al., 2003; Saito and Kataura, 2001). Defects are an example of the perturbations that cause shifts in the vibrational frequency of the phonons (Athalin and Lefrant, 2005). The G-band 1600 cm^{-1}, represents the graphitization of the CNTs, this is a peak that representative of highly –ordered pyrolitic graphite (Zhao et al., 2002). It is evidenced by the decrease in the D to G band ratio (ID/IG) from 19000 to 13000. The above finding agrees well with the result from HRTEM observation.

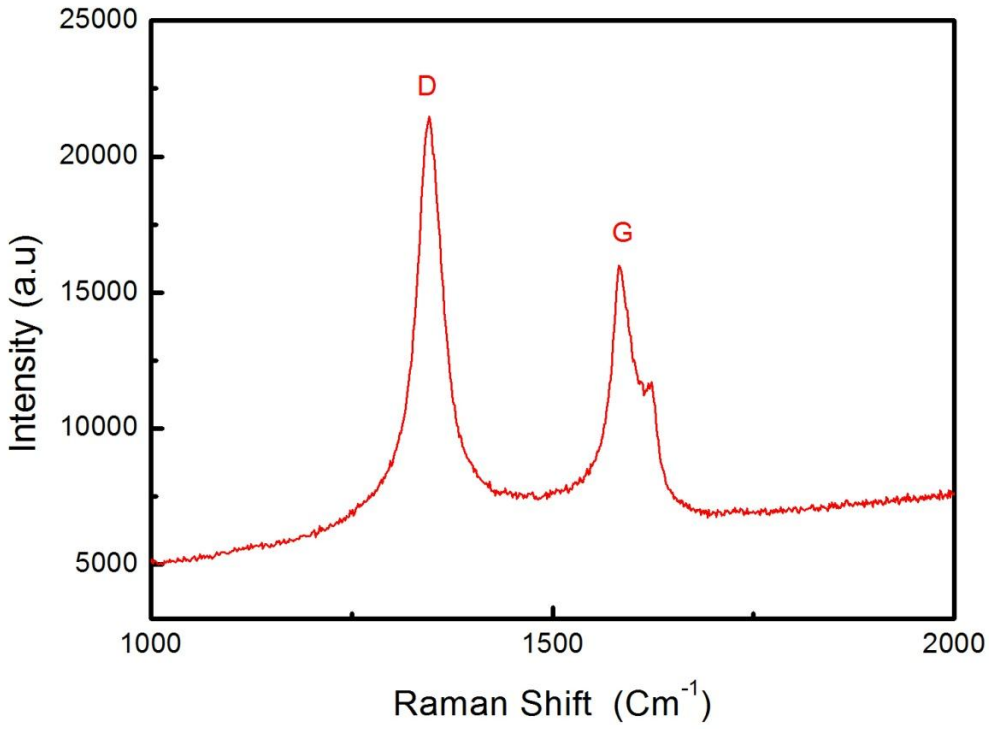

Figure 4.14: Raman spectra of CNT prepared at optimal conditions.

4.4.7 BET surface area

Fig. 4.14 (a) shows the N_2 sorption isotherms of CNTs. The hysteresis behavior apparent in the isotherms indicates the mesoporous nature of the carbon specimens. The adsorption isotherm features a combination of type I (the initial part is concave to the p/p° axis) and type IV isotherms (its apparent hysteresis loop). According to the IUPAC classification type I isotherm is given by microporous solids which have relatively small external surfaces and Type IV isotherm is given by many mesoporous industrial adsorbents (Carabineiro et al., 2011; Huang et al., 2011; Jiang and Zhao, 2004; Sing et al., 1985). Figure 4.14 (b) shows the pore size distribution (PSD) curves. The mean pore sizes estimated from the peak positions of the PSD curves was 3 nm. It also shows that a vast majority of the pores falls into the range of mesopore (Huang, et al., 2011). The BET surface area evaluated using N_2 adsorption isotherms prepared under optimum conditions was 206.45 m^2/g with a pore volume of 0.834 cm^3/g.

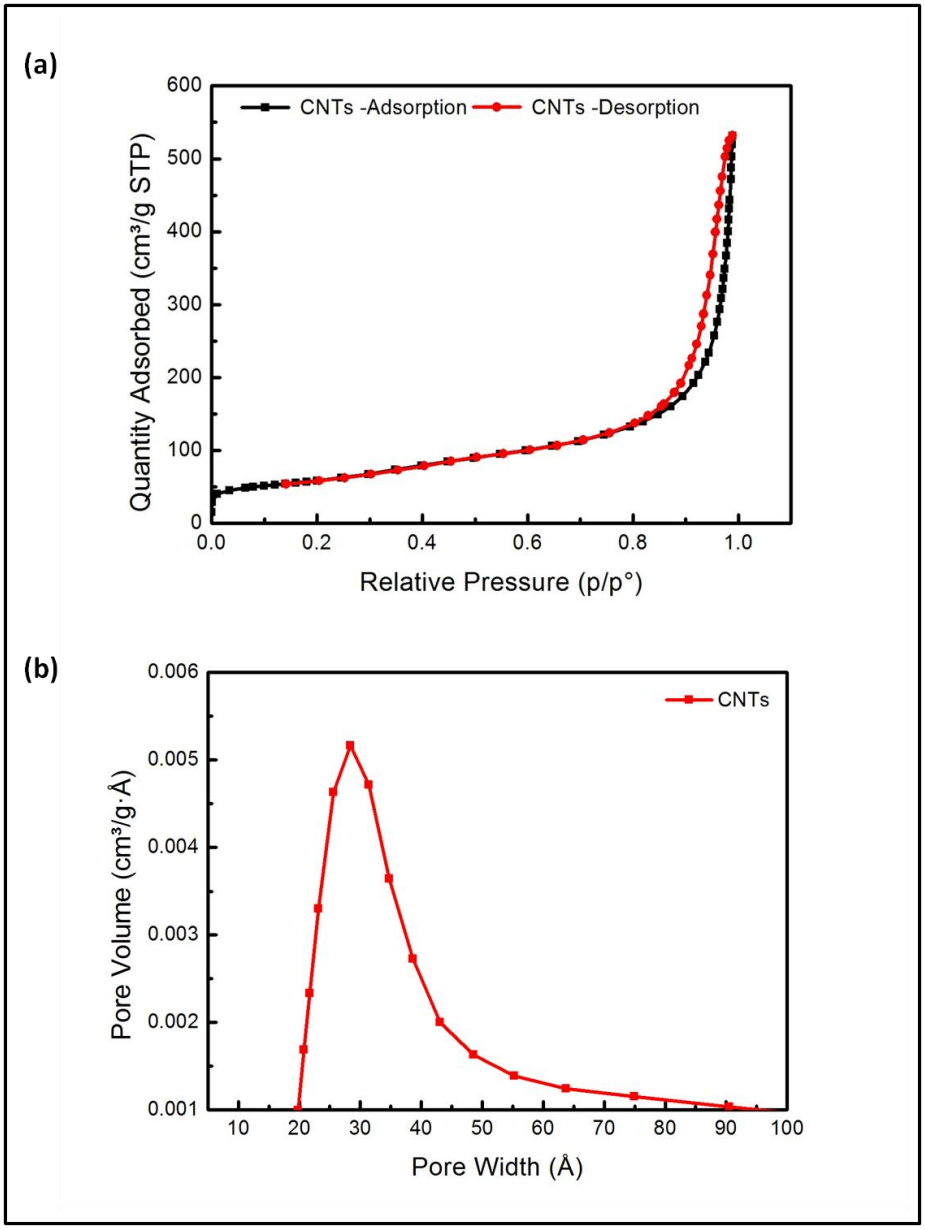

Figure 4.15: (a) N_2 adsorption/desorption isotherm of CNTs, (b) Pore size distribution curves of the CNTs prepared under optimal condition.

4.5 Heavy Metals removal

The heavy metal ions in waste water are becoming a major concern for environment conservative and human health. To reduce environmental problems, the CNTs are promising candidates for the adsorption of heavy metals. Statistical optimization of process

parameters such pH, CNTs dosage and agitation speed and time of removal of Pb (II), Cd (II), Cu (II) and Zn (II) were investigated using optimized MWCNTs conditions produced via microwave heating. The studies on the isotherm kinetic, isotherm model and thermodynamic parameters were developed and investigated as well.

4.5.1 Statistical optimization of removal of Pb (II) using CNTs

The initial stride in choosing the most suitable adsorbent with a higher adsorption capacity of Pb (II) would be the determination of the optimized condition of MWCNTs as a the adsorbent for removal of Pb (II) (Hu, et al., 2009; Kabbashi, 2011; Mubarak, et al., 2013). The precise numbers of runs for the optimized condition were regulated based on the design obtained from DOE. The detail experimental array of adsorption rate of removal of Pb (II) as shown in appendix B. The results obtained from this particular experiment were analyzed using the application of "analysis of variance" (ANOVA) obtained from the DOE and the optimized variables are attainable from Table 3.2. Results obtained from adsorption experiment were analyzed by employing ANOVA for the removal of Pb (II) using CNTs are indicated in Table 4.4. The fisher F-test value obtained from Table 4.4 which provides the comparative of the mean square of the residuals (errors). High F (19.6) value proves the efficiency of the model while the low probability, P value indicates higher significance of the regression model. This value indicates both models are significant. On the other hand, the correlation coefficient value, R-Squared and Adj R-Squared of CNTs were 0.99 and 0.97 respectively. This value defines the high efficiency and significance of both models. The model equation evolved for the removal of Pb (II) from aqueous solutions for CNTs is equation (4.2) is as follows:

Pb (II) % removal = 100.07 +0.48 * A +0.84 * B+0. 29 * C +1.02 * D -17.93 * A^2 - 7.73* B^2 -6.93 * C^2-11.43 * D^2 -0.48 * A * B -0.52 * A * C +1.48 * A * D +2.36 * B*C-1.64 *B*D+1. 64*C*D (4.2)

Consequently, variables A, B, C, D, AB, AC, AD, BC, BD and CD were significant model terms. This indicates that the pH (A), agitation speed (B), MWCNTs dosage (C) and time (D) were highly significant values of Probe >F was 0.0001. The coefficient of single factor represents the effect of its represented factor while the coefficients of double factors represent the interaction and effect of both represented factor. Hence, following up to the equation, the positive sign in the equation represents the synergistic effect while the negative sign represents antagonistic effect values. Fig. 4.15 shows theoretical values versus the experimental values for Pb (II) removal. It was clearly shown that the theoretical values obtained were quite close to experimental values, indicating that the model developed was successful in bridging the correlation between process parameters for removal of Pb (II).

Table 4.4: ANOVA for the selected quadratic model for removal of Pb (II).

Source	Sum of squares	DF	Mean square	F Value	Prob > F	Status
Model	8227.21	14	587.658	19.6	< .0001	Significant
A	4.205	1	4.205	0.1	0.7151	
B	12.66722	1	12.6672	0.4	0.5290	
C	1.560556	1	1.56055	0.1	0.8237	
D	18.605	1	18.605	0.6	0.4475	
A^2	823.0089	1	823.008	27.5	0.0003	
B^2	152.8938	1	152.893	5.1	0.0452	
C^2	122.8723	1	122.872	4.1	0.0679	
D^2	334.3833	1	334.383	11.2	0.0066	
AB	3.705625	1	3.70562	0.1	0.7318	
AC	4.305625	1	4.30562	0.1	0.7119	
AD	35.10563	1	35.1056	1.2	0.3023	
BC	88.83063	1	88.8306	3.0	0.1131	
BD	43.23062	1	43.2306	1.4	0.2550	
CD	43.23063	1	43.2306	1.4	0.2550	
Residual	329.7571	11	29.9779			
Lack of Fit	327.7571	10	32.775	16.4	0.190	Insignificant
Pure Error	2	1	2			
Cor Total	8556.97	25				

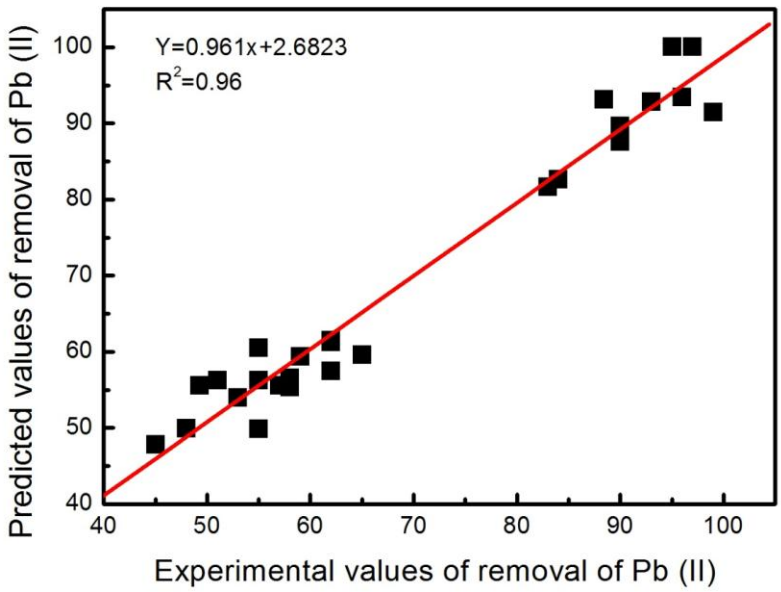

Figure 4.16: Relationship between Predicted values of removal of Pb (II).

Fig. 4.16 represents the 3-D plot for adsorption of Pb (II) prepared under optimized conditions of CNTs production affected by pH, CNTs dosage and agitation speed. Fig. 4.16 (a) visualized the interaction plot between pH and agitation speed. From the observation, the removal of Pb (II) reaches the maximum percentage when the interaction of both pH and agitation speed engaged at the middle point, 5 and 160 rpm respectively. By increasing and decreasing more values from the middle point for both parameters affected in decreasing of Pb (II) adsorption. The pH value of the aqueous solution plays a major role in the adsorption of heavy metals (Chen et al., 2007; Chen and Wang, 2006; Li, Ding, et al., 2003; Moradi, 2011; Xu, et al., 2008). The lead sorption capacity increased with the increase in pH and reached the maximum at pH around 5 and starts to decrease after that due to the effect of precipitation of lead hydroxide as between pH 5.4-6, more than 98% of Pb (II) species are Pb (II) (Machida, et al., 2004). Similar distribution of Pb (II) species in

aqueous solutions were also given by others (Abdel-Ghani et al., 2007; Faur-Brasquet et al., 2002; Herrera-Urbina and Fuerstenau, 1995; Meena, et al., 2008) and while above pH 6, Pb (II) starts precipitating as Pb $(OH)_2$ (Wang, Zhou, Peng, Yu, & Yang, 2007; Wang, Gong, et al., 2007) and hence studies in this range are not conducted. Regardless the precipitation phenomena, the increase in pH means a decrease in the total number of H^+ cations which are in competition with Pb (II) cations to occupy the active sites on adsorbent. Moreover, the high pH enhances the surface charge of the adsorbents (Li, Ding, et al., 2003; Wang, Zhou, Peng, Yu, & Chen, 2007). Fig. 4.16 (b) represents the 3-D interaction plot between pH and CNTs dosage. From the result, removal of Pb (II) obtained the highest value when the interaction between both factors were at the pH 5 and 0.1 CNTs dosage before it dropped linearly after the addition of both pH and dosage. The amount of Pb (II) adsorbed by the adsorbent increases with the increase of the CNTs dosage. The increase in adsorbent amount leads to increase in active sites concentration which helps in increasing the adsorption of the heavy metals. This observation agrees with the previously published works (Kabbashi, et al., 2009; Li, Wang, et al., 2002; Li, 2004). Furthermore, removal of Pb (II) was also studied by the interaction of pH and time as shown in Fig. 4.16 (c). Resulting of the same trend, removal of Pb (II) reached the highest adsorption at the time of 22.5 min with the pH of 5. Prolonged the time up to 40 min does not influence the removal of solute Pb (II) removal from aqueous solution (Li, et al., 2005; Ruparelia, et al., 2008).

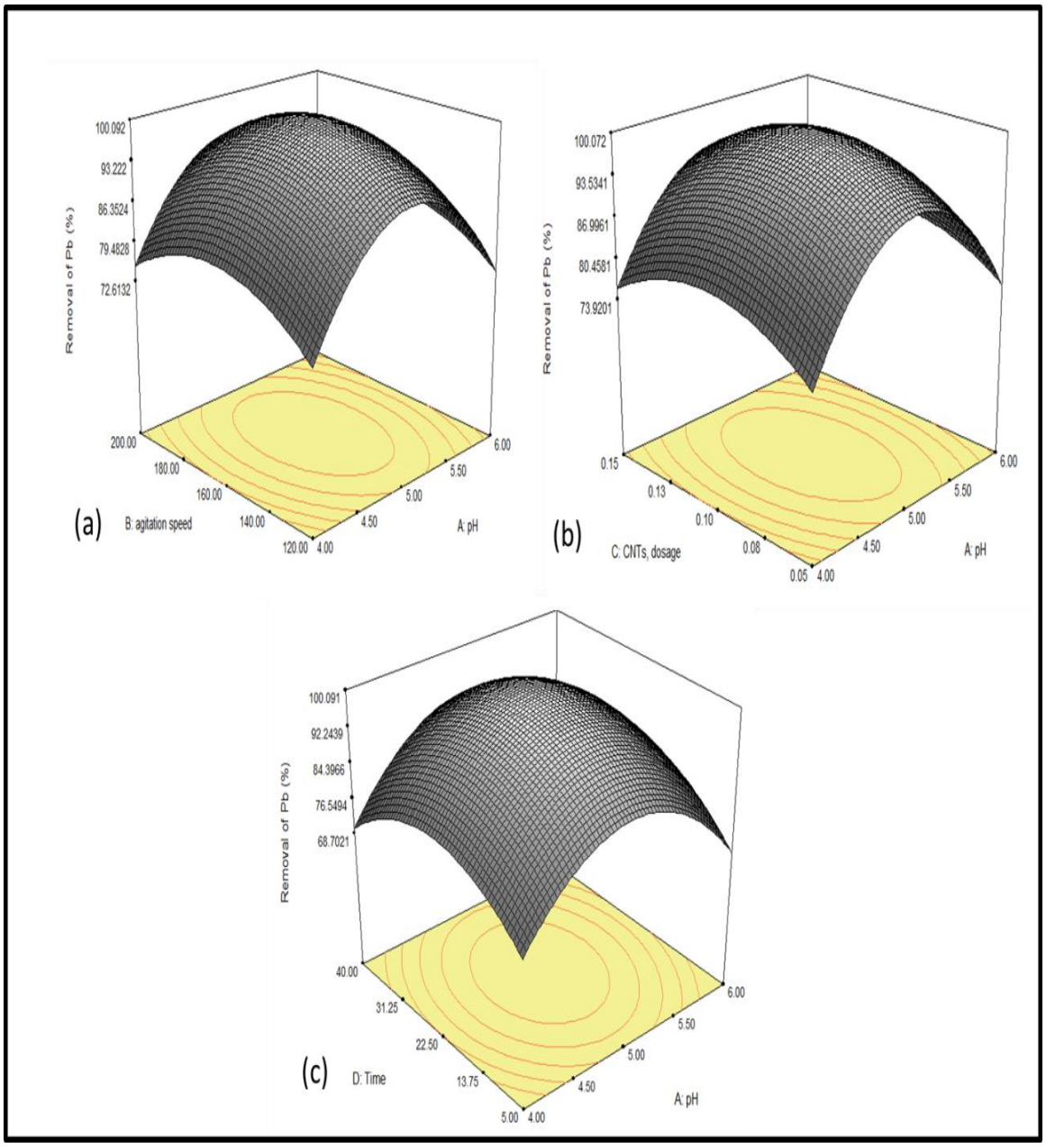

Figure 4.17: 3-D plots of removal of Pb (II) using optimized CNTs production, (a) interaction of agitation speed and pH, (b) interaction of CNTs dosage and pH, and (c) interaction of time and pH.

4.5.2 Adsorption isotherm of Pb (II)

Adsorption isotherm reflects the relationship between the amount of a solute adsorbed at constant temperature and its concentration in the equilibrium solution. It provides essential physciochemical data for assessing the applicability of the adsorption process as a complete unit operation. The successful representation of the dynamic adaptive separation of solute from solution onto an adsorbent depends upon a good description of the equilibrium separation between the two phases (Pehlivan, et al., 2008; Rao et al., 2010; Salmani et al., 2013). The relation between contact time (min) versus adsorption capacity (q_t) was plotted for different Pb (II) concentration as shown in Fig. 4.18. Adsorption of high initial Pb (II) concentration results in an increase in the adsorption uptake due to increase in mass transfer driving force leading to higher adsorption rate (Chen, et al., 2009; Chen and Wang, 2006). More than 95% of maximum equilibrium uptake capacity was reached after 20 min and complete equilibrium was reached in the 20 to 40 min. No significant additional adsorption was observed after 40 min of contact time. The contact time was thus maintained for 40 min to ensure that the equilibrium could be achieved (Chen and Wang, 2006; Li, Wang, et al., 2003; Stafiej and Pyrzynska, 2007). It indicates that carbon obtained has highly active sites with well developed pores, which is responsible for Pb (II) adsorption. The equilibrium uptake concentration (qe) of Pb (II) on solid phase adsorbent is directly proportional to Pb (II) connotation in the liquid phase as shown Fig 4.17 which mainly attributed to unsaturation of the adsorption sites or layers through the adsorption process. Such observation is usually reported by most of the researchers in the filed of sorption processes (Kabbashi, 2011; Li, Ding, et al., 2003; Vilar et al., 2006; Vuković, et al., 2010).

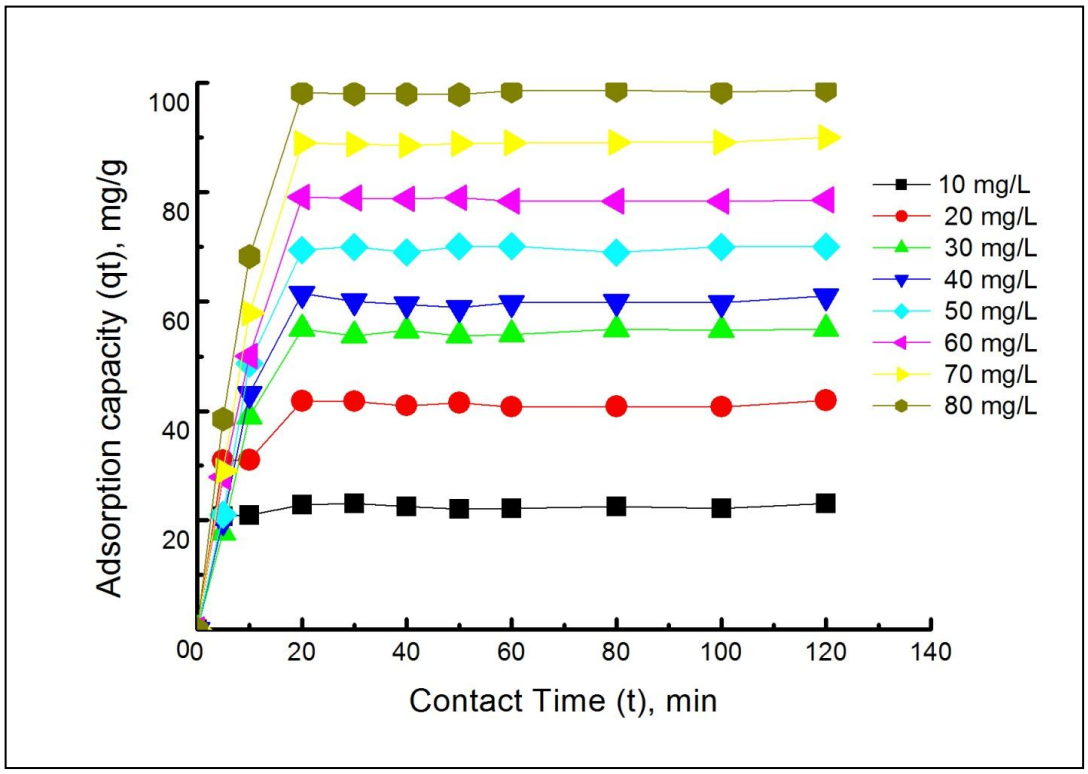

Figure 4.18: Adsorption capacity (qt) versus concentration (t) with different Pb (II) solution concentration.

4.5.3 Adsorption kinetics of Pb (II)

Adsorption kinetics is a powerful isotherm to demonstrate the unique relationship between carbonaceous adsorbents and the adsorbate. The interaction and affinity of equilibrium data are important and necessary for realistic and useful design and basic knowledge of adsorption system. The Langmuir isotherm, Freundlich isotherm and Temkin and Dubinin isotherm for Pb (II) have been successfully illustrated in Fig. 4.18 (a-d). As for this research study, four models were employed to determine the optimum model for the Pb (II) adsorption onto the CNTs surface. The Langmuir model is able to relate the solid phase

adsorbate concentration, q_e and the uptakes to the equilibrium liquid concentration, C_e as shown in the equation (4.3):

$$\frac{C_e}{q_e} = \frac{1}{K_L q_m} + \frac{C_e}{q_m} \quad (4.3)$$

where q_e (mg/g) represents the amount of adsorbed Pb (II) concentration per unit weight while the C_e (mg/L) represents an adsorbed Pb (II) concentration in solution at equilibrium. The Langmuir constant which relates to the affinity of the binding sites in the above equation is represented by K_L (L/mg) while the maximum adsorption capacity of the adsorbent is represented by q_m. A graph of C_e / q_e against C_e was plotted and the q_m and K_L values were calculated from the slope and the intercept of the graph. The relationship between Pb (II) uptake capacities (q_e) in mg/g of adsorbent the residual Pb (II) concentration C_e in mg/L at equilibrium is given by the following equation (4.4):

$$Inq_e = InK_F + \frac{1}{n} InC_e \quad (4.4)$$

Where K_F is a Freundlich constant that shows the adsorption capacity of the adsorbent and n is a constant, which shows the greatness of the relationship between the adsorbate and adsorbent. K_F and n were determined from the slope and intercept of the linear plot of ln q_e versus ln C_e. The Temkin equation (M.J. Temkin and Pyzhev, 1940) proposes a linear reduction in adsorption energy when the degree of completion of an adsorbent is raised. As a relationship between adsorbent-adsorbate, when the coverage is increased, the energy released by adsorption along the layer would decrease. The Temkin isotherm is introduced as shown in equations (4.5 & 4.6):

$$q_e = \frac{RT}{b} \ln(AC_e) \quad (4.5)$$

$$q_e = \text{B ln A} + \text{B ln } C_e \quad (4.6)$$

where B=RT/b, R is the universal gas constant (8.314 J mol^{-1} K^{-1}), T defined as absolute temperature (K), b is the Temkin constant related to the heat of adsorption (J mol^{-1}) and A the Temkin isotherm constant (L g^{-1}). The constants A and B are calculated from the slope and intercept of q_e versus lnC_e plot. Dubinin–Radushkevich isotherm is generally applied to express the adsorption mechanism with a Gaussian energy distribution onto a heterogeneous surface as shown in equitation (4.7). The model has often successfully fitted high solute activities and the intermediate range of concentration data well (Dąbrowski, 2001; Günay et al., 2007).

$$lnq_e = lnq_m - K\varepsilon^2 \quad (4.7)$$

Where K and ε^2 are Dubinin –Radushkevich isotherm constant. The saturation adsorption capacity q_m and K were calculated from the intercept and slope of lnq_e versus ε^2.

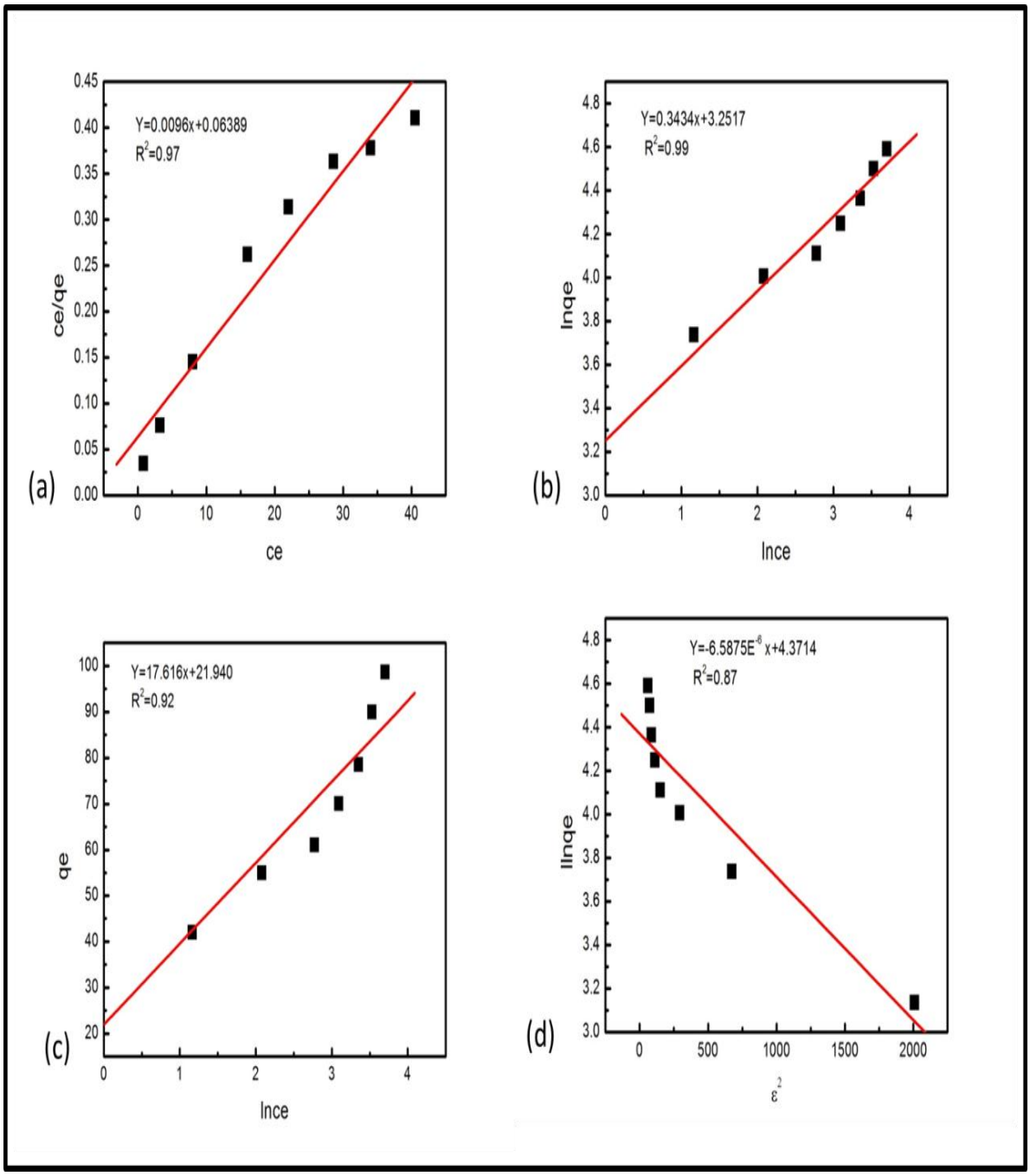

Figure 4.19: (a) Langmuir isotherm (b) Freundlich isotherm (c) Temkin isotherm, and (d) Dubinin –Radushkevich isotherm plots for adsorption of Pb (II).

Their constants and correlation coefficient were tabulated in Table 4.5. The isotherm data were collected through the measurements of Pb (II) metal ions after certain sorbent/ adsorbate contact intervals. The data collected throughout experiment were proving valid for Langmuir and Freundlich isotherm R^2= 0.97, and R^2= 0.99 respectively. However, Temkin and dubinin-Radushkevich isotherms do not show a good representation. Hence, high validity of Freundlich isotherm model proposes the adsorption process was taking place at the heterogeneous and consistent and well distribution of active sites along the CNTs surface. Review on Pb (II) removal using CNTs as shown in Table 4.6.

Table 4.5: Isotherm parameters for Pb (II) adsorption by CNTs.

Langmuir Isotherm		**Freundlich Isotherm**		**Temkin Isotherm**		**Dubinin-Radushkevich**	
q_m (mg g^{-1})	104.2	K_F (Lg^{-1})	25.83	A (Lg^{-1})	3.47	q_m	79.15
K_L (L mg^{-1})	0.1	n	2.91	B ($kJmol^{-1}$)	140.6	K $x10^{-6}$ (mol^2 kJ^{-2}	6.58
R^2	0.97	R^2	0.99	R^2	0.92	E (kJ mol^{-1})	0.27
						R^2	0.87

Table: 4.6 Summary of removal of Pb (II)

Adsorbent	**q_m (mg/g)**	**K_L (L/mg)**	**R^2**	**K_f (L/g)**	**n**	**R^2**	**References**
MWCNTs	104.2	0.1	0.97	25.83	2.91	0.99	This study
CNTs	11.23	0.04	0.993	0.68	1.52	0.97	(Hsieh and Horng, 2007)
CNT/Al_20_3	67.11	0.04	0.989	3.22	1.39	0.979	
CNT/MnO_2	82.6	1.65	0.998	43.43	3.9	0.867	(Wang, Gong, et al., 2007)
CNTs	17.44	0.586	0.995	5.99	1.91	0.987	(Li, Wang, et al., 2002)
MWCNT Oxidized	49.71	1.73	0.996	3.29	5.01	0.855	(Wang, Zhou, Peng, Yu, & Chen, 2007)
CNTs	62.5	0.11	0.964	-	-	-	(Hsieh, et al., 2006)
MWCNTs	6.71	3.71	0.96	4.76	7	0.98	(Tehrani, 2014)
MWCNTs oxidized	27.8	1.33	0.93	12.8	3.42	0.899	
MWCNT-TAA	71	0.13	0.945	8.34	1.43	0.99	
MWCNT oxidized	9.92	1.78	0.97	7.57	0.518	0.99	(Xu, et al., 2008)
CNTs oxidized	28	-	-	15.56	4.48	0.965	(Li, et al., 2005)
CNTs oxidized	97.08	1.51	0.987	-	-	-	(Li, Ding, et al., 2003)
CNTs oxidized	63.29	2.47	0.987	-	-	-	(Li, 2004)
CNTs oxidized	117.64	0.0038	0.933	5.4938	0.407	0.98	(Tofighy and Mohammadi, 2011)
SWCNT	29.851	0.691	0.99	20.61	9.91	0.99	(Moradi, 2011)
SWCNT-COOH	90.23	1.1	0.99	52.25	3.88	0.99	
CNTs-soaked in HNO_3	2.69	-	-	0.175	0.944	0.99	(Stafiej and Pyrzynska, 2007)
CNT refluxed in HNO_3	3.49	-	-	0.183	0.944	0.99	

In order to investigate the mechanism of Pb (II) adsorption on the CNTs surface and examine the potential rate-controlling step, the capability of pseudo-first order (Langergren, 1898) pseudo second order (Ho, 2006b; Ho and McKay, 1999b) kinetic models was examined in this study. The conformity between experimental data and the model predicted values was expressed by the correlation coefficients (R^2 values close or equal 1). A relatively high R^2 values indicate that the model successfully describes the kinetics of Pb (II) adsorption. Fig. 4.19 (a) shows the plot ln (qe-qt) against time representing the linear form of pseudo-first order kinetic model. The rate constant K_1 was calculated from the slope of straight line obtained. K_2 is the rate constant of pseudo second order adsorption kinetics (min.g/mg) was calculated from the intercept and slope of the straight line of t/qt against time as shown in Fig. 4.20 (b). From the observation, the kinetics of adsorption of Pb (II) ions adsorption on CNTs followed the pseudo second order with more conformity comparing pseudo first order as shown in Table 4.7. The pseudo second order rate has been applied widely to the sorption of metal ions, herbicides, oil and organic substances from aqueous systems (Ho, 2006b; Ho and McKay, 1999b).

Table 4.7: Experimental values of constants of adsorption kinetics model.

C_0 (mgL^{-1})	qe,exp. ($mg\ g^{-1}$)	Pseudo-First order			Pseudo-Second order		
		qe, cal ($mg\ g^{-1}$)	K_1 (min^{-1})	R^2	qe,cal. ($mg\ g^{-1}$)	K_2 ($min.g\ mg^{-1}$)	R^2
10	23	1.83	0.0111	0.12	24.5	0.080	0.999
20	42	3.29	0.0164	0.13	43.7	0.019	0.999
30	55.01	9.80	0.0406	0.48	57.04	0.0051	0.997
40	61.04	11.21	0.0275	0.46	62.69	0.0047	0.997
50	70.05	8.88	0.0390	0.36	72.8	0.0038	0.996
60	78.59	12.51	0.0404	0.53	81.43	0.0039	0.997
70	89.99	14.71	0.3326	0.49	93.37	0.0029	0.997
80	98.7	11.06	0.0457	0.39	101.18	0.0036	0.998

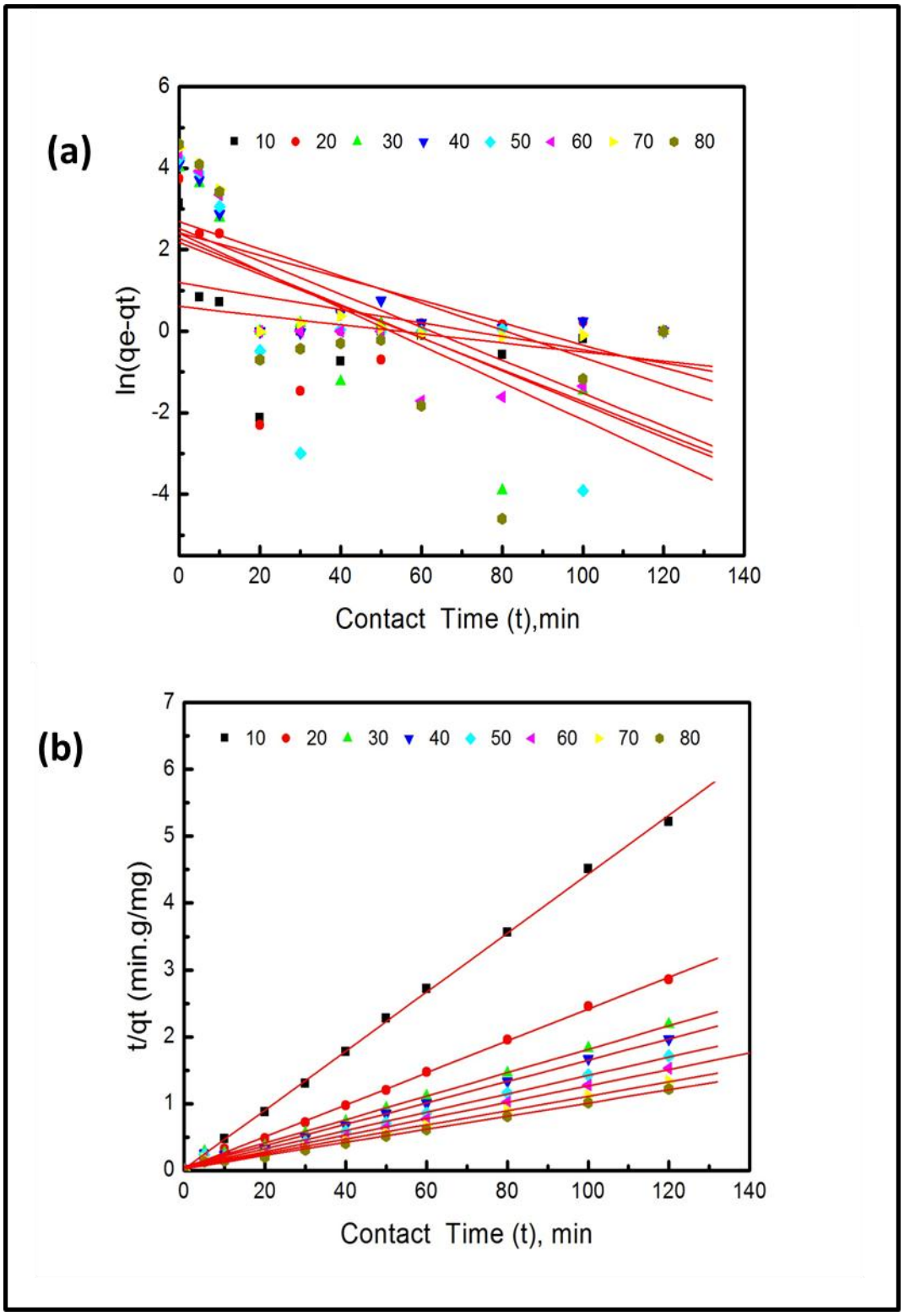

Figure 4.20: (a) Pseudo-first order kinetics (b) Pseudo second order kinetics for adsorption of Pb (II).

4.5.4 Thermodynamic study of Pb (II)

Generally, thermodynamic parameters are able to provide more information regarding the energetic change involved during the adsorption process. The adsorption isotherm of Pb (II) onto CNTs was measured at 293, 303, 308 and 323 K and the change in the thermodynamic parameters of the free energy of sorption (ΔG°), enthalpy (ΔH°), and entropy (ΔS°) were calculated using equations (4.9 & 4.8) from the variation of the thermodynamic equilibrium constant, K with a change in temperature. Free energy change (ΔG) can be calculated using equation (4.8), where R is the universal gas constant while T is the temperature in kelvin. Where K is the equilibrium constant and q_e and C_e are the amount of Pb (II) adsorbed per unit mass of CNTs and the equilibrium concentration of Pb (II) in the solution respectively. The enthalpy change value was obtained from the intercept of the ΔG° versus T plot. The values of the thermodynamic parameters obtained are shown in Table 4.8.

$$\Delta G = -RT\ lnK,\ K = \frac{Ce}{qe} \tag{4.8}$$

$$\ln K = \left(-\frac{\Delta H^{\circ}}{RT}\right) + \left(\frac{\Delta S^{\circ}}{R}\right) \tag{4.9}$$

The negative ΔG° value for the adsorption of Pb (II) on the CNTs surface at all temperatures proves that the sorption was spontaneous and thermodynamically favorable. In the same vein, the entropy change value, ΔS suggest that the randomness of the process at the solid-solution interface, increased when the Pb (II) ions attached to the active sites of adsorbent. The positive value of the enthalpy change value, ΔH proves that this adsorption experiment was an endothermic process (Li, Ding, et al., 2003; Pehlivan, et al., 2008).

Table 4.8: Thermodynamic parameters for Pb (II) adsorption.

Co Initial Conc (mgL^{-1})	**ΔH° ($kJ\ mol^{-1}$)**	**ΔS° $kJ\ mol^{-1}K^{-1}$**	**ΔG° ($kJmol^{-1}$)**			
			293 K	**303 K**	**308 K**	**323 K**
10	8.04	27.96	-8185	-8465	-8604	-9024
20	4.2	21.4	-6266	-6480	-6587	-6908
30	210.2	16.67	-4705	-4785	-4946	-5186
40	0.016	11.09	-3252	-3363	-3418	-3585

4.5.5 FTIR analysis of Pb (II) adsorption

The surface chemistry in terms of functional group which is adhered to the surface of CNTs during the adsorption of Pb (II) on the CNTs surface can be classified by employing Fourier Transform Infrared (FTIR) spectroscopy (Bruker, IFS66v/S). As for this research, FTIR was engaged as well to determine the functional groups attached on the surface of CNTs before and after adsorption of Pb (II). Fig 4.20 (a-b) shows the FTIR profile for adsorption of Pb (II) onto the CNTs surface before and after adsorption of Pb (II) respectively. Fig. 4.20 (a) demonstrates that there were few functional groups attached on the CNTs surface before the adsorption of Pb (II) while there were more peaks observed for after adsorption of Pb (II) on the CNTs as can be seen in Fig. 4.20 (b). The intensity of the band in the 3859-2519 cm^{-1} region contains –OH groups. The width and asymmetry of this band indicate the presence of strong hydrogen bonds. These hydrogen bonds could be a result of strongly adsorbed water on hydrophilic functional groups of the CNTs surfaces; The bands at 1965 and 1746 and from 2250-2400 cm^{-1}show carbonyl group (Li, et al., 2005; Li, Wang, et al., 2002), the bands at 996 cm^{-1} contains saturated carbon (methyl group $–CH_3$) which might be from the cracking of acetylene (Wang et al., 2004).

Absorption peaks at 766 and 702 cm^{-1} represent NO_2 bending vibrations (Mubarak, et al., 2014; Mubarak, et al., 2011).

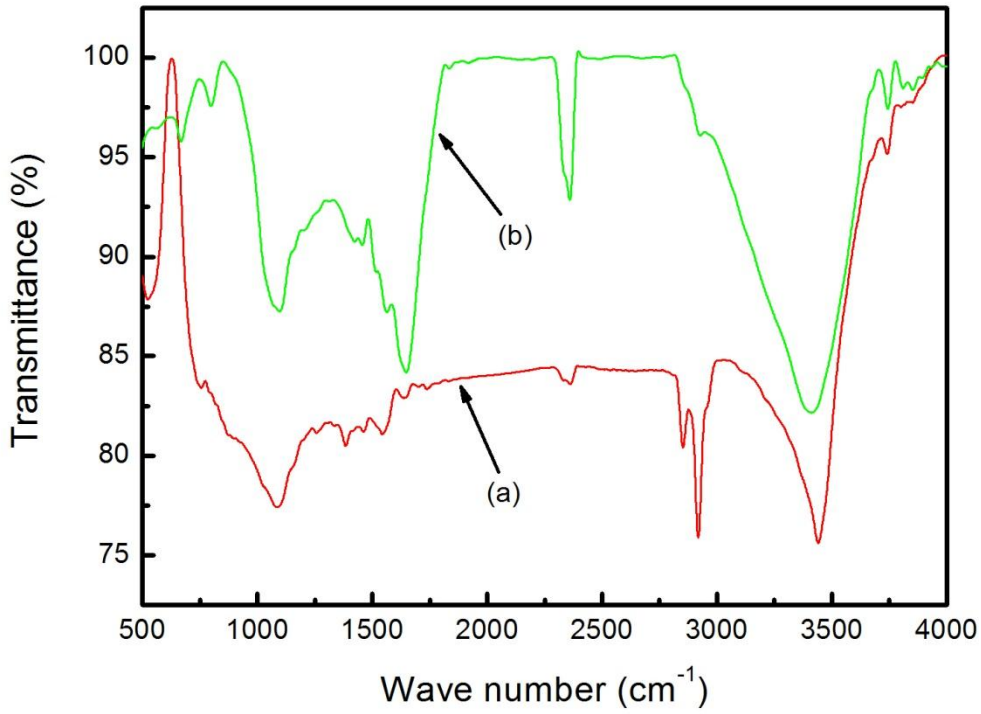

Figure 4.21: FTIR analysis of (a) CNTs before and (b) CNTs after adsorption of Pb (II).

4.6 Statistical optimization of removal of Cd (II) using CNTs

In order to determine the most suitable adsorbent with the highest adsorption capacity of Cd (II) from aqueous solutions, the first crucial step would be to determine the optimized condition of CNTs as a the adsorbent for removal of Cd (II). Specific runs for the optimized condition were conducted based on the design obtained from the DOE . The detail experimental array of adsorption rate of removal of Cd (II) as shown in appendix C. The results obtained from this particular experiment were analyzed using the application of "analysis of variance" (ANOVA) obtained from the DOE and the optimized variables are attainable from Table 3.3. The analyses obtained by the application of ANOVA for the

removal of Cd (II) using CNTs are indicated in Table 4.9. From the values obtained in Tables 4.9, the fisher F-test value can be related to the mean square of the regressed model which leads to the comparative mean square of the residuals (errors). The F value proves the efficiency of the model as its value increases. On the other hand, low probability, P value indicates higher significance of the regression model. Hence, from Tables 4.9, it can be seen that the F-test values using CNTs were 19, which indicates that the model are significant. Besides that, the values of the correlation coefficient, R-Squared and Adj R-Squared for CNTs were 0.96 and 0.90 respectively. This value implies that the model of the adsorbent is very close to each other, which indicates the high efficiency and significance of the model. The model equation evolved for the removal of Cd (II) from aqueous solutions for CNTs (3) are as follows:

Cd (II) Removal (%) = 96.50+0.61 * A-1.52 * B-0.26 * C+1.76 * D-10.19 * A^2-12.34 * B^2-6.34 * C^2-8.84* D^2-1.23 * A * B+2.86 * A * C+0.27 * A * D-0.27 * B * C+1.89 * B * D+1.23 * C * D (4.10)

Consequently, variables A, B, C, D, AB, AC, AD, BC, BD, and CD were significant model terms. This indicates that the pH (A), agitation speed (B), MWCNTs dosage (C) and time (D) were highly significant values of Probe >F was 0.001. The coefficient of single factor represents the effect of its represented factor while the coefficients of double factors represent the interaction and effect of both represented factor. Hence, following up to the equation, the positive sign in the equation represents the synergistic effect while the negative sign represents antagonistic effect values. Fig. 4.21 shows theoretical values versus the experimental values for Cd (II) removal. It was clearly shown that the theoretical values obtained were quite close to experimental values, indicating that the model

developed was successful in bridging the correlation between process parameters for removal of Cd (II).

Table 4.9: ANOVA for the selected factorial Model for removal of Cd (II).

Source	**Sum of squares**	**DF**	**Mean square**	**F Value**	**Prob > F**	**Status**
Model	6118.869	14	437.062	19.0	<.0001	Significant
A	6.7222	1	6.7222	0.3	0.5994	
B	41.405	1	41.405	1.8	0.2066	
C	1.2272	1	1.22722	0.1	0.8215	
D	55.827	1	55.827	2.4	0.1474	
A2	265.673	1	265.673	11.6	0.0059	
B2	389.673	1	389.673	17.0	0.0017	
C2	102.785	1	102.785	4.5	0.0581	
D2	199.913	1	199.913	8.7	0.0132	
AB	24.2556	1	24.2556	1.1	0.3263	
AC	130.530	1	130.530	5.7	0.0363	
AD	1.15562	1	1.15562	0.1	0.8267	
BC	1.15562	1	1.15562	0.1	0.8267	
BD	57.3806	1	57.380	2.5	0.1424	
CD	24.255	1	24.255	1.1	0.3263	
Residual	252.789	11	22.980			
Lack of Fit	252.28	10	25.228	50.5	0.1092	Insignificant
Pure Error	0.5	1	0.5			
Cor Total	6371.658	25				

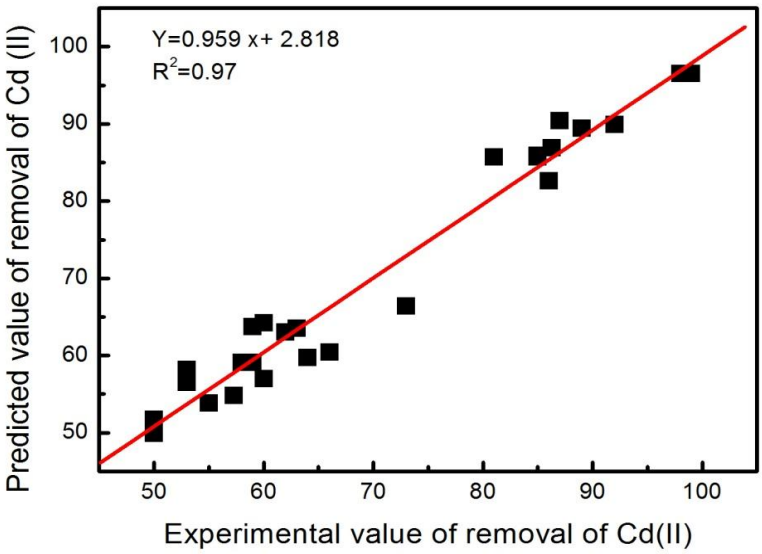

Figure 4.22: Relationship between actual value vs predicted values of removal of Cd (II).

Fig. 4.22 represents the 3-dimensional (3-D) plot for adsorption of Cd (II) prepared under optimized conditions of CNTs production affected by pH, CNTs dosage and agitation speed. The 3-D plot of the interaction between agitation speed and pH are as depicted in Fig. 4.22 (a) which shows that as pH increases with the increasing of agitation speed, removal of Cd (II) obtained the highest at pH 5 an 160 rpm agitation speed gave maximum removal of Cd (II). Further increase in pH and agitation speed resulted in decreased Cd (II) removal. This is due to the effects of precipitation of Cd (II) at relatively high values of pH (alkaline condition). The value of pH of the aqueous solution plays a major role in the adsorption of heavy metals (Li, Wang, et al., 2003; Stafiej and Pyrzynska, 2007; Vuković, et al., 2010). Fig. 4.22 (b) shows the interaction between pH and CNTs dosage where it was observed that removal of Cd (II) reached to the maximum when the pH and CNTs dosage is at its center point. Further increased in pH and CNTs dosage resulted in Cd (II) adsorption decreased. From the observation, increased in CNTs dosage from 0.05 to 0.1

increase the removal of cd linearly. Furthermore, the increase in the adsorbed amount leads to increase in active sites concentration which helps in adjusting the adsorption solution electrostatic charge to an adsorption preferable level by removing the competitive H^+ ions (Hsieh, et al., 2006; Li, Wang, et al., 2003). On the other hand, the adsorption capacity is highly dependent on the pH where H_2O_2 oxidizes the CNTs to reach an equilibrium state with a high adsorption capacity at lower pH (Li, Wang, et al., 2003). Fig. 4.22 (c) shows the interaction between time and pH. The elliptical plot indicated that there is good interaction between time and pH. The mid- point interaction for a time and pH shows the highest removal of Cd (II) obtained. Further increase in time 35 to 60 minutes and pH 5 to 6 resulted in decreased of Cd (II) removal (Gao, et al., 2009).

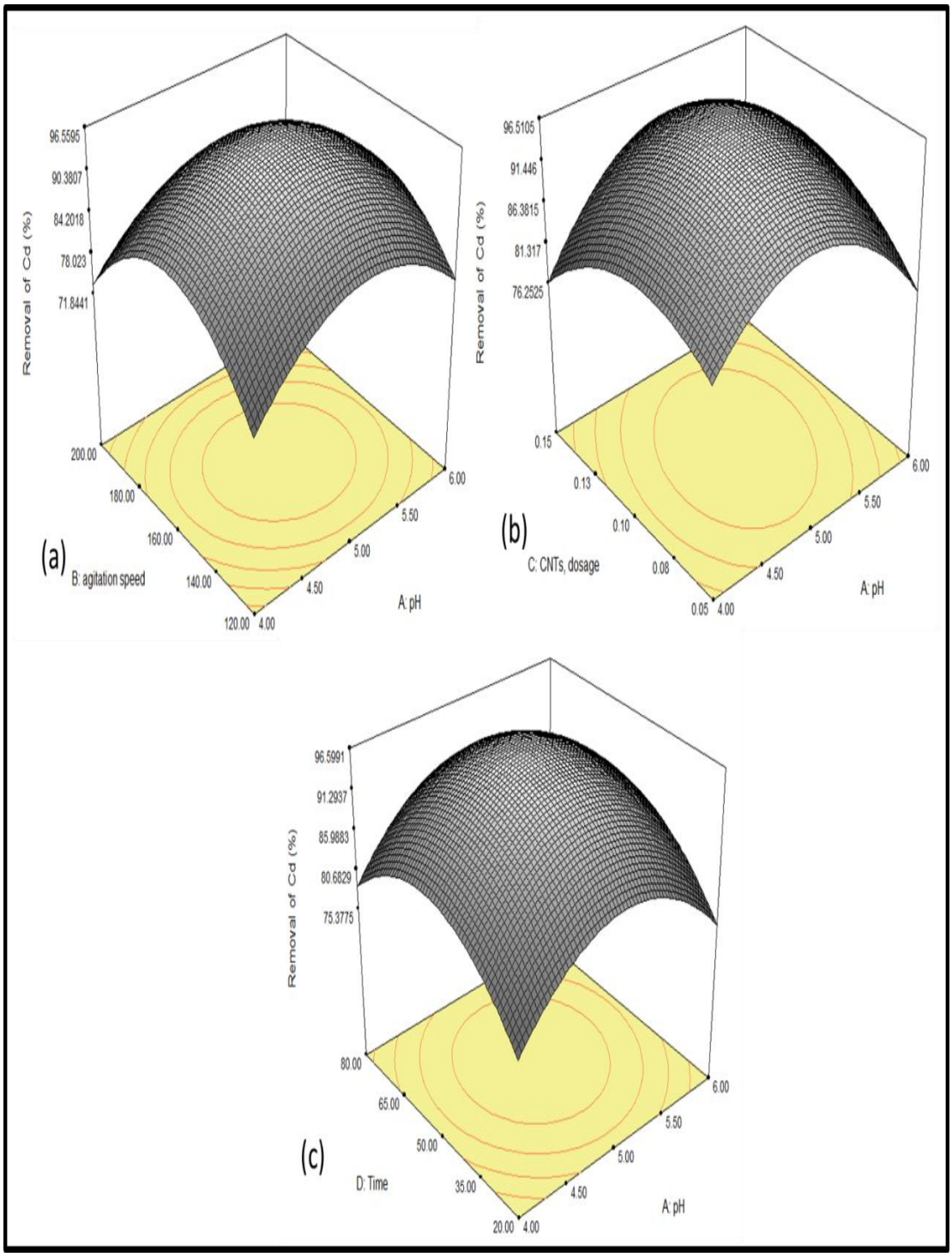

Figure 4.23: 3-D plots of removal of Cd (II) using optimized CNTs production, (a) interaction of agitation speed and pH, (b) interaction of CNTs dosage and pH, and (c) interaction of time and pH.

4.6.1 Adsorption isotherm of Cd (II)

Adsorption is the accumulation of mass transfer process that can generally be defined as material at the interface between solid and liquid phases. Equilibrium relationships between sorbent and sorbate are described by sorption isotherms, usually the relation between the quality sorbed and that remaining in the solution at a fixed temperature at equilibrium. Adsorption isotherms provide useful information for estimating performance in full scale stream (Pehlivan, et al., 2008; Rao, et al., 2010; Salmani, et al., 2013). The relation between contact time (min) versus adsorption capacity (q_t) was plotted for different Cd (II) concentration as shown in Fig. 4.23. Adsorption of high initial Cd (II) concentration results in an increase in the adsorption uptake due to increase in mass transfer driving force leading to higher adsorption rate (Chen, et al., 2009; Chen and Wang, 2006). More than 90% of maximum equilibrium uptake capacity was reached after 50 min and complete equilibrium was reached in the 50 min to 120 min. No significant additional adsorption was observed after 120 min of contact time. The contact time was thus maintained for 120 min to ensure that the equilibrium could be achieved (Chen and Wang, 2006; Li, Wang, et al., 2003; Stafiej and Pyrzynska, 2007). It indicates that carbon obtained has highly active sites with well developed pores, which is responsible for Cd (II) adsorption. The equilibrium uptake concentration (qe) of Cd (II) on solid phase adsorbent is directly proportional to Cd (II) connotation in the liquid phase as shown Fig. 4.23 which mainly attributed to unsaturation of the adsorption sites or layers through the adsorption process. Such observation is usually reported by most of the researchers in the filed of sorption processes (Kabbashi, 2011; Li, Ding, et al., 2003; Vilar, et al., 2006; Vuković, et al., 2010).

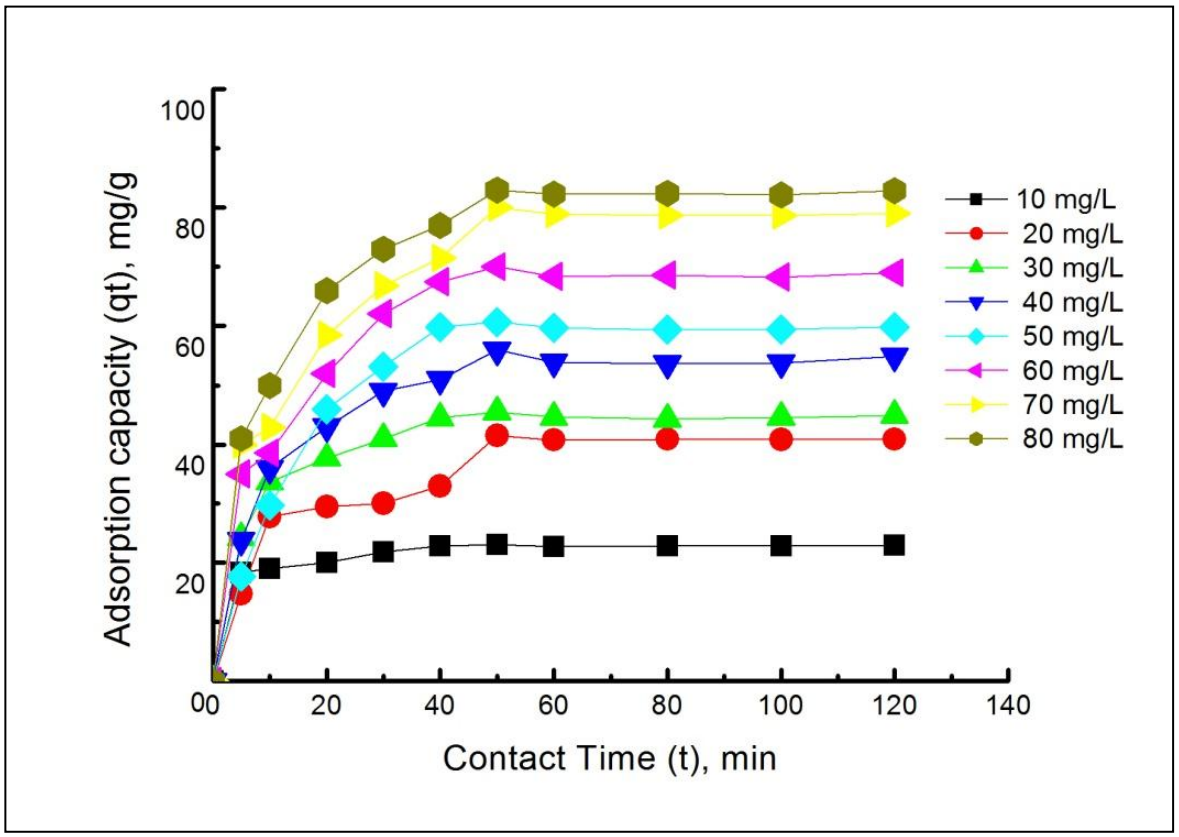

Figure 4.24: Adsorption capacity (qt) versus contact time (t) with different Cd (II) solution concentration.

4.6.1 Adsorption kinetics of Cd (II)

Adsorption isotherm is a powerful isotherm to demonstrate the unique relationship between carbonaceous adsorbents and the adsorbate. The interaction and affinity of equilibrium data are important and necessary for realistic and useful design and basic knowledge of adsorption system. The Langmuir isotherm (equation 4.3), Freundlich isotherm (equation 4.4) and Temkin (equation 4.5 and 4.6) and Dubinin isotherm (equation 4.7) for Cd (II) have been successfully illustrated in Fig. 4.24 (a-d). As for this research study, four models were employed to determine the optimum model for the Cd (II) adsorption onto the CNTs surface.

. Their constants and correlation coefficient were tabulated in Table 4.10. The isotherm data were collected through the measurements of Cd (II) metal ions after certain Sorbent/ adsorbate contact intervals. The data collected throughout the experiment were proving valid for Langmuir and Freundlich isotherm R^2= 0.97, and R^2= 0.98 respectively. However, Temkin and dubinin-Radushkevich isotherms do not show a good representation. Hence, high validity of Freundlich isotherm model proposes the adsorption process was taking place at the heterogeneous and consistent and well distribution of active sites along the CNTs surface. Review on Cd (II) removal using CNTs as shown in Table 4.11.

Table 4.10: Isotherm parameters for Cd (II) adsorption by CNTs

Langmuir Isotherm		**Freundlich Isotherm**		**Temkin Isotherm**		**Dubinin-Radushkevich**	
q_m (mg g^{-1})	88.62	K_F (Lg^{-1})	24.75	A (Lg^{-1})	4.76	q_m	66.56
K_L (L mg^{-1})	0.135	n	3.5	B ($kJmol^{-1}$)	181.18	K $x10^{-6}$ (mol^2 kJ^{-2}	5.62
R^2	0.97	R^2	0.98	R^2	0.87	E (kJ mol^{-1})	0.3
						R^2	0.81

Table 4.11: Review on Cd (II) removal using CNTs.

Adsorbent	**q_m (mg/g)**	**K_L (L/mg)**	**R^2**	**K_f (L/mg)**	**n**	**R^2**	**References**
MWCNTs	88.62	0.135	0.97	24.75	3.5	0.98	This study
CNTs/Al_2O_3	8.89	0.13	0.956	1.17	1.55	0.926	(Hsieh and Horng, 2007)
CNTs	6.19	0.18	0.997	1.94	1.94	0.964	
CNTs	9.41	0.37	0.957	-	-	-	(Hsieh, et al., 2006)
Oxidized CNTs	10.86	0.29	0.993	-	-	-	(Li, Ding, et al., 2003)
Oxidized CNTs	92.59	0.0029	0.906	4.119	0.401	0.95	(Tofighy and Mohammadi, 2011)
CNTs	34.34	-1.852	0.968	1.896	-0.208	0.968	(Kabbashi, 2011)
Raw-CNTs	1.26	0.135	0.996	0.0027	0.524	0.969	(Vuković, et al., 2010)
Oxidized CNTs	22.39	0.0317	0.996	0.127	0.601	0.97	
Oxidized CNTs	26	1.18	0.99	--	-	-	(Gao, et al., 2009)
CNTs oxidized	11.01	0.28	0.9926	-	-	-	(Li, 2004)
SWCNTs	18.86	0.544	0.99	13.13	11.07	0.99	(Moradi, 2011)
SWCNTs-COOH	52.356	1.002	0.999	37.856	10.593	0.983	

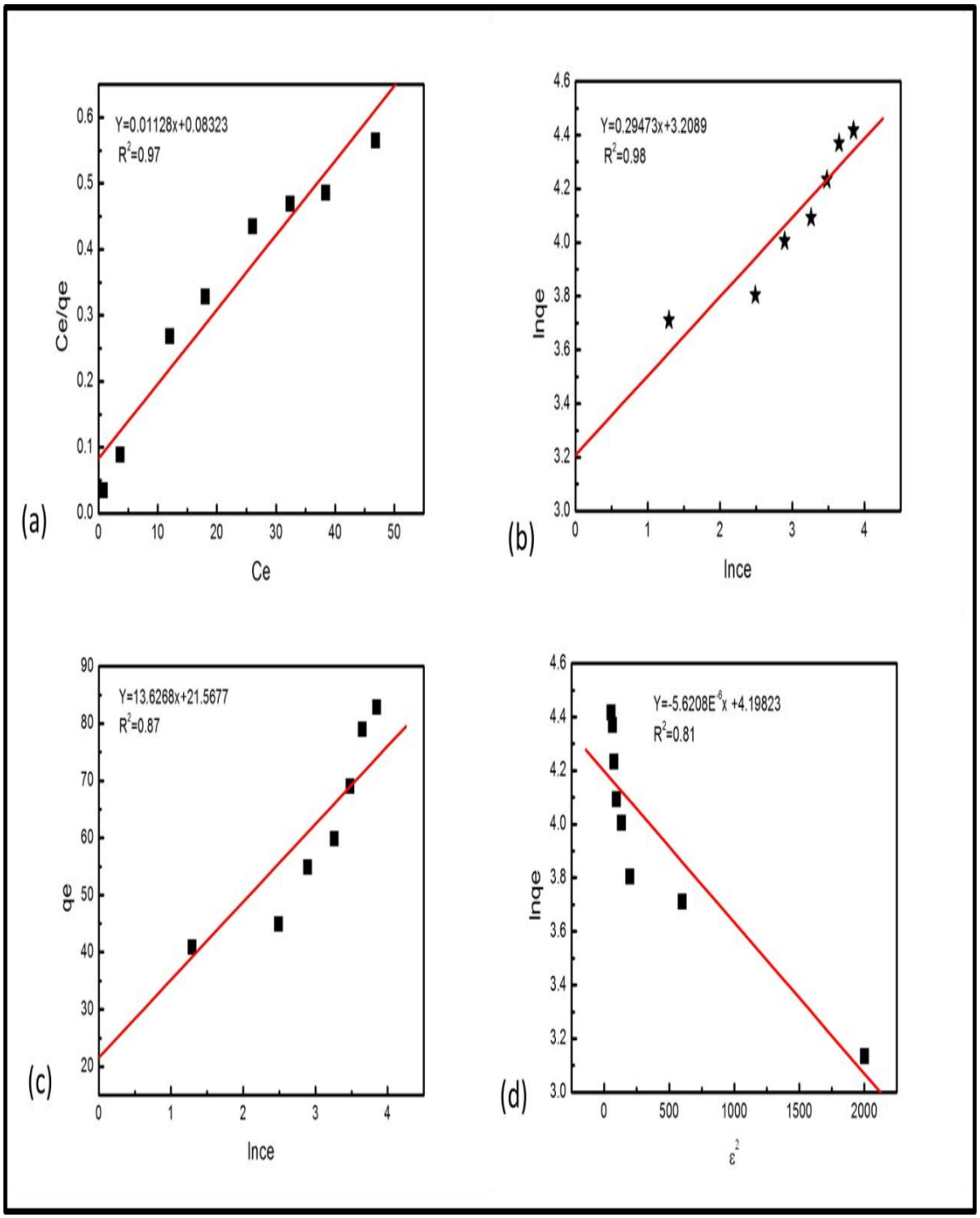

Figure 4.25: (a) Langmuir isotherm (b) Freundlich isotherm (c) Temkin isotherm, and (d) Dubinin –Radushkevich isotherm plots for adsorption of Cd (II).

Adsorption kinetics have been proposed to elucidate the adsorption mechanism. The mechanism of adsorption depends on the physical and chemical characteristic of the adsorbent as well as on the mass transfer process. In order to investigate the mechanism of adsorption of Cd (II) on CNTs and examine the potential rate, the capability of pseudo-first order (Langergren, 1898) pseudo second order (Ho, 2006b; Ho and McKay, 1999b). Kinetic models were examined in this study. The conformity between experimental data and the model predicted values was expressed by the correlation coefficients (R^2 values close or equal 1). A relatively high R^2 values indicate that the model successfully describes the kinetics of Cd (II) adsorption. Fig 4.25 (a) shows the plot ln (qe-qt) against time representing the linear form of pseudo-first order kinetic model. The rate constant K_1 was calculated from the slope of straight line obtained. K_2 is the rate constant of pseudo second order adsorption kinetics (min.g/mg) was calculated from the intercept and slope of the straight line of t/qt against time as shown in Fig 4.25 (b). From the observation, the kinetics of adsorption of Cd (II) ions adsorption on CNTs followed the pseudo second order with more conformity comparing pseudo first order as shown in Table 4.12. The pseudo second order rate has been applied widely to the sorption of metal ions, herbicides, oil and organic substances from aqueous systems (Ho, 2006b; Ho and McKay, 1999b).

Table 4.12: Experimental values of constants of adsorption kinetics model.

C_0 mgL^{-1}	qe,exp. ($mg\ g^{-1}$)	Pseudo-First order			Pseudo-Second order		
		qe, cal ($mg\ g^{-1}$)	K_1 (min^{-1})	R^2	qe,cal. ($mg\ g^{-1}$)	K_2 ($min.g\ mg^{-1}$)	R^2
10	22.99	4.11	0.0279	0.49	23.22	0.029	0.999
20	40.89	23.0	0.0536	0.59	43.63	0.003	0.994
30	44.9	11.54	0.0356	0.60	46.01	0.0081	0.999
40	54.9	21.30	0.0337	0.76	56.75	0.0041	0.998
50	59.87	16.66	0.0413	0.48	64.10	0.0024	0.995
60	69.01	25.0	0.0401	0.71	71.99	0.0031	0.997
70	79	33.3	0.0484	0.60	83.12	0.0025	0.997
80	82.9	33.51	0.0421	0.75	86.28	0.0026	0.998

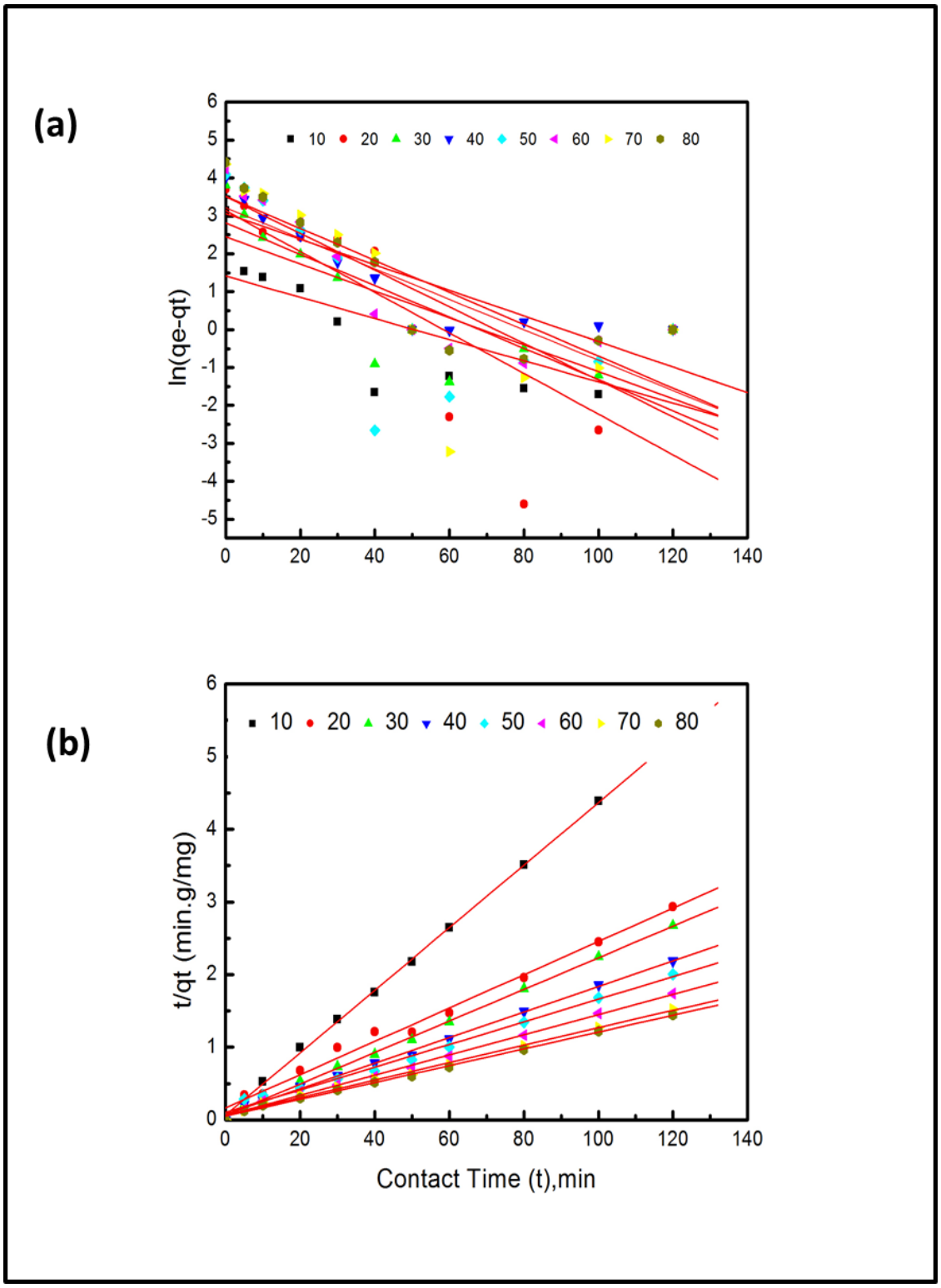

Figure 4.26: (a) pseudo-first order kinetics (b) pseudo second order kinetic for adsorption of Cd (II).

4.6.2 Thermodynamic study of Cd (II)

The evaluation of thermodynamic parameters provides in detail intuition into the mechanism of Cd (II) adsorption process. The adsorption isotherm of Cd (II) onto CNTs was measured at 293, 303, 308 and 323 K and the change in the thermodynamic parameters of the free energy of sorption (ΔG°), enthalpy (ΔH°), and entropy (ΔS°) were calculated using equations (4.8 & 4.9) from the variation of the thermodynamic equilibrium constant, K with a change in temperature. Free energy change (ΔG°) can be calculated using equation (4.8) below, where R is the universal gas constant while T is the temperature in Kelvin. Where K is the equilibrium constant and qe and Ce are the amount of Cd (II) adsorbed per unit mass of CNTs and the equilibrium concentration of Cd (II) in the solution respectively. The enthalpy change value was obtained from the intercept of the ΔG° versus T plot. The values of the thermodynamic parameters obtained are shown in Table 4.13.

The negative ΔG° value for the adsorption of Cd (II) on the CNTs surface at all temperatures proves that the sorption was spontaneous and thermodynamically favorable. In the same vein, the entropy change value, ΔS° suggest that the randomness of the process at the solid-solution interface, increased when the Cd (II) ions attached to the active sites of adsorbent. The negative value of the enthalpy change value, ΔH proves that this adsorption experiment was an exothermic process (Li, Ding, et al., 2003; Pehlivan, et al., 2008).

Table 4.13: Thermodynamic parameters for Cd (II) adsorption.

Co Initial Conc (mgL^{-1})	**ΔH° ($kJ\ mol^{-1}$)**	**ΔS° $kJ\ mol^{-1}K^{-1}$**	**ΔG° ($kJmol^{-1}$)**			
			293 K	**303 K**	**308 K**	**323 K**
10	-1.264	27.87	-8168	-8446	-8586	-9004
20	-0.584	20.1	-5859	-6090	-6191	-6192
30	-154.74	10.46	-3200	-3364	-3364	-3527
40	-1.44	9.23	-2708	-2800	-2847	-2985

4.6.3 FTIR analysis of Cd (II) adsorption

Adsorption behavior of any adsorbent is influenced by the chemical reactivity of the surface, especially when the chemically bonded oxygen exists on it in various forms of functional groups (Kandah and Meunier, 2007; Yang, et al., 2009). FTIR was engaged as well to determine the functional groups attached on the before and after adsorption of Cd (II) Fig. 4.26 (a-b) demonstrate the plot for CNTs before and after adsorption of Cd (II). Fig 4.26 (a) The peaks observed on before CNTs adsorption at a range of 1700 to 1900 cm^{-1} defines the carboxylic group, followed by aromatic C=C groups at 1450-1600 cm^{-1} and O-H groups at 2800-3000 cm^{-1} as well. Fig. 4.26 (b) shows after adsorption of Cd (II), it was observed several peaks were observed. The C= O and C–O are stretching frequencies shifted from 1705 and 1200 cm^{-1}. Peaks at 1600 cm^{-1} of amino-functionalized MWCNTs are due to the N–H stretching of amine groups. Peaks at 2930 and 2860 cm^{-1} are greatly enhanced because of the attachment of additional methyl groups. Peaks between 950 and 700 cm^{-1} are due to the stretching mode of aromatic amine groups, and peaks at 2370 cm^{-1} may be because of the existence of ammonium ions (Kuan et al., 2005; Peng et al., 2003; Stevens et al., 2003). The hydrophilic surface structure provides the functionalized CNTs an advantage of high dispersion in water, which eventually leads to a higher adsorption

capacity of Cd (II) ions from aqueous solution compared with before the adsorption of CNTs. This finding corresponds to many results reported by several previous researchers who studied on the surface chemistry of CNTs (Kuan, et al., 2005; Peng, et al., 2003; Smith, 1998; Stevens, et al., 2003; Zhang et al., 2010).

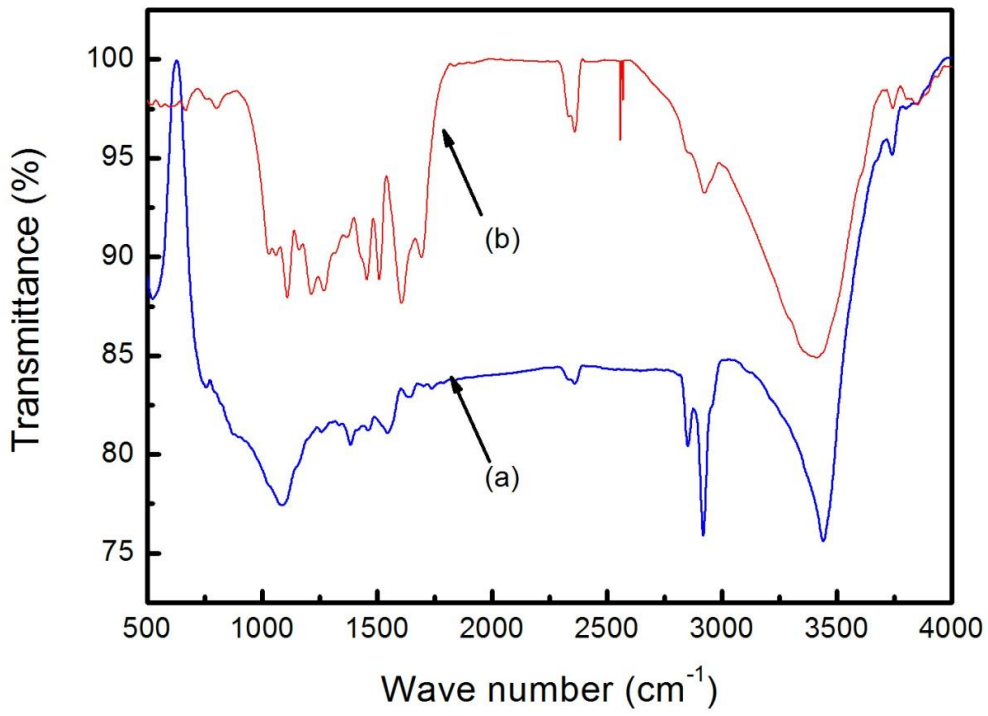

Figure 4.27: FTIR adsorption spectra for (a) CNTs before (b) CNTs after adsorption of Cd (II)

4.7 Statistical optimization of removal of Cu (II) using CNTs

The first crucial step in determining the most suitable adsorbent with the highest adsorption capacity of Cu (II) from aqueous solutions would be to find out the optimized condition of CNTs as a the adsorbent for removal of Cu (II). DOE is used to obtain the specific runs for the optimized condition. The detail experimental array of adsorption rate of removal of Cu

(II) as shown in appendix D. The results obtained from this particular experiment were analyzed using the application of "analysis of variance" (ANOVA) obtained from the DOE and the optimized variables are attainable from Table 3.4. The analyses obtained by the application of ANOVA for the removal of Cu (II) using CNTs are indicated in Table 4.14. From the values obtained in Tables 4.14, the fisher F-test value can be related to the mean square of the regressed model which leads to the comparative mean square of the residuals (errors). The F value proves the efficiency of the model as its value increases. On the other hand, low probability, P value indicates higher significance of the regression model. Hence, from Tables 4.14, it can be seen that the F-test values using CNTs were 9.96, which indicates that the model are significant. Besides that, the values of the correlation coefficient, R-Squared and Adj R-Squared for CNTs were 0.95 and 0.91 respectively. This value implies that the model of the adsorbent is very close to each other, which indicates the high efficiency and significance of the model. The model equation evolved for the removal of Cu (II) from aqueous solutions for CNTs (4.11) are as follows:

Removal of Cu (II) = 95.30+8.31 * A+1.25 * B+1.08 * C+1.68 * D-25.17 * A^2-10.67 * B^2-9.12 * C^2 -12.82 * D^2+1.53 * A * B-1.3* A * C+2.22 * A * D+1.66 * B * C-0.28*B*D+0.094*C*D (4.11)

Consequently, variables A, B, C, D, AB, AC, AD, BC, BD and CD were significant model terms. This indicates that the pH (A), agitation speed (B), MWCNTs dosage (C) and time (D) were highly significant values of Probe >F was 0.003. The coefficient of single factor represents the effect of its represented factor while the coefficients of double factors represent the interaction and effect of both represented factor. Hence, following up to the equation, the positive sign in the equation represents the synergistic effect while the negative sign represents antagonistic effect values. Fig. 4.27 shows theoretical values

versus the experimental values for Cu (II) removal. It was clearly shown that the theoretical values obtained were quite close to experimental values, indicating that the model developed was successful in bridging the correlation between process parameters for removal of Cu (II).

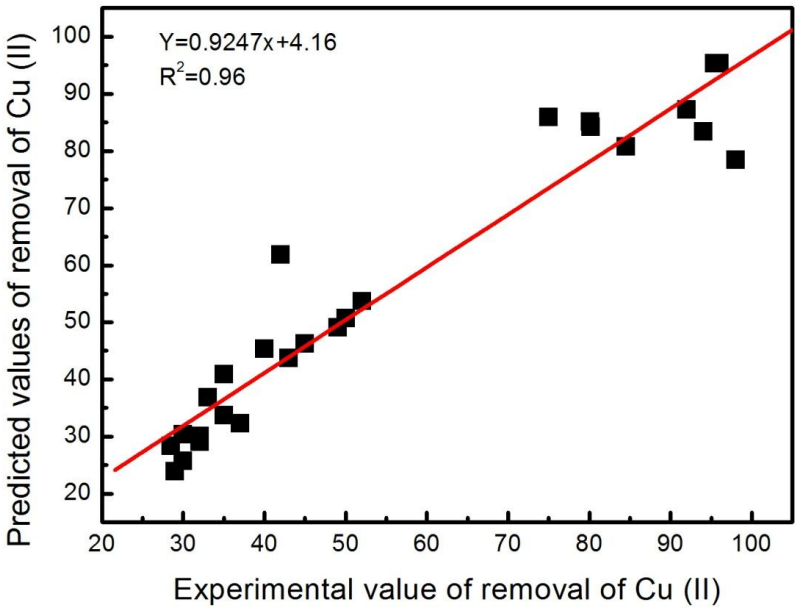

Figure 4.28: Relationship between actual value and predicted values of removal of Cu (II).

Table 4.14: ANOVA for the selected quadratic Model for removal of Cu (II).

Source	Sum of squares	DF	Mean square	F Value	Prob > F	Status
Model	15339.36	14	1095.66	9.66	0.0003	Significant
A	1241.681	1	1241.68	10.94	0.0070	
B	28.125	1	28.125	0.25	0.6284	
C	20.90889	1	20.9088	0.18	0.6760	
D	50.66889	1	50.6688	0.45	0.5177	
A^2	1622.759	1	1622.75	14.30	0.0030	
B^2	291.6944	1	291.694	2.57	0.1372	
C^2	213.1188	1	213.118	1.88	0.1978	
D^2	421.0588	1	421.058	3.71	0.0803	
AB	37.51563	1	37.5156	0.33	0.5768	
AC	28.89063	1	28.8906	0.25	0.6238	
AD	78.76563	1	78.7656	0.69	0.4225	
BC	43.89063	1	43.8906	0.39	0.5466	
BD	1.265625	1	1.26562	0.01	0.9178	
CD	0.140625	1	0.14062	0.001	0.9725	
Residual	1248.069	11	113.460			
Lack of Fit	1247.889	10	124.788	693.27	0.1295	Insignificant
Pure Error	0.18	1	0.18		0.0003	
Cor Total	16587.43	25			0.0070	

Fig. 4.28 represents the 3-dimensional plot for adsorption of Cu (II) prepared under optimized conditions of CNTs production affected by pH, MWCNTs dosage and agitation speed. Fig. 4.28 (a) shows the 3-D interaction plot of pH and agitation speed. The interaction of both factors curved a nice elliptical graph where it gives the highest percentage of Cu adsorption at pH 5.5 and agitation speed of 160 rpm. The pH value of the aqueous solution plays a major role in the adsorption of heavy metals (Chen, et al., 2007;

Chen and Wang, 2006; Li, Ding, et al., 2003; Moradi, 2011; Xu, et al., 2008). On the other hand, the minimum adsorption of Cu (II) was observed at low pH of 2 this is due to the fact that the presence of higher concentration and higher mobility of H^+ ions favoured its adsorption compared to Cu (II) ions and furthermore, due to the high solubility and ionization of Cu (II) salt in the acidic medium (Li, Ding, et al., 2003; Li, 2004). It would be plausible to suggest that at lower pH value, the surface of the adsorbent is surrounded by H^+, thereby preventing the metal ions from approaching the binding sites of the CNTs. This means that at the higher H^+ concentration, the CNTs surface becomes more positively charged such that attraction between adsorbents and metal cations is reduced (Li et al., 2007; Tumin et al., 2008; Wu, 2007). In contrast, with an increase in pH, more negative sites offered by these functional groups are becoming available for the adsorption of Cu (II), thus the Cu (II) removal efficiency increases quickly at high pH (Li, et al., 2010). This is due to the fact, sorption of metal cations increased with increasing pH as the metal ionic species become less stable in the solution and thus facilitating greater Cu (II) removal (Li, Luan, et al., 2003b). The maximum adsorption observed at pH 5 it is due to partial hydrolysis of Cu (II) ions, resulting in the formation of Cu (OH^+) ions and Cu $(OH)_2$, which would be adsorbed to a greater extent on a less-polar carbon surface of the adsorbents compares to Cu (II) ions. Furthermore the low solubility of hydrolyzed Cu (II) species may be another reason for a maximum adsorption at pH5 (Gabaldon et al., 2000; Ngah and Fatinathan, 2008). It is known that a precipitate of copper hydroxide will be produced within the higher pH region (at pH> 5.8) (Corapcioglu and Huang, 1987). In order to eliminate the precipitation effect on the Cu (II) adsorption by the adsorbents, adsorption isotherm experiments were carried out at the optimum pH of 5 (Corapcioglu and Huang, 1987). Fig. 4.28 (b) shows a linear increment of Cu (II) removal when the pH start

to increase from 2 to 4 before it reached the maximum adsorption at about pH 5.5 when interacted with CNTs dosage of 0.1. Further increased in pH and CNTs dosage resulted in Cu (II) adsorption decreased. From the observation, increased in CNTs dosage from 0.05 to 0.1 increase the removal of Cu (II) linearly. Furthermore, the increase in the adsorbent amount leads to increase in active sites concentration which helps in adjusting the adsorption solution electrostatic charge to an adsorption preferable level by removing the competitive H^+ ions (Hsieh, et al., 2006; Li, Wang, et al., 2003). On the other hand, the adsorption capacity is highly dependent on the pH where H_2O_2 oxidizes the CNTs to reach an equilibrium state with a high adsorption capacity at lower pH (Li, Wang, et al., 2003). Fig. 4.28 (c) shows the interaction of pH and time for the removal of Cu (II). It was observed that the Cu (II) was removed more than 95% at the time of 35 minutes. Further increase in time 35 to 60 minutes and pH 5.5 to 6 resulted in decreased of Cu (II) removal (Gao, et al., 2009; Li, et al., 2005; Li, Luan, et al., 2003b; Mubarak et al., 2012).

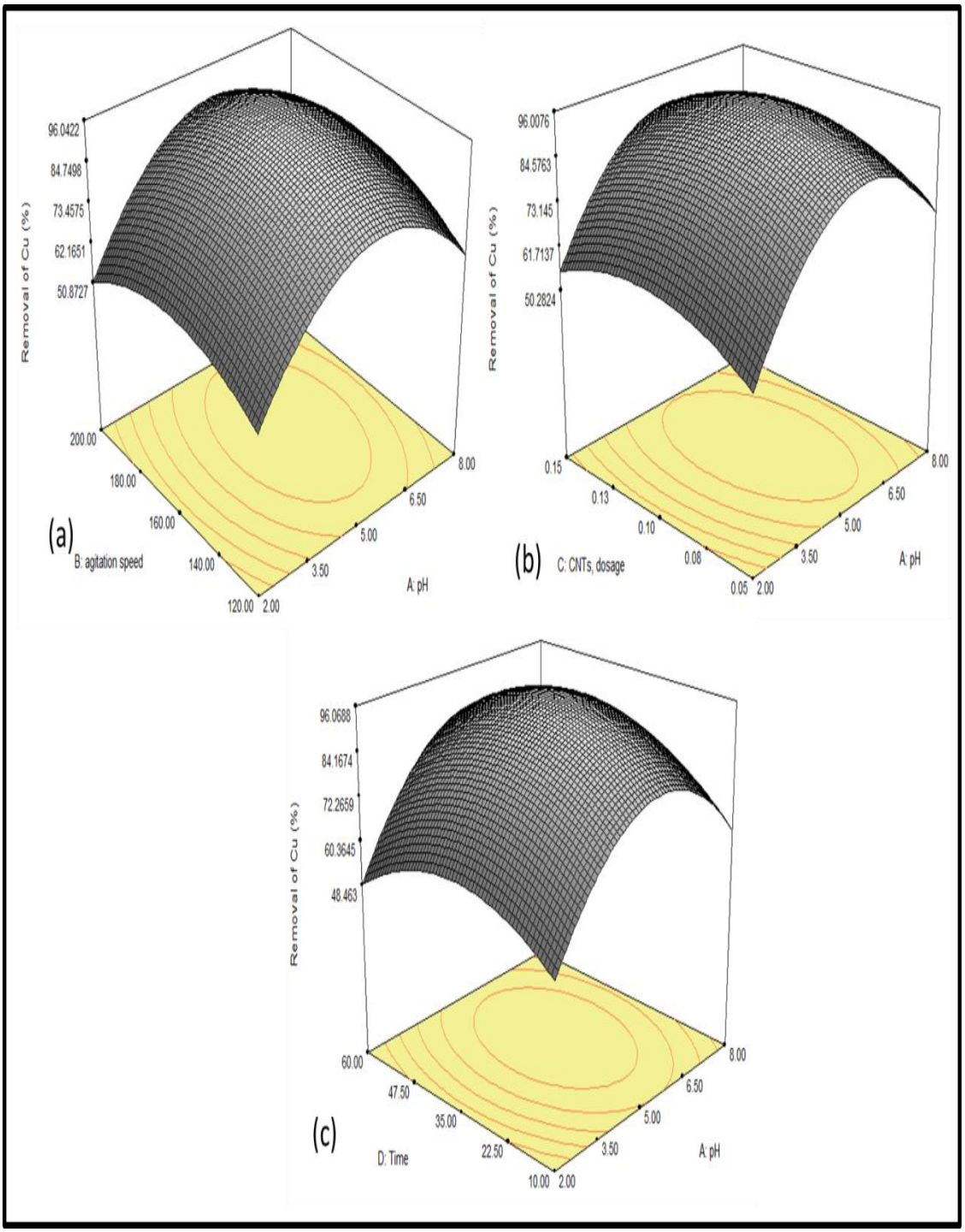

Figure 4.29:3-D plots of removal of Cu (II) using optimized CNTs production, (a) interaction of agitation speed and pH, (b) interaction of CNTs dosage and pH, and (c) interaction of time and pH.

4.7.1 Adsorption isotherm of Cu (II)

The correlation between the amount of a solute adsorbed at constant temperature and its concentration in the equilibrium solution is reflected by adsorption isotherm. It gives important physciochemical data to measure the applicability of the adsorption process as a complete unit operation. The successful representation of the dynamic adaptive separation of solute from solution onto an adsorbent depends upon a good description of the equilibrium spearation between the thow phase (Pehlivan, et al., 2008; Rao, et al., 2010; Salmani, et al., 2013). The relation between contact time (min) versus adsorption capacity (q_t) was plotted for different Cu (II) concentration as shown in Fig. 4.29. Adsorption of high initial Cu (II) concentration results in an increase in the adsorption uptake due to increase in mass transfer driving force leading to higher adsorption rate (Chen, et al., 2009; Chen and Wang, 2006). It was observed that adsorption of Cu (II) by CNTs was rapid during first 35 min. Beyond the 35 min, the rate of adsorption was observed to decline with increment in time, till equilibrium concentration was reached. This rapid adsorption at the initial time was expected, as the amount of Cu (II) ions present in solution and available sites on the adsorbent were still high, resulting in high adsorption sites on the adsorbents reduced, which resulted in a reduction in the rate of adsorption Cu (II) till equilibrium conentations were noticed. Furthermore, at the lower concentration, it becomes more difficult for less-polar adsorbents to adsorb Cu (II) from a more polar solvent (Stafiej and Pyrzynska, 2007; Wu, 2007; Yang, et al., 2009). More than 90% of maximum equilibrium uptake capacity was reached after 35 min and complete equilibrium was reached in the 35 min to 120 min. No significant additional adsorption was observed after 120 min of contact time. The contact time was thus maintained for 120 min to ensure that

the equilibrium could be achieved (Chen and Wang, 2006; Li, Wang, et al., 2003; Stafiej and Pyrzynska, 2007).

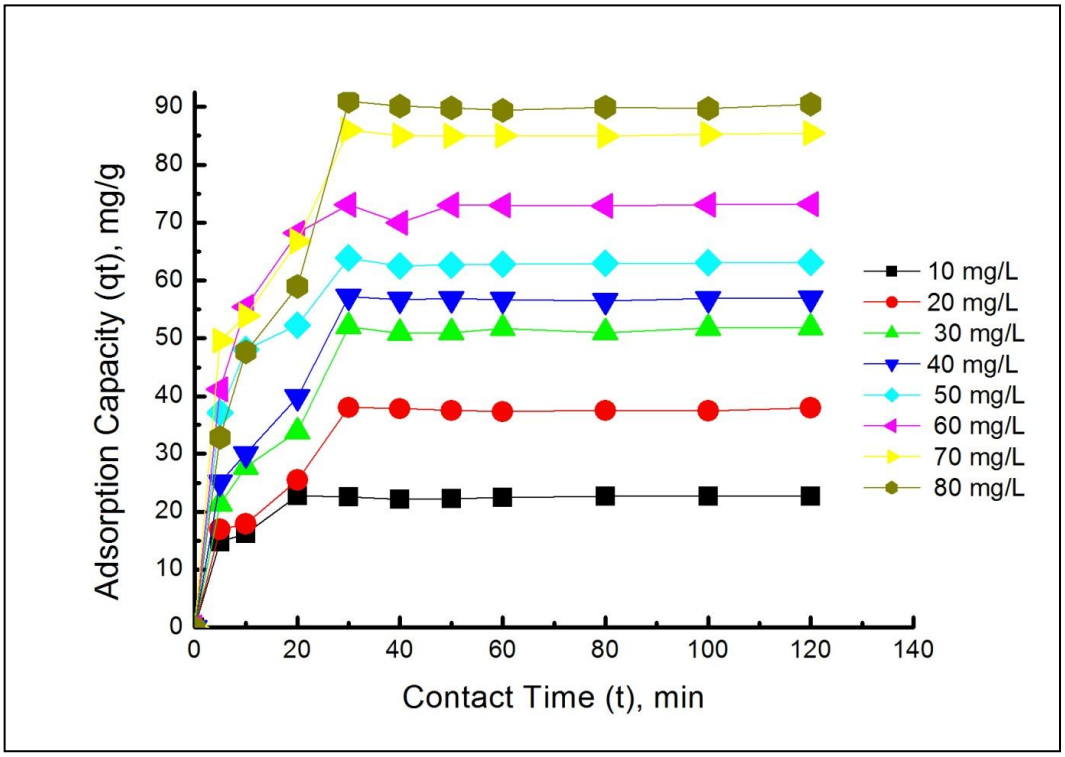

Figure 4.30: Adsorption capacity (qt) versus contact time (t) with different Cu (II) solution.

4.7.2 Adsorption kinetics of Cu (II)

The unique relationship between carbonaceous adsorbents and the adsorbate can be demonstrated by this powerful isotherm so called adsorption isotherm. The interaction and affinity of equilibrium data are essential for practical and functional design and basic knowledge of adsorption system. The Langmuir isotherm (equation 4.3), Freundlich isotherm (equation 4.4) and Temkin (equation 4.5 and 4.6) and Dubinin isotherm (equation 4.7) for Cu (II) have been successfully illustrated in Fig 4.30 (a-d). As for this research study, four models were employed to determine the optimum model for the Cu (II)

adsorption onto the CNTs surface. Their constants and correlation coefficient were tabulated in Table 4.15. The isotherm data were collected through the measurements of Cu (II) metal ions after certain sorbent/ adsorbate contact intervals. The data collected throughout experiment were proving valid for Langmuir and Freundlich isotherm R^2= 0.96, and R^2= 0.99 respectively. However, Temkin and dubinin-Radushkevich isotherms do not show a good representation. Hence, high validity of Freundlich isotherm model proposes the adsorption process was taking place at the heterogeneous and consistent and well distribution of active sites along the CNTs surface. Review on Cu (II) removal using CNTs as shown in Table 4.16.

Table 4.15: Isotherm parameters for Cu (II) adsorption by CNTs.

Langmuir Isotherm		**Freundlich Isotherm**		**Temkin Isotherm**		**Dubinin-Radushkevich**	
q_m (mg g^{-1})	99	K_F (Lg^{-1})	22.56	A (Lg^{-1})	2.71	q_m	71.8
K_L (L mg^{-1})	0.012	n	2.85	b ($kJmol^{-1}$)	146.79	K $x10^{-6}$ (mol^2 kJ^{-2}	6.97
R^2	0.96	R^2	0.99	R^2	0.89	E (kJ mol^{-1})	0.26
						R^2	0.81

Table 4.16: Review on Cu (II) removal using CNTs

Adsorbent	**qm (mg/g)**	**K_L (L/mg)**	**R^2**	**K_f (L/g)**	**n**	**R^2**	**References**
MWCNTs	99	0.012	0.96	22.56	2.85	0.99	This study
CNTs	27.03	0.05	0.969	-	-	-	(Hsieh, et al., 2006)
CNT	8.25	0.023	0.842	0.498	1.739	0.863	(Wu, 2007)
CNTs Modified with HNO_3	13.87	0.0542	0.96	1.542	2.33	0.986	
CNTs modified with NaOCl	47.39	2.951	0.974	21.0	5.33	0.98	
Oxidized MWCNT	28.49	3.82	0.982	-	-	-	(Li, Luan, et al., 2003b)
Oxidized CNT	64.93	0.002	0.89	1.2356	0.5170	0.988	(Tofighy and Mohammadi, 2011)
Oxidized CNT	40.4	0.885	0.996	-	-	-	(Gao, et al., 2009)
CNTs	26.41	0.94	0.99	12.77	3.87	0.96	(Li, et al., 2010)
CNTs-CA	84.88	0.78	0.99	32.01	1.84	0.955	
SWCNT-COOH	68.96	1.028	0.99	46.65	7.97	0.99	(Moradi, 2011)
SWCNTs	21.08	0.638	0.99	14.28	9.86	0.99	
CNTs-soaked in HNO_3	3.49	-	-	0.183	1.005	0.99	(Stafiej and Pyrzynska, 2007)
CNTs refluxed in HNO_3	2.69	-	-	0.189	0.992	0.992	
CNTs	7.14	0.12	0.996	0.99	1.86	0.980	(Hsieh and Horng, 2007)
CNTs-AL_2O_3	26.59	0.10	0.987	2.91	1.66	0.980	
CNTs-oxidized	28.33	3.84	0.9809	-	-	-	(Li, 2004)

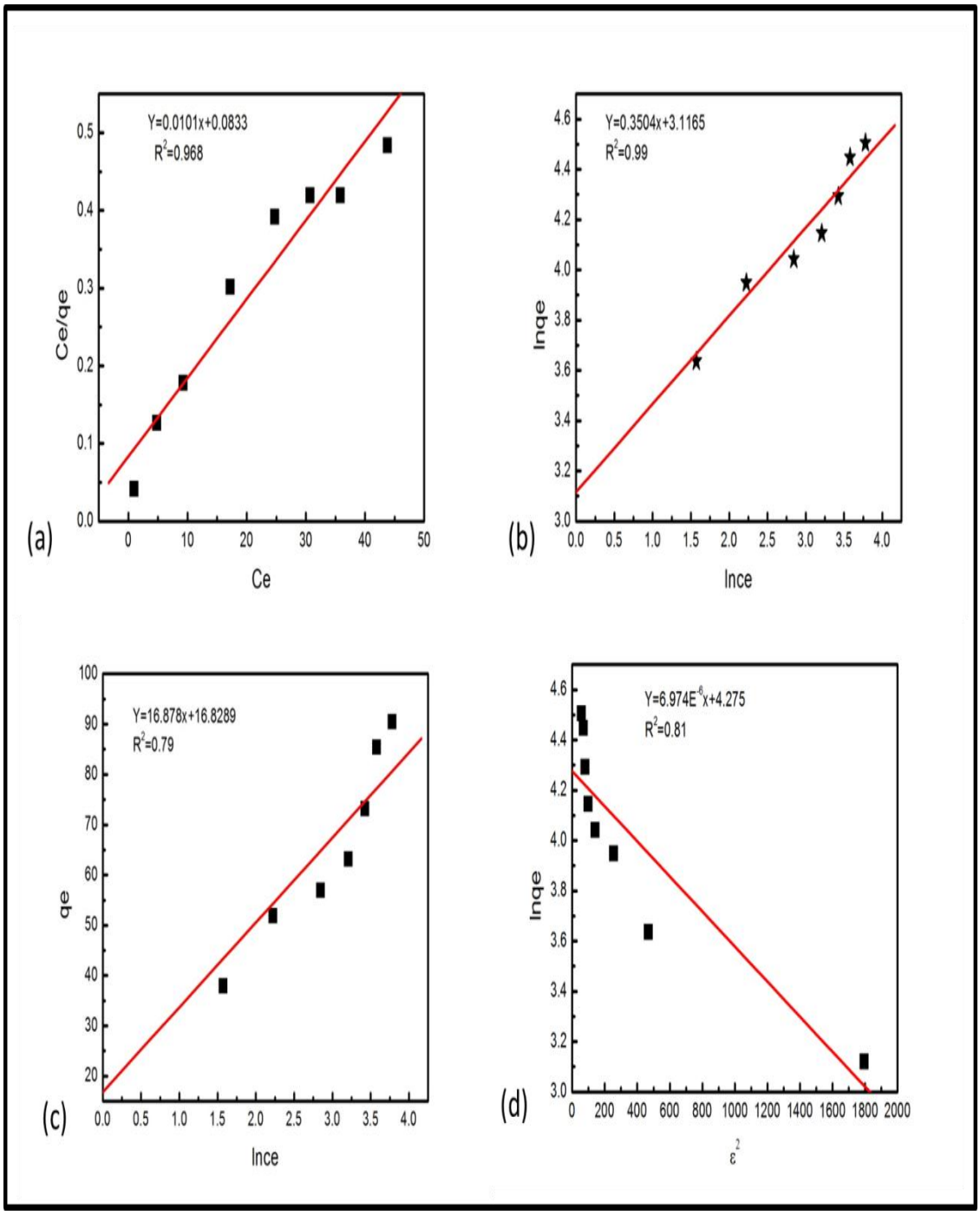

Figure 4.31 :(a) Langmuir isotherm (b) Freundlich isotherm (c) Temkin isotherm, and (d) Dubinin –Radushkevich isotherm plots for adsorption of Cu (II).

In order to investigate the mechanism of Cu (II) adsorption on the CNTs surface and examine the potential rate-controlling step, the capability of pseudo-first order (Langergren, 1898) pseudo second order (Ho, 2006b; Ho and McKay, 1999b) kinetic models was examined in this study. The conformity between experimental data and the model predicted values was expressed by the correlation coefficients (R^2 values close or equal 1). A relatively high R^2 values indicate that the model successfully describes the kinetics of Cu (II) adsorption. Fig 4.31 (a) shows the plot ln (q_e-q_t) against time representing the linear form of pseudo-first order kinetic model . The rate constant K_1 was calculated from the slope of straight line obtained. K_2 is the rate constant of pseudo second order adsorption kinetics (min.g/mg) was calculated from the intercept and slope of the straight line of t/qt against time as shown in Fig 4.31 (b). From the observation, the kinetics of adsorption of Cu (II) ions adsorption on CNTs followed the pseudo second order with more conformity comparing pseudo first order as shown in Table 4.17. The pseudo second order rate has been applied widely to the sorption of metal ions, herbicides, oil and organic substances from aqueous systems (Ho, 2006b; Ho and McKay, 1999b).

Table 4.17: Experimental values of constants of adsorption kinetics model.

C_0 mgL^{-1}	qe,exp. ($mg\ g^{-1}$)	Pseudo-First order			Pseudo-Second order		
		qe, cal ($mg\ g^{-1}$)	K_1 (min^{-1})	R^2	qe,cal. ($mg\ g^{-1}$)	K_2 ($min.g\ mg^{-1}$)	R^2
10	22.65	2.36	0.0173	0.15	23.03	0.027	0.999
20	37.97	9.84	0.0335	0.47	40.0	0.0044	0.995
30	51.9	`16.66	0.0422	0.60	54.82	0.0033	0.995
40	56.99	13.07	0.0434	0.51	59.98	0.0034	0.996
50	63.16	13.46	0.0437	0.62	64.59	0.0061	0.999
60	73.2	10.04	0.0397	0.44	74.62	0.0067	0.999
70	85.44	18.48	0.0442	0.60	88.18	0.0037	0.998
80	90.5	23.10	0.0403	0.54	96.06	0.0017	0.995

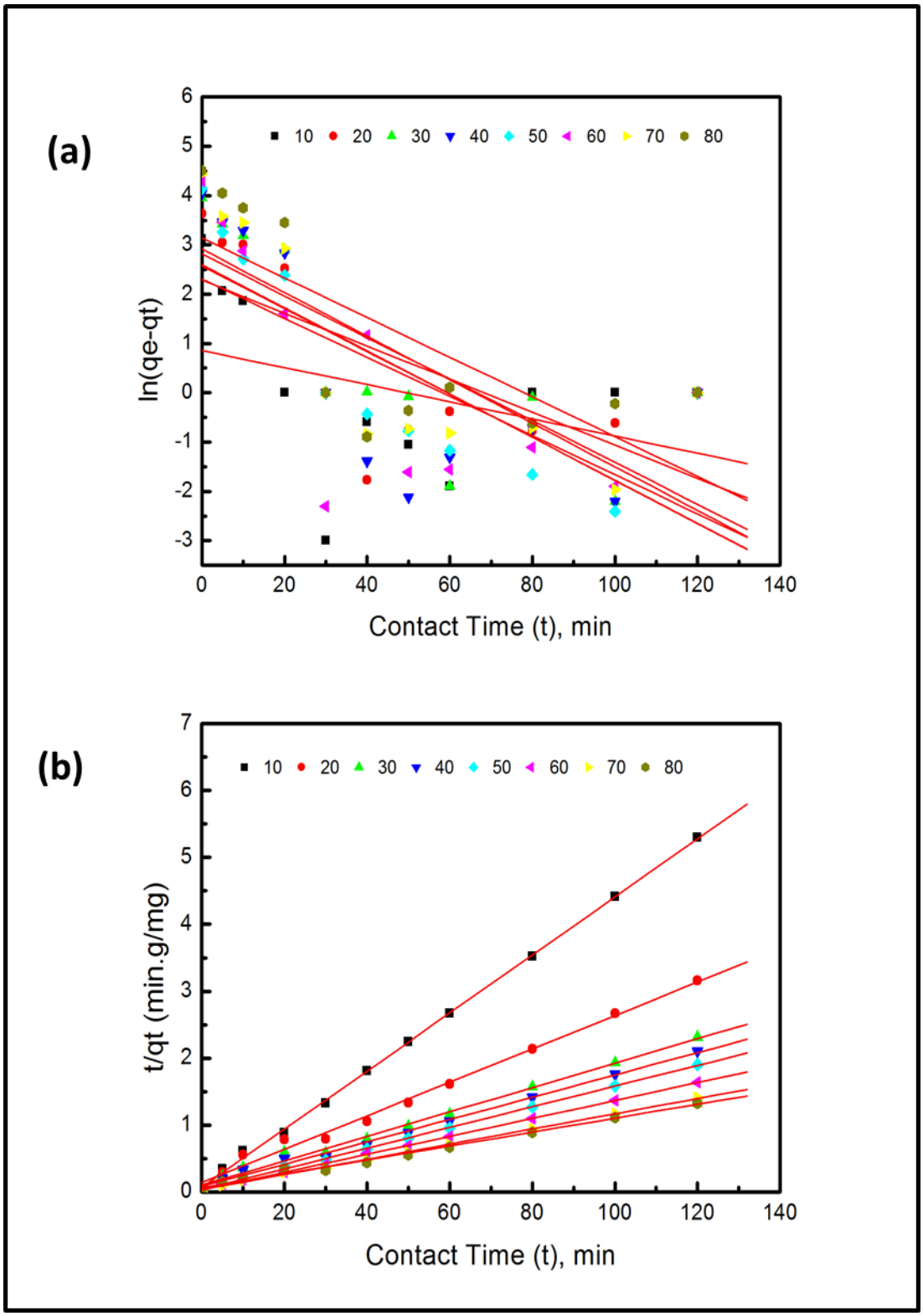

Figure 4.32: (a) Pseudo-first order kinetics (b) Pseudo second order kinetics for adsorption of Cu (II).

4.7.3 Thermodynamic study of Cu (II)

Thermodynamic parameters are used to present an essential data on the energetic change involved during the adsorption process. The adsorption isotherm of Cu (II) onto CNTs was measured at 293, 303, 308 and 323 K and the change in the thermodynamic parameters of the free energy of sorption (ΔG°), enthalpy (ΔH°), and entropy (ΔS°) were calculated using equations (4.8 & 4.9) from the variation of the thermodynamic equilibrium constant, K with a change in temperature. Free energy change (ΔG°) can be calculated using equation (4.8), where R is the universal gas constant while T is the temperature in kelvin. Where K is the equilibrium constant and qe and Ce are the amount of Cu (II) adsorbed per unit mass of CNTs and the equilibrium concentration of Cu (II) in the solution respectively. The enthalpy change value was obtained from the intercept of the ΔG° versus T plot. The values of the thermodynamic parameters obtained are shown in Table 4.18.

The negative ΔG° value for the adsorption of Cu (II) on the CNTs surface at all temperatures proves that the sorption was spontaneous and thermodynamically favorable. In the same vein, the entropy change value, ΔS° suggest that the randomness of the process at the solid-solution interface, increased when the Cu (II) ions attached to the active sites of adsorbent. The positive value of the enthalpy change value, ΔH proves that this adsorption experiment was an endothermic and spontaneous process (Li, Ding, et al., 2003; Pehlivan, et al., 2008).

Table 4.18: Thermodynamic parameters for Cu (II) adsorption.

Co Initial Conc (mgL^{-1})	**ΔH° ($kJ\ mol^{-1}$)**	**ΔS° $kJ\ mol^{-1}K^{-1}$**	**ΔG° ($kJmol^{-1}$)**			
			293	303	308	323
10	0.38	26.45	-7751	-8015	-8148	-8545
20	0.09	17.17	-5031	-5203	-5289	-5546
30	0.15	14.34	-4203	-4347	-4418	-4634
40	0.015	9.956	-2917	-3016	-3066	-3215

4.7.4 FTIR analysis of Cu (II) adsorption

FTIR is a versatile technique to identify the surface chemistry in terms of functional groups. It was used to analyze functional groups attached on the before and after adsorption of Cu (II) Fig. 4.32 (a) and (b) demonstrate the plot for CNTs before and after adsorption of Cu (II). Fig. 4.32 (a) The peaks observed on before CNTs adsorption at a range of 1700 to 1900 cm^{-1} defines the carboxylic group, followed by aromatic C=C groups at 1450-1600 cm^{-1} and O-H groups at 2800-3000 cm^{-1} as well. Fig. 4.32 (b) shows after adsorption of Cu (II), it was observed several peaks were observed. The C= O and C–O are stretching frequencies shifted from 1705 and 1200 cm^{-1}. Peaks at 1600 cm^{-1} of amino-functionalized MWCNTs are due to the N–H stretching of amine groups. Peaks at 2930 and 2860 cm^{-1} are greatly enhanced because of the attachment of additional methyl groups. Peaks between 950 and 700 cm^{-1} are due to the stretching mode of aromatic amine groups, and peaks at 2370 cm^{-1} may be because of the existence of ammonium ions (Kuan, et al., 2005; Peng, et al., 2003; Stevens, et al., 2003). The hydrophilic surface structure provides the functionalized CNTs an advantage of high dispersion in water, which eventually leads to a higher adsorption capacity of Cu (II) ions from aqueous solution compared with before the adsorption of CNTs. This finding corresponds to many results reported by several

previous researchers who studied on the surface chemistry of CNTs (Kuan, et al., 2005; Peng, et al., 2003; Smith, 1998; Stevens, et al., 2003; Zhang, et al., 2010).

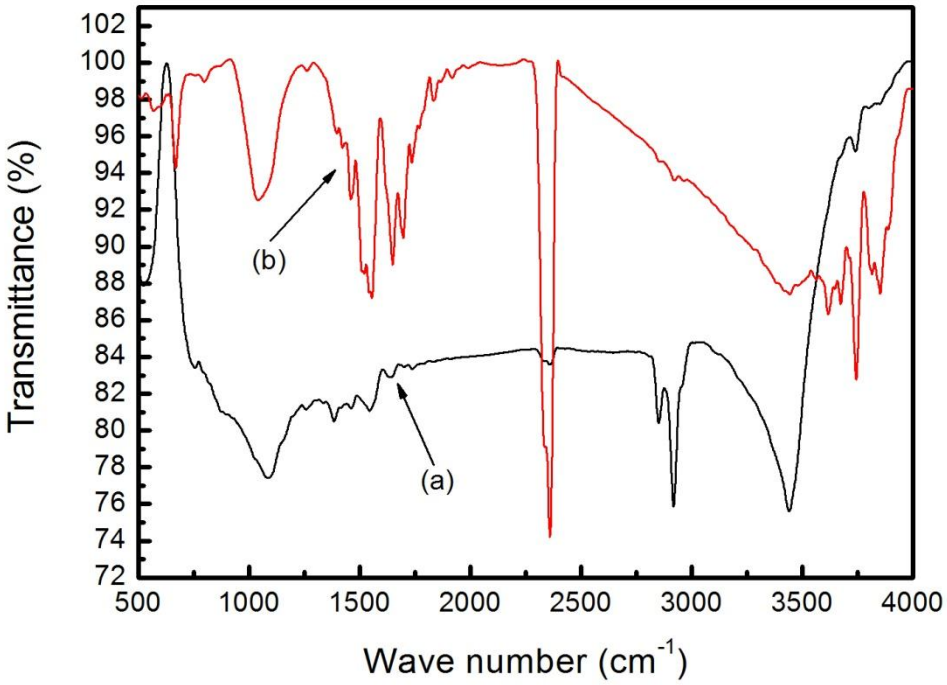

Figure 4.33: FTIR adsorption spectra for (a) CNTs before (b) CNTs after adsorption of Cu (II).

4.8 Statistical optimization of removal of Zn (II) using CNTs

The highest adsorption capacity of Zn (II) from aqueous solutions can be determined by the optimized condition of CNTs as the adsorbents for Zn (II) removal. Specific runs provided by the DOE were conducted accordingly. The detail experimental array of adsorption rate of removal of Pb (II) as shown in appendix E. The results obtained from this particular experiment were analyzed using the application of "analysis of variance" (ANOVA) and the optimized variables are attainable from Table 3.5. The analyses achieved by the

application of ANOVA for the removal of Zn (II) using CNTs are indicated in Table 4.19. From the values in Tables 4.19, the fisher F-test value can be related to the mean square of the regressed model which leads to the comparative mean square of the residuals (errors). The F value proves the efficiency of the model as its value increases. On the other hand, low probability, P value indicates higher significance of the regression model. Hence, from Tables 4.19, it can be seen that the F-test values using CNTs were 32, which indicates that the models are significant. Besides, the values of the correlation coefficient, R-Squared and Adj R-Squared for CNTs were 0.97 and 0.94 respectively. This value implies that the models of adsorbent are very close to each other, which indicates the high efficiency and significance of the models. The model equation evolved for the removal of Zn (II) from aqueous solutions for CNTs as Eq. (4.12) are as follows:

Removal of Zn (II) = = 110.30-3.27 * A-0.67 * B+0.63 * C-0.81 * D-25.68 * A^2-15.33 * B^2-15.33 C^2-15.73 * D^2+0.031 * A * B+2.90 * A * C+1.58 * A * D-1.74 * B*C+0.69*B*D+2.06*C*D (4.12)

Consequently, variables A, B, C, D, AB, AD and CD were significant model terms. This indicates that the pH (A), agitation speed (B), MWCNTs dosage (C) and time (D) were highly significant values of Probe >F was 0.001. The coefficient of single factor represents the effect of its represented factor while the coefficients of double factors represent the interaction effect of both represented factor. Hence, following up to the equation, the positive sign in the equation represents the synergistic effect while the negative sign represents antagonistic effect values. Fig 4.33 shows theoretical values versus the experimental values for Zn (II) removal. It was clearly shown that the theoretical values obtained were quite close to experimental values, indicating that the model developed was successful in bridging the correlation between process parameters for removal of Zn (II).

Table 4.19: ANOVA for the selected quadratic Model for removal of Zn (II).

Source	Sum of squares	DF	Mean square	F Value	Prob > F	Status
Model	21649.43	14	1546.38	32.0	< 0.0001	Significant
A	192.7339	1	192.73	4.0	0.0710	
B	8	1	8	0.2	0.6917	
C	7.10645	1	7.106	0.1	0.7085	
D	11.84222	1	11.84	0.2	0.6301	
A^2	1688.604	1	1688.60	35.0	0.0001	
B^2	601.695	1	601.69	12.5	0.0047	
C^2	602.0876	1	602.08	12.5	0.0047	
D^2	633.5085	1	633.50	13.1	0.0040	
AB	0.015625	1	0.0156	0.0	0.09860	
AC	134.56	1	134.56	2.8	0.1231	
AD	40.00563	1	40.005	0.8	0.03821	
BC	48.3025	1	48.302	1.0	0.03386	
BD	7.700625	1	7.7006	0.2	0.06972	
CD	68.0625	1	68.062	1.4	0.2600	
Residual	530.7995	11	48.254			
Lack of Fit	530.7945	10	53.0794	10615.9	0.176	Insignificant
Pure Error	0.005	1	0.005			
Cor Total	22180.22	25				

Fig. 4.34 shows the 3-dimensional interaction plot for adsorption of Zn (II) prepared under optimized condition of pH, MWCNTs dosage, agitation speed and time. The pH of an aqueous solution is one of the major parameters that control the adsorption of ion at the solid water interfaces. In addition to that it affects the solubility of the metal ions, concentration of the counter ions on the functional groups of adsorbent and the degree of ionization of the adsorbate during the reaction (Diniz et al., 2002). The 3-D plot of the

interaction between agitation speed and pH are as depicted in Fig. 4.35 (a) which shows the optimum condition for the removal of Zn (II) were at pH 10 and agitation speed of 160 rpm. These conditions gave the highest Zn (II) adsorption. PH 10 was observed to be the most favorable condition for Zn (II) removal as the adsorption decreased when the pH was set to less than 10 as well as if it was set to be more than 10. This is due to that zinc species can be present in deionized water in the forms of Zn (II), $Zn(OH)^{+1}$, $Zn(OH)_2^{0}$, $Zn(OH)_3^{-1}$ and $Zn(OH)_4^{2-}$ (Fu and Wang, 2011; Leyva Ramos et al., 2002; Lu et al., 2006a). At pH<8, the predominant zinc species are always Zn (II) and the removal of Zn (II) is mainly accomplished by adsorption reaction. Therefore, the low Zn (II) adsorption that took place at low pH can be attributed in part to competition between H^+ and Zn (II) ions on the same sites (Lu and Chiu, 2006b; Weng and Huang, 2004; Yin et al., 2012). Furthermore, the zeta potential of CNTs becomes more negative with the increase of pH, which causes electrostatic attraction and thus results in the adsorption of more Zn (II) onto CNTs. In the pH range of 8–10, the removal of Zn remained constant and reached maximum. The main species are $Zn(OH)^{+1}$, $Zn(OH)_2^{0}$ and $Zn(OH)_3^{-1}$ and thus the removal of Zn (II) is possibly accomplished by simultaneous precipitation of $Zn(OH)_2$(s) and adsorption of $Zn(OH)^{+1}$ and $Zn(OH)_3^{-1}$. Further increase in pH above 10, the predominant zinc species are the negative spaces $Zn(OH)_3^{-1}$ and $Zn(OH)_2^{-4}$ (Leyva Ramos, et al., 2002). Therefore, the decrease in Zn (II) removal that took place at a pH of above 10 can be attributed in part to competition among OH^-, $Zn(OH)_3^{-1}$ and $Zn(OH)_2^{-4}$ ions on the same sites (Lu and Chiu, 2006b). On the other hand, the increase of agitation speed, improves the diffusion of Zn (II) ions towards the surface of the CNTs (Lu et al., 2007; Mubarak, et al., 2013). Fig. 4.35 (b) shows the interaction between CNTs dosage and pH. It was observed highest removal of Zn (II) was obtained at CNTs dosage 0.10 and pH10, further increase increase in pH

decreases the removal of Zn (II) was observed. On the other hand, as the CNTs dosage increases, there is more surface of CNTs available for the interaction with the respective Zn (II) metal ions for a higher adsorption capacity. This suggests that after the solution reaches saturated phase, the maximum adsorption sets in and hence the amount of ions bound to the adsorbent and the amount of free ions remain constant even further addition of CNTs dose of adsorbent. Thus, the removal percentage of Zn (II) from aqueous solution can be escalated by increasing the CNTs dosage (Lu, et al., 2006a; Tofighy and Mohammadi, 2011). Fig. 4.35 (c) shows the interaction between time and pH. It was observed that at 60 min and pH 10 gives the highest removal of Zn (II) was observed. As the contact time increases, the interaction time between the Zn (II) ions and the adsorbent's surface ions increases, this leads to higher removal percentage of Zn (II) (Atieh, 2011b; Lu and Chiu, 2006b).

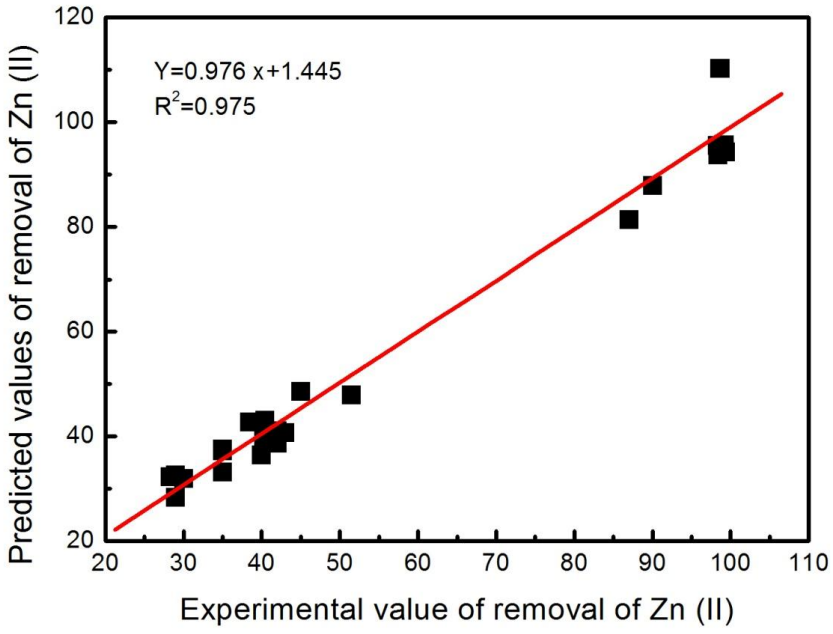

Figure 4.34: Relationship between actual value and predicted values of removal of Zn (II).

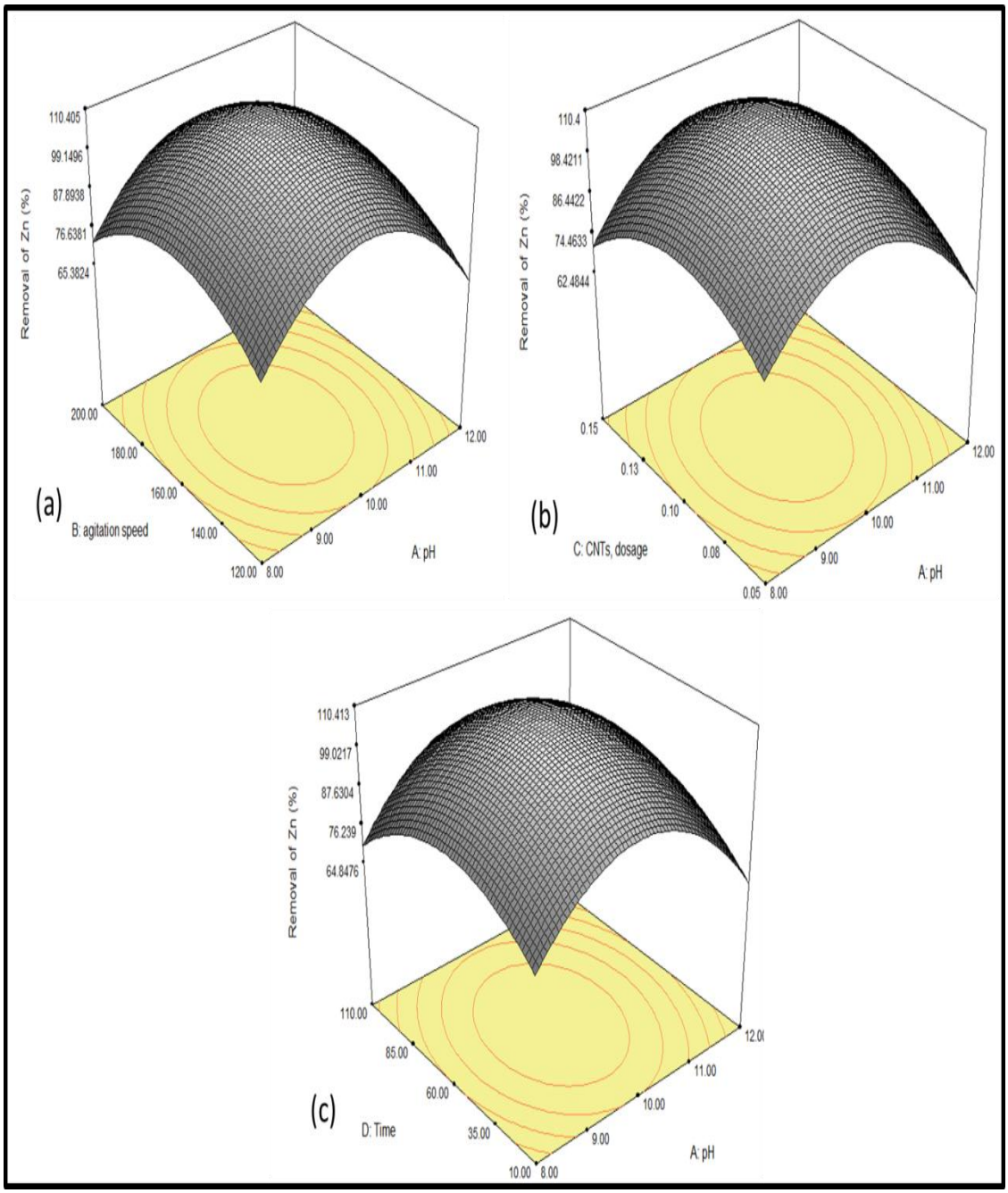

Figure 4.35: 3-D plots of removal of Zn (II) using optimized CNTs production, (a) interaction of agitation speed and pH, (b) interaction of CNTs dosage and pH,and (c) interaction of time and pH.

4.8.1 Adsorption isotherm of Zn (II)

The quantity of absorbent that can be taken up by a particular adsorbent at equilibrium is a function of both adsorbate concentration and temperature. When experiments are conducted at constant temperature, the resulting function is commonly referred to as an adsorption isotherm. The adsorption isotherm is the most extensively employed methods for representing the equilibrium states of an adsorption system. It gives useful information regarding the adsorbate, the adsorbent, and the adsorption process (Bansal, 2005). Theoretically, the adsorption capacity of an adsorbent is achieved at equilibrium when the rate of adsorption equals the rate of desorption. The successful representation of the dynamic adaptive separation of solute from solution onto an adsorbent depends upon a good description of the equilibrium separation between the two phases (Pehlivan, et al., 2008; Rao, et al., 2010; Salmani, et al., 2013). The relation between contact time (min) versus adsorption capacity (qt) was plotted for different Zn (II) concentration as shown in Fig. 4.35. Adsorption of high initial Zn (II) concentration results in an increase in the adsorption uptake due to increase in mass transfer driving force leading to higher adsorption rate (Chen, et al., 2009; Chen and Wang, 2006). It was observed that adsorption of Zn (II) by CNTs increase was rapidly during the first 35 min. Beyond the 60 min, the rate of adsorption was observed to decline with increment in 60 times, till equilibrium concentration was reached. This rapid adsorption at the initial time was expected, as the amount of Zn (II) ions present in solution and available sites on the adsorbent were still high, resulting in high adsorption sites on the adsorbents reduced, which resulted in a reduction in the rate of adsorption Zn (II) till equilibrium concentrations were noticed. Furthermore, at the lower concentration, it becomes more difficult for less-polar adsorbents to adsorb Zn (II) from a more polar solvent (Stafiej and Pyrzynska, 2007; Wu, 2007; Yang,

et al., 2009). More than 90% of maximum equilibrium uptake capacity was reached after 60 min and complete equilibrium was reached in the 60 min to 120 min. No significant additional adsorption was observed after 120 min of contact time. The contact time was thus maintained for 120 min to ensure that the equilibrium could be achieved (Chen and Wang, 2006; Li, Wang, et al., 2003; Stafiej and Pyrzynska, 2007).

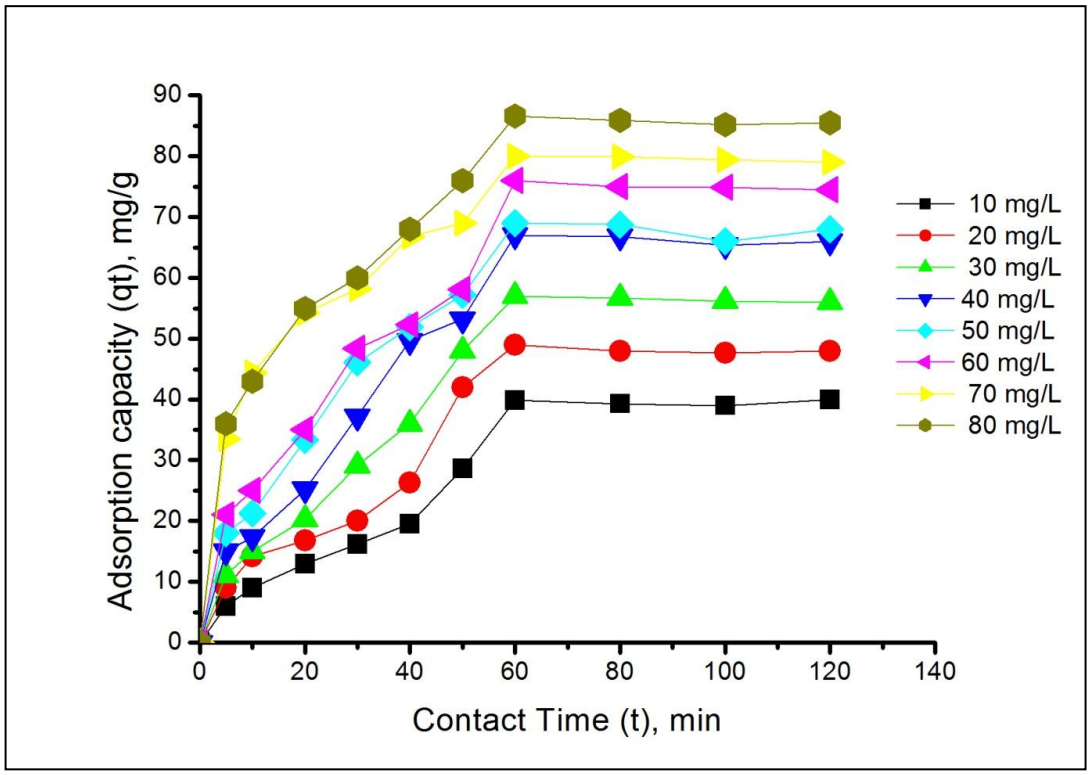

Figure 4.36: Adsorption capacity (qt) versus contact time (t) with different Zn (II) solution concentration.

4.8.2 Adsorption kinetics of Zn (II)

Same with other heavy metals, adsorption kinetics is used to determine the unique relationship between carbonaceous adsorbents and the adsorbate. Useful design and basic knowledge of adsorption system would be provided by the interaction and affinity of

equilibrium data. The Langmuir isotherm (equation 4.3), Freundlich isotherm (equation 4.4) and Temkin (equation 4.5 and 4.6) and Dubinin isotherm (equation 4.7) for Zn (II) have been successfully illustrated in Fig. 4.36 (a-d). As for this research study, four models were employed to determine the optimum model for the Zn (II) adsorption onto the CNTs surface. Their constants and correlation coefficient were tabulated in Table 4.20. The isotherm data were collected through the measurements of Zn (II) metal ions after certain Sorbent/ adsorbate contact intervals. The data collected throughout experiment were proving valid for Langmuir and Freundlich isotherm R^2= 0.98, and R^2= 0.94 respectively. However, Temkin and dubinin-Radushkevich isotherms did not show a good representation. Hence, high validity of the Langmuir isotherm model proposes the adsorption process was taking place at the heterogeneous and consistent and well distribution of active sites along the CNTs surface. Review on Zn (II) removal using CNTs as shown in Table 4.21.

Table 4.20: Isotherm parameters for Zn (II) adsorption using CNTs.

Langmuir Isotherm		**Freundlich Isotherm**		**Temkin Isotherm**		**Dubinin-Radushkevich**	
q_m (mg/g)	90.9	K_F (L/g)	31.62	A (L/g)	6.77	q_m	66.56
K_L (L/mg)	0.11	n	4.52	b (kJ/mol)	192.2	K x10^{-4} (mol^2 kJ^{-2}	4.22
R^2	0.98	R^2	0.94	R^2	0.89	E (kJ/mol)	0.39
						R^2	0.4

Table 4.21: Review on Zn (II) removal using CNTs

Adsorbent	**qm (mg/g)**	**K_L (L/mg)**	**R^2**	**K_f (L/g)**	**n**	**R^2**	**References**
MWCNTs	90.9	0.11	0.98	31.52	4.52	0.94	This study
Oxidized CNTs	74.9	0.0019	0.88	1.296	0.502	0.942	(Tofighy and Mohammadi, 2011)
Oxidized CNTs	5.2	0.825	0.99	-	-	-	(Gao, et al., 2009)
Oxidized CNTs	47.62	0.205	0.99	-	-	-	(Lu et al., 2009)
MWCNTs	39.37	0.116	0.98	-	-	-	84[3]
SWCNTs	41.84	0.161	0.997	12.37	3.40	0.984	(Lu, et al., 2006a)
MWCNTs	33.33	0.118	0.982	10.62	4.03	0.984	
MWCNTs	10.21	0.007	0.471	0.17	0.714	0.928	(Lu and Chiu, 2008)
MWCNTs-HNO_3	27.2	0.15	0.99	6.14	0.33	0.95	
MWCNTs-$KMnO_4$	28.01	0.16	0.99	9.89	0.236	0.982	
MWCNTs-NaCl	32.68	0.22	0.99	11.84	0.244	0.99	
SWCNTs	43.66	0.19	0.99	13.24	0.292	0.945	(Lu and Chiu, 2006a)
MWCNT-oxidized	1.05	0.06	0.98	4.41	0.33	0.99	(Mubarak, et al., 2013)

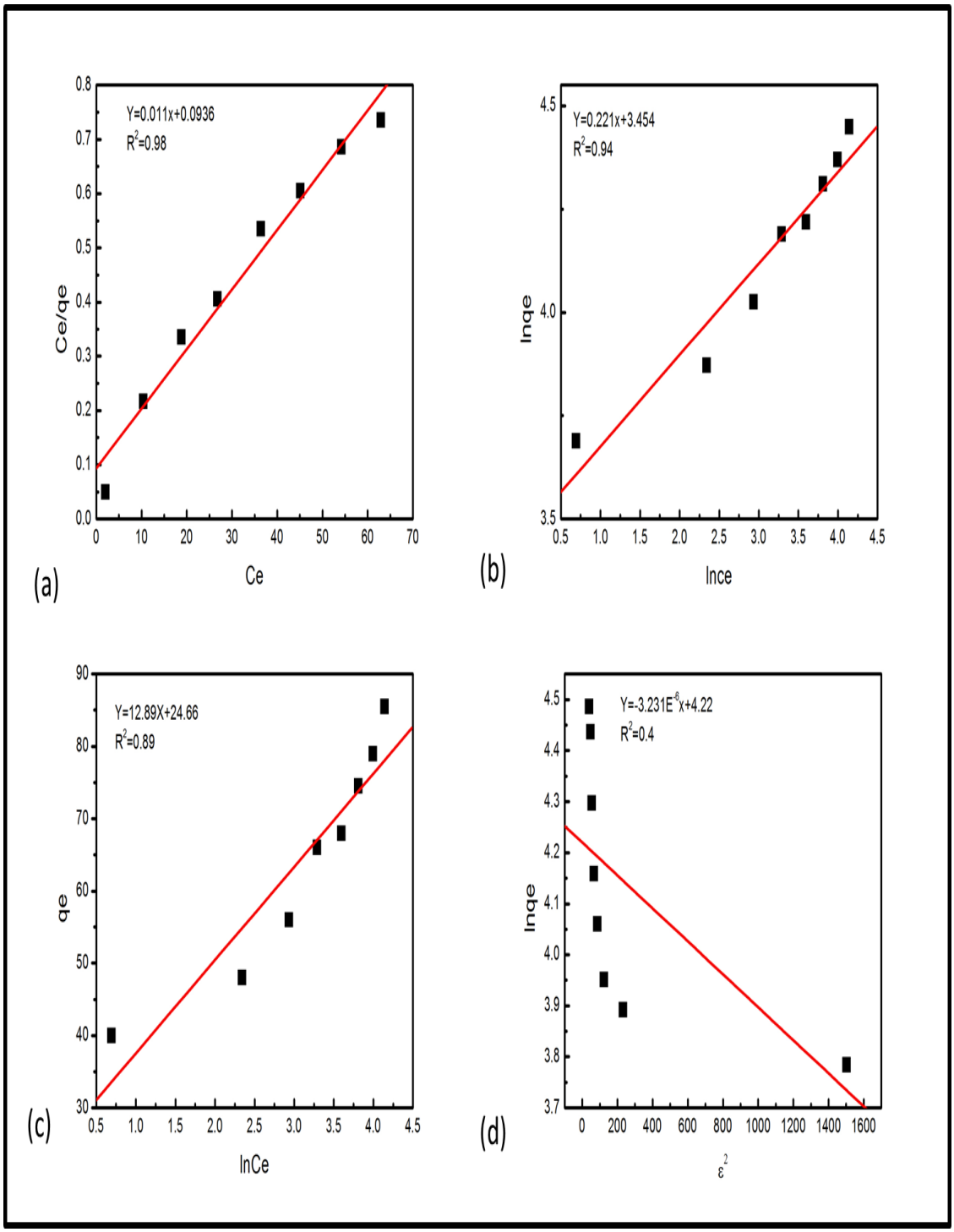

Figure 4.37: (a) Langmuir isotherm (b) Freundlich isotherm (c) Temkin isotherm, and (d) Dubinin –Radushkevich isotherm plots for adsorption of Zn (II).

In order to investigate the mechanism of Zn (II) adsorption on the CNTs surface and examine the potential rate-controlling step, the capability of pseudo-first order (Langergren, 1898) and pseudo second order (Ho, 2006b; Ho and McKay, 1999b) kinetic models were examined in this study. The conformity between experimental data and the model predicted values was expressed by the correlation coefficients (R^2 values close or equal to 1). A relatively high R^2 values indicate that the model successfully describes the kinetics of Zn (II) adsorption. Fig. 4.37 (a) shows the plot ln (q_e-q_t) against time representing the linear form of pseudo-first order kinetic model. The rate constant K_1 was calculated from the slope of straight line obtained. K_2 is the rate constant of pseudo second order adsorption kinetics (min.g/mg) was calculated from the intercept and slope of the straight line of t/qt against time as shown in Fig. 4.37 (b). From the observation, the kinetics of adsorption of Zn (II) ions adsorption on CNTs followed the pseudo second order with more conformity comparing pseudo first order as shown in Table 4.22. The pseudo second order rate has been applied widely to the sorption of metal ions, herbicides, oil and organic substances from aqueous systems (Ho, 2006b; Ho and McKay, 1999b).

Table 4.22: Experimental values of constants of adsorption kinetics model.

C_0 mgL^{-1}	qe,exp. ($mg\ g^{-1}$)	Pseudo-First order			Pseudo-Second order		
		qe, cal ($mg\ g^{-1}$)	K_1 (min^{-1})	R^2	qe,cal. ($mg\ g^{-1}$)	K_2 ($min.g\ mg^{-1}$)	R^2
10	40	47.31	0.0239	0.84	45.22	0.00057	0.82
20	48	58.56	0.0296	0.83	56.9	0.00051	0.86
30	56	61.57	0.0266	0.86	61.46	0.00060	0.92
40	66	76.78	0.0383	0.94	79.05	0.00050	0.93
50	68	65.23	0.0358	0.99	77.16	0.00074	0.97
60	74.5	73.77	0.0325	0.97	82.50	0.00068	0.98
70	79	62.07	0.0350	0.97	82.64	0.0013	0.99
80	85.5	84.52	0.0405	0.86	90.57	0.0009	0.99

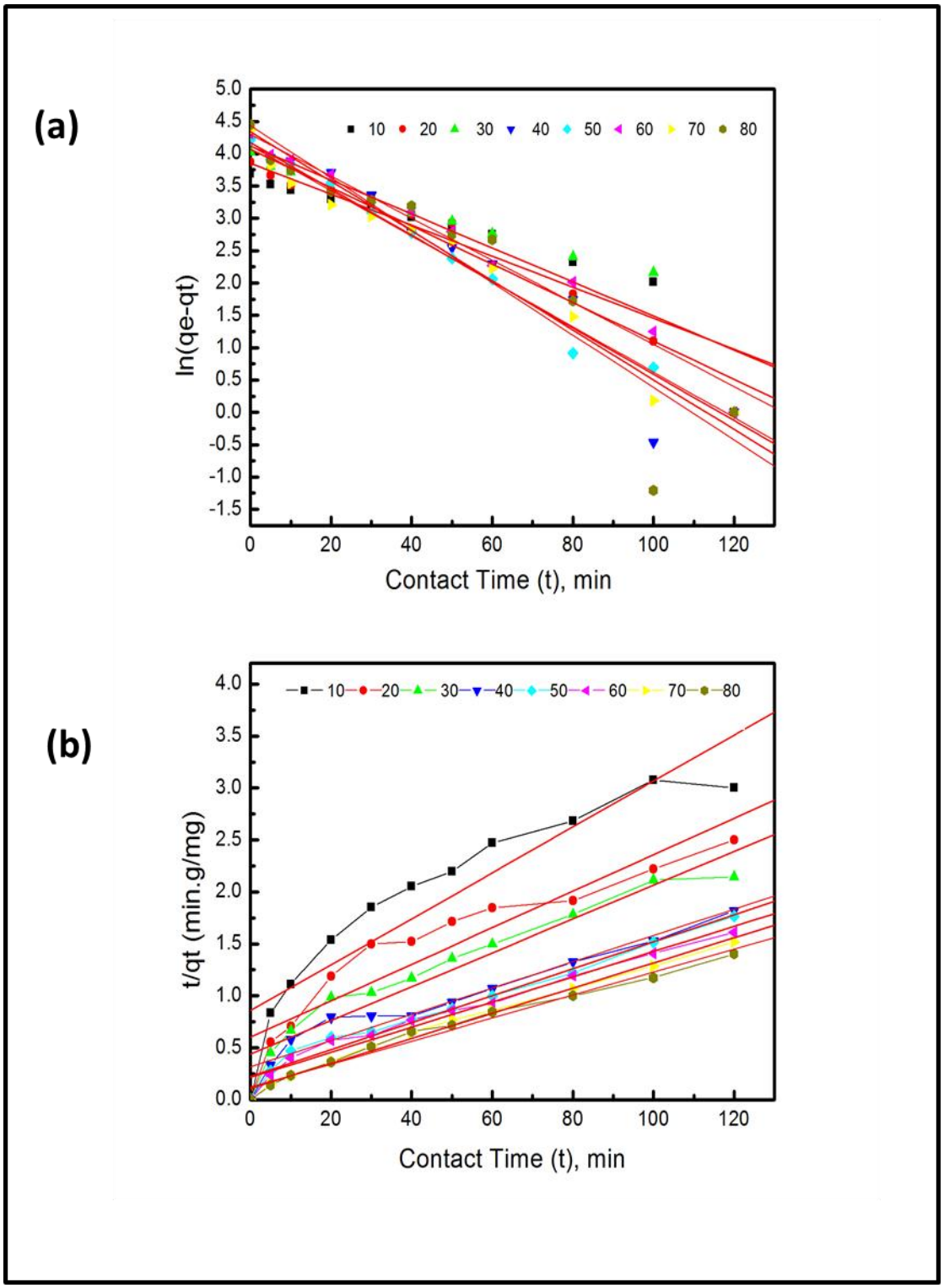

Figure: 4.38: (a) Pseudo-first order kinetics (b) Pseudo second order kinetic for adsorption of Zn (II).

4.8.3 Thermodynamic study

The adsorption isotherm of Zn (II) onto CNTs was measured at 293, 303, 308 and 323 K and the change in the thermodynamic parameters of the free energy of sorption (ΔG°), enthalpy (ΔH°), and entropy (ΔS°) were calculated using equatations (4.8 & 4.9) from the variation of the thermodynamic equilibrium constant, K with a change in temperature. Thermodynamic parameters are used to provide more information regarding the energetic change involved during the adsorption process. Free energy change (ΔG) can be calculated using (4.8), where R is the universal gas constant while T is the temperature in Kelvin. Where K is the equilibrium constant and q_e and C_e are the amount of Zn (II) adsorbed per unit mass of CNTs and the equilibrium concentration of Zn (II) in the solution respectively. The enthalpy change value was obtained from the intercept of the ΔG° versus T plot. The values of the thermodynamic parameters obtained are shown in Table 4.23.

The negative ΔG° value for the adsorption of Zn (II) on the CNTs surface at all temperatures proves that the sorption was spontaneous and thermodynamically favorable. In the same vein, the entropy change value, ΔS° suggested that the randomness of the process at the solid-solution interface, increased when the Zn (II) ions attached to the active sites of adsorbent. The positive value of the entropy change value, ΔH proves that this adsorption experiment was an endothermic process and a negative value indicates adsorption was an exothermic process (Li, Ding, et al., 2003; Pehlivan, et al., 2008).

Table 4.23: Thermodynamic parameters for Zn (II) adsorption.

Co Initial Conc (mgL^{-1})	**ΔH° ($kJ\ mol^{-1}$)**	**ΔS° ($kJ\ mol^{-1}K^{-1}$)**	**ΔG° ($kJmol^{-1}$)**			
			293 K	**303 K**	**308 K**	**323 K**
10	-1.01	24.90	-7297	-7546	-7671	-8044
20	3.81	12.69	-3717	-3844	-3907	-4098
30	4.03	8.86	-2593	-2682	-2726	-2859
40	5.2	7.6	-2232	-2308	-2346	-2460

4.8.4 FTIR analysis of Zn (II) adsorption

In order to investigate the successful functionalization groups attached on the surface of CNTs were analyzed by using FTIR. FTIR was engaged as well to determine the functional groups attached on the before and after adsorption of Zn (II). Fig. 4.38 (a-b) demonstrates the plot for CNTs before and after adsorption of Zn (II). Fig. 4.38 (a) The peaks observed on before CNTs adsorption at a range of 1700 to 1900 cm^{-1} defines the carboxylic group, followed by aromatic C=C groups at 1450-1600 cm^{-1} and O-H groups at 2800-3000 cm^{-1} as well. Fig. 4.38 (b) shows after adsorption of Zn (II), it was observed several peaks were observed. The C=O and C–O is stretching frequencies shifted from 1705 and 1200 cm^{-1}. Peaks at 1600 cm^{-1} of amino-functionalized MWCNTs are due to the N–H stretching of amine groups. Peaks at 2930 and 2860 cm^{-1} are greatly enhanced because of the attachment of additional methyl groups. Peaks between 950 and 700 cm^{-1} are due to the stretching mode of aromatic amine groups, and peaks at 2370 cm^{-1} may be because of the existence of ammonium ions (Kuan, et al., 2005; Peng, et al., 2003; Stevens, et al., 2003). The hydrophilic surface structure provides the functionalized CNTs an advantage of high dispersion in water, which eventually leads to a higher adsorption capacity of Zn (II) ions from aqueous solution compared with before the adsorption of CNTs. This finding

corresponds to many results reported by several previous researchers who studied on the surface chemistry of CNTs (Kuan, et al., 2005; Peng, et al., 2003; Smith, 1998; Stevens, et al., 2003; Zhang, et al., 2010).

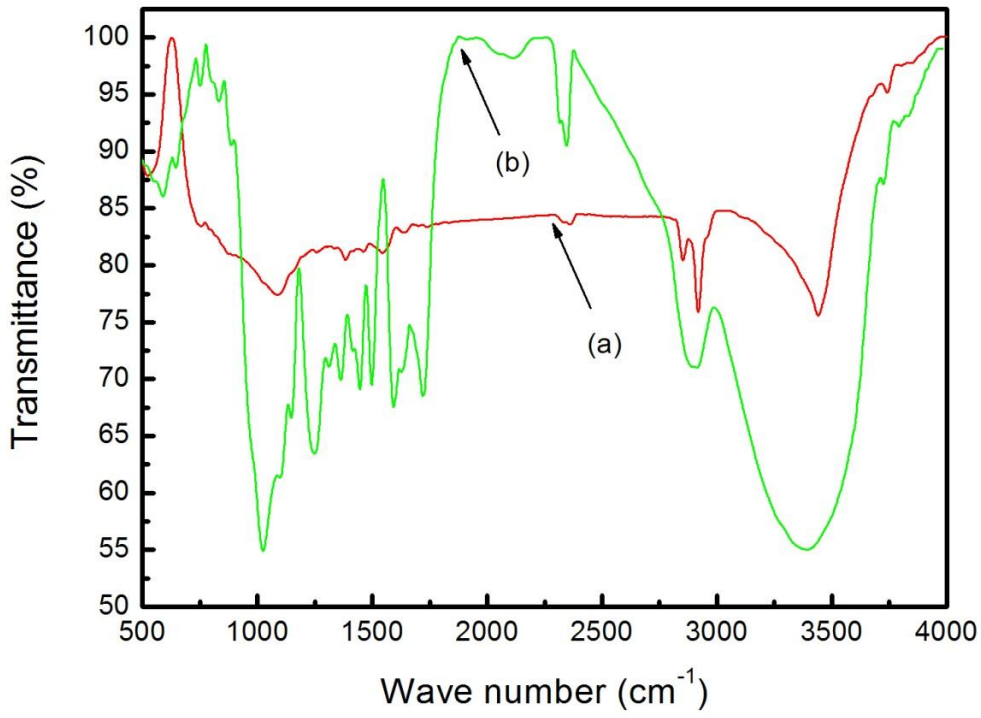

Figure 4.39: FTIR adsorption spectra for (a) CNTs before (b) CNTs after adsorption of Zn (II).

4.8.5 Zeta potential of MWCNTs

Zeta potential was measured for MWCNTs before and after adsorption of heavy metals. The zeta potential for MWCNTs was -42.5 mV that made this material lay in the region of the good stability aqueous system and its surface become more hydrophilic due to the presence of oxygen-containing functional groups on the surface such as carbonyl and

aliphatic carboxylic acids resulting in increasing of electron density and increasing the electron negativity which is thought to play an important role in the adsorption mechnasim. After the adsorption process the value of Zeta potential was 6.48, 6, 4.95 and +5.86 mV because of the saturation of the surface with positive charged of Pb (II), Cd (II), Cu (II) and Zn (II) ions respectively. That relatively low zeta value has an advantage in the process of removal of heavy metals by making the adsorbent more hydrophobic and reducing the stability and as a result the separation of poisoned adsorbent become easier by settling, coagulation or flocculation (Lu and Chiu, 2006; Lu et al., 2006).

CHAPTER V

CONCLUSIONS AND RECOMMENDATIONS

5.1 Conclusions

Microwave synthesis, including fast CNTs growth and ambient reaction condition and simplifies the procedure leading to a high yield synthesis of high-quality CNTs with minimal impurity. Unlike conventional heating, microwave heating has a higher heating rate, which results from the intrinsic transition of electromagnetic energy to thermal energy by a molecular interaction with the electromagnetic field, rather than heat transfer by conduction or convection. One such possibility is the use of microwave radiation, which over the past few years has played an important role as a thermal tool in organic synthesis due to considerable advantages over conventional methods. Another major advantage of the MA-CVD approach is that CNTs can be produced continuously, which could provide a very good way to synthesize large quantities of CNTs under relatively, controlled conditions. Major findings made from this research are summarized as follows.

i. A novel MWCNTs have been successfully synthesized by MA-CVD using acetylene and hydrogen as the precursor gases, and ferrocene as catalyst.

ii. MWCNTs has been successfully produced by MA-CVD and the statistical analysis reveal that the optimized conditions for the high yield MWCNTs production were microwave power of 900 W, radiation time of 35 min and gas ratio of C_2H_2/H_2 was 0.6.

iii. The TGA analysis showed that the purity of MWCNTs produced was almost 98% purity. FESEM and TEM analyses revealed that the uniformly dispersed MWCNTs have diameters ranging from 10 to 23 nm and 30 micron long.

iv. The produced MWCNTs have a high BET surface area of 206 m^2/g and the zeta potential for MWCNTs was -42.5 mV.

v. The interaction of process parameters on MWCNTs productions between hydrogen, acetylene and microwave power were the three key parameters to achieve high yield and high purity of MWCNTs.

vi. Statistical analysis has been examined for validation of the results, and the observation showed that 97.0% of desirability was achieved, which indicated that these MWCNTs were high in purity and high yield.

vii. A novel MWCNTs proved to be an outstanding adsorbent for the removal of heavy metals from aqueous solution.

viii. Characterization has shown a clear demarcation in the physicochemical properties of MWCNTs.

ix. The optimization and kinetic study on the removal of Pb (II), Cd (II), Cu (II) and Zn (II) using MWCNTs is conducted. Maximum adsorption capacities (q_m) for Pb (II), Cd (II), Cu (II) and Zn (II) ions were obtained at 104.2, 88.63, 99 and 90.9 mg/g respectively.

x. Analysis results revealed that the optimum conditions for the highest removal of (99.9%) Pb (II) and (98%) Cd (II) were recorded to have pH 5, MWCNTs dosage 0.1 g, contact time 22.5 and 50 min and agitation speed of 160 rpm respectively.

xi. The statistical analysis revealed that the optimum conditions for the highest removal of (99%) Cu (II) and (99.9%) Zn (II) were recorded to have pH 5.5, and pH 10 MWCNTs dosage 0.1 and 0.05 g, contact time 35 and 60 min and agitation speed of 160 and 120 rpm respectively.

xii. Four models such as Langmuir, Freundlich, Temkin and Dubinin isotherm model were tested for each heavy metals. The system was found more likely to follow Langmuir and Freundlich models match the experimental data very well for each heavy metals since R^2=0. 99.

xiii. Two kinetic models were studied which were pseudo first order and the pseudo second order for each heavy metals, it was found that adsorption kinetic obeyed pseudo-second order for each heavy metals since R^2=0. 999

xiv. Different thermodynamic parameters, viz., ΔH°, ΔS° and ΔG° have also been evaluated and it has been found that the adsorption was feasible, spontaneous and endothermic in nature for Pb (II), Cu (II) and Zn (II).

xv. The thermodynamic analysis revealed that the sorption of Cd (II) onto MWCNTs is exothermic and spontaneous in nature.

xvi. Hence, MWCNTs are the most promising candidate for removal of heavy metals from waste water treatment and separation process.

5.2 Recommendations

Some recommendations can be made from the results obtained and observations throughout this research study, it is summarized as follows:

i. Wide ranges of hydrocarbon precursors have been successfully used in the synthesis of carbon nanomaterials. However, there are still many more types of hydrocarbon precursors that can be studied to produce these materials such as methane, ethylene, and benzene. Therefore the study of using other hydrocarbon precursors for synthesis of carbon nanotubes should be continued.

ii. Catalyst plays a very important role to produce high purity and high yield of carbon material. Therefore, the study of using the other types of catalyst like nickel and cobalt needs to be investigated.

iii. The MA-CVD reactor can be scaled up to a pilot plant, including a continuous reaction to increase the rate of production of MWCNTs.

iv. MWCNTs are an excellent adsorbent that can be used for removal of other toxic materials such as heavy metals (As (V), Hg, Ni etc.).

v. MWCNTs exhibited high BET surface area, thus it can be used for gas adsorption applications such as NOx removal from flue gases or H_2 storage.

vi. MWCNTs can be used in immobilization of enzymes and proteins for several biotechnology applications

vii. A column study can be carried out to determine the breakthrough conditions in the adsorption process.

viii. MWCNTs material can be fixed in a packed bed filter to be used for continuous adsorption process for future investigations.

Bibliography

Abdel-Ghani, N., Hefny, M., & El-Chaghaby, G. A. (2007). Removal of lead from aqueous solution using low cost abundantly available adsorbents. *International Journal of Environmental Science & Technology, 4*(1), 67-73.

Abdullahi, I., Sakulchaicharoen, N., & Herrera, J. E. (2012). A mechanistic study on the growth of multi-walled carbon nanotubes by methane decomposition over nickel–alumina catalyst. *Diamond and Related Materials, 23*(0), 76-82.

Ago, H., Komatsu, T., Ohshima, S., Kuriki, Y., & Yumura, M. (2000). Dispersion of metal nanoparticles for aligned carbon nanotube arrays. *Applied Physics Letters, 77*(1), 79-81.

Amelinckx, S., Bernaerts, D., Zhang, X. B., Van Tendeloo, G., & Van Landuyt, J. (1995). A structure model and growth mechanism for multishell carbon nanotubes. *Science, 267*(5202), 1334-1338.

Amirhasan, N., Bahram, G., Mostafa, Z., & Ezatollah, A. (2007). Morphology optimization of ccvd-synthesized multiwall carbon nanotubes, using statistical design of experiments. *Nanotechnology, 18*(11), 115715.

Ando, Y., & Zhao, X. (2006). Synthesis of carbon nanotubes by arc-discharge method. *New Diamond and Frontier Carbon Technology, 16*(3), 123-137.

Ando, Y., Zhao, X., Hirahara, K., Suenaga, K., Bandow, S., & Iijima, S. (2000). Mass production of single-wall carbon nanotubes by the arc plasma jet method. *Chemical Physics Letters, 323*(5–6), 580-585.

Ando, Y., Zhao, X., Sugai, T., & Kumar, M. (2004). Growing carbon nanotubes. *Materials Today, 7*(10), 22-29.

Andriotis, A., Menon, M., & Froudakis, G. (2000). Catalytic action of ni atoms in the formation of carbon nanotubes: A combined ab-initio and molecular dynamics study. *Microelectronics, Microsystems and Nanotechnology, papers presented at MMN*.

Ata, M., Kijima, Y., Imoto, H., Matsuzawa, N., & Takahashi, N. (1994). Carbon microfibers grown on graphite electrode during fullerene generation using composite graphite rods. *Japanese Journal of Applied Physics, Part 1: Regular Papers and Short Notes and Review Papers, 33*(7 A), 4032-4038.

Athalin, H., & Lefrant, S. (2005). A correlated method for quantifying mixed and dispersed carbon nanotubes: Analysis of the raman band intensities and evidence of wavenumber shift. *Journal of Raman Spectroscopy, 36*(5), 400-408.

Atieh, M. A. (2011a). Removal of chromium (vi) from polluted water using carbon nanotubes supported with activated carbon. *Procedia Environmental Sciences, 4*(0), 281-293.

Atieh, M. A. (2011b). *Removal of zinc from water using modified and non-modified carbon nanofibers.* Paper presented at the Proceedings of the 2nd International Conference on Environmental Science and Technology IPCBEE Singapore.

Atthipalli, G., Epur, R., Kumta, P. N., Yang, M., Lee, J.-K., & Gray, J. L. (2011). Nickel catalyst-assisted vertical growth of dense carbon nanotube forests on bulk copper. *The Journal of Physical Chemistry C, 115*(9), 3534-3538.

Ausman, K. D., Piner, R., Lourie, O., Ruoff, R. S., & Korobov, M. (2000). Organic solvent dispersions of single-walled carbon nanotubes: Toward solutions of pristine nanotubes. *The Journal of Physical Chemistry B, 104*(38), 8911-8915.

Aziz, H. A., Adlan, M. N., & Ariffin, K. S. (2008). Heavy metals (cd, pb, zn, ni, cu and cr (iii)) removal from water in malaysia: Post treatment by high quality limestone. *Bioresource Technology, 99*(6), 1578-1583.

Azouaou, N., Sadaoui, Z., Djaafri, A., & Mokaddem, H. (2010). Adsorption of cadmium from aqueous solution onto untreated coffee grounds: Equilibrium, kinetics and thermodynamics. *Journal of Hazardous Materials, 184*(1), 126-134.

Bacon, R. (1960). Growth, structure, and properties of graphite whiskers. *Journal of Applied Physics, 31*(2), 283-290.

Baker, R. T. K., Barber, M. A., Harris, P. S., Feates, F. S., & Waite, R. J. (1972). Nucleation and growth of carbon deposits from the nickel catalyzed decomposition of acetylene. *Journal of Catalysis, 26*(1), 51-62.

Ball, P. (2001). Roll up for the revolution. [10.1038/35102721]. *Nature, 414*(6860), 142-144.

Bandow, S., Asaka, S., Saito, Y., Rao, A. M., Grigorian, L., Richter, E., et al. (1998). Effect of the growth temperature on the diameter distribution and chirality of single-wall carbon nanotubes. *Physical Review Letters, 80*(17), 3779-3782.

Bansal, R. C. a. G., M. (2005). Activated carbon adsorption. 351-353.

Baughman, R. H., Zakhidov, A. A., & de Heer, W. A. (2002). Carbon nanotubes--the route toward applications. *Science, 297*(5582), 787-792.

Bazargan, A., & McKay, G. (2012). A review – synthesis of carbon nanotubes from plastic wastes. *Chemical Engineering Journal, 195–196*(0), 377-391.

Bekarevich, R. V., Miura, S., Ogino, A., Rahachou, A. U., & Nagatsu, M. (2012). Low temperature growth of carbon nanomaterials on the polymer substrates by microwave plasma technique. *Transactions of the Materials Research Society of Japan, 37*(2), 157-160.

Benito, P., Herrero, M., Labajos, F., Rives, V., Royo, C., Latorre, N., et al. (2009a). Production of carbon nanotubes from methane: Use of co-zn-al catalysts prepared by microwave-assisted synthesis. *Chemical Engineering Journal, 149*(1), 455-462.

Benito, P., Herrero, M., Labajos, F. M., Rives, V., Royo, C., Latorre, N., et al. (2009b). Production of carbon nanotubes from methane: Use of co-zn-al catalysts prepared by microwave-assisted synthesis. *Chemical Engineering Journal, 149*(1–3), 455-462.

Bethune, D. S., Klang, C. H., de Vries, M. S., Gorman, G., Savoy, R., Vazquez, J., et al. (1993). Cobalt-catalysed growth of carbon nanotubes with single-atomic-layer walls. [10.1038/363605a0]. *Nature, 363*(6430), 605-607.

Biškup, B., & Subotić, B. (2005). Removal of heavy metal ions from solutions using zeolites. Iii. Influence of sodium ion concentration in the liquid phase on the kinetics of exchange processes between cadmium ions from solution and sodium ions from zeolite a. *Separation Science and Technology, 39*(4), 925-940.

Bonard, J., x, Marc, Salvetat, J.-P., Sto, ckli, T., et al. (1998). Field emission from single-wall carbon nanotube films. *Applied Physics Letters, 73*(7), 918-920.

Bower, C., Suzuki, S., Tanigaki, K., & Zhou, O. (1998). Synthesis and structure of pristine and alkali-metal-intercalated single-walled carbon nanotubes. *Applied Physics A, 67*(1), 47-52.

Bower, C., Zhou, O., Zhu, W., Werder, D., & Jin, S. (2000). Nucleation and growth of carbon nanotubes by microwave plasma chemical vapor deposition. *Applied Physics Letters, 77*(17), 2767-2769.

Bower, C., Zhu, W., Jin, S., & Zhou, O. (2000). Plasma-induced alignment of carbon nanotubes. *Applied Physics Letters, 77*(6), 830-832.

Brunetti, F. G., Herrero, M. A., Muñoz, J. d. M., Giordani, S., Díaz-Ortiz, A., Filippone, S., et al. (2007). Reversible microwave-assisted cycloaddition of aziridines to carbon nanotubes. *Journal of the American Chemical Society, 129*(47), 14580-14581.

Bustero, I., Ainara, G., Isabel, O., Roberto, M., Inés, R., & Amaya, A. (2006). Control of the properties of carbon nanotubes synthesized by cvd for application in electrochemical biosensors. *Microchimica Acta, 152*(3-4), 239-247.

Byszewski, P., Lange, H., Huczko, A., & Behnke, J. F. (1997). Fullerene and nanotube synthesis. Plasma spectroscopy studies. *Journal of Physics and Chemistry of Solids, 58*(11), 1679-1683.

Calderón, J., Navarro, M. E., Jimenez-Capdeville, M. E., Santos-Diaz, M. A., Golden, A., Rodriguez-Leyva, I., et al. (2001). Exposure to arsenic and lead and neuropsychological development in mexican children. *Environmental Research, 85*(2), 69-76.

Cao, Z., Sun, Z., Guo, P., & Chen, Y. (2007). Effect of acetylene flow rate on morphology and structure of carbon nanotube thick films grown by thermal chemical vapor deposition. *Frontiers of Materials Science in China, 1*(1), 92-96.

Carabineiro, S., Pereira, M., Pereira, J., Caparros, C., Sencadas, V., & Lanceros-Mendez, S. (2011). Effect of the carbon nanotube surface characteristics on the conductivity and dielectric constant of carbon nanotube/poly(vinylidene fluoride) composites. *Nanoscale Research Letters, 6*(1), 302.

Cassell, A. M., Raymakers, J. A., Kong, J., & Dai, H. (1999). Large scale cvd synthesis of single-walled carbon nanotubes. *The Journal of Physical Chemistry B, 103*(31), 6484-6492.

Chatterjee, S. K., Bhattacharjee, I., & Chandra, G. (2010). Biosorption of heavy metals from industrial waste water by geobacillus thermodenitrificans. *Journal of Hazardous Materials, 175*(1–3), 117-125.

Che, G., Lakshmi, B. B., Fisher, E. R., & Martin, C. R. (1998). Carbon nanotubule membranes for electrochemical energy storage and production. *Nature, 393*(6683), 346-349.

Chen, B., & Wu, P. (2005). Aligned carbon nanotubes by catalytic decomposition of c2h2 over ni–cr alloy. *Carbon, 43*(15), 3172-3177.

Chen, C.-W., Kao, C.-M., Chen, C.-F., & Dong, C.-D. (2007). Distribution and accumulation of heavy metals in the sediments of kaohsiung harbor, taiwan. *Chemosphere, 66*(8), 1431-1440.

Chen, C., Hu, J., Shao, D., Li, J., & Wang, X. (2009). Adsorption behavior of multiwall carbon nanotube/iron oxide magnetic composites for ni(ii) and sr(ii). *Journal of Hazardous Materials, 164*(2–3), 923-928.

Chen, C., Hu, J., Xu, D., Tan, X., Meng, Y., & Wang, X. (2008). Surface complexation modeling of sr (ii) and eu (iii) adsorption onto oxidized multiwall carbon nanotubes. *Journal of Colloid and Interface Science, 323*(1), 33-41.

Chen, C., & Wang, X. (2006). Adsorption of ni(ii) from aqueous solution using oxidized multiwall carbon nanotubes. *Industrial & Engineering Chemistry Research, 45*(26), 9144-9149.

Chen, M., Chen, C.-M., & Chen, C.-F. (2002). Preparation of high yield multi-walled carbon nanotubes by microwave plasma chemical vapor deposition at low temperature. *Journal of Materials Science, 37*(17), 3561-3567.

Chen, M., Chen, C.-M., Koo, H.-S., & Chen, C.-F. (2003). Catalyzed growth model of carbon nanotubes by microwave plasma chemical vapor deposition using ch4 and co2 gas mixtures. *Diamond and Related Materials, 12*(10–11), 1829-1835.

Chen, R. J., Zhang, Y., Wang, D., & Dai, H. (2001). Noncovalent sidewall functionalization of single-walled carbon nanotubes for protein immobilization. *Journal of the American Chemical Society, 123*(16), 3838-3839.

Chen, X. H., Chen, C. S., Chen, Q., Cheng, F. Q., Zhang, G., & Chen, Z. Z. (2002). Non-destructive purification of multi-walled carbon nanotubes produced by catalyzed cvd. *Materials Letters, 57*(3), 734-738.

Cheng, J., Zhang, X., Liu, F., Tu, J., Lu, H., Sun, Y., et al. (2004). Long bundles of aligned carbon nanofibers obtained by vertical floating catalyst method. *Materials Chemistry and Physics, 87*(2), 241-245.

Cheung, C. L., Kurtz, A., Park, H., & Lieber, C. M. (2002). Diameter-controlled synthesis of carbon nanotubes. *The Journal of Physical Chemistry B, 106*(10), 2429-2433.

Chhowalla, M., Teo, K., Ducati, C., Rupesinghe, N., Amaratunga, G., Ferrari, A., et al. (2001). Growth process conditions of vertically aligned carbon nanotubes using plasma enhanced chemical vapor deposition. *Journal of Applied Physics, 90*(10), 5308-5317.

Chiang, W.-H., & Sankaran, R. M. (2008). Synergistic effects in bimetallic nanoparticles for low temperature carbon nanotube growth. *Advanced Materials, 20*(24), 4857-4861.

Cho, H.-H., Wepasnick, K., Smith, B. A., Bangash, F. K., Fairbrother, D. H., & Ball, W. P. (2009). Sorption of aqueous zn [ii] and cd [ii] by multiwall carbon nanotubes: The relative roles of oxygen-containing functional groups and graphenic carbon. *Langmuir, 26*(2), 967-981.

Choi, J. H., Kim, S. D., Noh, S. H., Oh, S. J., & Kim, W. J. (2006). Adsorption behaviors of nano-sized ets-10 and al-substituted-etas-10 in removing heavy metal ions, pb2+ and cd2+. *Microporous and Mesoporous Materials, 87*(3), 163-169.

Choi, Y. C., Bae, D. J., Lee, Y. H., Lee, B. S., Han, I. T., Choi, W. B., et al. (2000). Low temperature synthesis of carbon nanotubes by microwave plasma-enhanced chemical vapor deposition. *Synthetic Metals, 108*(2), 159-163.

Clauss, C., Schwarz, M., & Kroke, E. (2010). Microwave-induced decomposition of nitrogen-rich iron salts and cnt formation from iron (iii)–melonate fe [c< sub> 9</sub> n< sub> 13</sub>]. *Carbon, 48*(4), 1137-1145.

Colbert, D. T., Zhang, J., McClure, S. M., Nikolaev, P., Chen, Z., Hafner, J. H., et al. (1994). Science. *266*, 1218-1284.

Collins, P. G., & Avouris, P. (2000). Nanotubes for electronics. *Scientific American, 283*(6), 62-69.

Collins, P. G., Zettl, A., Bando, H., Thess, A., & Smalley, R. E. (1997). Nanotube nanodevice. *Science, 278*(5335), 100-102.

Colomer, J. F., Stephan, C., Lefrant, S., Van Tendeloo, G., Willems, I., Kónya, Z., et al. (2000). Large-scale synthesis of single-wall carbon nanotubes by catalytic chemical vapor deposition (ccvd) method. *Chemical Physics Letters, 317*(1–2), 83-89.

Colt, J. (2006). Water quality requirements for reuse systems. *Aquacultural Engineering, 34*(3), 143-156.

Corapcioglu, M. O., & Huang, C. P. (1987). The adsorption of heavy metals onto hydrous activated carbon. *Water Research, 21*(9), 1031-1044.

Couteau, E., Hernadi, K., Seo, J. W., Thiên-Nga, L., Mikó, C., Gaál, R., et al. (2003). Cvd synthesis of high-purity multiwalled carbon nanotubes using caco3 catalyst support for large-scale production. *Chemical Physics Letters, 378*(1–2), 9-17.

Cumings, J., Mickelson, W., & Zettl, A. (2003). Simplified synthesis of double-wall carbon nanotubes. *Solid State Communications, 126*(6), 359-362.

Dąbrowski, A. (2001). Adsorption—from theory to practice. *Advances in Colloid and Interface Science, 93*(1), 135-224.

Dai, H., Rinzler, A. G., Nikolaev, P., Thess, A., Colbert, D. T., & Smalley, R. E. (1996). Single-wall nanotubes produced by metal-catalyzed disproportionation of carbon monoxide. *Chemical Physics Letters, 260*(3–4), 471-475.

Dai, L., & Mau, A. W. H. (2001). Controlled synthesis and modification of carbon nanotubes and c60: Carbon nanostructures for advanced polymeric composite materials. *Advanced Materials, 13*(12-13), 899-913.

Dallinger, D., & Kappe, C. O. (2007). Microwave-assisted synthesis in water as solvent. *Chemical Reviews, 107*(6), 2563-2591.

Danafar, F., Fakhru'l-Razi, A., Salleh, M. A. M., & Biak, D. R. A. (2009). Fluidized bed catalytic chemical vapor deposition synthesis of carbon nanotubes—a review. *Chemical Engineering Journal, 155*(1–2), 37-48.

Das, N., Dalai, A., Soltan Mohammadzadeh, J. S., & Adjaye, J. (2006). The effect of feedstock and process conditions on the synthesis of high purity cnts from aromatic hydrocarbons. *Carbon, 44*(11), 2236-2245.

Davis, W. R., Slawson, R. J., & Rigby, G. R. (1953). An unusual form of carbon. [10.1038/171756a0]. *Nature, 171*(4356), 756-756.

Delzeit, L., Nguyen, C. V., Chen, B., Stevens, R., Cassell, A., Han, J., et al. (2002). Multiwalled carbon nanotubes by chemical vapor deposition using multilayered metal catalysts. *The Journal of Physical Chemistry B, 106*(22), 5629-5635.

Di, Z.-C., Ding, J., Peng, X.-J., Li, Y.-H., Luan, Z.-K., & Liang, J. (2006). Chromium adsorption by aligned carbon nanotubes supported ceria nanoparticles. *Chemosphere, 62*(5), 861-865.

Dillon, A. C. G., T. , Alleman,J.L., Jones,K.M. Parilla,P.A. Heben M.J. . (2001). Optimization of single-wall nanotube synthesis for hydrogen storage iea task 12. *Metal Hydrides and Carbon for Hydrogen Storage NREL/CH*, 91-95.

Diniz, C. V., Doyle, F. M., & Ciminelli, V. S. (2002). Effect of ph on the adsorption of selected heavy metal ions from concentrated chloride solutions by the chelating resin dowex m-4195. *Separation Science and Technology, 37*(14), 3169-3185.

Douven, S., Pirard, S. L., Chan, F.-Y., Pirard, R., Heyen, G., & Pirard, J.-P. (2012). Large-scale synthesis of multi-walled carbon nanotubes in a continuous inclined mobile-bed rotating reactor by the catalytic chemical vapour deposition process using methane as carbon source. *Chemical Engineering Journal, 188*(0), 113-125.

Dresselhaus, M., & Avouris, P. (2001). Introduction to carbon materials research. In M. Dresselhaus, G. Dresselhaus & P. Avouris (Eds.), *Carbon nanotubes* (Vol. 80, pp. 1-9): Springer Berlin Heidelberg.

Dresselhaus, M. S., Dresselhaus, G., & Eklund, P. C. (1996). *Science of fullerenes and carbon nanotubes: Their properties and applications*: Academic Press.

Dresselhaus, M. S., Dresselhaus, G., & Saito, R. (1995). Physics of carbon nanotubes. *Carbon, 33*(7), 883-891.

Ebbesen, T. W. (1997a). *Carbon nanotubes: Preparartion and properties*: CRC press.

Ebbesen, T. W. (1997b). Production and purification of carbon nanotubes, in carbon nanotubes: Preparation and properties,. *T.W. Ebbesen, Ed. Boca Raton, FL :CRC* 139-162.

Ebbesen, T. W., & Ajayan, P. M. (1992). Large-scale synthesis of carbon nanotubes. [10.1038/358220a0]. *Nature, 358*(6383), 220-222.

Ebbesen, T. W., Hiura, H., Fujita, J., Ochiai, Y., Matsui, S., & Tanigaki, K. (1993). Patterns in the bulk growth of carbon nanotubes. *Chemical Physics Letters, 209*(1–2), 83-90.

Eftekhari, A., Manafi, S., & Moztarzadeh, F. (2006). Catalytic chemical vapor deposition preparation of multi-wall carbon nanotubes with cone-like heads. *Chemistry Letters, 35*(1), 138-139.

Eklund, P. C., Holden, J. M., & Jishi, R. A. (1995). Vibrational modes of carbon nanotubes; spectroscopy and theory. *Carbon, 33*(7), 959-972.

Eklund, P. C., Pradhan, B. K., Kim, U. J., Xiong, Q., Fischer, J. E., Friedman, A. D., et al. (2002). Large-scale production of single-walled carbon nanotubes using ultrafast pulses from a free electron laser. *Nano Letters, 2*(6), 561-566.

Endo, M., Muramatsu, H., Hayashi, T., Kim, Y. A., Terrones, M., & Dresselhaus, M. S. (2005). Nanotechnology: /`buckypaper/' from coaxial nanotubes. [10.1038/433476a]. *Nature, 433*(7025), 476-476.

Endo, M., Takeuchi, K., Igarashi, S., Kobori, K., Shiraishi, M., & Kroto, H. W. (1993). The production and structure of pyrolytic carbon nanotubes (pcnts). *Journal of Physics and Chemistry of Solids, 54*(12), 1841-1848.

Endo, M. F., H. , Fukunaga, E. . (1991). 18th meeting japanese carbon society, japanese carbon society. *Japanese Carbon Society, Saitama,December*, 34-35.

Endo, M. T., K. Igarashi,S , Kobori, K. Shiraishi, M., Kroto,H. W. . (1992). 19th meeting japanese carbon society. *Japanese Carbon Society, Kyoto, December* 192.

Fan, J., Wan, M., Zhu, D., Chang, B., Pan, Z., & Xie, S. (1999). Synthesis, characterizations, and physical properties of carbon nanotubes coated by conducting polypyrrole. *Journal of Applied Polymer Science, 74*(11), 2605-2610.

Fan, S., Chapline, M. G., Franklin, N. R., Tombler, T. W., Cassell, A. M., & Dai, H. (1999). Self-oriented regular arrays of carbon nanotubes and their field emission properties. *Science, 283*(5401), 512-514.

Faur-Brasquet, C., Reddad, Z., Kadirvelu, K., & Le Cloirec, P. (2002). Modeling the adsorption of metal ions (cu< sup> 2+</sup>, ni< sup> 2+</sup>, pb< sup>

2+</sup>) onto accs using surface complexation models. *Applied Surface Science, 196*(1), 356-365.

Flahaut, E., Bacsa, R., Peigney, A., & Laurent, C. (2003). Gram-scale ccvd synthesis of double-walled carbon nanotubes. [10.1039/B301514A]. *Chemical Communications*(12), 1442-1443.

Flahaut, E., Laurent, C., & Peigney, A. (2005). Catalytic cvd synthesis of double and triple-walled carbon nanotubes by the control of the catalyst preparation. *Carbon, 43*(2), 375-383.

Fonseca, A., Hernadi, K., Nagy, J. B., Bernaerts, D., & Lucas, A. A. (1996). Optimization of catalytic production and purification of buckytubes. *Journal of Molecular Catalysis A: Chemical, 107*(1–3), 159-168.

Fonseca, A., Hernadi, K., Piedigrosso, P., Colomer, J.-F., Mukhopadhyay, K., Doome, R., et al. (1998). Synthesis of single-and multi-wall carbon nanotubes over supported catalysts. *Applied Physics A, 67*(1), 11-22.

Franklin, N. R., Li, Y., Chen, R. J., Javey, A., & Dai, H. (2001). Patterned growth of single-walled carbon nanotubes on full 4-inch wafers. *Applied Physics Letters, 79*(27), 4571-4573.

Freundlich, H. M. F. (1906). Over the adsorption in solution *journal of physical chemistry, 57*, 385-470.

Friberg, L., Nordberg, G.F. and Vouk, V.B. . (1979). Handbook on the toxicology of metals. *New York: Elsevier North Holland*, 345.

Fu, D., Ma, Q., Zeng, X., Chen, J., Zhang, W., & Li, D. (2013). Synthesis and magnetic properties of aligned carbon nanotubes by microwave-assisted pyrolysis of acetylene. *Physica E: Low-dimensional Systems and Nanostructures, 54*, 185-190.

Fu, F., & Wang, Q. (2011). Removal of heavy metal ions from wastewaters: A review. *Journal of Environmental Management, 92*(3), 407-418.

Gabaldon, C., MARZAL, P., SECO, A., & GONZALEZ, J. A. (2000). Cadmium and copper removal by a granular activated carbon in laboratory column systems. *Separation Science and Technology, 35*(7), 1039-1053.

Gamaly, E. G., & Ebbesen, T. W. (1995). Mechanism of carbon nanotube formation in the arc discharge. *Physical Review B, 52*(3), 2083-2089.

Gao, Z., Bandosz, T. J., Zhao, Z., Han, M., & Qiu, J. (2009). Investigation of factors affecting adsorption of transition metals on oxidized carbon nanotubes. *Journal of Hazardous Materials, 167*(1–3), 357-365.

Geng, J., Singh, C., Shephard, D. S., Shaffer, M. S., Johnson, B. F., & Windle, A. H. (2002). Synthesis of high purity single-walled carbon nanotubes in high yield. *Chemical Communications*(22), 2666-2667.

Gibson, J. A. E. (1992). Early nanotubes? [10.1038/359369c0]. *Nature, 359*(6394), 369-369.

Gogotsi, Y. (2006). *Nanomaterials handbook*: CRC press.

Gulino, G., Vieira, R., Amadou, J., Nguyen, P., Ledoux, M. J., Galvagno, S., et al. (2005). C2h6 as an active carbon source for a large scale synthesis of carbon nanotubes by chemical vapour deposition. *Applied Catalysis A: General, 279*(1–2), 89-97.

Günay, A., Arslankaya, E., & Tosun, İ. (2007). Lead removal from aqueous solution by natural and pretreated clinoptilolite: Adsorption equilibrium and kinetics. *Journal of Hazardous Materials, 146*(1), 362-371.

Guo, T., Nikolaev, P., Thess, A., Colbert, D. T., & Smalley, R. E. (1995). Catalytic growth of single-walled manotubes by laser vaporization. *Chemical Physics Letters, 243*(1–2), 49-54.

Guo, T., Nikolaev, P. Rinzler, A.G., Tomanek, D., Colbert, D.T., Smalley, R.E. (1995). Self-assembly of tubular fullerenes. *J. Phys. Chem* 10964-10697.

Han, J. H., Choi, S. H., Lee, T. Y., Yoo, J. B., Park, C. Y., Jeong, T. W., et al. (2002). Field emission properties of modified carbon nanotubes grown on fe-coated glass using pecvd with carbon monoxide. *Physica B: Condensed Matter, 323*(1–4), 182-183.

Harris, J. D., Raffaelle, R. P., Gennett, T., Landi, B. J., & Hepp, A. F. (2005). Growth of multi-walled carbon nanotubes by injection cvd using cyclopentadienyliron dicarbonyl dimer and cyclooctatetraene iron tricarbonyl. *Materials Science and Engineering: B, 116*(3), 369-374.

Harris, P. J., & Harris, P. J. P. J. F. (2001). *Carbon nanotubes and related structures: New materials for the twenty-first century*: Cambridge university press.

Harutyunyan, A. R., Pradhan, B. K., Kim, U. J., Chen, G., & Eklund, P. C. (2002). Cvd synthesis of single wall carbon nanotubes under "soft" conditions. *Nano Letters, 2*(5), 525-530.

Hatta, N., & Murata, K. (1994). Very long graphitic nano-tubules synthesized by plasma-decomposition of benzene. *Chemical Physics Letters, 217*(4), 393-402.

Hayashi, Y., Tokunaga, T., Kaneko, K., Henley, S. J., Stolojan, V., Carey, J. D., et al. (2006). Microstructure analyses of metal-filled carbon nanotubes synthesized by microwave plasma-enhanced chemical vapor deposition. *Nanotechnology, IEEE Transactions on, 5*(5), 485-490.

He, D., Li, H., Li, W., Haghi-Ashtiani, P., Lejay, P., & Bai, J. (2011). Growth of carbon nanotubes in six orthogonal directions on spherical alumina microparticles. *Carbon, 49*(7), 2273-2286.

Hernadi, K., Fonseca, A., Nagy, J. B., Bernaerts, D., & Lucas, A. A. (1996). Fe-catalyzed carbon nanotube formation. *Carbon, 34*(10), 1249-1257.

Herrera-Urbina, R., & Fuerstenau, D. (1995). The effect of pb (ii) species, ph and dissolved carbonate on the zeta potential at the quartz/aqueous solution interface. *Colloids and Surfaces A: Physicochemical and Engineering Aspects, 98*(1), 25-33.

Ho, Y.-S. (2006a). Review of second-order models for adsorption systems. *Journal of Hazardous Materials, 136*(3), 681-689.

Ho, Y.-S. (2006b). Second-order kinetic model for the sorption of cadmium onto tree fern: A comparison of linear and non-linear methods. *Water Research, 40*(1), 119-125.

Ho, Y., & McKay, G. (1999a). The sorption of lead (ii) ions on peat. *Water Research, 33*(2), 578-584.

Ho, Y. S., & McKay, G. (1999b). Pseudo-second order model for sorption processes. *Process Biochemistry, 34*(5), 451-465.

Hone, J. (2001). Phonons and thermal properties of carbon nanotubes. In M. Dresselhaus, G. Dresselhaus & P. Avouris (Eds.), *Carbon nanotubes* (Vol. 80, pp. 273-286): Springer Berlin Heidelberg.

Hong, E. H., Lee, K. H., Oh, S. H., & Park, C. G. (2003). Synthesis of carbon nanotubes using microwave radiation. *Advanced Functional Materials, 13*(12), 961-966.

Hou, B. X., R. Inoue,T. Einarsson,E. . Chiashi,S Shiomi,J. Miyoshi,A. Maruyama, S. (2011). Decomposition of ethanol and dimethyl ether during chemical vapour deposition synthesis of single-walled carbon nanotubes. *Jpn J Appl Phys 50*(6), 0651011-0651014.

Hsieh, S.-H., & Horng, J.-J. (2007). Adsorption behavior of heavy metal ions by carbon nanotubes grown on microsized al< sub> 2</sub> o< sub> 3</sub> particles. *Journal of University of Science and Technology Beijing, Mineral, Metallurgy, Material, 14*(1), 77-84.

Hsieh, S.-H., Horng, J.-J., & Tsai, C.-K. (2006). Growth of carbon nanotube on micro-sized al2o3 particle and its application to adsorption of metal ions. *Journal of Materials Research, 21*(05), 1269-1273.

Hu, J., Chen, C., Zhu, X., & Wang, X. (2009). Removal of chromium from aqueous solution by using oxidized multiwalled carbon nanotubes. *Journal of Hazardous Materials, 162*(2–3), 1542-1550.

Huang, C.-W., Hsu, C.-H., Kuo, P.-L., Hsieh, C.-T., & Teng, H. (2011). Mesoporous carbon spheres grafted with carbon nanofibers for high-rate electric double layer capacitors. *Carbon, 49*(3), 895-903.

Huang, J. H., Chuang, C. C., & Tsai, C. H. (2003). Effect of nickel thickness and microwave power on the growth of carbon nanotubes by microwave-heated chemical vapor deposition. *Microelectronic Engineering, 66*(1–4), 10-16.

Huang, W., Wang, Y., Luo, G., & Wei, F. (2003). 99.9% purity multi-walled carbon nanotubes by vacuum high-temperature annealing. *Carbon, 41*(13), 2585-2590.

Huang, Z., Xu, J., Ren, Z., Wang, J., Siegal, M., & Provencio, P. (1998). Growth of highly oriented carbon nanotubes by plasma-enhanced hot filament chemical vapor deposition. *Applied Physics Letters, 73*(26), 3845-3847.

Hugh, O. P. (1999). Handbook of chemical vapor deposition (cvd) principles, technology, and applications. *Second EditionWilliam Andrew publishing, llc Norwich, New York, USA*.

Hughes, T. V., & Chambers, C. R. Manufacture of carbon filaments,.

Huh, Y., Lee, J. Y., Cheon, J., Hong, Y. K., Koo, J. Y., Lee, T. J., et al. (2003). Controlled growth of carbon nanotubes over cobalt nanoparticles by thermal chemical vapor deposition. *Journal of Materials Chemistry, 13*(9), 2297-2300.

Hyung, H., & Kim, J.-H. (2008). Natural organic matter (nom) adsorption to multi-walled carbon nanotubes: Effect of nom characteristics and water quality parameters. *Environmental Science & Technology, 42*(12), 4416-4421.

Iijima, S. (1991). Helical microtubules of graphitic carbon. [10.1038/354056a0]. *Nature, 354*(6348), 56-58.

Iijima, S., & Ichihashi, T. (1993). Single-shell carbon nanotubes of 1-nm diameter. [10.1038/363603a0]. *Nature, 363*(6430), 603-605.

Ikeda, T., Kamo, T., & Danno, M. (1995). New synthesis method of fullerenes using microwave‐induced naphthalene‐nitrogen plasma at atmospheric pressure. *Applied Physics Letters, 67*(7), 900-902.

Ikuno, T., Ryu, J. T., Oyama, T., Ohkura, S., Baek, Y. G., Honda, S., et al. (2002). Characterization of low temperature growth carbon nanofibers synthesized by using plasma enhanced chemical vapor deposition. *Vacuum, 66*(3-4), 341-345.

Ishigami, M., Cumings, J., Zettl, A., & Chen, S. (2000). A simple method for the continuous production of carbon nanotubes. *Chemical Physics Letters, 319*(5–6), 457-459.

Ishioka, M., Okada, T., & Matsubara, K. (1993). Preparation of vapor-grown carbon fibers in straight form by floating catalyst method in linz-donawitz converter gas. *Carbon, 31*(1), 123-127.

Ishioka, M., Okada, T., Matsubara, K., & Endo, M. (1992). Formation of vapor-grown carbon fibers in co-co2-h2 mixtures, i. Influence of carrier gas composition. *Carbon, 30*(6), 859-863.

Javey, A., Guo, J., Wang, Q., Lundstrom, M., & Dai, H. (2003). Ballistic carbon nanotube field-effect transistors. [10.1038/nature01797]. *Nature, 424*(6949), 654-657.

Jennifer, R., and Lukes H. Z. . (2007). Thermal conductivity of individual single-wall carbon nanotubes. *J. Heat Transfer, 129*(6), 705 -712.

Jiang, Q., & Zhao, Y. (2004). Effects of activation conditions on bet specific surface area of activated carbon nanotubes. *Microporous and Mesoporous Materials, 76*(1–3), 215-219.

Jiang, W., Ferkel, H., & Molian, P. (2004). Rapid production of carbon nanotubes by high-power laser ablation. *Journal of Manufacturing Science and Engineering, 127*(3), 703-707.

José-Yacamán, M., Miki-Yoshida, M., Rendón, L., & Santiesteban, J. G. (1993). Catalytic growth of carbon microtubules with fullerene structure. *Applied Physics Letters, 62*(2), 202-204.

Journet, C., & Bernier, P. (1998). Production of carbon nanotubes. *Applied Physics A, 67*(1), 1-9.

Journet, C., Maser, W. K., Bernier, P., Loiseau, A., Lamy de la Chapelle, M., Lefrant, S., et al. (1997). Large-scale production of single-walled carbon nanotubes by the electric-arc technique. *Nature, 388*(6644), 756-758.

Jung, S. H., Kim, M. R., Jeong, S. H., Kim, S. U., Lee, O. J., Lee, K. H., et al. (2003). High-yield synthesis of multi-walled carbon nanotubes by arc discharge in liquid nitrogen. *Applied Physics A, 76*(2), 285-286.

Kabbashi, N. A., Atieh, M. A., Al-Mamun, A., Mirghami, M. E. S., Alam, M. D. Z., & Yahya, N. (2009). Kinetic adsorption of application of carbon nanotubes for pb(ii) removal from aqueous solution. *Journal of Environmental Sciences, 21*(4), 539-544.

Kabbashi, N. A., Daoud, J.I., Isam, Y.Q., Mirghami, M.E.S., Rosli, N.F. and Nurhasni, F.R. (2011). Statistical analaysis for removal of cadmium from aqueous solution at high ph. *Aust. J. Basic. Appl. Sci., 5(6)*, 440–446.

Kandah, M. I., & Meunier, J.-L. (2007). Removal of nickel ions from water by multi-walled carbon nanotubes. *Journal of Hazardous Materials, 146*(1–2), 283-288.

Kasumov, Y. A., Shailos, A., Khodos, I. I., Volkov, V. T., Levashov, V. I., Matveev, V. N., et al. (2007). Cvd growth of carbon nanotubes at very low pressure of acetylene. *Applied Physics A, 88*(4), 687-691.

Kataura, H., Kimura, A., Ohtsuka, Y., Suzuki, S., Maniwa, Y., Hanyu, T., et al. (1998). Formation of thin single-wall carbon nanotubes by laser vaporization of rh/pd-graphite composite rod. *Japanese Journal of Applied Physics, Part 2: Letters, 37*(5 B), L616-L618.

Kato, T., Matsumoto, T., Saito, T., Hayashi, J.-I., Kusakabe, K., & Morooka, S. (1993). Effect of carbon source on formation of vapor-grown carbon fiber. *Carbon, 31*(6), 937-940.

Kharissova, O. V. (2004). Vertically aligned carbon nanotubes fabricated by microwaves. *Review Advances Materials Science, 7*, 50.

Kiang, C.-H., Goddard Iii, W. A., Beyers, R., & Bethune, D. S. (1995). Carbon nanotubes with single-layer walls. *Carbon, 33*(7), 903-914.

Kiang, C.-H., Goddard Iii, W. A., Beyers, R., Salem, J. R., & Bethune, D. S. (1996). Catalytic effects of heavy metals on the growth of carbon nanotubes and nanoparticles. *Journal of Physics and Chemistry of Solids, 57*(1), 35-39.

Kiang, C.-H., Goddard, W. A., III, Beyers, R., Salem, J. R., & Bethune, D. S. (1994). Catalytic synthesis of single-layer carbon nanotubes with a wide range of diameters. *The Journal of Physical Chemistry, 98*(26), 6612-6618.

Kiang, C. H., Dresselhaus, M. S., Beyers, R., & Bethune, D. S. (1996). Vapor-phase self-assembly of carbon nanomaterials. *Chemical Physics Letters, 259*(1–2), 41-47.

Kiang, C. H., Endo, M., Ajayan, P. M., Dresselhaus, G., & Dresselhaus, M. S. (1998). Size effects in carbon nanotubes. *Physical Review Letters, 81*(9), 1869-1872.

Kim, D. H., & Anderson, M. A. (1994). Photoelectrocatalytic degradation of formic acid using a porous titanium dioxide thin-film electrode. *Environmental Science & Technology, 28*(3), 479-483.

Kim, K.-E., Kim, K.-J., Jung, W. S., Bae, S. Y., Park, J., Choi, J., et al. (2005). Investigation on the temperature-dependent growth rate of carbon nanotubes using

chemical vapor deposition of ferrocene and acetylene. *Chemical Physics Letters, 401*(4–6), 459-464.

Kim, N. S., Lee, Y. T., Park, J., Han, J. B., Choi, Y. S., Choi, S. Y., et al. (2003). Vertically aligned carbon nanotubes grown by pyrolysis of iron, cobalt, and nickel phthalocyanines. *The Journal of Physical Chemistry B, 107*(35), 9249-9255.

Kim, Y., Hayashi, T., Endo, M., Kaburagi, Y., Tsukada, T., Shan, J., et al. (2005a). Synthesis and structural characterization of thin multi-walled carbon nanotubes with a partially facetted cross section by a floating reactant method. *Carbon, 43*(11), 2243-2250.

Kim, Y. A., Hayashi, T., Endo, M., Kaburagi, Y., Tsukada, T., Shan, J., et al. (2005b). Synthesis and structural characterization of thin multi-walled carbon nanotubes with a partially facetted cross section by a floating reactant method. *Carbon, 43*(11), 2243-2250.

Kinniburgh, D. G. (1986). General purpose adsorption isotherms. *Environmental Science & Technology, 20*(9), 895-904.

Kitiyanan, B., Alvarez, W. E., Harwell, J. H., & Resasco, D. E. (2000). Controlled production of single-wall carbon nanotubes by catalytic decomposition of co on bimetallic co–mo catalysts. *Chemical Physics Letters, 317*(3–5), 497-503.

Klinke, C., Bonard, J.-M., & Kern, K. (2001). Comparative study of the catalytic growth of patterned carbon nanotube films. *Surface Science, 492*(1–2), 195-201.

Kobayashi, Y., Nakashima, H., Takagi, D., & Homma, Y. (2004). Cvd growth of single-walled carbon nanotubes using size-controlled nanoparticle catalyst. *Thin Solid Films, 464*, 286-289.

Kokai, F., Takahashi, K., Kasuya, D., Yudasaka, M., & Iijima, S. (2002). Growth dynamics of single-wall carbon nanotubes and nanohorn aggregates by co2 laser vaporization at room temperature. *Applied Surface Science, 197–198*(0), 650-655.

Kong, J., Cassell, A. M., & Dai, H. (1998). Chemical vapor deposition of methane for single-walled carbon nanotubes. *Chemical Physics Letters, 292*(4–6), 567-574.

Konno, K., Onoe, K., Takiguchi, Y., & Yamaguchi, T. (2013). Direct preparation of hydrogen and carbon nanotubes by microwave plasma decomposition of methane over fe/si activated by biased hydrogen plasma. *Green and Sustainable Chemistry, 3*, 19.

Kroto, H. W., Heath, J. R., O'Brien, S. C., Curl, R. F., & Smalley, R. E. (1985). C60: Buckminsterfullerene. [10.1038/318162a0]. *Nature, 318*(6042), 162-163.

Kuan, H.-C., Ma, C.-C. M., Chang, W.-P., Yuen, S.-M., Wu, H.-H., & Lee, T.-M. (2005). Synthesis, thermal, mechanical and rheological properties of multiwall carbon nanotube/waterborne polyurethane nanocomposite. *Composites Science and Technology, 65*(11–12), 1703-1710.

Kuang, M. H., Wang, Z. L., Bai, X. D., Guo, J. D., & Wang, E. G. (2000). Catalytically active nickel {110} surfaces in growth of carbon tubular structures. *Applied Physics Letters, 76*(10), 1255-1257.

Kumar, M., & Ando, Y. (2010). Chemical vapor deposition of carbon nanotubes: A review on growth mechanism and mass production. *Journal of Nanoscience and Nanotechnology, 10*(6), 3739-3758.

Kuo, C.-S., Bai, A., Huang, C.-M., Li, Y.-Y., Hu, C.-C., & Chen, C.-C. (2005). Diameter control of multiwalled carbon nanotubes using experimental strategies. *Carbon, 43*(13), 2760-2768.

Kuo, D. H., Su, M. Y., & Chen, W. R. (2006). Fast rate growth of organized carbon nanotubes by cvd using iron pentacarbonyl as gas-phase catalyst. *Chemical Vapor Deposition, 12*(6), 395-402.

Küttel, O. M., Groening, O., Emmenegger, C., & Schlapbach, L. (1998). Electron field emission from phase pure nanotube films grown in a methane/hydrogen plasma. *Applied Physics Letters, 73*(15), 2113-2115.

Lacerda, R., Teo, K., Teh, A., Yang, M., Dalal, S., Jefferson, D., et al. (2004). Thin-film metal catalyst for the production of multi-wall and single-wall carbon nanotubes. *Journal of Applied Physics, 96*(8), 4456-4462.

Lacerda, R. G., Teh, A. S., Yang, M. H., Teo, K. B. K., Rupesinghe, N. L., Dalal, S. H., et al. (2004). Growth of high-quality single-wall carbon nanotubes without amorphous carbon formation. *Applied Physics Letters, 84*(2), 269-271.

Lambert, J. M., Ajayan, P. M., & Bernier, P. (1995). Synthesis of single and multi-shell carbon nanotubes. *Synthetic Metals, 70*(1–3), 1475-1476.

Langergren, S. S., B.K,. (1898). The theory of adsorption of solutes. *Veternskapsakad Handlingar, 24*(4), 1-39.

Langmuir, I. (1918). The adsorption of gases on plane surfaces of glass, mica and platinum. *Journal of the American Chemical Society, 40*(9), 1361-1403.

Lee, C. J., Lyu, S. C., Kim, H.-W., Park, C.-Y., & Yang, C.-W. (2002). Large-scale production of aligned carbon nanotubes by the vapor phase growth method. *Chemical Physics Letters, 359*(1–2), 109-114.

Lee, C. J., & Park, J. (2000). Growth model of bamboo-shaped carbon nanotubes by thermal chemical vapor deposition. *Applied Physics Letters, 77*(21), 3397-3399.

Lee, J.-H., Lee, S. H., Kim, D., & Park, Y. S. (2013). The structural and surface properties of carbon nanotube synthesized by microwave plasma chemical vapor deposition method for superhydrophobic coating. *Thin Solid Films, 546*, 94-97.

Lee, K.-H. (2007). Low temperature synthesis of carbon nanotubes by direct microwave irradiation: DTIC Document.

Lee, S. J., Kim, K., Kim, D. H., Park, J. O., & Park, G. T. (2002). *Multiple magnification images based micropositioning for 3d micro assembly*.

Leyva Ramos, R., Bernal Jacome, L., Mendoza Barron, J., Fuentes Rubio, L., & Guerrero Coronado, R. (2002). Adsorption of zinc (ii) from an aqueous solution onto activated carbon. *Journal of Hazardous Materials, 90*(1), 27-38.

Li, H., He, D., Li, T., Genestoux, M., & Bai, J. (2010). Chemical kinetics of catalytic chemical vapor deposition of an acetylene/xylene mixture for improved carbon nanotube production. *Carbon, 48*(15), 4330-4342.

Li, J., Bai, G., Feng, J., & Jiang, W. (2005). Microstructure and mechanical properties of hot-pressed carbon nanotubes compacted by spark plasma sintering. *Carbon, 43*(13), 2649-2653.

Li, W. Z., Xie, S. S., Qian, L. X., Chang, B. H., Zou, B. S., Zhou, W. Y., et al. (1996). Large-scale synthesis of aligned carbon nanotubes. *Science, 274*(5293), 1701-1703.

Li, Y.-H., Di, Z., Ding, J., Wu, D., Luan, Z., & Zhu, Y. (2005). Adsorption thermodynamic, kinetic and desorption studies of pb2+ on carbon nanotubes. *Water Research, 39*(4), 605-609.

Li, Y.-H., Ding, J., Luan, Z., Di, Z., Zhu, Y., Xu, C., et al. (2003). Competitive adsorption of pb2+, cu2+ and cd2+ ions from aqueous solutions by multiwalled carbon nanotubes. *Carbon, 41*(14), 2787-2792.

Li, Y.-H., Luan, Z., Xiao, X., Zhou, X., Xu, C., Wu, D., et al. (2003a). Removal of cu2⁺ ions from aqueous solutions by carbon nanotubes. *Adsorption Science & Technology, 21*(5), 475-485.

Li, Y.-H., Luan, Z., Xiao, X., Zhou, X., Xu, C., Wu, D., et al. (2003b). Removal of cu2+ ions from aqueous solutions by carbon nanotubes. *Adsorption Science & Technology, 21*(5), 475-485.

Li, Y.-H., Wang, S., Cao, A., Zhao, D., Zhang, X., Xu, C., et al. (2001). Adsorption of fluoride from water by amorphous alumina supported on carbon nanotubes. *Chemical Physics Letters, 350*(5–6), 412-416.

Li, Y.-H., Wang, S., Luan, Z., Ding, J., Xu, C., & Wu, D. (2003). Adsorption of cadmium(ii) from aqueous solution by surface oxidized carbon nanotubes. *Carbon, 41*(5), 1057-1062.

Li, Y.-H., Wang, S., Wei, J., Zhang, X., Xu, C., Luan, Z., et al. (2002). Lead adsorption on carbon nanotubes. *Chemical Physics Letters, 357*(3–4), 263-266.

Li, Y.-H., Zhu, Y., Zhao, Y., Wu, D., & Luan, Z. (2006). Different morphologies of carbon nanotubes effect on the lead removal from aqueous solution. *Diamond and Related Materials, 15*(1), 90-94.

Li, Y.-M., Sun, S.-Q., Zhou, Q., Qin, Z., Tao, J.-X., Wang, J., et al. (2004). Identification of american ginseng from different regions using ft-ir and two-dimensional correlation ir spectroscopy. *Vibrational Spectroscopy, 36*(2), 227-232.

Li, Y., Cui, R., Ding, L., Liu, Y., Zhou, W., Zhang, Y., et al. (2010). How catalysts affect the growth of single-walled carbon nanotubes on substrates. *Advanced Materials, 22*(13), 1508-1515.

Li, Y., Liu, F., Xia, B., Du, Q., Zhang, P., Wang, D., et al. (2010). Removal of copper from aqueous solution by carbon nanotube/calcium alginate composites. *Journal of Hazardous Materials, 177*(1–3), 876-880.

Li, Y., Zhao, Y., Hu, W., Ahmad, I., Zhu, Y., Peng, X., et al. (2007). *Carbon nanotubes-the promising adsorbent in wastewater treatment.* Paper presented at the Journal of Physics: Conference Series.

Li, Y. H., Di, Z.C., Luan, Z.K., Ding, J., Zuo, H., Wu, X.Q., Xu, C.L. and Wu, D.H. . (2004). Removal of heavy metals from aqueous solution by carbon nanotubes: Adsorption equilibrium and kinetics. *J. Environ. Sci. China, 16*, 208–211.

Li, Z., Chen, J., Zhang, X., Li, Y., & Fung, K. K. (2002). Catalytic synthesized carbon nanostructures from methane using nanocrystalline ni. *Carbon, 40*(3), 409-415.

Lidström, P., Tierney, J., Wathey, B., & Westman, J. (2001). Microwave assisted organic synthesis—a review. *Tetrahedron, 57*(45), 9225-9283.

Lin, X., Wang, X. K., Dravid, V. P., Chang, R. P. H., & Ketterson, J. B. (1994). Large scale synthesis of single-shell carbon nanotubes. *Applied Physics Letters, 64*(2), 181-183.

Ling, T. Y., Lipan, S., and Singh, H. (2010). Performance of oxidation ponds in removing heavy metals from pig farm wastewater. *Middle-East Journal of Scientific Research, 5*, 163-169.

Liu, B., Ren, W., Gao, L., Li, S., Pei, S., Liu, C., et al. (2009). Metal-catalyst-free growth of single-walled carbon nanotubes. *Journal of the American Chemical Society, 131*(6), 2082-2083.

Liu, B. C., Lyu, S. C., Lee, T. J., Choi, S. K., Eum, S. J., Yang, C. W., et al. (2003). Synthesis of single- and double-walled carbon nanotubes by catalytic decomposition of methane. *Chemical Physics Letters, 373*(5–6), 475-479.

Liu, C., Cheng, H. M., Cong, H. T., Li, F., Su, G., Zhou, B. L., et al. (2000). Synthesis of macroscopically long ropes of well-aligned single-walled carbon nanotubes. *Advanced Materials, 12*(16), 1190-1192.

Liu, J., Fan, S., & Dai, H. (2004). Recent advances in methods of forming carbon nanotubes. *MRS Bulletin, 29*(04), 244-250.

Liu, J., Jiang, Z., Yu, H., & Tang, T. (2011). Catalytic pyrolysis of polypropylene to synthesize carbon nanotubes and hydrogen through a two-stage process. *Polymer Degradation and Stability, 96*(10), 1711-1719.

Liu, J., Zubiri, M. R. i., Vigolo, B., Dossot, M., Fort, Y., Ehrhardt, J.-J., et al. (2007). Efficient microwave-assisted radical functionalization of single-wall carbon nanotubes. *Carbon, 45*(4), 885-891.

Liu, R.-M., & Ting, J.-M. (2003). Growth of carbon nanotubes using microwave plasma-enhanced chemical vapor deposition process. *Materials Chemistry and Physics, 82*(3), 571-574.

Long, R. Q., & Yang, R. T. (2001). Carbon nanotubes as superior sorbent for dioxin removal. *Journal of the American Chemical Society, 123*(9), 2058-2059.

Lu, C., & Chiu, H. (2006b). Adsorption of zinc(ii) from water with purified carbon nanotubes. *Chemical Engineering Science, 61*(4), 1138-1145.

Lu, C., & Chiu, H. (2008). Chemical modification of multiwalled carbon nanotubes for sorption of zn< sup> 2+</sup> from aqueous solution. *Chemical Engineering Journal, 139*(3), 462-468.

Lu, C., Chiu, H., & Bai, H. (2007). Comparisons of adsorbent cost for the removal of zinc (ii) from aqueous solution by carbon nanotubes and activated carbon. *Journal of Nanoscience and Nanotechnology, 7*(4-5), 4-5.

Lu, C., Chiu, H., & Liu, C. (2006b). Removal of zinc(ii) from aqueous solution by purified carbon nanotubes: Kinetics and equilibrium studies. *Industrial & Engineering Chemistry Research, 45*(8), 2850-2855.

Lu, C., & Liu, C. (2006). Removal of nickel(ii) from aqueous solution by carbon nanotubes. *Journal of Chemical Technology & Biotechnology, 81*(12), 1932-1940.

Lu, C., Liu, C., & Rao, G. P. (2008). Comparisons of sorbent cost for the removal of ni2+ from aqueous solution by carbon nanotubes and granular activated carbon. *Journal of Hazardous Materials, 151*(1), 239-246.

Lu, C., Liu, C., & Su, F. (2009). Sorption kinetics, thermodynamics and competition of ni2+ from aqueous solutions onto surface oxidized carbon nanotubes. *Desalination, 249*(1), 18-23.

Lu, C., & Su, F. (2007). Adsorption of natural organic matter by carbon nanotubes. *Separation and Purification Technology, 58*(1), 113-121.

Luo, J. Z., Gao, L. Z., Leung, Y. L., & Au, C. T. (2000). The decomposition of no on cnts and 1 wt% rh/cnts. *Catalysis Letters, 66*(1-2), 91-97.

M.J. Temkin, & Pyzhev, V. (1940). Acta physiochim. *URSS, 12*, 217.

Machida, M., Kikuchi, Y., Aikawa, M., & Tatsumoto, H. (2004). Kinetics of adsorption and desorption of pb (ii) in aqueous solution on activated carbon by two-site adsorption model. *Colloids and Surfaces A: Physicochemical and Engineering Aspects, 240*(1), 179-186.

Magrez, A., Smajda, R., Seo, J. W., Horváth, E., Ribič, P. R., Andresen, J. C., et al. (2011). Striking influence of the catalyst support and its acid–base properties: New insight into the growth mechanism of carbon nanotubes. *ACS Nano, 5*(5), 3428-3437.

Maroto Valiente, A., Navarro López, P., Rodríguez Ramos, I., Guerrero Ruiz, A., Li, C., & Xin, Q. (2000). In situ study of carbon nanotube formation by c2h2 decomposition on an iron-based catalyst. *Carbon, 38*(14), 2003-2006.

Maruyama, S., Kojima, R., Miyauchi, Y., Chiashi, S., & Kohno, M. (2002). Low-temperature synthesis of high-purity single-walled carbon nanotubes from alcohol. *Chemical Physics Letters, 360*(3–4), 229-234.

Masao Yamaguchi, L. P., Seiji Akita, and Yoshikazu Nakayama (2008). Effect of residual acetylene gas on growth of vertically aligned carbon nanotubes. *Jpn. J. Appl. Phys, 47*, 1937-1940.

Masciangioli, T., & Zhang, W.-X. (2003). Peer reviewed: Environmental technologies at the nanoscale. *Environmental Science & Technology, 37*(5), 102A-108A.

Maser, W. K., Muñoz, E., Benito, A. M., Martínez, M. T., de la Fuente, G. F., Maniette, Y., et al. (1998). Production of high-density single-walled nanotube material by a simple laser-ablation method. *Chemical Physics Letters, 292*(4–6), 587-593.

McKee, G. S. B., Deck, C. P., & Vecchio, K. S. (2009). Dimensional control of multi-walled carbon nanotubes in floating-catalyst cvd synthesis. *Carbon, 47*(8), 2085-2094.

MDC. (1997). Laws of malaysia-environmental quality act 1974 and regulations, fourth ed.Kuala lumpur. *Sdn.Bhd.*

Meena, A. K., Kadirvelu, K., Mishraa, G., Rajagopal, C., & Nagar, P. (2008). Adsorption of pb (ii) and cd (ii) metal ions from aqueous solutions by mustard husk. *Journal of Hazardous Materials, 150*(3), 619-625.

Méndez, U. O., Kharissova, O. V., & Rodríguez, M. (2003). Synthesis and morphology of nanostructures via microwave heating. *Review Advance Materials Science, 5*, 398.

Monthioux, M., & Kuznetsov, V. L. (2006). Who should be given the credit for the discovery of carbon nanotubes? *Carbon, 44*(9), 1621-1623.

Moon, J.-M., An, K. H., Lee, Y. H., Park, Y. S., Bae, D. J., & Park, G.-S. (2001). High-yield purification process of singlewalled carbon nanotubes. *The Journal of Physical Chemistry B, 105*(24), 5677-5681.

Moradi, O., Zare, K. and Yari, M. . (2011). Interaction of some heavy metal ions with single walled carbon nanotube. *Int. J. Nano. Dim, 1(3)*(203-220).

Mordkovich, V. Z., Yoshimura, S., & Chang, R. P. H. (1998). In supercarbon: Synthesis, properties and applications. *Springer*, 107-118.

Muataz, A. A., Fakhrul-Razi, A. A., Dayang, B. A. R., Lsadig, M. E., Chuah, G. T., Ma'an, F. A., et al. (2003). Carbon nanofiber and carbon nanotube production by floating catalyst chemical vapour deposition (fc-cvd). *Update on Microscopy and Microanalysis*, 14-17.

Muataz, A. A. F.-R., A. . Dayang,B.A.R . EL-Sadig,M Chuah,G.T. . Maan,F. A . Sunny,I Faizah, Y. Abdul Hamid,M, Mohd Halim, I.S. . (2003). Production of vapor growth carbon fiber (vgcf) by using cvd. *Somche*, 596-602.

Mubarak, N., Daniel, S., Khalid, M., & Tan, J. (2012). Comparative study of functionalize and non-functionalized carbon nanotube for removal of copper from polluted water. *International Journal of Chemical & Environmental Engineering, 3*(5), 314-317.

Mubarak, N. M., Alicia, R. F., Abdullah, E. C., Sahu, J. N., Haslija, A. B. A., & Tan, J. (2013). Statistical optimization and kinetic studies on removal of zn2+ using functionalized carbon nanotubes and magnetic biochar. *Journal of Environmental Chemical Engineering, 1*(3), 486-495.

Mubarak, N. M., Ruthiraan, M., Sahu, J. N., Abdullah, E. C., Jayakumar, N. S., Sajuni, N. R., et al. (2014). Adsorption and kinetic study on sn2+ removal using modified

carbon nanotube and magnetic biochar. *International Journal of Nanoscience*, 1350044.

Mubarak, N. M., Yusof, F., & Alkhatib, M. F. (2011). The production of carbon nanotubes using two-stage chemical vapor deposition and their potential use in protein purification. *Chemical Engineering Journal, 168*(1), 461-469.

Mukhopadhyay, K., Koshio, A., Sugai, T., Tanaka, N., Shinohara, H., Konya, Z., et al. (1999). Bulk production of quasi-aligned carbon nanotube bundles by the catalytic chemical vapour deposition (ccvd) method. *Chemical Physics Letters, 303*(1–2), 117-124.

Muñoz, E., Maser, W. K., Benito, A. M., Martínez, M. T., de la Fuente, G. F., Maniette, Y., et al. (2000). Gas and pressure effects on the production of single-walled carbon nanotubes by laser ablation. *Carbon, 38*(10), 1445-1451.

Murakami, Y., Miyauchi, Y., Chiashi, S., & Maruyama, S. (2003). Characterization of single-walled carbon nanotubes catalytically synthesized from alcohol. *Chemical Physics Letters, 374*(1), 53-58.

Muyibi, S. A., Ambali, A. R., & Eissa, G. S. (2008). Development-induced water pollution in malaysia: Policy implications from an econometric analysis. [Article]. *Water Policy, 10*(2), 193-206.

N. Grobert, J. P. H., W.-K. Hsu, H. W. Kroto, M. Terrones,, & Zhu, D. R. M. W. a. Y. Q. (1999). New advances in the creation of nanostructured materials. *Pure Appl. Chem, 71*(11), 2125-2130.

Nagaraju, N., Fonseca, A., Konya, Z., & Nagy, J. B. (2002). Alumina and silica supported metal catalysts for the production of carbon nanotubes. *Journal of Molecular Catalysis A: Chemical, 181*(1–2), 57-62.

Narkiewicz, U., Podsiadły, M., Jędrzejewski, R., & Pełech, I. (2010). Catalytic decomposition of hydrocarbons on cobalt, nickel and iron catalysts to obtain carbon nanomaterials. *Applied Catalysis A: General, 384*(1–2), 27-35.

Ngah, W., & Fatinathan, S. (2008). Adsorption of cu (ii) ions in aqueous solution using chitosan beads, chitosan–gla beads and chitosan–alginate beads. *Chemical Engineering Journal, 143*(1), 62-72.

Nie, H., Cui, M., & Russell, T. P. (2013). A route to rapid carbon nanotube growth. *Chemical Communications, 49*(45), 5159-5161.

Nikolaev, P. (2004). Gas-phase production of single-walled carbon nanotubes from carbon monoxide: A review of the hipco process. *Journal of Nanoscience and Nanotechnology, 4*(4), 307-316.

Nikolaev, P., Bronikowski, M. J., Bradley, R. K., Rohmund, F., Colbert, D. T., Smith, K. A., et al. (1999). Gas-phase catalytic growth of single-walled carbon nanotubes from carbon monoxide. *Chemical Physics Letters, 313*(1–2), 91-97.

Ning, Y., Zhang, X., Wang, Y., Sun, Y., Shen, L., Yang, X., et al. (2002). Bulk production of multi-wall carbon nanotube bundles on sol–gel prepared catalyst. *Chemical Physics Letters, 366*(5–6), 555-560.

Nuchter, M., Ondruschka, B., Bonrath, W., & Gum, A. (2004). Microwave assisted synthesis - a critical technology overview. [10.1039/B310502D]. *Green Chemistry, 6*(3), 128-141.

Oberlin, A., Endo, M., & Koyama, T. (1976). Filamentous growth of carbon through benzene decomposition. *Journal of Crystal Growth, 32*(3), 335-349.

Odom, T. W., Huang, J.-L., Kim, P., & Lieber, C. M. (1998). Atomic structure and electronic properties of single-walled carbon nanotubes. [10.1038/34145]. *Nature, 391*(6662), 62-64.

Otsuka, K., Abe, Y., Kanai, N., Kobayashi, Y., Takenaka, S., & Tanabe, E. (2004). Synthesis of carbon nanotubes on ni/carbon-fiber catalysts under mild conditions. *Carbon, 42*(4), 727-736.

Palizdar, M., Ahgababazadeh, R., Mirhabibi, A., Brydson, R., & Pilehvari, S. (2011). Investigation of fe/mgo catalyst support precursors for the chemical vapour deposition growth of carbon nanotubes. *Journal of Nanoscience and Nanotechnology, 11*(6), 5345-5351.

Pan, S.-C., Lin, C.-C., & Tseng, D.-H. (2003). Reusing sewage sludge ash as adsorbent for copper removal from wastewater. *Resources, Conservation and Recycling, 39*(1), 79-90.

Pan, Z., Xie, S., Lu, L., Chang, B., Sun, L., Zhou, W., et al. (1999). Tensile tests of ropes of very long aligned multiwall carbon nanotubes. *Applied Physics Letters, 74*(21), 3152-3154.

Park, Y. S., Kim, T. H., Lee, M. H., & Kwon, S. C. (2002). Study on the effect of ultrasonic waves on the characteristics of electroless nickel deposits from an acid bath. *Surface and Coatings Technology, 153*(2–3), 245-251.

Pehlivan, E., Yanık, B., Ahmetli, G., & Pehlivan, M. (2008). Equilibrium isotherm studies for the uptake of cadmium and lead ions onto sugar beet pulp. *Bioresource Technology, 99*(9), 3520-3527.

Peng, H., Alemany, L. B., Margrave, J. L., & Khabashesku, V. N. (2003). Sidewall carboxylic acid functionalization of single-walled carbon nanotubes. *Journal of the American Chemical Society, 125*(49), 15174-15182.

Peng, X., Luan, Z., Di, Z., Zhang, Z., & Zhu, C. (2005). Carbon nanotubes-iron oxides magnetic composites as adsorbent for removal of pb(ii) and cu(ii) from water. *Carbon, 43*(4), 880-883.

Pérez-Cabero, M., Monzón, A., Rodríguez-Ramos, I., & Guerrero-Ruíz, A. (2004). Syntheses of cnts over several iron-supported catalysts: Influence of the metallic precursors. *Catalysis Today, 93–95*(0), 681-687.

Pimenta, M. A., Jorio, A., Brown, S. D. M., Souza Filho, A. G., Dresselhaus, G., Hafner, J. H., et al. (2001). Diameter dependence of the raman d-band in isolated single-wall carbon nanotubes. *Physical Review B, 64*(4), 041401.

Pinault, M., Mayne-L'Hermite, M., Reynaud, C., Pichot, V., Launois, P., & Ballutaud, D. (2005). Growth of multiwalled carbon nanotubes during the initial stages of aerosol-assisted ccvd. *Carbon, 43*(14), 2968-2976.

Pinheiro, J. P., Schouler, M. C., & Gadelle, P. (2003). Nanotubes and nanofilaments from carbon monoxide disproportionation over co/mgo catalysts: I. Growth versus catalyst state. *Carbon, 41*(15), 2949-2959.

Qian, D., Wagner, G. J., Liu, W. K., Yu, M.-F., & Ruoff, R. S. (2002). Mechanics of carbon nanotubes. *Applied Mechanics Reviews, 55*(6), 495-533.

Qian, W., Liu, T., Wei, F., & Yuan, H. (2003). Quantitative raman characterization of the mixed samples of the single and multi-wall carbon nanotubes. *Carbon, 41*(9), 1851-1854.

Qiu, J., An, Y., Zhao, Z., Li, Y., & Zhou, Y. (2004a). Catalytic synthesis of single-walled carbon nanotubes from coal gas by chemical vapor deposition method. *Fuel processing technology, 85*(8), 913-920.

Qiu, J., An, Y., Zhao, Z., Li, Y., & Zhou, Y. (2004b). Catalytic synthesis of single-walled carbon nanotubes from coal gas by chemical vapor deposition method. *Fuel processing technology, 85*(8–10), 913-920.

Quinton, B. T., Barnes, P. N., Varanasi, C. V., Burke, J., Tsao, B.-H., Yost, K. J., et al. (2013). A comparative study of three different chemical vapor deposition techniques of carbon nanotube growth on diamond films. *Journal of Nanomaterials, 2013*, 9.

Radushkevich, L. V., & Lukyanovich, V. M. (1952). *J. Phys. Chem. Russia, 1*, 88.

Rao, G. P., Lu, C., & Su, F. (2007). Sorption of divalent metal ions from aqueous solution by carbon nanotubes: A review. *Separation and Purification Technology, 58*(1), 224-231.

Rao, K., Mohapatra, M., Anand, S., & Venkateswarlu, P. (2010). Review on cadmium removal from aqueous solutions. *International Journal of Engineering, Science and Technology, 2*(7).

Ren, Z. F., Huang, Z. P., Wang, D. Z., Wen, J. G., Xu, J. W., Wang, J. H., et al. (1999). Growth of a single freestanding multiwall carbon nanotube on each nanonickel dot. *Applied Physics Letters, 75*(8), 1086-1088.

Rinzler, A. G., Liu, J., Dai, H., Nikolaev, P., Huffman, C. B., Rodríguez-Macías, F. J., et al. (1998). Large-scale purification of single-wall carbon nanotubes: Process, product, and characterization. *Applied Physics A, 67*(1), 29-37.

Rohmund, F., Falk, L. K. L., & Campbell, E. E. B. (2000). A simple method for the production of large arrays of aligned carbon nanotubes. *Chemical Physics Letters, 328*(4–6), 369-373.

Ru, C. (2000). Effect of van der waals forces on axial buckling of a double-walled carbon nanotube. *Journal of Applied Physics, 87*(10), 7227-7231.

Ruparelia, J. P., Duttagupta, S. P., Chatterjee, A. K., & Mukherji, S. (2008). Potential of carbon nanomaterials for removal of heavy metals from water. *Desalination, 232*(1–3), 145-156.

Saito, R. (1998). Physical properties of carbon nanotubes (paperback).

Saito, R., & Kataura, H. (2001). Optical properties and raman spectroscopy of carbon nanotubes. In M. Dresselhaus, G. Dresselhaus & P. Avouris (Eds.), *Carbon nanotubes* (Vol. 80, pp. 213-247): Springer Berlin Heidelberg.

Saito, Y., Hamaguchi, K., Nishino, T., Hata, K., Tohji, K., Kasuya, A., et al. (1997). Field emission patterns from single-walled carbon nanotubes. *Jpn. J. Appl. Phys, 36*(10).

Saito, Y., Kawabata, K., & Okuda, M. (1995). Single-layered carbon nanotubes synthesized by catalytic assistance of rare-earths in a carbon arc. *The Journal of Physical Chemistry, 99*(43), 16076-16079.

Saito, Y., Nishikubo, K., Kawabata, K., & Matsumoto, T. (1996). Carbon nanocapsules and single-layered nanotubes produced with platinum-group metals (ru, rh, pd, os, ir, pt) by arc discharge. *Journal of Applied Physics, 80*(5), 3062-3067.

Saito, Y., Okuda, M., Tomita, M., & Hayashi, T. (1995). Extrusion of single-wall carbon nanotubes via formation of small particles condensed near an arc evaporation source. *Chemical Physics Letters, 236*(4–5), 419-426.

Saito, Y., Yoshikawa, T., Bandow, S., Tomita, M., & Hayashi, T. (1993). Interlayer spacings in carbon nanotubes. *Physical Review B, 48*(3), 1907-1909.

Salmani, M. H., Davoodi, M., Ehrampoush, M. H., Ghaneian, M. T., & Fallahzadah, M. H. (2013). Removal of cadmium (ii) from simulated wastewater by ion flotation technique. *Iranian Journal of Environmental Health Science and Engineering, 10*(1), 16.

Santangelo, S., Messina, G., Faggio, G., Lanza, M., Pistone, A., & Milone, C. (2010). Calibration of reaction parameters for the improvement of thermal stability and crystalline quality of multi-walled carbon nanotubes. *Journal of Materials Science, 45*(3), 783-792.

Satio, Y. O., M., Fujimoto, N. Yoshikawa,T. Tomita,M, Hayashi,T.J. (1994). Single-wall carbon nanotubes growing radially from ni fine particles formed by arc evaporation. *J. Appl. Phys, 33*, L526-L529.

Satishkumar, B., Thomas, P. J., Govindaraj, A., & Rao, C. (2000). Y-junction carbon nanotubes. *Applied Physics Letters, 77*(16), 2530-2532.

Satishkumar, B. C., Govindaraj, A., & Rao, C. N. R. (1999). Bundles of aligned carbon nanotubes obtained by the pyrolysis of ferrocene–hydrocarbon mixtures: Role of the metal nanoparticles produced in situ. *Chemical Physics Letters, 307*(3–4), 158-162.

Satishkumar, B. C., Govindaraj, A., Sen, R., & Rao, C. N. R. (1998). Single-walled nanotubes by the pyrolysis of acetylene-organometallic mixtures. *Chemical Physics Letters, 293*(1–2), 47-52.

Schadler, L., Giannaris, S., & Ajayan, P. (1998). Load transfer in carbon nanotube epoxy composites. *Applied Physics Letters, 73*, 3842.

Schujman, S., Vajtai, R., Biswas, S., Dewhirst, B., Schowalter, L., & Ajayan, P. (2002). Electrical behavior of isolated multiwall carbon nanotubes characterized by scanning surface potential microscopy. *Applied Physics Letters, 81*(3), 541-543.

Sen, R., Govindaraj, A., & Rao, C. N. R. (1997). Carbon nanotubes by the metallocene route. *Chemical Physics Letters, 267*(3–4), 276-280.

Seraphin, S., & Zhou, D. (1994). Single-walled carbon nanotubes produced at high yield by mixed catalysts. *Applied Physics Letters, 64*(16), 2087-2089.

Seraphin, S., Zhou, D., Jiao, J., Minke, M. A., Wang, S., Yadav, T., et al. (1994). Catalytic role of nickel, palladium, and platinum in the formation of carbon nanoclusters. *Chemical Physics Letters, 217*(3), 191-195.

Seraphin, S., Zhou, D., Jiao, J., Withers, J. C., & Loutfy, R. (1993). Effect of processing conditions on the morphology and yield of carbon nanotubes. *Carbon, 31*(5), 685-689.

Shi, Z., Lian, Y., Liao, F. H., Zhou, X., Gu, Z., Zhang, Y., et al. (2000). Large scale synthesis of single-wall carbon nanotubes by arc-discharge method. *Journal of Physics and Chemistry of Solids, 61*(7), 1031-1036.

Shi, Z., Zhou, X., Jin, Z., Gu, Z., Wang, J., Feng, S., et al. (1996). High yield synthesis and growth mechanism of carbon nanotubes. *Solid State Communications, 97*(5), 371-375.

Shirazi, Y., Tofighy, M. A., Mohammadi, T., & Pak, A. (2011). Effects of different carbon precursors on synthesis of multiwall carbon nanotubes: Purification and functionalization. *Applied Surface Science, 257*(16), 7359-7367.

Shukla, B., Saito, T., Ohmori, S., Koshi, M., Yumura, M., & Iijima, S. (2010). Interdependency of gas phase intermediates and chemical vapor deposition growth of single wall carbon nanotubes. *Chemistry of Materials, 22*(22), 6035-6043.

Sing, K. S. W., Everett, D. H., Haul, R. A. W., Moscou, L., Pierotti, R. A., Rouquerol, J., et al. (1985). *Pure and Applied Chemistry, 57*, 603-V.

Singh, C., Shaffer, M. S. P., & Windle, A. H. (2003). Production of controlled architectures of aligned carbon nanotubes by an injection chemical vapour deposition method. *Carbon, 41*(2), 359-368.

Sinha, A. K., Hwang, D. W., & Hwang, L.-P. (2000). A novel approach to bulk synthesis of carbon nanotubes filled with metal by a catalytic chemical vapor deposition method. *Chemical Physics Letters, 332*(5–6), 455-460.

Sinha, N., & Yeow, J. T. W. (2005). Carbon nanotubes for biomedical applications. *NanoBioscience, IEEE Transactions on, 4*(2), 180-195.

Sinnott, S. B., Andrews, R., Qian, D., Rao, A. M., Mao, Z., Dickey, E. C., et al. (1999). Model of carbon nanotube growth through chemical vapor deposition. *Chemical Physics Letters, 315*(1–2), 25-30.

Smith, B. C. (1998). *Infrared spectral interpretation: A systematic approach*: CRC press.

Srivastava, D., Wei, C., & Cho, K. (2003). Nanomechanics of carbon nanotubes and composites. *Applied Mechanics Reviews, 56*(2), 215-230.

Stafiej, A., & Pyrzynska, K. (2007). Adsorption of heavy metal ions with carbon nanotubes. *Separation and Purification Technology, 58*(1), 49-52.

Stevens, J. L., Huang, A. Y., Peng, H., Chiang, I. W., Khabashesku, V. N., & Margrave, J. L. (2003). Sidewall amino-functionalization of single-walled carbon nanotubes through fluorination and subsequent reactions with terminal diamines. *Nano Letters, 3*(3), 331-336.

Strano, M. S., Doorn, S. K., Haroz, E. H., Kittrell, C., Hauge, R. H., & Smalley, R. E. (2003). Assignment of (n, m) raman and optical features of metallic single-walled carbon nanotubes. *Nano Letters, 3*(8), 1091-1096.

Su, M., Zheng, B., & Liu, J. (2000). A scalable cvd method for the synthesis of single-walled carbon nanotubes with high catalyst productivity. *Chemical Physics Letters, 322*(5), 321-326.

Takizawa, M., Bandow, S., Torii, T., & Iijima, S. (1999). Effect of environment temperature for synthesizing single-wall carbon nanotubes by arc vaporization method. *Chemical Physics Letters, 302*(1–2), 146-150.

Taniguchi, M., Nagao, H., Hiramatsu, M., Ando, Y., & Hori, M. (2005). Preparation of dense carbon nanotube film using microwave plasma-enhanced chemical vapor deposition. *Diamond and Related Materials, 14*(3), 855-858.

Tans, S. J., Devoret, M. H., Dai, H., Thess, A., Smalley, R. E., Geerligs, L., et al. (1997). Individual single-wall carbon nanotubes as quantum wires. *Nature, 386*(6624), 474-477.

Tapasztó, L., Kertész, K., Vértesy, Z., Horváth, Z. E., Koós, A. A., Osváth, Z., et al. (2005). Diameter and morphology dependence on experimental conditions of carbon nanotube arrays grown by spray pyrolysis. *Carbon, 43*(5), 970-977.

Tatsuki, H., Tomoju, K., & Junichi, K. (2003). Selective synthesis of double-wall carbon nanotubes by ccvd of acetylene using zeolite supports. *Chemical Physics Letters, 382*, 679-685.

Tehrani, M. S., Azar, P.A.,Namin,P.E.,Dehagi,S.M. (2014). Removal of lead ions from aqueous solution using multiwalled carbon nanotubes:The effect of functionalization. *J. Appl. Environ. Biol. Sci., 4(2)*, 316-326.

Teng, I.-J., Hsu, H.-L., Jian, S.-R., Wang, L.-C., Chen, K.-L., Kuo, C.-T., et al. (2013). Temperature-dependent electrical and photo-sensing properties of horizontally-oriented carbon nanotube networks synthesized by sandwich-growth microwave plasma chemical vapor deposition. *Thin Solid Films, 529*, 190-194.

Teo, K. B., Singh, C., Chhowalla, M., & Milne, W. I. (2003). Catalytic synthesis of carbon nanotubes and nanofibers. *Encyclopedia of nanoscience and nanotechnology, 10*(1).

Terrones, M. (2003). Science and technology of the twenty-first century: Synthesis, properties, and applications of carbon nanotubes. *Annual Review of Materials Research, 33*(1), 419-501.

Thess, A., Lee, R., Nikolaev, P., Dai, H., Petit, P., Robert, J., et al. (1996). Crystalline ropes of metallic carbon nanotubes. *Science, 273*(5274), 483-487.

Tofighy, M. A., & Mohammadi, T. (2011). Adsorption of divalent heavy metal ions from water using carbon nanotube sheets. *Journal of Hazardous Materials, 185*(1), 140-147.

Tomie, T., Inoue, S., Kohno, M., & Matsumura, Y. (2010). Prospective growth region for chemical vapor deposition synthesis of carbon nanotube on c–h–o ternary diagram. *Diamond and Related Materials, 19*(11), 1401-1404.

Tsai, W., Chang, C., Lin, M., Chien, S., Sun, H., & Hsieh, M. (2001). Adsorption of acid dye onto activated carbons prepared from agricultural waste bagasse by zncl< sub> 2</sub> activation. *Chemosphere, 45*(1), 51-58.

Tumin, N. D., Chuah, A. L., Zawani, Z., & Rashid, S. A. (2008). Adsorption of copper from aqueous solution by elais guineensis kernel activated carbon. *Journal of Engineering Science and Technology, 3*(2), 180-189.

Vajtai, R., Wei, B., Zhang, Z., Jung, Y., Ramanath, G., & Ajayan, P. (2002). Building carbon nanotubes and their smart architectures. *Smart Materials and Structures, 11*(5), 691.

Vázquez, E., & Prato, M. (2009). Carbon nanotubes and microwaves: Interactions, responses, and applications. *ACS Nano, 3*(12), 3819-3824.

Veziri, C. M., Pilatos, G., Karanikolos, G. N., Labropoulos, A., Kordatos, K., Kasselouri-Rigopoulou, V., et al. (2008). Growth and optimization of carbon nanotubes in activated carbon by catalytic chemical vapor deposition. *Microporous and Mesoporous Materials, 110*(1), 41-50.

Vilar, V. J., Botelho, C., & Boaventura, R. A. (2006). Equilibrium and kinetic modelling of cd (ii) biosorption by algae< i> gelidium</i> and agar extraction algal waste. *Water Research, 40*(2), 291-302.

Vivas-Castro, J., Rueda-Morales, G., Ortega-Cervantez, G., Moreno-Ruiz, L., Ortega-Aviles, M., & Ortiz-Lopez, J. (2011). Synthesis of carbon nanostructures by microwave irradiation.

Vuković, G. D., Marinković, A. D., Čolić, M., Ristić, M. Đ., Aleksić, R., Perić-Grujić, A. A., et al. (2010). Removal of cadmium from aqueous solutions by oxidized and ethylenediamine-functionalized multi-walled carbon nanotubes. *Chemical Engineering Journal, 157*(1), 238-248.

Wagner, H. D., Lourie, O., Feldman, Y., & Tenne, R. (1998). Stress-induced fragmentation of multiwall carbon nanotubes in a polymer matrix. *Applied Physics Letters, 72*(2), 188-190.

Wang, H., Zhou, A., Peng, F., Yu, H., & Yang, J. (2007). Mechanism study on adsorption of acidified multiwalled carbon nanotubes to pb(ii). *Journal of Colloid and Interface Science, 316*(2), 277-283.

Wang, H. J., Zhou, A. L., Peng, F., Yu, H., & Chen, L. F. (2007). Adsorption characteristic of acidified carbon nanotubes for heavy metal pb(ii) in aqueous solution. [Article]. *Materials Science and Engineering a-Structural Materials Properties Microstructure and Processing, 466*(1-2), 201-206.

Wang, S.-G., Gong, W.-X., Liu, X.-W., Yao, Y.-W., Gao, B.-Y., & Yue, Q.-Y. (2007). Removal of lead(ii) from aqueous solution by adsorption onto manganese oxide-coated carbon nanotubes. *Separation and Purification Technology, 58*(1), 17-23.

Wang, S., Zhu, W., Liao, D., Ng, C., & Au, C. (2004). In situ ftir studies of no reduction over carbon nanotubes (cnts) and 1wt.% pd/cnts. *Catalysis Today, 93*, 711-714.

Wang, X., Chen, C., Hu, W., Ding, A., Xu, D., & Zhou, X. (2005). Sorption of 243am(iii) to multiwall carbon nanotubes. *Environmental Science & Technology, 39*(8), 2856-2860.

Wang, X., Hu, Z., Chen, X., & Chen, Y. (2001). Preparation of carbon nanotubes and nano-particles by microwave plasma-enhanced chemical vapor deposition. *Scripta Materialia, 44*(8–9), 1567-1570.

Wei, B. Q., Vajtai, R., Jung, Y., Ward, J., Zhang, R., Ramanath, G., et al. (2002). Microfabrication technology: Organized assembly of carbon nanotubes. [10.1038/416495a]. *Nature, 416*(6880), 495-496.

Weng, C.-H., & Huang, C. (2004). Adsorption characteristics of zn (ii) from dilute aqueous solution by fly ash. *Colloids and Surfaces A: Physicochemical and Engineering Aspects, 247*(1), 137-143.

Wiles, P. G., & Abrahamson, J. (1978). Carbon fibre layers on arc electrodes—i: Their properties and cool-down behaviour. *Carbon, 16*(5), 341-349.

Willems, I., Konya, Z., Colomer, J.-F., Van Tendeloo, G., Nagaraju, N., Fonseca, A., et al. (2000). Control of the outer diameter of thin carbon nanotubes synthesized by catalytic decomposition of hydrocarbons. *Chemical Physics Letters, 317*(1), 71-76.

Willems, I., Kónya, Z., Colomer, J. F., Van Tendeloo, G., Nagaraju, N., Fonseca, A., et al. (2000). Control of the outer diameter of thin carbon nanotubes synthesized by catalytic decomposition of hydrocarbons. *Chemical Physics Letters, 317*(1–2), 71-76.

Wirojanagud, W., Tantemsapya, N., & Tantriratna, P. (2004). Precipitation of heavy metals by lime mud waste of pulp and paper mill. *Songklanakarin J. Sci. Technol, 26*, 45-53.

Wójtowicz, A., & Stoklosa, A. (2002). Removal of heavy metal ions on smectite ion-exchange column. *Polish Journal of Environmental Studies, 11*(1), 97-101.

Wu, C.-H. (2007). Studies of the equilibrium and thermodynamics of the adsorption of cu2+ onto as-produced and modified carbon nanotubes. *Journal of Colloid and Interface Science, 311*(2), 338-346.

Xu, D., Tan, X., Chen, C., & Wang, X. (2008). Removal of pb(ii) from aqueous solution by oxidized multiwalled carbon nanotubes. *Journal of Hazardous Materials, 154*(1–3), 407-416.

Xu, Y.-j., Rosa, A., Liu, X., & Su, D.-s. (2011). Characterization and use of functionalized carbon nanotubes for the adsorption of heavy metal anions. *New Carbon Materials, 26*(1), 57-62.

Xu, Z.-X., Lin, J.-D., Roy, V. A. L., Ou, Y., & Liao, D.-W. (2005). Catalytic synthesis of carbon nanotubes and carbon spheres using kaolin supported catalyst. *Materials Science and Engineering: B, 123*(2), 102-106.

Y. Maniwa, R. F., H. Kira, H. Tou, E. Nishibori, M. Takata, M. Sakata, A. Fujiwara, X. Zhao, S. Iijima, Y. Ando. (2001). Multiwalled carbon nanotubes grown in hydrogen atmosphere: An x-ray diffraction study. *Phys. Rev. B, 64*, 0731051-0731054.

Yang, S., Li, J., Shao, D., Hu, J., & Wang, X. (2009). Adsorption of ni(ii) on oxidized multi-walled carbon nanotubes: Effect of contact time, ph, foreign ions and paa. *Journal of Hazardous Materials, 166*(1), 109-116.

Yang, Z., Zhang, Q., Luo, G., Huang, J.-Q., Zhao, M.-Q., & Wei, F. (2010). Coupled process of plastics pyrolysis and chemical vapor deposition for controllable synthesis of vertically aligned carbon nanotube arrays. *Applied Physics A, 100*(2), 533-540.

Ye, H., & Yu, Z. (2010). Adsorption of pb (ii) onto modified rice bran. *Analysis, 5*, 10.

Yin, Q., Chen, Q., Sun, M., & Wang, L. (2012). Spectrophotometric determination of zinc using carboxylic carbon nanotubes. *International Journal of Electrochemical Science, 7*(12).

Yong, Z., Fang, L., & Zhi-hua, Z. (2011). Synthesis of heterostructured helical carbon nanotubes by iron-catalyzed ethanol decomposition. *Micron, 42*(6), 547-552.

Yudasaka, M., Ichihashi, T., Komatsu, T., & Iijima, S. (1999). Single-wall carbon nanotubes formed by a single laser-beam pulse. *Chemical Physics Letters, 299*(1), 91-96.

Yudasaka, M., Kikuchi, R., Matsui, T., Ohki, Y., Yoshimura, S., & Ota, E. (1995). Specific conditions for ni catalyzed carbon nanotube growth by chemical vapor deposition. *Applied Physics Letters, 67*(17), 2477-2479.

Yudasaka, M., Kokai, F., Takahashi, K., Yamada, R., Sensui, N., Ichihashi, T., et al. (1999). Formation of single-wall carbon nanotubes: Comparison of co2 laser ablation and nd:Yag laser ablation. *The Journal of Physical Chemistry B, 103*(18), 3576-3581.

Yudasaka, M., Komatsu, T., Ichihashi, T., & Iijima, S. (1997). Single-wall carbon nanotube formation by laser ablation using double-targets of carbon and metal. *Chemical Physics Letters, 278*(1–3), 102-106.

Yudasaka, M., Sensui, N., Takizawa, M., Bandow, S., Ichihashi, T., & Iijima, S. (1999). Formation of single-wall carbon nanotubes catalyzed by ni separating from y in laser ablation or in arc discharge using a c target containing a niy catalyst. *Chemical Physics Letters, 312*(2–4), 155-160.

Zajíčková, L., Jašek, O., Synek, P., Eliáš, M., Kudrle, V., Kadlečíková, M., et al. (2009). Synthesis of carbon nanotubes in mw plasma torch with different methods of catalyst layer preparation and their applications: Nanocon.

Zeng, X., Fu, D., Sheng, H., Xie, S., Li, X., Hu, Q., et al. (2010). Growth and morphology of carbon nanostructures by microwave-assisted pyrolysis of methane. *Physica E: Low-dimensional Systems and Nanostructures, 42*(8), 2103-2108.

Zeng, X., Sun, X., Cheng, G., Yan, X., & Xu, X. (2002). Production of multi-wall carbon nanotubes on a large scale. *Physica B: Condensed Matter, 323*(1–4), 330-332.

Zhang, H., Guo, H., Deng, X., Gu, P., Chen, Z., & Jiao, Z. (2010). Functionalization of multi-walled carbon nanotubes via surface unpaired electrons. *Nanotechnology, 21*(8), 085706.

Zhao, X., Ando, Y., Qin, L. C., Kataura, H., Maniwa, Y., & Saito, R. (2002). Characteristic raman spectra of multiwalled carbon nanotubes. *Physica B: Condensed Matter, 323*(1–4), 265-266.

Zheng, B., Li, Y., & Liu, J. (2002). Cvd synthesis and purification of single-walled carbon nanotubes on aerogel-supported catalyst. *Applied Physics A, 74*(3), 345-348.

Zheng, L. X., O'Connell, M. J., Doorn, S. K., Liao, X. Z., Zhao, Y. H., Akhadov, E. A., et al. (2004). Ultralong single-wall carbon nanotubes. [10.1038/nmat1216]. *Nat Mater, 3*(10), 673-676.

Zhou, D., Seraphin, S., & Wang, S. (1994). Single-walled carbon nanotubes growing radially from yc2 particles. *Applied Physics Letters, 65*(12), 1593-1595.

Zhu, S., Su, C.-H., Lehoczky, S. L., Muntele, I., & Ila, D. (2003). Carbon nanotube growth on carbon fibers. *Diamond and Related Materials*, *12*(10–11), 1825-1828.

APPENDICES

APPENDIX A

Table A1: Experimental array of CNTs production via microwave heating

Microwave power W,(A)	Radiation time min, (B)	Gas Ratio (C_2H_2/H_2) (C)	Weight of CNTs, gram
600	35	0.6	0.48
600	60	0.2	0.3
1200	60	0.2	1.75
600	10	1	0.08
900	35	1	3.5
600	10	0.2	0.25
1200	10	1	0.23
900	35	0.2	3.8
1200	10	0.2	1
900	60	0.6	4.5
600	60	1	0.58
1200	60	1	0.9
600	10	1	0.38
900	35	0.6	5.8
1200	10	0.2	0.85
1200	60	0.2	0.42
600	60	1	0.2
1200	35	0.6	4.6
1200	60	1	1.15
600	60	0.2	0.5
900	35	0.6	5.56
1200	10	1	0.35
600	10	0.2	0.48
900	10	0.6	4.2

APPENDIX B

Table B1: Experimental array of Pb (II) removal using MWCNTs

pH (A)	Agitation speed rpm, (B)	MWCNTs dosage g, (C)	Adsorption time min, (D)	C_t (mg/L)	Removal of Pb (II) %	q_t (mg/g)
4	200	0.15	5	4.5	55	13.75
4	200	0.05	40	5.2	48	12
5	160	0.1	22.5	0.01	99.9	24.97
6	120	0.15	5	5.5	45	11.25
6	200	0.15	5	4.2	58	14.5
6	120	0.05	5	4.5	55	13.75
5	200	0.1	22.5	1.16	88.4	22.1
4	160	0.1	22.5	1.7	83	20.75
5	160	0.05	22.5	0.7	93	23.25
5	160	0.1	40	1	90	22.5
4	120	0.15	40	5.07	49.3	12.32
4	120	0.05	40	4.2	58	14.5
4	120	0.05	5	4.9	51	12.75
6	160	0.1	22.5	1.6	84	21
4	120	0.15	5	4.5	55	13.75
6	120	0.15	40	4.1	59	14.75
4	200	0.05	5	3.8	62	15.5
5	160	0.1	5	1	90	22.5
6	120	0.05	40	3.8	62	15.5
6	200	0.05	40	4.7	53	13.25
5	160	0.15	22.5	0.4	96	24
6	200	0.15	40	3.8	62	15.5
5	120	0.1	22.5	0.1	99	24.75
5	160	0.1	22.5	0.5	95	23.75
6	200	0.05	5	4.3	57	14.25
4	200	0.15	40	3.5	65	16.25

MWCNTs dose= 0.1 gram, Initial Pb (II) aqueous solution C_o=10 mg/L, Temperature= 26± 1 ^oC

% removal= $[(C_o-C_t)/C_o]x100$
Adsorption of Pb (II) mg/L= C_o-C_t
Adsorption capacity at time t (qt) in mg/g= $[(C_o-C_t)/M]xV$
V-volume of Pb (II) aqueous solution= 0.25L
M-mass of MWCNTs dosage= 0.1 gram

APPENDIX C

Table C1: Experimental array of Cd (II) removal using MWCNTs

pH (A)	Agitation speed rpm, (B)	MWCNTs dosage g, (C)	Adsorption time min, (D)	C_t (mg/L)	Removal of Cd (II) %	q_t (mg/g)
6	160	0.1	50	1.37	86.3	21.575
5	160	0.1	50	0.2	98	24.5
6	200	0.05	20	5	50	12.5
4	200	0.15	20	5	50	12.5
6	120	0.05	80	4.7	53	13.25
5	160	0.1	80	1.1	89	22.25
6	200	0.15	20	4.5	55	13.75
5	160	0.1	20	1.5	85	21.25
5	120	0.1	50	1.9	81	20.25
4	200	0.05	20	4.2	58	14.5
6	200	0.05	80	4	60	15
4	120	0.05	20	3.8	62	15.5
5	160	0.1	50	0.1	99	24.75
4	120	0.15	80	4.7	53	13.25
5	200	0.1	50	1.4	86	21.5
6	120	0.05	20	3.4	66	16.5
5	160	0.15	50	0.8	92	23
4	120	0.15	20	4.27	57.3	14.325
4	200	0.05	80	3.7	63	15.75
6	120	0.15	20	4.1	59	14.75
4	160	0.1	50	1.5	85	21.25
4	200	0.15	80	4.1	59	14.75
6	120	0.15	80	2.7	73	18.25
4	120	0.05	80	3.6	64	16
5	160	0.05	50	1.3	87	21.75
6	200	0.15	80	4	60	15

MWCNTs dose= 0.1 gram, Initial Cd (II) aqueous solution C_o=10 mg/L, Temperature= 26± 1 ^oC.

% removal= $[(C_o-C_t)/C_o]x100$
Adsorption of Cd (II) mg/L= C_o-C_t
Adsorption capacity at time t (qt) in mg/g= $[(C_o-C_t)/M]xV$
V-volume of Cd (II) aqueous solution= 0.25L
M-mass of MWCNTs dosage= 0.1 gram

APPENDIX D

Table D1: Experimental array of Cu (II) removal using MWCNTs

pH (A)	Agitation speed rpm, (B)	MWCNTs dosage g, (C)	Adsorption time min, (D)	C_t (mg/L)	Removal of Cu (II) %	q_t (mg/g)
8	120	0.05	10	6.6	34	8.5
8	200	0.15	10	5.5	45	11.25
5	160	0.15	35	0.8	92	23
2	120	0.05	60	7.15	28.5	7.125
5	160	0.1	60	1.98	80.2	20.05
5	160	0.1	35	0.4	96	24
5	120	0.1	35	0.6	94	23.5
2	120	0.15	10	7	30	7.5
8	120	0.15	60	6	40	10
2	120	0.05	10	6.8	32	8
2	200	0.15	60	6.3	37	9.25
2	200	0.15	10	6.5	35	8.75
8	120	0.15	10	6.7	33	8.25
5	160	0.1	35	0.46	95.4	23.85
2	200	0.05	10	7	30	7.5
8	200	0.15	60	4.8	52	13
2	200	0.05	60	7.1	29	7.25
8	200	0.05	60	5	50	12.5
2	120	0.15	60	6.8	32	8
8	120	0.05	60	5.1	49	12.25
5	160	0.1	10	1.55	84.5	21.125
2	160	0.1	35	5.8	42	10.5
5	160	0.05	35	1.99	80.1	20.025
5	200	0.1	35	2.5	75	18.75
8	160	0.1	35	0.2	98	24.5
8	200	0.05	10	5.7	43	10.75

MWCNTs dose= 0.1 gram, Initial Cu (II) aqueous solution Co=10 mg/L, Temperature= 26± 1 ^{o}C.

% removal= [(Co-Ct)/Co]x100
Adsorption of Cu (II) mg/L= Co-Ct
Adsorption capacity at time t (qt) in mg/g= [(Co-Ct)/M]xV
V-volume of Cu (II) aqueous solution= 0.25L
M-mass of MWCNTs dosage= 0.1 gram

APPENDIX E

Table E1: Experimental array of Zn (II) removal using MWCNTs

pH (A)	Agitation speed rpm, (B)	MWCNTs dosage g, (C)	Adsorption time min, (D)	C_t (mg/L)	Removal of Zn (II) %	q_t (mg/g)
8	200	0.15	110	6.5	35	17.5
12	200	0.15	110	5.97	40.3	20.15
12	160	0.1	60	1.3	87	43.5
12	120	0.05	110	7.1	29	14.5
10	160	0.1	10	0.15	98.5	49.25
8	120	0.15	10	6.155	38.45	19.225
8	200	0.05	110	5.8	42	21
8	120	0.05	110	6.5	35	17.5
8	200	0.15	10	6	40	20
10	200	0.1	60	0.15	98.5	49.25
12	200	0.05	110	7	30	15
8	120	0.05	10	4.855	51.45	25.725
8	200	0.05	10	5.5	45	22.5
10	160	0.05	60	0.1	99.0	49.5
8	120	0.15	110	5.7	43	21.5
8	160	0.1	60	1	90	45
12	200	0.05	10	6.5	35	17.5
12	120	0.15	10	5.8	42	21
10	160	0.15	60	0.17	98.3	49.15
12	200	0.15	10	7.1	29	14.5
12	120	0.15	110	5.96	40.4	20.2
10	160	0.1	60	0.14	98.6	49.3
12	120	0.05	10	7.17	28.3	14.15
10	160	0.1	110	0.16	98.4	49.2
10	120	0.05	60	0.08	99.2	49.6
10	160	0.1	60	0.13	98.7	49.35

MWCNTs dose= 0.05 gram, Initial Zn (II) aqueous solution Co=10 mg/L, Temperature= 26± 1 ^{o}C.

% removal= [(Co-Ct)/Co]x100
Adsorption of Zn (II) mg/L= Co-Ct
Adsorption capacity at time t (qt) in mg/g= [(Co-Ct)/M]xV
V-volume of Zn (II) aqueous solution= 0.25L
M-mass of MWCNTs dosage= 0.05 gram

APPENDIX F

Design Expert Soft were overview

Design –Expert software version 6.08 was used in this research study to develop, optimize and statically analyses the experimental data. It provides highly efficient design of experiment (DOE). Design-expert program offers rotatable 3D plot for visualization of response surfaces.

Central composite model is used to identify the vital factors that affect the process of product. CCD model was used for determination of CNTs production run. It was also used to analyses the adsorption of heavy metals to CNTs sample prepared as a response for view to select best quality of CNT sample.

A response surface method (RSM) designs is used to find the ideal process settings to achieve optimal performance. It helps to quantify the relationship between one or more measured responses and the vital input factor.

Definitions for each statistic in the analysis of variance (ANOVA) are summarized as follows.

Sum of squares: Total of the sum of squares for the terms in the model, as reported in the effects list for factorial and on the model screen.

DF: Degrees of freedom for the model: It is the number of model terms, including the intercept, minus one.

Std Dev: (Root MSE) square root of the residual mean square. Considered this to be an estimate of the standard deviation with the experiment.

Mean Square: Estimate of the model variance, calculated by the model sum of squares divided by model degrees of freedom.

F Value: Test for comparing model variance with residual (error) variance. If the variance are close to the same, the ratio will be close to one and it is less likely that any of the factors have a significant effect on the response.

Prob > F: Probability of seeing the observed F value if the null hypothesis is true (there is no factor effect). Small probability values call for rejection of the null hypothesis. The probability equals the proportion of the area under the curve of the F – distribution that lies beyond the observed F value. The F distribution itself is determined by the degrees of freedom associated with the variances being compared.

Residual: consists of terms used to estimate experimental error (for 2-level factorials, the insignificant factors and interactions that fall on the normal probability line on the effect plot).

Lack of fit: This is the variation of the data around the fitted model. If the model does not fit the data well, this will be significant.

Pure Error: Amount of variation in the response in replicated design points.

Cor Total: Totals of all information corrected for the mean.

Curvature: (2 –level Factorials only) compares the average response of the factorial points to test for non-linearity between the factorial points.

Adj R-Squared; A measure of the amount of variation around the mean explained by the model, adjusted for the number of terms in the model. The adjusted R-squared decrease as the number of terms in the model increases if those additional terms don't add value to the model.

Pred R-Squared: A measure of the amount of variation in new data explained by the model.

Adequate Precision: This is a signal to noise ratio. It compares the range of the predicted values at the design points to the average prediction error. Ratios greater than 4 indicates adequate model discrimination

APPENDIX G

List of Achievements

List of publications

i. N.M. Mubarak, J.N. Sahu, E.C. Abdullah,N.S.Jayakumar. Removal of Heavy Metals from Wastewater Using Carbon Nanotubes. Separation &purification review. 43:311–338, (2014): ISI: Q1; IF: 3.154. (ISI-Cited Publication).

ii. N.M. Mubarak, E.C. Abdullah, N. S. Jayakumar, J.N. Sahu. An overview on methods for the production of carbon nanotubes. Journal of Industrial and Engineering Chemistry. 20(4):1186-1197, (2014): ISI: Q1; IF: 2.145. (ISI-Cited Publication).

iii. N.M. Mubarak, J.N. Sahu, E.C. Abdullah, N.S. Jayakumar, P. Ganesan. Novel microwave-assisted multiwall carbon nanotubes enhancing Cu (II) adsorption capacity in water .Journal of the Taiwan Institute of Chemical Engineers. Accepted on 8th February, 2015 ISI:Q1;IF 2.637. (ISI-Cited Publication)

iv. N.M. Mubarak, J.N. Sahu, E.C. Abdullah,N.S.Jayakumar, P. Ganesan. Single stage production of carbon nanotubes using microwave technology, Diamond & Related Materials. 48,52-59, (2014): ISI:Q2; IF: 1.740. (ISI-Cited Publication).

v. N.M. Mubarak, J.N. Sahu, E.C. Abdullah, N.S. Jayakumar, P. Ganesan. Microwave assisted multiwall carbon nanotubes enhancing Cd (II)

adsorption capacity in aqueous media. Journal of Industrial and Engineering Chemistry. In Press (2014): ISI: Q1; IF: 2.063. (ISI-Cited Publication).

vi. N.M. Mubarak, J.N. Sahu, E.C. Abdullah, N.S. Jayakumar, P. Ganesan. Thermodynamic and isotherm study for enhancement on Zn (II) removal from aqueous solution using Microwave assisted synthesis of multiwall carbon nanotubes. Clean soil-Air, water – provisionally accepted on 1 October (2014) -3rd Revision submitted. ISI:Q1:IF; 1.838.(ISI-Cited Publication).

vii. N.M. Mubarak, J.R.Wong, K.W.Tan, J.N. Sahu, E.C. Abdullah, N.S. Jayakumar, P. Ganesan. Immobilization of cellulase enzyme on functionalized multiwall carbon nanotubes. Journal of Molecular Catalysis B: Enzymatic, 107, 124-131,(2014): ISI:Q2; IF: 2.823. (ISI-Cited Publication).

viii. N.M Mubarak,R.K. Thines, N.R. Sajuni, E.C. Abdullah, J.N. Sahu , P. Ganesan , N.S.Jayakumar. Adsorption of chromium (VI) on functionalized and non-functionalized carbon nanotubes. Korean Journal of Chemical Engineering. 31(9),1582-1591 (2014): ISI: Q3; IF: 1.059. (ISI-Cited Publication

ix. R.K. Thines, N.M Mubarak, M.Ruthiraan, E.C. Abdullah, J.N.Sahu, N.S.Jayakumar,P. Ganesan , N.R.Sajuni. Adsorption isotherm and thermodynamics studies of Zn (II) on functionalized and non – functionalized carbon nanotubes. Advanced Science, Engineering and Medicine. 6(9), 974-984 (2014).(Scopous Cited Publication)

x. N.M. Mubarak, E.C. Abdullah, J.N. Sahu, N.S.Jayakumar, P. Ganesan. Mass Production of Carbon Nanofibers Using Microwave Technology. Journal of nanoscience and nanotechnology. In Press ISI:Q3 : IF: 1.339 (ISI-Cited publication) .

xi. M. Ruthiraan, N.M. Mubarak, R.K. Thines, E.C. Abdullah, J.N. Sahu, N.S.Jayakumar,P.Ganesan. Comparative kinetic study of functionalized carbon nanotubes and magnetic biochar for removal of Cd^{2+} ions from waste water. Korean J. Chem. Eng. 32(3), 446-457 (2015) . ISI: Q3; IF: 1.241. (ISI-Cited Publication).

xii. N.M. Mubarak, J.N. Sahu, E.C. Abdullah, N.S. Jayakumar, N.R. Sajuni, J. Tan. Adsorption and kinetic study on Sn^{2+} removal using modified carbon nanotube and magnetic biochar.International journal of nanoscience, 12(6),1350044-14, (2013), World Scientific Publisher.

xiii. N.M. Mubarak, S. Daniel, M. Khalid, and J.Tan. Comparative study of functionalize and non-functionalized carbon nanotube for Removal of Copper from polluted water. International Journal of Chemical and Environmental Engineering (IJCEE). 3(5), 314-317, (2012).

xiv. N.M Mubarak, R.F Alicia, E.C.Abdullah, J.N.Sahu, A.B Ayu Haslija , J.Tan. Statistical optimization and kinetic studies on removal of Zn2+ using functionalized carbon nanotubes and magnetic biochar. Journal of Environmental Chemical Engineering, 1(3) 486–495,(2013) (Scopus cited publication).

Paper under review

i. Rapid adsorptive removal of toxic Pb (II) ions from aqueous solution using microwave assisted multiwall carbon nanotubes. Chemical Engineering Research and Design- Revision submitted..

ii. Optimization of carbon nanofibers production using microwave assisted chemical vapour deposition. Journal of cleaner production – Under review.

iii. Optimization of multiwall carbon nanotubes synthesis by tubular microwave chemical vapour deposition technique. Arbian journal of chemistry- Under review.

iv. Comparative kinetic study on removal of zinc and copper using carbon nanofibers synthesized via microwave technology. Arabian Journal of chemistry- Under Review .

v. Application potential of carbon nanomaterials in water and wastewater treatment: a review. Chemosphere- Under review.

Conference presentation

i. N.M Mubarak,N. Sazila, Sahu J.N,Abdullah E.C, N.R. Sajuni,J.Tan, Comparative Study on phenol removal from aqueous solution by using carbon nanotubes and magnetic biochar. 27th Regional conference on solid state science & technology (RCSSST27) 20-22 December 2013, Kota Kinabalu, Sabah,Malayasia.

ii. N.M. Mubarak, S. Daniel, M. Khalid, J. Tan , M Khalid Comparative study of functionalize and no functionalized carbon nanotubes for removal of

copper from polluted water . International conference on chemical and biological processes-ICCBP 21-23 June 2012, Kuala Lumpur, Malaysia.

Book Chapter

i. N.M. Mubarak, J.N. Sahu, E.C. Abdullah, N. S. Jayakumar, P. Ganesan, Chemical Functionalization of Carbon Nanomaterials: Chemistry and Applications" Book chapter 4 “Overview on functionalization of carbon nanotubes” Page 83-101. Taylors and Francis Publisher USA. In Press 2015

Patent

i. Production of nanostructured materials using microwave heating, J.N. Sahu, N.M. Mubarak, E.C. Abdullah. Malaysia Patent File number: **PI 2013 701556**

Exhibitions

i. Malaysia Technology Expo (MTE-2014) 20-22 February Won **Gold Medal** for the poster title” Mass production of carbon nanotubes using microwave technology”

ii. Malaysia Technology Expo (MTE-2014) 20-22 February Won **Best Award** for the poster title” Mass production of carbon nanotubes using microwave technology.

iii. International Engineering invention &innovation exhibition (I-ENVEX 2014) 11 -13April won **Gold Medal** for poster title “Immobilization of cellulase enzyme on functionalized multiwalled carbon nanotubes.

Other research achievement

i. N. M. Mubarak, A. Kundu, J.N. Sahu, E.C. Abdullah, N. S. Jayakumar. Synthesis of palm oil empty fruit bunch magnetic pyrolytic char impregnating with $FeCl_3$ by microwave heating technique. Biomass and Bioenergy, 61:265-275, (2014): ISI: Q1; IF: 2.975. (ISI-Cited Publication).

ii. Suchithra Thangalazhy-Gopakumar, Wail Mohammed Ahmed Al-Nadheri, Dinesh Jegarajan, JN Sahu, NM Mubarak, S Nizamuddin. Utilization of Palm Oil Sludge through Pyrolysis for Bio-oil and Bio-char Production. Bioresource technology, In Press 2014. ISI:Q1;IF 5.04. (ISI-Cited Publication).

iii. N. M. Mubarak, R.F Alicia, E.C.Abdullah,J.N.Sahu, A.B Ayu Haslija , J.Tan. Statistical Optimization of Zinc Removal Using Activated Carbon and Magnetic Biochar. Advances in Environmental Biology, 8(3) Special 2014, Pages: 686-691; Scopus cited publication.

iv. N. Sabzoi, N. S. JayaKumar, J. N. Sahu, P. Ganesan, N. M. Mubarak, S. A. Mazari, Synthesis and characterization of hydrochars produced by hydrothermal carbonization of oil palm shell. The Canadian Journal of Chemical Engineering, Accepted 19th Jan 2015. ISI:Q3;IF 1.313. (ISI-Cited Publication)

v. N. Sabzoi, N. S. JayaKumar, J. N. Sahu, P. Ganesan, N. M. Mubarak, S. A. Mazari, Hydrothermal carbonization of oil palm shell. Korean journal of chemical engineering. Accepted 18 December 2014. ISI: Q3; IF 1.241. (ISI-Cited Publication

vi. M. Shyamsundar, S. Z. M. Shamshuddin, N. M. Mubarak, S. R. Prathap. Catalytic Synthesis of Salicylate Esters over Cordierite Honeycomb Coated with Mo (VI)/ZrO2. Modern Research in Catalysis, 2013, 2, 39-41 (2013).

vii. N. M. Mubarak, N. Sazila, E.C. Abdullah, J. N. Sahu, N.S .Jayakumar, P. Ganesan. Comparative Study on Phenol Removal from Aqueous Solution by Using Carbon Nanotubes and Magnetic Biochar. Journal of Solid State Science & Technology. Accepted 13th October-2014. Scopus Cited publication.

viii. N.M. Mubarak, J.N. Sahu, E.C. Abdullah, N.S.Jayakumar, P. Ganesan. Plam oil empty fruit bunch based magnetic biochar composite comparison for synthesis by microwave-assisted and conventional heating. Microporous and Mesoporous Materials –Under review

ix. N. M. Mubarak, Y.T.Fo, Hikmat Said Al-Salim, J.N. Sahu, E.C. Abdullah, S. Nizamuddin, N.S.Jayakumar, P.Ganesan. Removal of methylene blue and orange-G from waste water using magnetic biochar. International Journal of nanoscience. Accepted on 15th January 2015, DOI: 10.1142/S0219581X1550009X (Scopus cited publication).

x. Nizamuddin, N.S Jayakumar, J.N Sahu, P. Ganesan, N.M Mubarak, Manoj Tiripathi. Chemical, dielectric and structural characterization of optimized hydrochar produced from hydrothermal carbonization of oil palm shell. Fuel, Under Review.

xi. Nizamuddin, W.E Yong, N.S Jayakumar, J.N Sahu, P. Ganesan, N.M Mubarak, Shaukat A. Mazari. An optimization study for catalytic hydrolysis of oil palm shell using response surface methodology. Journal of Oil Palm Research. Revision submitted.

xii. Nizamuddin, N.S Jayakumar, J.N Sahu, P. Ganesan, N.M Mubarak. Oil Palm shell from oil palm industry as a feed material for hydrochar production. Biomass and Bioenergy, Under Review.

xiii. N.M Mubarak, S.Shapnathayammal, Suchithra Thangalazhy-Gopakumar, J.N. Sahu, E.C. Abdullah3, P. Ganesan , N.S.Jayakumar Adsorption and Kinetic Study on Mg2+ Removal from Waste Water using Rice Husk based Magnetic Biochar. International Journal of nanoscience.Under Review.

Conference presentation.

i. N.M Mubarak, R.F. Alicia, E.C. Abdullah, J.N. Sahu, A.B Ayu Haslija , J.Tan. Statistical optimization of zinc removal using activated carbon and magnetic biochar. Third International Conference on Biotechnology Engineering (ICBIoE 2013) 2-4 July 2013, Kula Lumpur, Malaysia.

ii. N.M. Mubarak, C. Evon, L. Lisa, J.N. Sahu, E.C. Abdullah, N.S. Jayakumar, P. Ganesan. Removal of Zn^{2+} using magnetic biochar produced from coconut shell via microwave heating. 27th Symposium of malaysian chemical engineers (SOMChE 2014) 29-30 october.2014 Taylor's University Lakeside campus, subangjaya, Kula Lumpur, Malaysia.

Patent

i. Synthesis of magnetic biomass materials using microwave heating, J.N. Sahu, E.C. Abdullah, N.M. Mubarak. Malaysia Patent File number: **PI 2013700218.**

Awards

i. International Engineering invention &innovation exhibition (I-ENVEX- 2014) 11 -13April won **Gold Medal** for poster title "By products from palm oil sludge: A promising route for sustainable world".

ii. International engineering invention &innovation exhibition (I-ENVEX- 2014) 11 -13April Won **Sepcial Award MINDS** (Malaysian Invention And Design Society) for poster tittle"By products from palm oil sludge: A promising route for sustainable world".

iii. International Engineering invention &innovation exhibition (I-ENVEX- 2014) 11 -13April won **Silver Medal** for poster title "Adsorption and kinetic study on removal of Mg2+ from waste water using rice husk based magnetic.

iv. Novel Research and Innovation Competition (NRIC- 2013) 19-23 August won **Gold Medal** for poster title"Synthesis of magnetic biochar using microwave heating for removal of heavy-metals and dye from waste water"

v. International Engineering invention &innovation exhibition (I-ENVEX -2013) 16 -19April won **Gold Medal** for poster title "Synthesis of novel magnetic biochar using microwave heating for removal of lead from waste water".

vi. Material Lecture competition UM level 17 April 2013, won **Gold Medal** for the poster title Synthesis of novel magnetic biochar using microwave heating for removal of cadmium from waste water".

vii. 24th International invention, innovation & Technology Exhibition (ITEX-2013) 9-11May won **Gold Medal** for poster title Synthesis of novel magnetic biochar using microwave heating for removal of arsenic from waste water.

viii. Biomalaysia & Bioeconomy Asia Pacific Exhibition (BioInnovation Awards 2013-21 October) won **Silver medal** for the poster title "Enhancement of heavy metal removal from waste water using magnetic biochar synthesized by microwave technology".

ix. Biomalaysia & Bioeconomy Asia Pacific Exhibition (BioInnovation Awards 2013-21 October) won **Silver medal** for the poster title "Sustainably production of magnetic biochar from agriculture waste biomass by using microwave technology".